OPEN ACCESS

University of BRISTOL

This electronic thesis or dissertation has been downloaded from Explore Bristol Research, http://research-information.bristol.ac.uk

Author:
George, Daniel Bernard Francois

Title:
Determination of residual stresses in large section stainless steel welds.

General rights
Access to the thesis is subject to the Creative Commons Attribution - NonCommercial-No Derivatives 4.0 International Public License. A copy of this may be found at https://creativecommons.org/licenses/by-nc-nd/4.0/legalcode This license sets out your rights and the restrictions that apply to your access to the thesis so it is important you read this before proceeding.

Take down policy
Some pages of this thesis may have been removed for copyright restrictions prior to having it been deposited in Explore Bristol Research. However, if you have discovered material within the thesis that you consider to be unlawful e.g. breaches of copyright (either yours or that of a third party) or any other law, including but not limited to those relating to patent, trademark, confidentiality, data protection, obscenity, defamation, libel, then please contact collections-metadata@bristol.ac.uk and include the following information in your message:

• Your contact details
• Bibliographic details for the item, including a URL
• An outline nature of the complaint

Your claim will be investigated and, where appropriate, the item in question will be removed from public view as soon as possible.

DETERMINATION OF RESIDUAL STRESSES IN LARGE SECTION STAINLESS STEEL WELDS

By

Daniel Bernard François George

A thesis submitted to the University of Bristol
In accordance with the requirements of
The degree of Doctor of Philosophy
In the Department of Mechanical Engineering
In the Faculty of Engineering

July 2000

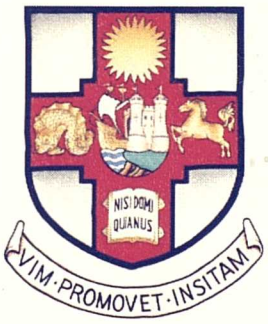

Advanced Materials and Structural Integrity Group
Department of Mechanical Engineering
University of Bristol
BRISTOL BS8 1TR – UK

ABSTRACT

Thick-section steel welds can be found in many engineering applications such as in the mining, offshore and the nuclear industries. The distribution of residual stresses in these components can play a crucial role in the integrity of the overall fabrication. Residual stresses may contribute to localised plastic behaviour or crack initiation. Techniques that can quantify these residual stresses are therefore an important part of ensuring safety of the component.

The deep-hole residual stress measurement technique was investigated to assess its reliability in measuring residual stresses in thick section stainless steel welded components. It is a semi-destructive technique that involves drilling a small hole through the specimen thickness, whose diameter is measured accurately. The removal of a cylinder containing this reference hole enables a strain relaxation in this core. This generates a variation of the reference hole diameter, which is remeasured and enables pre-existent residual stress state to be determined. New analysis was developed to take into account more complex residual stress states.

Validation of the technique was undertaken through calibration work on simple components containing known applied stress distributions. Bending and torsion tests were carried out and results comparisons between theory, FE simulation and experiments were made. The effect of a steep residual stress gradient was investigated using an autofrettaged tube.

An extensive set of experimental measurements was undertaken on welded specimens. These experimental results were compared with finite element analyses carried out by British Energy plc. The effects of section size and weld geometry were investigated as well as the influence of post weld heat treatment and weld repair on the residual stress distributions.

Overall, the experimental measurements in welded components did not agree with recommended code distributions. This work has illustrated that continued experimental measurement of residual stresses is required in thick section components to avoid non-conservative estimates of structural Integrity.

DECLARATION

The accompanying dissertation entitled "Determination of Residual Stresses in Large Section Steel Welds" is submitted in support of an application for the degree of Doctor of Philosophy in Engineering at the University of Bristol. The candidate bases the dissertation on independent work unless otherwise acknowledged or referenced in the text. This work has not been submitted for any other degree or diploma at the University or any other institution. The views expressed in the dissertation are those of the author and not of the University.

I declare that the above statements are true.

Daniel B.F. George

July 2000.

PUBLICATIONS

The papers :

A.A. Garcia-Granada, D. George and D.J. Smith, "*Assessment of Distortions in the Deep-hole Technique for Measuring Residual Stresses*", Proceedings of the 11th International Conference on Experimental Mechanics, Oxford, UK, pp. 1301-1306, August 1998.

D.J. Smith, D. George, P.J. Bouchard and C. Watson, "*Prediction and Measurement of Residual Stress in Thick-Section Stainless Steel Welds*", I.Mech.E Seminar, London, UK, November 1999.

D. George, P.J. Bouchard and D.J. Smith, "*Evaluation of Through Wall Residual Stresses in Stainless Steel Welds Repairs*", Materials Science Forum, vol. 347-349, pp. 646-651, 2000.

D.J. Smith, D. George and J. Bouchard, "*Measurement And Prediction Of Through Thickness Residual Stresses In Thick Section Welds*", Journal of Strain Analysis, Special Issue, vol. 35, no. 4, pp. 287-305, 2000.

D. George and D.J. Smith, "*The Application of the Deep-hole Technique for Measuring Residual Stresses in Autofrettaged Tubes*", PVP High Pressure Technology, vol. 406, pp. 25-31, 2000.

D. George and D.J. Smith, "*Residual Stress Measurement in Thick Section Components*", PVP Assessment Methodologies for Preventing Failure: Deterministic and Probabilistic Aspects and Weld Residual Stress, vol. 410-1, pp. 275-282, 2000.

are based on the results of this study.

And the papers :

P.J. Bouchard, R.H. Leggatt, D. George, S.K. Bates and A.G. Youtssos, "*Thermal Relaxation of Residual Stresses in Thick Section Type 316 Stainless Steel Girth Welds*", 6th International Conference on Residual Stresses, Oxford, UK, July 2000.

S.K. Bates, R.H. Leggatt, D. George, A.G. Youtssos, and P.J. Bouchard, "*Measurement and Modelling of Residual Stresses in Thick Section Type 316 Stainless Steel Welds*", 6th International Conference on Residual Stresses, Oxford, UK, July 2000.

Used results carried out during this project.

ACKNOWLEDGEMENTS

My sincere gratitude is expressed to Professor David J. Smith, the supervisor of this project, for his continuous advice, encouragement and commitment and help regarding the content of this dissertation. I also would like to thank Professor Smith for giving me the chance to come over Bristol to undertake this work.

I would like to thank Mr. Peter J. Bouchard of British Energy (BE) plc. for his help in providing most relevant information and results regarding the finite element analysis aspects and numerical simulations. Also the financial support for this research project was provided by British Energy (contract reference : IMC Reference PC/GNSR/5051).

I also would like to thank the VORSAC team, which provided valuable information under the project FI4S-CT96-0040 and also financially supported this research for a period of one year.

The staff of the Mechanical Engineering workshop performed much important work on my behalf. In particular, I wish to thank Mr. Ian Milnes for his very considerable efforts regarding the experimental equipment of the deep-hole method. This was a very time consuming undertaking, which he approached with patience and much dedication.

I also would like to thank the Structural Integrity Group, which provided a friendly and dynamic atmosphere in which to carry out my work during the period of this research.

Many thanks as well to my family and friends who encouraged me at various stages of this project.

CONTENTS

LIST OF TABLES

LIST OF FIGURES

NOMENCLATURE

The following lists the symbols used in the main text.

d	Distance which the weld cap lay over the parent metal
$\vec{F}$	Vector of body forces
$\overrightarrow{M'}$	Vector of body momentum
$\bar{\varepsilon}$	Vector of measured reference hole strains
$\bar{\sigma}$	Optimised stress vector
$\bar{\varepsilon}$	Optimised strain vector
σ_0	Constant or hydrostatic term of the Fourier analysis
σ^{ci}, σ^{si}	Stress coefficients of the Fourier analysis for *cos* and *sin* functions
$\sigma_{rr}, \sigma_{\theta\theta}$	Radial and hoop stress coefficient of the Fourier analysis for stress evaluation around the reference hole
Φ	Stress function of the Fourier analysis
ν	Poisson's ratio
ε_θ	Reference hole hoop strain
σ_{xx}, σ_{yy}	Evaluated residual stresses in the plane normal to the reference hole axis
ε_z	Reference hole through thickness strain
σ_{zz}	Evaluated residual stress in the direction parallel to the reference hole axis
$[M]$	Compliance matrix
$[M]^*$	Pseudo-inverse of the matrix M
a, b	Inner and outer radius of the core for the Fourier analysis
$A[z]$	A parameter representing uniform expansion of the reference hole
b, h	Dimensions of square beam in calibration test
$B[z]$	A parameter representing eccentric deformation of the reference hole
c_{ii}	Single crystal constants for anisotropic analysis
d_0	Reference hole diameter
d_c	Calibration distance for the capacitance gauges
d_c	Diameter of circular cross section for calibration test
E	Young's modulus

$f[\theta,z], g[\theta,z], h[\theta,z]$	Angular and through thickness functions
F_{max}	Maximum load applied in calibration test
I_x	Quadratic moment of area
J	Quadratic moment of area for the torsion calibration test
k_2	Constant for modified torsion theory
M^t	Applied moment in calibration tests
n	Number of measured angles around the gun drilled reference hole
p_i, p_0	Inner and outer pressure of the tube in the hydrostatic calibration test
r	Radius of measured specimen
r_c	Radius to neutral axis in calibration test
t	Specimen wall thickness
t	Specimen or sample thickness
T_{max}	Maximum applied torque
u_r	Radial displacement of reference hole
x, y	Co-ordinates in the plane normal to the axis of the reference hole
y_c	Distance to neutral axis in calibration test
z	Position through thickness
z_l	Distance along the beam in calibration test
z_n	Number of measured points or increments through the specimen wall thickness
T	Applied torque in calibration test
λ	Coefficient of distribution of load between x and y directions in local plasticity around the hole.
θ	Angle around the reference hole
σ_{max}	Maximum stress applied in calibration test
σ_y	Yield stress
τ	Shear stress in calibration test
τ_{max}	Maximum shear stress

CHAPTER 1 : INTRODUCTION

Thick-section steel welds can be found in many different engineering components, including systems for pressurised water reactors (PWRs) and joints employed in the petro-chemical industry. The nature and distributions of residual stresses in these components can have a crucial effect on their integrity during normal operation. This arises primarily from the combined effect of residual and in-service stresses, which can bring localised plastic deformation or crack initiation. A previous project by Bonner [1996] addressed the development of the deep-hole method to measure residual stresses in thick section welds. The method was developed but further validation was required and a more extensive set of results was desirable for a range of component thickness and geometry.

The main aims of this research was to validate the deep-hole technique for use on thick stainless steel welds, to provide a reliable tool to evaluate accurately residual stress distributions and finally to compare the measurements with numerical simulations. The technique involves drilling a reference hole through the specimen thickness and accurately measures the diameter of the hole through the depth and at a number of angles around the hole. A cutting operation follows the first set of measurements, and consists of trepanning a cylindrical core containing the reference hole. This is followed by remeasuring the reference hole diameter at the same locations as before. The relaxed strains are subsequently converted into residual stresses formerly present in the specimen using a 2D plane stress analysis.

One part of the project was to compare measured residual stresses with results available in the literature. However, this research project carried out measurements only in stainless steel specimens and very little earlier work has been carried out. A literature review is presented in chapter 2. The main areas covered are the definition, distribution, origin and characteristics of residual stresses, their advantages and disadvantages particularly in stress relief and weld repairs. A broad overview of the different techniques available to measure residual stresses is also presented. The methods are separated into three categories, namely non-destructive, semi-destructive

and destructive. The review also examines residual stress distributions or redistributions in stainless steel welds after post weld heat treatment and weld repairs.

The second stage of the research was to undertake developments and provide validation of the deep-hole technique. These features are presented in chapter 3 and 4. An assessment of the technique is given in chapter 3 together with new developments undertaken during this project. Also, new developments in the analysis are presented together with assessment of the validity of the current analysis. Chapter 4 presents results from different calibration tests undertaken to assess the measurement accuracy and reliability of the technique. Experimental calibrations were undertaken by applying known stress distributions and measuring these using the deep-hole method. Constant and linear stress distributions using hydrostatic pressure and simple bending were assessed. Non-linear stress distributions in the torsion test and using an autofrettaged tube were also examined. In the case of the autofrettaged tube the assessment was more complex because of the presence of a residual stress gradient through the thickness of the specimen. Finally, numerical simulations were carried out to assess the influence of localised plasticity in evaluating residual stresses.

The project carried out an extensive set of experimental measurements on a variety of stainless steel welded components. The components and the measurements are presented in detail in chapter 5 where aspects related to specimen size and geometry, as well as the influence of post weld heat treatment, ageing and weld repairs are presented. The experimental measurements are compared in chapter 6 with finite element simulations of welding carried out by British Energy. Also, experimental results using different experimental techniques are compared with deep-hole measurements.

An overall discussion of the research is presented in chapter 7 where an assessment is made of the deep-hole method in measuring through-wall residual stress distributions in welded components. Also, the measured results from welded specimens are compared with earlier work. The conclusions and future work of the research project are presented in chapter 8.

CHAPTER 2 : LITERATURE REVIEW

2.1. Introduction

The literature reviewed in this chapter focuses on the generation and characterisation of residual stresses in welded components, a description of different techniques to measure these residual stresses and the result of specific treatments applied to components such as post weld heat treatment (PWHT), ageing and weld repairs. It is not intended to provide a complete overview on the subject of residual stresses since this would be far too long. Rather the focus will be on the subjects relevant to the thesis and particularly in relation to stainless steel welded specimens.

The aspects related to the definition, origin, nature of residual stresses and different techniques to measure these are developed in detail in Bonner [1996]. These are summarised here. New published literature has been added to expand this earlier review.

2.2. Residual stresses in engineering components

Residual stress may be defined as the self-equilibrating internal stress existing in a free body under uniform temperature conditions and with no external load applied. It is the most common term used since it may be "left over" by a previous manufacturing operation. At equilibrium, without external load, both the resultant force and the resultant moment of the body must be equal to zero.

A classification of residual stress into three categories has been suggested by Macherauch et al. [1986], using the term "homogeneous" to mean "constant in magnitude and direction" :

1st category : Macro residual stress which are homogeneous across several grains of the material and equilibrated over the body.

2nd category : Nearly homogeneous micro residual stress which are homogeneous only on a part of a grain or one grain and equilibrated over several grains.

3rd category : Inhomogeneous micro residual stress which are inhomogeneous even over sub-microscopic distances inside the body but in equilibrium on small parts of a grain.

One or a superposition of these three categories define all the residual stress states. However, from an engineering point of view, the first category has more importance than the 2nd and 3rd categories because any modification to equilibrium may also modifies the external dimensions of the body.

2.2.1. Origin and nature of residual stresses

Residual stresses always arise when material is deformed inhomogeneously and permanently, or plastically [Macherauch, 1987]. As stated earlier, the main engineering sources of residual stresses are for the first category and examples are as follows ; machining, forming, elasto-plastic loading, heat treating, joining, coating and founding. Most of these sources will be briefly reviewed in the following sub-sections.

(i) Machining (Grinding, turning, drilling, milling)

These processes used on metallic materials usually generate compressive stresses in the working directions of the cutting zone [Bainbridge, 1969]. The intensity of the residual stress depends on different parameters like cutting speed, cut depth, geometry and material properties. Different investigations on the surface residual stresses of steel show compressive values from 250MPa going up to 600MPa in the case of turning. The cutting speed and tool sharpness are two important parameters especially in milling and grinding where residual stresses may vary widely because of local heating.

(ii) Forming (rolling, shot-peening, stretch-forming)

The shot-peening process generates compressive stresses in the material. A high velocity shot is used to cause local plastic yielding at the outside surface, which elongates relative to the interior. Results presented by Noyan et al. [1981], show that the interior constrains the surface causing high local compressive residual stress near the surface, balanced by tensile stress in the interior.

In the case of rolling, the magnitude of stress is dependent on the material yield stress, the sample thickness, the roll size and the degree of reduction [Baldwin, 1949].

(iii) Elasto-plastic loading (bending, torsion, tension, compression)

On releasing external loading after plastic deformation, residual stresses can occur [Noyan, 1987]. For example, if the surface has a higher yield strength than the interior, for a tensile plastic stress, the independent elastic contraction after releasing the stress would leave the surface shorter than the interior (figure 2.1). Since the deformation must be the same, tensile residual stress remain at the surface balanced by compressive residual stress inside the material.

In the case of bending, yielding takes place on both the tensile and compressive outer surfaces. The stresses are then non-linearly distributed close to the outside faces (figure 2.2). On load release, the beam springs back elastically resulting in a residual stress distribution through the depth of the beam.

(iv) Heat treatment

This procedure can cause residual stresses even without crystalline structure change (Noyan et al., 1987). For example, when a material is cooled down rapidly after heat treatment, dissimilar rates of contraction appear at the surface and interior of the material. Once at room temperature, the surface extends relative to the interior resulting in residual compression.

If a phase transformation occurs during heat treatment, compressive surface residual stresses are produced because these deformations dominate the local yielding

due to heat treatment. Near to room temperature, the permanently deformed interior material forces the surface into residual tension, which can promote cracking. Local yielding can prevent this occurring and generally, the material must be cooled down sufficiently slowly after heat treatment.

(v) Joining (welding, soldering, brazing, adhering)

There are many factors in welding which create residual stresses and therefore their calculation can become difficult and complex. The main source of residual stresses, shown in figure 2.3, is the localised shrinkage of cooling weld metal which is restrained by surrounding colder sections of the fabrication. Other less important factors can influence the final distribution; for example, residual stresses remaining in the parent metal due to cutting processes, preheating or the welding process employed.

The real state of residual stresses inside the material is still more complex, being continually modified during the welding process. A controlled study of this problem is therefore an extremely difficult exercise, since at any instant any of the influencing parameters may be different. Hence, any endeavour to estimate the final distribution should take into account all the influencing parameters.

Most of the sources of residual stresses arising from welding and their relative importance are reviewed below :

- Shrinkage

The principal origin of residual stresses in welded components is the localised shrinkage of cooling weld metal opposed by colder adjacent material. For the simple case of a longitudinal weld in a plate, depending on factors such as plate thickness and boundary conditions, plastic deformation is unnecessary for the production of residual stresses.

- Quenching

The cooling process after welding is rarely homogeneous across the specimen thickness (Macherauch et al., 1977). In a thick specimen, the outside usually cools

down more rapidly than the interior, even with cooling with air. This effect increases if the weld is quenched. If the temperature gradient is large between the outside and the interior during cooling, inhomogeneous plastic deformation arises as the thermal stresses exceed the yield stress.

- Phase transformation

Welded specimens heated above temperatures where crystalline structure changes occur usually have phase transformations on cooling and for some materials, significant volume variation at the same time. For example, the phase transformations, in welded steel, from austenite to ferrite, pearlite, bainite or martensite can occur. The expansion of the transformed region will induce compressive residual stress.

It is possible to shift the phase transformation temperature by alloying the specimen but different alloying can result in increased [Macherauch et al., 1977] or decreased [Parlane, 1981] magnitude of residual stresses. These opposite effects can then make the choice of alloying very difficult.

- Superimposition of (a), (b) and (c)

In real situations, the different sources of residual stresses detailed above are usually combined resulting in a complex final state. The simplest way to combine these effects is to assume a linear superimposition, shown in figure 2.4, which tend to show that the maximum residual tensile stress is always outside the weld centre line. Experiments conducted by Macherauch et al. [1977] showed a good agreement with the linear superimposition. However, recent work [Macherauch et al., 1986] on the simple superimposition described above, show only a limited understanding of the sources of residual stress distributions.

- Plastic deformation imposed on parent material

Darbyshire [1985], suggested that the above mechanisms can be further complicated by the effect of heat transfer from the weld to the adjacent material. After welding, the weld starts to cool down accompanied with a cycle of heating and cooling of the parent material. The resulting effect varies from place to place and reduces as the distance from the weld increases. It appears that the parent material in contact with the heated weld yields in compression and reverts to residual tension on

cooling. The tensile residual stresses present in the weld can therefore be extended to the parent material.

- Expansion coefficient mismatch

Another important factor characteristic for the phase transformation is the difference between the coefficients of thermal expansion in the weld and in the parent material. That difference can produce very steep stress gradients at the interface due to the cooling process. These changes are characteristic of a discontinuity in material properties and are more important than moderate changes arising from other sources [Darbyshire, 1985].

- Other factors

There are other factors influencing the distribution of welding residual stresses, usually less important than those described above. One of the most significant is restraint. This effect, caused by previously deposited weld, can sometimes be difficult to predict. For example the degree of restraint increases after each pass in a multi-pass weld. On the other hand, external restraint is usually more easily understood and Parlane [1981], suggests that restraint acts to balance the generated residual stresses.

Usually, in the determination of residual stresses in welded components, consideration is only given to the sources directly involved in the welding process while the preparation of the sample is overlooked. For example, the cutting processes for preparation also generate residual stresses since they produce a local thermal gradient. The use of preheating the sample before welding may be another way to reduce residual stresses after welding.

Other less important factors such as geometry and thickness of the sample can influence the final distribution of residual stresses.

2.2.2. Distributions of Residual Stresses in Welds

The geometry of welds used in this project (for butt-welded pipes) was always in the form of a 'V' as shown in figure 2.5. The weld beads are deposited incrementally from the bottom (root pass) to the top, alternatively on the left and right hand side of

the weld groove. When each layer is deposited, between hot and cold metal shrinkage occur (as presented in section 2.2.1). This phenomenom is amplified as the weld groove is filled up since the size of the weld width is increasing. Ultimately, the increasing generated tensile residual stress on the last bead conteract the smaller residual stress of the initial beads. This globally generates a compressive residual stress at the inner surface of the specimen, while the outer surface remains in tension. This, of course assumes that stresses are symetrically distributed on each side of the weld centre line and that no other effects disturb the residual stress distribution. Also, this global stress distribution depends on the location of measurement.

2.3. Measuring residual stress distributions

2.3.1. Introduction

Different techniques available to measure residual stresses are presented in this section. Almost all of these techniques involve strain measurements, which are converted into stresses. These strain measurement techniques can be classified into three different categories :

non-destructive : the measurements are done without causing any damage to the material (such as optical methods, X-ray and neutron diffraction).

semi-destructive : where the analysis involves removing only small quantities of material without significantly affecting the structural integrity (and measuring strain relaxation).

destructive : removing large quantities of material (and also measuring strain relaxation).

2.3.2. Non-destructive techniques

(a) X-ray diffraction

Recent work by Hutchings [1990] shows that specific lattice planes in metallic crystalline structures distort under applied loading and this is directly proportional to the stress. If isotropic elasticity is assumed, the strain is related to the stress by :

$$\varepsilon_{\psi} = \frac{1+\nu}{E}\sigma \cdot \sin^2 \psi - \frac{\nu}{E}\sigma \qquad (2.1)$$

where E is the Young's modulus, ν is the Poisson's ratio and ε_{ψ} is the measured strain at angle ψ to the surface. This measurement technique relies directly on the interference of X-ray radiation, which is diffracted by the atomic lattice structure. The diffraction angle is given by Bragg's Law :

$$n\lambda = 2d \cdot \sin\theta \qquad (2.2)$$

where n is an integer, λ is the radiation wavelength, d is the spacing between reflecting planes and θ is the complement of angle of incidence on these planes (figure 2.6). Differentiation of equation (2.2) gives :

$$\varepsilon = \frac{\Delta d}{d} = -\cot\theta \cdot \Delta\theta \qquad (2.3)$$

Measurement of changes in the locations of diffracted X-ray peaks recorded from the lattice plane at different angles ψ allows the determination of the strains ε_{ψ}. The substitution of ε_{ψ} from equation (2.3) into equation (2.1) gives :

$$2\Delta\theta = -2 \cdot \tan\theta \cdot \frac{1+\nu}{E} \cdot \sigma \cdot \sin^2 \psi + C \qquad (2.4)$$

where $2\Delta\theta$ is the angular shift of a diffracted peak recorded from different angles ψ and C is a constant. A plot of $2\Delta\theta$ versus $\sin^2 \psi$ results in a straight line of gradient $-2.\tan\theta.(1+\nu).(\sigma/E)$ and then, σ can be determined.

The stresses obtained by this method can be very localised to the extent of being only associated with the surface region. In practice, in steel X-ray can penetrate only to a depth of about 0.1mm where a more complex state of stress occurs. For these conditions, more complicated formulae must be employed to determine the residual stresses (see Doig et al. [1985] or Noyan et al. [1987]).

Usually, the X-ray diffraction method gives a very good precision and resolution [Parlane, 1977]. However, there are several disadvantages: it is very time-consuming (2 hours for one stress value), E and ν have to be assumed and may be different from the bulk value. It may be also unreliable when plastic deformation occurred due to lattice disorientation and the surface finish has to be very good.

(b) Neutron diffraction

This measurement method, as with the X-ray method, gives directly the strains obtained from the changes of the lattice spacing (Webster et al., 1985). However, neutrons are more energetic than X-ray and can therefore penetrate several centimetres into most metals.

The relationship used to obtain residual stresses using the neutron diffraction method is again Bragg's law, equation (2.2). Two different approaches are possible in the neutron diffraction technique; the first is based on the use of a monochromatic neutron beam involving the same analysis as with X-ray and the second is based on a polychromatic neutron beam requiring fixed angle measurement between stressed and unstressed samples.

In general, to completely define a stress tensor, it is necessary to have measurements at different angles [Webster et al., 1985]. For specific conditions such as plane stress or plane strain where the principal stress directions are known, a complete definition of the stress tensor can be obtained using only three orthogonal measurements.

(c) Ultrasonic

Many forms of experiments use ultrasound to measure residual stresses. In most cases, these techniques use the fact that the ultra sound propagation speed varies with the anisotropy due to the stress state.

Different methods using the ultrasonic method are presented by Parlane [1977] :

+ birefringence	: where the stress dependent velocity is observed; only uniform stresses can be determined.
+ attenuation	: affected by stress state and material properties.
+ surface waves	: to measure the stresses to a depth of about 1 mm (also called Rayleigh waves).
+ goniometry	: depending on the nature of stress of the three critical angles of incidence (shear, longitudinal and Rayleigh).
+ beam interaction	: where interacting beams are used to create a third beam in the sample.

The ultrasonic method can give errors up to 3% but an average of 5% to 10% appears to be more realistic. The important disadvantages of this method are, the area measured which is only usually about 30 mm^2 and the variation of sample geometry that can make the use of waves difficult.

(d) Electro-magnetism

In contrast to diffraction and ultrasonic techniques, the magnetic stress measurement method is restricted to ferromagnetic materials. Keller et al. [1989], proposed a method to solve the relationship used to determine residual stresses which integrate a form of comparative measurement and calibrated material and cannot be described in physical terms. However, dependence between structural variables and magnetic quantities has been established.

The basic principle of the electromagnetic method is that different domains of the material have separate electromagnetic properties dependent on the stress state. This

stress state can then be determined by measuring the variation of these electromagnetic properties as a function of the magnetic field strength.

Problems can arise from measured properties varying with structural state, materials must be magnetostrictive, calibration must be done for each material, and stress measurements can be expensive due to time and measurement system. One advantage is that the results are insensitive to a surface roughness ≤ 0.1 mm.

2.3.3. Semi-destructive techniques

In this section, methods of residual stress measurement which cause only slight damage to the specimen and do not compromise its integrity are reviewed.

(a) Centre-hole drilling

This technique is based on the partial stress relief of the specimen surface through the drilling of a hole. The radial stress σ_r at the hole edge is equal to zero and increases with the radial distance [Procter, 1985]. The variation of that radial stress is measured by strain gauges aligned 'radially' at the specimen surface (see figure 2.7).

The stress field is assumed to be biaxial and principal stress directions are unknown. The stress state can be calculated using a three-element strain rosette where:

$$\sigma_{max},\sigma_{min} = \frac{E}{2K_1}\left[\frac{\varepsilon_1+\varepsilon_3}{1-\upsilon\cdot\frac{K_2}{K_1}} \pm \frac{\sqrt{(\varepsilon_1-\varepsilon_3)^2+(\varepsilon_1+\varepsilon_3-2\varepsilon_2)^2}}{1+\upsilon\cdot\frac{K_2}{K_1}}\right] \qquad (2.5)$$

$$\phi = \frac{1}{2}\tan^{-1}\left(\frac{\varepsilon_1+\varepsilon_3-2\varepsilon_2}{\varepsilon_3-\varepsilon_1}\right)$$

and σ_{max}, σ_{min} are the values of the maximum and minimum principal stresses; $\varepsilon_{1,2,3}$ are the measured relaxed strains at 0, 45 and 90°; E is the Young's modulus; ν is the

Poisson's ratio; and Φ is the direction of the principal stresses (relative to ε_1). The constants $1/K_1$ and $\nu K_2/K_1$ are directly determined using a uniaxial stress field by :

$$\frac{1}{K_1} = \frac{\varepsilon_A}{\varepsilon_{A'}} \quad and \quad \frac{\nu K_2}{K_1} = -\frac{\varepsilon_{T'}}{\varepsilon_{A'}}$$

where ε_A is the applied strain in axial direction, $\varepsilon_{A'}$ is the relaxed strain in axial direction (due to hole drilling) and $\varepsilon_{T'}$ is the corresponding relaxed strain in the transverse direction.

The strain measurements are usually done with rosettes that have been specially designed for this purpose. The hole has to be at an identical known distance from each rosette element, perfectly circular and drilled to a known diameter.

It is important that the drilling process does not induce additional residual stresses and can produce high quality flat-bottomed holes. Different drilling techniques have been used (Keller et al., 1989). For example air abrasion generates the least stress and high speed drilling and produces the best hole shape. The different hole diameters employed are 0.8, 1.6 and 3.2 mm and the depth can be up to 1.5 times the diameter of the hole.

It should be noted that the residual stress field is disturbed by the addition of a hole over a region of about 5 times the hole diameter. Therefore measurements have to be obtained away from the specimen boundaries. Other potential errors in the results can occur from the values of $1/K_1$ and $\nu K_2/K_1$, quality of drilling and strain measurement.

The errors caused by local yielding around the hole in the hole drilling strain-gauge method were studied by Lin et al. [1995]. The material used was 304 stainless steel. If residual stresses inside the hole before drilling exceed 1/3 of the yield strength, due to a stress concentration factor of 3 around the hole in uniaxial loading, plastic flow will start during the drilling procedure and the elastic equation used in this case is no longer valid. If the error induced by local yielding is neglected, the residual stress measured will always be overestimated. The results show that the error

is negligible when the residual stresses are less than about 65% of the yield strength of the test material (figure 2.8).

Lin and Chou [1995] show that at 95% of the yield strength, the error induced in a 304 stainless steel sample was 44%. It was also found that with stainless steel a larger error occurred compared to samples using 1018 low carbon steel and 5052 H32 aluminium alloy. It is important to note that Lin and Chou examined plastic deformation around the hole due to the stress concentration arising from elastic residual stresses and not from plasticity associated with drilling.

(b) Ring coring

The basic principle of this method is similar to the centre-hole method. The difference is that an annular groove is used instead of a hole. A ring-core rosette is fixed in the centre of an annular grove, which is trepanned in steps. This trepanning releases the stresses in the core and the strain variations are recorded through the ring-core rosette. Keil [1993], proposed the following relaxation functions to calculate the original principal residual stresses as a function of depth :

$$\sigma_1(z),\sigma_2(z)=\frac{\sigma_a(z)+\sigma_c(z)}{2}\pm\sqrt{\frac{[\sigma_b(z)-\sigma_a(z)]^2-[\sigma_b(z)-\sigma_c(z)]^2}{2}}$$

$$\alpha=\frac{1}{2}\tan^{-1}\left[\frac{2\sigma_b(z)-\sigma_a(z)-\sigma_c(z)}{\sigma_a(z)-\sigma_c(z)}\right] \qquad (2.6)$$

where

$$\sigma_{a,c}(z)=\frac{E}{K_1(z)^2-\nu^2K_2(z)^2}\left[K_1(z)\frac{d\varepsilon_{a,c}(z)}{dz}+\nu K_2(z)\frac{d\varepsilon_{c,a}(z)}{dz}\right] \qquad (2.7)$$

$$\sigma_b(z)=\frac{E}{K_1(z)^2-\nu^2K_2(z)^2}\left\{K_1(z)\frac{d\varepsilon_b(z)}{dz}+\nu K_2(z)\left[\frac{d\varepsilon_a(z)}{dz}-\frac{d\varepsilon_b(z)}{dz}+\frac{d\varepsilon_c(z)}{dz}\right]\right\}$$

and z is the current groove depth. σ_1, σ_2 are the principal stresses (at depth z). α is the σ_1 direction. $\varepsilon_{a,b,c}$ are the measured relaxed strains at 0, 45 and 90° at surface. E is the Young's modulus and ν is the Poisson's ratio. Finally, the relaxation functions $K_1(z)$ and $K_2(z)$ are dependent on the geometry and can be determined in advance by a direct uniaxial tensile stress.

Different processes are available for trepanning the circular groove. A special hollow mill can be used. However, there are problems like removing the strain gauge leads before each milling operation. Usually, electrical discharge machining (E.D.M.) is used because it overcomes the problems associated with the hollow milling technique.

Keller et al. [1989] presents a general process for a circular groove of about 5mm depth, which gives good results to a depth up to 25mm. The outside diameter of the groove is generally 18mm and the overall dimensions makes it a more destructive method than the centre-hole technique. However, its better accuracy makes it a preferred option to calculate stresses at a greater depth [De Angelis et al., 1990]. Misra et al. [1982], point out that there is the potential for greater precision in the ring-coring method compared to the centre-hole technique. In the ring core method, 90% of the stresses are released whereas in the centre-hole method only 25% of the residual stresses are released.

(c) Deep hole drilling method

The deep-hole method consists of drilling a hole through the specimen and trepanning a core containing the hole. The hole diameter is measured before and after trepanning and the changes in diameter are used to calculate the residual stresses. Initial studies using the deep-hole method were developed by Zhdanov et al. [1978], Beaney [1978] and Jesensky et al. [1981]. Zhdanov examined residual stresses in steel welds in which 8mm diameter hole were drilled. In each case, the shape of the hole was precisely measured with special devices. A core of 40mm diameter was then incrementally trepanned to be able to measure the height variation at different points. Assuming uniformity and linear stress-strain behaviour on stress relief, and that the

axis of the hole was a principal direction of stress ($\tau_{xz} = \tau_{yz} = 0$), the stresses $\sigma_{x,y,z}$ could be calculated.

Beaney [1978] proposed an approach using gun drilling to provide a very smooth and straight 3.175 mm diameter hole in the direction of one principal stress and measure the diameter at 0, 45 and 90° each 2mm in depth. The change in the hole diameter is measured by using strain gauges fixed onto two parallel beams fixed together and drawn along the hole. The variations of diameter along the hole generate deflection of the beams, which are measured by the strain gauges. A core was then trepanned by electro chemical machining (E.C.M.) and the diameter of the hole was remeasured.

Jesensky et al. [1981] measured residual stresses in steel weldments. This technique used two blind drilled holes on the opposite faces of the sample and strain gauges placed inside the two holes and on the two faces. The technique permitted, after trepanning two cores of 32 mm in the component was carried out, measurement of the complete residual stress state in the three directions x, y and z.

Beaney's method [1978] was updated by Procter et al. [1987], and included important improvements to the experimental procedure. The main improvements were associated with averaging of residual stress in the smallest possible area, ensuring that the drilling process did not modify the weld stress state and displacements were no longer recorded using strain gauges. Further improvements included the use of capacitance gauges to measure the change in hole diameter (figure 2.9).

Significant developments and improvements to these procedures have been achieved in the earlier research project at Bristol University [Bonner, 1996] and also in the current research project. The main interest in using the deep hole technique is that it is a semi-destructive method and allows reasonably accurate results for depths greater than about 20mm.

Leggatt et al. [1996] assessed the deep-hole method through a calibration test using a rectangular ferritic steel bar. The specimen was 875mm long, 100mm deep

and 52mm wide. A tensile test of the same specimen was carried out to determine the stress/strain characteristics of the material at room temperature. The rectangular bar was subjected to four-point elastic-plastic bending, and the deep-hole method applied to measure the residual stress inside the bar after plastic deformation. An analytical solution for determining the residual stresses from the measured strains was also presented. The measurements and the analytical solution show a very good agreement as shown in figure 2.10.

Detailed results from the previous research project are presented by Bonner [1996] and the details of the analytical procedure is given by Smith and Bonner [1996]. Smith and Bonner [1996] also discuss several sources of errors obtained from residual stresses measured in a heat-treated sample. The reliability of the measuring device was of the order of $\pm 1.5\mu m$, which corresponds to about 30MPa.

The deep-hole technique was also applied by Bouchard et al. [1997] to obtain residual stresses in a thick section AISI type 316H austenitic stainless steel component. Results are compared with Finite Element analysis.

The principal reasons giving rise to differences between the predicted and measured residual stresses were the assumptions made in the Finite Element analysis as well as in the experimental process. The parameter, which had the main influence on the FE results, was the variation of yield stress.

2.3.4. Destructive techniques

In this section, methods that significantly damage the material for residual stress measurement, are considered. They essentially employ different kinds of sectioning, which cause relaxation of strain. Three methods in this category are reviewed : Sachs, Rosenthal and Norton and crack compliance.

(a) Sachs method

The basic principle of this method is to measure partial relaxation of strain by removing incrementally several layers of material [De Angelis, 1990]. Sachs [1927],

showed that the calculations remain simple if the geometry of the sample is axisymmetric but is difficult to use in the other cases due to the complexity of the analytical expressions. Ueda et al. [1975], demonstrated that the Sachs method should be used only in cases where the residual stresses have a rotational symmetry and are uniform in the axial direction.

The potential use of that method is for example on tubes or solid cylinders and the equations used to estimate residual stresses are :

$$\sigma_{rr}(r) = \frac{E}{1-\nu^2}\frac{A(r_0)-A(r)}{2A(r)}\Theta$$

$$\sigma_{\theta\theta}(r) = \frac{E}{1-\nu^2}\left\{\left[A(r_0)-A(r)\right]\frac{d\Theta}{dA(r)} - \frac{A(r_0)+A(r)}{2A(r)}\Theta\right\} \qquad (2.8)$$

$$\sigma_{zz}(r) = \frac{E}{1-\nu^2}\left\{\left[A(r_0)-A(r)\right]\frac{d\Lambda}{dA(r)} - \Lambda\right\}$$

where $\Theta = \varepsilon_{\theta\theta} + \nu\,\varepsilon_{zz}$ and $\Lambda = \varepsilon_{zz} + \nu\,\varepsilon_{\theta\theta}$

with $\sigma_{rr,\theta\theta,zz}$ equal to the residual stresses in the radial, tangential and axial directions respectively, r is the radius from the specimen axis and r_o the outside radius, and E is the Young's modulus and ν the Poisson's ratio. A is the enclosed area. The above relations assume an elastic behaviour and plastic deformation can arise. The values of Θ and Λ versus $A(r)$ must be plotted carefully because of the necessity of determining the derivative functions. In this way, continuous distribution of residual stresses may be obtained.

The necessary devices to perform the above procedure are strain gauges, micrometer and a tool to conduct layer removal. The more sensible choice for the layer removal tool is usually E.C.M. because of its stress free operation, usable for high strength materials, smooth finish and temperature control.

(b) Rosenthal and Norton method

This method uses similar equations to the Sachs method relating the stresses to the relaxed strains. It has been developed for flat rectangular bars where layers are removed from one face [Rosenthal et al., 1945]. However, the Rosenthal and Norton (RN) method is superior to Sachs method because it can measure more general stress states. The limitation of the method is that it can only measure residual stress state in a small element of material removed from the main body. The RN method is particularly suitable for thick welded plates. The details of the procedure are given by Leggatt et al. [1991] and shown in figure 2.11. The analysis assumes that the residual stress in the plate must be longitudinally invariant or symmetrical about the weld centre. If the blocks removed from the plate are narrow and long, it is assumed that stresses are completely relieved across their width and are linear along their length. In this case, it is assumed that simple beam theory can be applied. The calculation procedure is given in Leggatt et al. [1991]. The total residual stresses at depth z are given by :

$$\sigma_{xx,yy}(z) = \frac{S_{1x,y}(z) + S_{2x,y}(z) + S_{3x,y}(z) + \nu\left[S_{1y,x}(z) + S_{2y,x}(z) + S_{3y,x}(z)\right]}{1-\nu^2}. \quad (2.9)$$

where S_i are stress components in the blocks removed. $\tau_{xy}(z)$ can also be calculated from the same procedure and $\sigma_{zz}(z)$ is determined from the differential equations of equilibrium [Rosenthal et al., 1945].

The accuracy of the RN method has been found to be poor [Ueda et al., 1975]. Ueda et al. [1986, 1989] proposed a more complex method involving new parameters called 'inherent strains' to be able to predict the residual stress state in welded plates with a relatively good accuracy.

There are several problems associated with the RN method. The method does not provide local values of stress. Improving this however does disturb the assumption that the stresses are considered to be linear in the beam removed. The method also assumes constant value of $\sigma_{zz}(z)$. This assumption is not valid for thickness over

25mm. Therefore, the RN method may only be suitable for samples of simple geometric shape [De Angelis et al., 1990], i.e. without large section changes or curvature.

(c) Crack compliance method

The basic process of this method is to cut a thin slot of increasing depth into a specimen and measure released strain using strain gauges. The assumptions are that linear relaxation occurs on machining and there is no stress variation along the length of the slot. The calculation of stresses is done by mathematical model involving for example decomposition using a series of Legendre polynomials proposed by Cheng et al. [1986] or Schindler et al. [1994]. It is claimed that the analytical model is preferable to using Finite Element analysis since it involves simpler calculations. These calculations can be applied to different forms of geometry.

The main advantages of that method are that it is simple and quick to use. There is a relatively good accuracy particularly in measuring localised residual stresses. However, disadvantages include difficulty in determining the appropriate crack compliance if it is not known. In addition, analytical solutions can be complex.

2.4. Residual stresses in steel welds

2.4.1. Introduction

The origin, nature and distribution of residual stresses in welded components and different ways to measure them were presented in section 2.2 and 2.3. Some welded components will be subjected to different treatments during their lifetime, whether post weld heat treatment for residual stress relief or weld repair for extension of lifetime. Relevant literature on these treatments is presented in the following section.

2.4.2. As-welded

Here, an overview of typical residual stress distributions in multi-pass welds is given. Attention is focused mainly on development and distribution of residual stresses in stainless steel specimens.

An early model for the prediction of stress accumulation in steels during welding is given by Jones et al. [1977]. The effect of material deformation behaviour on stress buildup during continuous cooling is determined. The results for three different steels, 2CrMo, 9CrMo and AISI 316 steels were presented in the study. Jones resolved the previous uncertainties of residual stress predictions by taking into account the material transformation behaviour.

The model is developed around a restrained uniaxial specimen under cooling periods of simulated weld thermal cycles from a detailed knowledge of the mechanical properties and transformation behaviour. The specimen is subjected to thermal cycle by resistance heating and conduction cooling. Strain is measured through extensometry. The buildup of stress in restrained 2CrMo, 9CrMo and AISI 316 steels during the thermal cycle is shown in Figure 2.12. Initially, when the material is austenitic, it is weak and only a small tensile stress can develop in the specimen. This stress increases as the temperature decreases. During transformation, the expansion caused by the phase change more than counteracts the contraction resulting from cooling and produces a compressive stress. When the phase transformation is complete the tensile stress increases rapidly as the material cools down. This pattern is typical of that observed in ferritic steels. However, AISI 316 does not transform to a ferritic structure and therefore does not exhibit any off-loading during the thermal cycle but builds up stress continuously as cooling proceeds.

For the three materials studied, high tensile stresses develop only after transformation is complete (for 2CrMo and 9CrMo) and their magnitude is determined by the temperature interval between completion of transformation and preheat and by the strength of the weakest structure in the component. These observations imply that the absolute level of residual stress in a welded joint would be

reduced by material components of low strength, low transformation temperature or by welding with high preheat.

The approach by Jones only takes account of the phase transformation of the material for the residual stress generation during welding procedure. It is clear that the origin and distribution of these stresses may be due to many different factors. More recent work [Leggatt, 1997] presents a more detailed approach to the magnitudes and distributions of residual stresses that occur in common types of welded joints. Leggatt explains that the maximum tensile residual stresses are typically of yield strength magnitude in carbon manganese and stainless steels. The distribution of longitudinal (parallel to the weld) residual stresses are primarily a function of the maximum temperature reached at any point and transverse residual stresses mainly depend on the degree of restraint acting at the joint. The effects of weld repair and post weld heat treatment are also assessed by Leggatt. These aspects are presented later in more detail.

Leggatt [1997] shows that if the thermal contraction strain, $\alpha(T_s-T_0)$ is greater than the yield strain $\varepsilon_Y = \sigma_Y/E$, then yielding will occur during cooling and the maximum residual stress will typically be of yield magnitude. T_s and T_0 represent respectively the softening temperature above which the strength of the material is very low and the uniform temperature of the component after cooling. However, if the thermal contraction strain is less than the yield strain, then the maximum residual stresses will be no greater than $E\alpha(T_s-T_0)$. Table 2.1 gives illustrative values of contraction strain and yield strain for four materials. Leggatt also shows that the approach by Jones [1977] works only for a single pass weld since the stress distribution for a multipass weld reveals a saw-tooth stress distribution as shown in figure 2.13. The beneficial effect of preheat in low alloy steels only applies to the last bead since the stress magnitude of the previous beads depends on the other deposited beads with new temperature cycles [Hepworth, 1980].

Results of through-wall distribution of hoop, axial and radial stresses calculated by Josephson [1983] at the centre of a hoop weld are also shown and reported in figure 2.14. Other residual stress distributions are shown in figure 2.15 for a 32mm

thick butt-welded pipe and for a T-butt weld on tubular connection in Figure 2.16. These will be compared with results obtained during this research project and reported in chapters 5 and 6.

Faure et al. [1996] report measurements of residual stresses in austenitic stainless steel orbital TIG weld. Results are shown for thickness stress distributions measured using the centre-hole drilling and block removal, sectioning and layering (BRSL) techniques. The two techniques were calibrated with similar materials containing known stress fields. Through thickness stresses were obtained at the weld centre line of the specimen and surface stresses obtained at 0mm, 20mm and 40mm from the weld centre line. The orbital TIG weld was in a pipe 700mm long. The measured residual stress distributions are shown in Figure 2.17 to 2.19 respectively for surface distributions, weld centre line and 20mm away from the weld centre line (HAZ). As will be shown later very similar trends are observed compared with the results obtained in this project. The results will be compared directly to results presented in chapter 4 and 5. The residual stresses shown in figure 2.18 at the weld centre line revealed that the axial tensile stress at the outside face was 200MPa and changing to compression at 1/3 of the depth to a maximum value of -400MPa. For the hoop stress, the distribution is almost the same with the intensity changing from +200MPa to -300MPa.

Yen et al. [1994] present results from a study of residual stresses on weld overlay repair type 304 stainless steel pipe. This repair technique is mainly used for pipes suffering from Inter-Granular Stress Corrosion Cracking (IGSCC). It is desirable that the inner surface of the pipe is restrained so that a compressive residual stress state is created to prevent IGSCC. The residual stresses on the two faces of the weld overlay were measured using the hole-drilling strain gauge method. The specimen was a 267mm outside diameter pipe of 15mm thick and 152mm long. The overlay was 140mm long and 9mm thick. The experimental procedure used strain gauge rosettes mounted every 90° on the hoop axis of the weld, and on the inside and outside faces of the sample. No stress relief was used during welding repair. Residual stresses were measured at nine different depths using an incremental hole drilling technique. There is good agreement between experiment and finite element results for the axial residual

stress on the outside surface across the overlay. The tensile residual stress was about 300MPa to 350MPa in the middle part of the weld overlay. The distribution of residual stresses on the inside face was in compression between 0MPa and 200MPa.

Residual stress measurements were undertaken during the previous research project [Bonner, 1996] on thick butt-welded pipes as a validation for the deep-hole technique. Measurements were carried out on an 84mm thick cylindrical butt-weld of axial length 1520mm and 292mm bore shown in figure 2.20. The component was made of carbon steel and used a single-V edge preparation (figure 2.21) of 70mm width. Measurements were undertaken at two locations, respectively the weld centre line (say location A) and 24mm away from the weld centre line (say location B). Results are shown in figure 2.22 and 2.23. The results obtained in these two cases show the non-symetrical residual stress distribution on each side of the weld centre line. The maximum residual stress intensity reached in the hoop direction was obtained at location B since the last deposited bead was not at the weld centre line. Note also that the characteristic residual stress distribution obtained in most cases and presented in chapter 5 and 6 is similar to location B of the carbon steel pipe where the residual stress intensity is maximum.

Brust [1981] presented a finite element analysis study on a 40mm thick butt-welded austenitic pipe. A very similar trend was observed in this case with experimental and finite element results presented in chapter 5 and 6. The results are shown on figure 2.24 and 2.25. Note that a reasonably good comparison was also observed between experiment and finite element results shown in figures 2.24 and 2.25.

2.4.3. Post weld heat-treatment

Leggatt [1997] shows results produced by Josephson [1983] of the typical effect of PWHT on the residual stresses in a cylindrical butt-weld. Results are shown in figure 2.26. The maximum longitudinal (hoop) residual stresses were reduced from about 500MPa to 75MPa and the maximum transverse (axial) stresses from 250MPa to 50MPa. The shape of the relaxed residual stress distribution reflects the as-welded residual stress distribution. In addition, figure 2.27 shows the effect of PWHT time on

the variation of residual stresses. The results presented by Debiez and Granjon [1977] show that most of the residual stress relaxation occurs during the first 3 hours of the PWHT at 650°C (this correspond almost to the heating part of the process) and remain almost constant thereafter. There was a small increase of the residual stresses when the specimen was cooled down.

Fidler [1982] also examined the effect of time and temperature on residual stresses in austenitic welds. Surface residual stress measurements were undertaken using the surface hole drilling technique at various distances from the weld centre line before and after post weld heat treatment. The overall as-welded residual stresses were close to the yield stress at the weld centre line and decreasing rapidly further away from it. Residual stress distributions before and after one hour PWHT at various temperatures are shown in figure 2.28 and the effect of time of PWHT is shown in figure 2.29. Note the two following aspects: The intensity of residual stresses was of the order of 0.2% proof stress before and after PWHT for one hour and a PWHT longer than two hours did not significantly further decrease the residual stress intensity.

More recent work carried out by Spooner et al. [1994] presents the residual stress distributions before and after thermal stress relief in austenitic stainless steel plate. This study was undertaken in a half inch thick 304 stainless steel welded plate using gas tungsten arc welding (GTAW) process. The thermal stress relief consisted of heating the specimen to 1150°F (621°C), holding the temperature for one hour and air-cooling the specimen. Stresses were determined in the longitudinal, transverse and normal directions. It is noticeable that the stress intensity in the weld region was reduced to about 30% after PWHT. Stress distributions are shown in figure 2.30.

Bonner [1996] also presented some results on the influence of post weld heat treatment on a 85mm thick carbon steel butt-welded pipe. This is the same component as shown in figure 2.20 and was examined before and after PWHT. The results for the post weld heat treated condition are shown in figure 2.31. A significant residual stress relief was observed compared with results shown in figure 2.22. The location of the two measurements was at the weld centre line. Note that in the heat treated condition,

the low residual stresses on the edges were not relaxed but redistributed. Only the more tensile residual stresses towards the centre of the wall thickness decreased from about 200MPa to about 60MPa for the hoop stress and from 100MPa to 40MPa for the axial stress.

2.4.4. Weld repair

Residual stresses at repair welds are often more severe than those in planned construction welds because the restraint is usually higher. Hence the residual stresses at repair welds should always be taken into consideration of the integrity of a welded structure. In practice they are often overlooked, because their locations are not known at the design stage, and may not be recorded at the fabrication stage. Very little literature is available on measurement of residual stresses in steel repair welds. Leggatt [1997] presents measured through-wall distribution of residual stresses in a deep as-welded repair (28mm long) at the edge of a heat-treated butt-weld in 75mm thick C-Mn steel plate. Figure 2.32 shows the measured through-wall residual stress distributions where the intensity of the stress is highly tensile (between 400MPa and 500MPa for the hoop stress) over most of the repair depth. The intensity of the stresses decays rapidly once outside the weld repair. It is shown by Leggatt [1997] that the distribution of the repair residual stresses is not only due to the repair depth but also from the repair length and specimen thickness.

2.5. Concluding remarks

The available literature on welding in general, residual stresses and heat treatment is large. For this thesis the intention is to focus on aspects directly relevant to this research project and particularly on stainless steel welds. However, it was more difficult to find published literature, and consideration has been given to papers, which are concerned only with the study of residual stresses in stainless steel welded components mostly after 1990. The deep hole measurement technique has not been used widely in the reviewed papers and comparison between the results obtained in the current project and available results in the literature may not be very easy.

Nevertheless a number of concluding remarks based on the results reviewed can be made :

- The distribution of residual stresses in a weld is primarily dependent on the effect of restraint during the cooling process. Also, other aspects influence the residual stress distribution and intensity but to a lower extent.

- The maximum intensity of residual stresses in austenitic welds is of the order of the yield stress due to the maximum temperature reached at any point. The effect of preheat has not shown any significant effect in reducing the residual stress intensity.

- Residual stresses in welded pipe components with a 'V' weld preparation tend to have a distribution changing from tension on the outside surface of the weld to compression on the inside surface. It is important to generate compressive residual stresses at the inner surface since it usually prevents crack initiation in pressure vessels.

- In welded pipes, it is generally accepted that the hoop stress at the weld centre line is usually more important than the axial stress.

- Centre hole drilling techniques have shown a good correlation with other experimental techniques and are used widely where drilling a small hole into the surface of the component is not critical.

- The deep-hole technique is semi-destructive, since a hole has to be drilled through the specimen thickness so stress distributions can be determined through the wall. A good correlation was observed with other experimental techniques and numerical analysis to evaluate through thickness stress variations. This technique is of particular interest for component thickness greater than 20mm.

- Sachs boring technique can be used to measure residual stresses which are completely axisymmetric.

- Post weld heat treatment showed a big influence on the residual stress distributions. Stresses relief of up to 80% were presented, however, this very much depends on the time and temperature applied to the specimen. It is also observed that most of the residual stress relief occurs during heating up since the yield strength of the material decreases with increasing temperature.

- Only limited literature is available on residual stresses in stainless steel weld repairs. Where information is available the results show that repair stresses can be higher than as-welded stresses and should be taken into account in integrity assessment. However, more studies are necessary to assess their effects.

CHAPTER 3 : DEEP-HOLE TECHNIQUE

3.1. Introduction

This chapter presents the work carried out during the project on the assessment of the deep-hole technique. Two aspects of the work are presented: Description of the experimental setup and analysis. The sections presented on the calibration tests and finite element analysis related to the validation of the deep-hole technique will be presented in chapter 4. The description of the experimental setup contains technical aspects about the accuracy and reliability of the equipment. The analysis part looks at the influence of different parameters on the evaluation of residual stresses.

3.2. Summary and improvements to the method

3.2.1. Introduction

A full description of the basic technique can be found in Bonner (1996) and will not be repeated here. Only a brief description of the technique is given together with a number of aspects of the experimental technique. In particular the different steps used to carry out the residual stress measurements are described. The technique uses the following apparatus in the experimental setup: A table for specimen orientation and fixing a reference frame to support various devices such as a gun-drilling motor, an Electro Discharge Machining (EDM) system, and a Mercer air probe to carry out measurements. Finally, a data logging system is used to record information. The overall layouts are shown in Figures 3.1a and 3.1b.

The technique is divided into five different steps:

- Attach bushes on the front and back faces (when possible) of the specimen to act as reference (since they are stress free).
- Gun-drill a reference hole of 3.175mm diameter at the location of measurement, with the desired orientation through the specimen thickness.

- Measure the reference hole diameter at n angles around the hole and z_n points through the wall thickness. This provides a complete mapping of the reference hole after gun drilling.
- Trepan a core around and containing the reference hole as its axis and measure the change in height of the core during trepanning.
- Re-measure the reference hole diameter, at the same position as before trepanning, to obtain radial strain relaxation of the hole. The hole diameters are recorded through an air-electric transducer and converted into diameter distances.

Each step of the technique, shown in Figure 3.2 with relevant modifications is discussed in the following. An assessment of characteristics examined through the research project is also given.

3.2.2. Reference Bushes

At the start of the project, the attachment of the bushes onto the specimen was only to ensure that there was a reference point in the evaluation of residual stresses. It was found later, through calibration tests using known stress distributions, that using pins to fix the front bush to the specimen introduced a local stress concentration around the reference hole and influenced the evaluation of the residual stresses. A schematic of the bushes attached onto the specimen is shown in Figure 3.3a. Subsequently, the bushes were glued onto the specimen to overcome the stress concentration problem. Figure 3.3b shows a residual stress distribution using the pinned bushes on a steel bar. It is clear that the pins, which are inserted about 5mm into the specimen, generate an elastically balanced local residual stress field around the reference hole and prevent an accurate evaluation over a distance of about 20mm, which is four times longer than the pins.

Another aspect related to the use of bushes was the air probe sensitivity close to the edge of the specimen and the accuracy of measurements close to the specimen surface. Bushes are included on both sides of the specimen to provide a continuous hole from the specimen to the bush so that the airflow of the probe is constrained. A schematic of the attached bushes onto the specimen is shown in Figure 3.4. Pictures of the attached front bushes are shown in Figure 3.5. Calibration work undertaken on the

air probe sensitivity showed that there was excellent reliability up to a distance of about 0.2mm close to the edge of the specimen but bushes were still necessary for obtaining a stress free reference. The second requirement for the front bush (presented later) was for the start of the gun drilling process, and to ensure that initial "bell-mouthing" obtained during the start of drilling was contained in the front bush.

The newest configuration is shown in Figure 3.4 together with the fixture for air probe location using an automated device. A stepper motor controls the rotation of the air probe around the reference hole at n angles using a conical roller bearing. The number of angles n is currently 18. This device replaces a previous configuration where each angle around the reference hole was set manually through a pin inserted in a bush with holes at the specified angles (respectively 8 and 16). A picture of the original location bush is shown in Figure 3.6.

3.2.3. Gun drilling

The gun drilling is a very precise hole drilling process. It has been well defined in "The Gun-drilling Guidebook" and provides very accurate holes, which do not need any other secondary operation. Standard holes can have a straightness up to 0.1μm per millimetre depth, a hole diameter tolerance of ±15μm and a surface finish as low as 0.1μm. These figures are often quoted by the manufacturers and measured tolerances during this project will be presented later.

The drilling process needs the front bush to start and prevent a non-circular hole into the specimen. Once the process is started, the cutting forces are distributed in a balanced way around the hole such that the drill is kept along a straight line and produces a high standard surface finish. High-pressure coolant oil is used to counteract the cutting forces, support the tool, cool the cutting edges and expel dirt through the gun-drill flute. Figure 3.7a shows a schematic of the gun-drilling process. Figure 3.7b shows a picture of the head of the gun-drill.

One important quality of the hole generated by gun drilling is the accuracy of the surface roughness of the gun-drilled hole. Throughout this project, all measurements carried out in stainless steel specimens had an average surface roughness of about

15μm (experimentally observed). This was considered to be well below the measurement range of the air probe system, which is very accurate within about 50μm to 70μm of the calibration range. However, the surface roughness becomes more critical as the hole diameter becomes smaller since the air probe range of measurement decreases with the diameter of the air probe itself. In other words, the surface roughness of the drilled hole must improve (i.e. it must be smaller) with decreasing diameter. Some work was carried out during this project to measure the surface roughness of the reference hole. A comparative measurement was obtained using a tallysurf machine (which has a much higher reading accuracy than the air probe device) together with air probe readings of the surface of the hole. To obtain the surface roughness measurements using the tallysurf, an extracted core had to be cut along the axis of the reference hole. The comparative reading is shown in Figure 3.8 (the tallysurf readings are plotted only to follow the air probe scale).

It is difficult to compare directly the readings between air probe and tallysurf since the core has to be cut in two parts and aligned properly under the tallysurf reading machine. However, measurements were carried out over a distance of about 15mm and the comparison of readings is very good. The tallysurf machine takes 5 readings every micron and the air probe takes 5 readings every millimetre. The air probe only gives an approximation of the reference hole diameter variation. The surface area of measurement of the air probe (diameter of airflow) is probably too big to increase this accuracy. The air probe is not able to pick up sharp changes of diameter over a very small distance (less than 0.2mm). It is therefore very important for the purposes of measurement accuracy to obtain the best possible surface roughness. In the case of the butt-welded specimens measured during the period of this project, an average accuracy of 1μm in reading the reference hole diameter was achieved, which gives approximately an error band of about ±30MPa for a Young's modulus E=200GPa and Poisson's ratio of 0.3.

A possible way to improve the surface roughness of the hole was thought to be by honing. This was attempted and results did not show any improvement. The only modification observed in using this honing process was an average increase of the hole diameter. Figure 3.9 shows a picture of the flex hone used for this purpose.

Figure 3.10 shows the air probe readings for one hole using the flex hone. No direct evidence was observed that the surface roughness of the reference hole was improved, rather there was only increase of the average hole diameter.

3.2.4. Electro Discharge Machining

The Electro Discharge Machining (EDM) system was only installed part way through the project. Before this, an Electro Chemical Machining (ECM) process was used. The two separate systems are described thereafter. Both procedures are considered as a stress free operations.

Electro Chemical Machining

ECM is a process of metal removal in which electrolysis is used to dissolve workpiece metal. An ionic electrolyte in a dissolved or molten state is obtained by the passage of an electric current between conducting electrodes (the tubular cutting tool and the specimen). The electrolyte is pumped at a high pressure through the gap between the tool and the workpiece and the action of the current flowing through the electrolyte causes metallic particles at the workpiece surface to go into the solution. Figure 3.11 shows a schematic layout of the ECM system. A number of inherent problems arise from the ECM system; no change in core diameter was available from that system, since it was very difficult to control the extension of material removal. These problems are discussed in more detail later.

The remaining core of the specimen was approximately 11mm ±1mm diameter. The hole left in the specimen was about 30mm diameter. The widths of the welds in various specimens (discussed later) were between 20mm and 50mm. The trepanned core would be partly in the weld metal and partly in the parent metal, which influenced the evaluation of residual stresses, particularly in the heat affected zone (HAZ) of the weld. Figure 3.12 shows a schematic of the core extracted from a specimen using the ECM system and Figure 3.13 show pictures of several extracted cores. The stop-start nature of the ECM system often led to highly variable core diameters.

Electro Discharge Machining

Electrical-discharge machining (EDM), or spark machining, is also a process of metal removal with repetitive spark discharges from a pulsating DC power supply, with a dielectric flowing between the workpiece and the tool. The tool is mounted on the chuck attached to the machine spindle whose motion is controlled by a servo-controlled feed drive. The tool and workpiece are connected to a DC power supply. Dielectric is circulated under pressure by a pump in the tool electrode. The servomotor maintains a spark gap between 0.025 and 0.05mm. Each spark generates a localised high temperature of the order of 12000°C in its immediate vicinity. This heat causes part of the surrounding dielectric fluid to evaporate and melts and vaporises to form a small crater on the work surface. The metal globules formed during this operation are carried away by the coolant fluid. As the process progresses, the electrode is advanced by the servo-drive towards the workpiece to maintain a constant gap distance until the final cavity is produced. The motor must be reversible because if the servomechanism overshoots as a result of accumulation of swarf in the gap, the tool must be withdrawn. Changing the settings of the variable resistance may vary the exact value of gap distance.

Figure 3.14a shows a schematic layout of the EDM system and Figure 3.14b shows a schematic of the geometry of the core extracted using the EDM process. Compared to the geometry of the core in the ECM system, the quantity of material removed is much lower and changing the dimensions of the electrode can change the core diameter. Figure 3.15 shows a picture of extracted cores using EDM with 20mm and 10mm diameter electrodes.

Two main improvements in the EDM system were made. The quantity of metal removed from the specimen was much lower, and the diameter of the core was increased from 11mm to 20mm and the hole left in the specimen decreased from 30mm to 23mm. The second important point was that the core diameter could be changed by changing the size of the electrode.

The diameter of the trepanned core, in comparison with the ECM system, was increased to be outside the stress concentration zone generated by the 3.175mm diameter reference hole. Although it is not clear what is the volume fraction of the

core over which the residual stresses are measured, the analysis assumes that the stress distribution across the core is constant. It was then decided to decrease the diameter of the core to explore the influence of core diameter. However, there is a maximum diameter where the relaxation of residual stresses will start to decrease and this should be considered. On the other hand, as will be presented later, even if the relaxed strains are within the stress concentration zone, which could bring about plastic deformation, the evaluation of residual stresses would not be very much affected as long as the plastic deformation does not exceed 60% of the yield stress. This will be explained in more detail later in chapter 4.

Some recent work was carried out using a 10mm diameter core and a 3.175mm diameter hole. Experimental results were found to be in accordance with other measurement techniques and finite element analysis.

3.2.5. Capacitance gauge measurements

One of the main assumptions in the deep-hole method is that the axis, z, of the gun drilled reference hole is a principal axis of stress and that the through-thickness stress σ_z is zero. This means that the conventional plane stress analysis by Bonner et al in the *(x, y)* plane is correct. However, if this is not the case (for example in a shrink fit cylinder, or perpendicular cross-weld, or quenched balls, or centre of ring welds), the measured residual stresses in the *(x, y)* plane are not representative of the correct stress state within the specimen. The deformation of the trepanned core can be simple expansion/contraction or a combination with shear in the x and/or y directions (Figure 3.16). For this reason, a system was designed to measure through thickness changes in core height. It is important to note that the shape of specimens measured during this project does not enable this measurement to be made easily. Experimental tests were carried out to assess the reliability of the capacitance gauge design.

Figure 3.17 shows the layout of the capacitance gauge arrangement and Figure 3.18 shows a picture of the arrangement in situ. The working process of the device is as follows. A ceramic rod of diameter smaller than the reference hole is introduced. The capacitance gauge head is then fixed on the rod at the back face of the specimen. The calibration distance d_c between the capacitance head and the back face of the

specimen is provided by a micro-thread screw on the outside of the front bush and an elastic spring between the rod's head and the front bush. When the trepanned core expands or contracts, the distance d_c varies the same amount and this variation is recorded. Four capacitance gauges were designed so that variations can be recorded in both the x and y directions.

A calibration test was carried out to assess the displacement accuracy of the capacitance gauge device. Figure 3.19 shows the schematic layout of the test carried out. The test consisted of simple displacement measurement of a tensile test specimen. The material characteristics were known so that the displacements of the specimen were directly related to strains and stresses through Young's modulus and specimen geometry. The displacement was measured both by the test machine and capacitance gauges. The calculated Young's modulus from the test results was the same as the expected value of 200GPa. Results are shown in Figure 3.20. From this test, it was shown that the measurement device worked well but results are more difficult to interpret on the real welded specimens. Since most measured specimens during the project were butt-welded pipes, the radial component of stress was always found to be small, therefore difficult to measure. Another factor was that the EDM process generated heat during cutting, which made the core expand and since this was a transient effect, it is very difficult to assess its influence on the capacitance readings. Usually, only an average of the radial displacement was obtained. A possible way to assess the influence of heat generation is to simulate the EDM process using a finite element analysis and to determine the relation between core expansion and heat input. This is being examined in a new research project.

Two experimental measurements were nonetheless important in the assessment of the capacitance gauge system. These were a 65mm thick nozzle component and a 110mm thick butt-welded end cap to cylinder stainless steel specimens (presented in chapters 5 and 6). The results for these are discussed later in the thesis.

3.2.6. Air probe measurements

Measurement of the reference hole diameter is performed using a MERCER air probe of diameter slightly smaller than the gun drilled hole. An air-electric transducer

converts the air pressure variation into an electric signal displayed by a digital meter. An air compressor provides a constant air pressure through the air probe device. The schematic layout of the system is shown in Figure 3.21.

Figure 3.22 shows a picture of the head of the air probe device and Figure 3.23 shows the rig used to hold the air probe and perform the measurements. Compressed air flows to atmosphere via the air probe resulting in a pressure variation depending on the size of the hole diameter. The air probe consists of a thin hollow tube capped at one end with two small diametrically opposite holes. In the absence of any surface near the holes, the pressure is at a minimum and when the probe is passed down the hole, the air jet pressure increases. The pressure depends on the range and linearity of the air electric-transducer, air probe calibration, precision of angle measured and depth of measurement for the calculation procedure and axis location of the air probe inside the hole. In order to assess the accuracy and reliability of the air probe system, different tests were carried out. The surface area of each hole in the air probe head is of the order of 0.7mm^2 and the squared area of measurement around each hole on the air probe head of about 3mm^2. The probe head diameter is of 3.16mm. The air probe is driven via a micrometric screw thread, which allows accurate reading of the measurement depth.

Figure 3.24 shows a typical calibration curve for the air probe system and figure 3.25 shows a schematic response of the air probe reading with distance. To read accurately the reference hole diameter, it is necessary to calibrate the air probe using known diameter calibration rings. These are set onto the air probe head before test measurement. It is assumed that the range and linearity reading of the air electric transducer are accurate so that variations in the readings are only due to the air probe device. There is a good linear response in a small range of diameter variation close to the probe. When the reference hole diameter increases to larger values, the response of the air probe becomes less accurate although calibration is still possible. Since the point measurement is made over a small square area and airflow is diverging, the accuracy of measurement decreases and depends on the surface roughness of the reference hole. A linear response of the air probe was found to be within a hole diameter variation of approximately 50μm larger than the 3.175mm reference hole diameter.

The repeatability of identical measurement is critical since it is directly related to the intensity of measured residual stresses. Effectively, in this project, with 200GPa for Young's modulus, changes in diameter of 1μm gives rise to a variation of stress of 30MPa (compared to a 3.175mm diameter reference hole). Figure 3.26 shows diameter measurement repeated at the same location. This shows good accuracy of the air probe reading but also shows a possible potential error in the stress evaluation. The small variations between the two readings (because of average reading) cannot decrease the system sensitivity. This could only be done by decreasing the surface area of reading.

Another point in the accuracy of the air probe is the area over which the air probe takes a reading (approximately $3mm^2$). This gives an average value of the diameter over this area. However, since the measurements were taken every 0.2mm along the axis of the reference hole and the surface roughness of the hole does not allow residual stress evaluation over such short distances, the variation of surface roughness over this distance did not modify the evaluated results. However, the evaluation of the residual stresses with a sharp stress gradient was problematic and will be discussed later.

An evaluation of the possible errors concerning air probe measurements was carried out. A summary of the different conditions used and results for 95% confidence interval are shown in Table 3.1. The air probe calibration was tested for different combination of parameters related to the choice of scale and calibration rings. The scale was used in either μinch or μm and calibration rings were tested as a function of position on the measurement device. It appeared from the different tests carried out that the best calibration procedure (see table 3.1) was obtained when the global error is 1.028μm with 95% confidence interval. It was also shown that the air probe readings were not dependent on time or temperature.

The air probe is driven accurately through the specimen thickness via an accurate screw thread controlled through a stepper motor. This enables removal of the distance interpolation necessary before this device on the standard screw thread. An average accuracy of the new screw thread is about 0.01mm for a step reading of 0.2mm. This

means that diameters are read more accurately at a depth in the reference hole minimising the errors on stress evaluation through diameter reading. Second, the new rig rotates the probes at accurate angles around the reference hole also via a stepper motor. The stepper motor is able to rotate the air probe each 0.2° angle, which can provide as many angles necessary to obtain an accurate fit through the experimental data. This is particularly useful when a random stress distribution is present around the reference hole. Note that this cannot be achieved with the present analysis since it evaluates only stress in two main directions (x, y).

The microthread screw to drive the air probe through the reference hole was implemented during this project and enabled more accurate readings of the position along the reference hole so that the same measured point will be corresponding between before and after the EDM process. Since the surface roughness of the reference hole is of the order of 15μm, it was evident that obtaining a diameter at a peak or in a trough would give rise to significant stress variation. This is illustrated in Figure 3.27, where the effect of incorrect measurement of location in the reference hole gives rise to large errors in strain.

One concern in using the air probe system was the ability of the system to evaluate accurately residual stresses near the entry and exit face of the specimen. This problem becomes more important as the specimen thickness decreases below 20mm or 15mm since the air probe area of measurement is of the order of 3mm². The problem arises when the pressurised air flowing out of the probe moves from in the hole to the edge of the hole. A test specimen was gun-drilled and air-probe measurements undertaken through the specimen thickness. Then, the test specimen surface was ground accurately and air-probe measurements carried out again. The comparison between the two readings is shown in Figure 3.28. It can be observed that the accuracy of the near entry reading is of the order of 0.5mm for the non-ground test and of the order of 0.1mm for the ground test.

Although many parameters seem to influence the accuracy of the air probe measurement (Rouvenot and Wotling, 1997), the important aspect that enables reliable results to be obtained is that measurements are carried out between before and

after the EDM process. Indeed, since a difference is measured, the error in the two readings is similar, consequently the errors are eliminated and only the strain relaxation is measured.

3.3. Developments in Analysis

3.3.1. Introduction

The analysis to evaluate residual stresses in the deep-hole technique assumes a geometrically simple case. A careful assessment of the analysis is necessary if more complex cases need be carried out. A brief description of the analysis will be given together with the corresponding assumptions. Later, in this section, further aspects related to the analysis are examined.

In applying an analysis to convert measured strains to stresses, the following lemma is used to overcome the difficulty concerning the equivalence of an imposed stress field and prescribed displacement state (Bonner, 1996):

"*In general, the imposition of a stress system, S, on a region of material, R, resulting in elastic behaviour in that material, will produce the same stress field in a bounded sub-region of R, say R', as does the imposition of the same displacements on the boundary of R' as were caused by the system S*".

This lemma forms an important part of some of the theoretical derivations, which are used in the theory. This is described in more detail in Bonner (1996).

The analysis is developed by assuming that the specimen thickness is divided into a number of blocklengths or plates. Each blocklength is bounded by two imaginary parallel planes, which are normal to the reference hole axis. The main assumptions of the analysis are as follows:

- The gun drilled reference hole is a principal stress direction
- At each point measured through the specimen thickness, a 2D plane stress analysis is carried out.

- Each measurement in the thickness direction is independent from each other (see figure 3.29).
- The relaxed strains in the core occur elastically after the EDM process.
- The material properties of the specimen are isotropic.

The theoretical analysis provides a solution for three components of the stress tensor σ_{xx}, σ_{yy} and σ_{xy}, as a function of the strain ε_θ measured around the reference hole at n angles assuming that z is the reference hole axis. It will be shown later that the number of angles in the analysis influences the results, and account can be taken of the strain ε_{zz} along the axis of the hole.

The radial displacements at the hole edge, u_r, are measured as a function of angle, θ, of the reference hole, (of diameter, d_o), and through-thickness position, z. The change in thickness is measured also when residual stress is released as a result of trepanning. The relaxed normalised displacements, $2u_r/d_o$ are therefore related to the residual stresses, σ_{xx}, σ_{yy}, σ_{xy}, where:

$$\left.\begin{aligned} \varepsilon_\theta[\theta,z].E = E\frac{2u_r}{d_0} &= -\left\{\sigma_{xx}.f[\theta,z]+\sigma_{yy}.g[\theta,z]+\tau_{xy}.h[\theta,z]-\upsilon.\sigma_{zz}\right\} \\ E.\varepsilon_{zz} &= -\sigma_{zz}-\nu\left(\sigma_{xx}+\sigma_{yy}\right) \end{aligned}\right\} \quad (3.1)$$

The functions $f[\theta,z]$, $g[\theta,z]$, and $h[\theta,z]$ are given by

$$\left.\begin{aligned} f[\theta,z] &= A[z].\{1+B[z].2\cos(2\theta) \\ g[\theta,z] &= A[z].\{1-B[z].2\cos(2\theta) \\ h[\theta,z] &= 4.A[z].\{B[z].\sin(2\theta) \end{aligned}\right\} \quad (3.2)$$

The parameter $A[z]$ and $B[z]$ represent uniform expansion and eccentricity of the hole, respectively.

At a given through thickness position, z_1, a minimum of four strains including ε_{zz} must be measured to obtain the residual stresses. For example $\varepsilon_\theta[\theta,z_1]$ at $\theta = 0°$, 45° and 90° and also ε_{zz}.

Alternatively, as proposed by Bonner (1996), and Bonner and Smith (1996), if measurements are obtained at n angles a least squares fit to the diametral strains can be used to determine the stresses. For a given through thickness position z_1 the stress equation (1) is rewritten in matrix form as:

$$\bar{\varepsilon} = -[M].\bar{\sigma} \tag{3.3}$$

where the strain and stress vectors are

$$\bar{\varepsilon} = [\, \varepsilon_\theta[\theta_1,z_1],\ \varepsilon_\theta[\theta_2,z_1],\ \ldots,\ \varepsilon_\theta[\theta_n,z_1],\ \varepsilon_{zz}\,]^T$$

$$\bar{\sigma} = [\, \sigma_{xx},\ \sigma_{yy},\ \sigma_{xy},\ \sigma_{zz}\,]^T \tag{3.4}$$

The compliance matrix M is given by

$$[M] = \begin{bmatrix} f[\theta_1,z_1] & g[\theta_1,z_1] & h[\theta_1,z_1] & -\upsilon \\ f[\theta_2,z_1] & g[\theta_2,z_1] & h[\theta_2,z_1] & -\upsilon \\ \cdot & \cdot & \cdot & \cdot \\ \cdot & \cdot & \cdot & \cdot \\ f[\theta_n,z_1] & g[\theta_n,z_1] & h[\theta_n,z_1] & -\upsilon \\ -\upsilon & -\upsilon & 0 & 1 \end{bmatrix} \tag{3.5}$$

The optimum residual stress can be obtained by using Pseudo-Inverse or Moore-Penrose inverse matrix with:

$$\bar{\sigma} = -[M]^*.\bar{\varepsilon} \tag{3.6}$$

where $[M]^* = (M^T.M)^{-1}.M^T$ is the Pseudo-Inverse of the matrix $[M]$ and $\bar{\sigma}$ is the optimum stress vector $[\sigma_{xx},\ \sigma_{yy},\ \sigma_{xy},\ \sigma_{zz}]^T$ that best fits the measured strains ε.

Elastic finite element (FE) analyses were carried out by Garcia Granada et al (1998) to determine the coefficients A and B as a function of depth z for different

thickness $2t$. These analyses revealed that the hole distortion was a function of depth z. The diametral distortions given by equations 1 and 2 were such that A was approximately 1 for all z and B varied with depth. For a 20mm plate, B varies from 0.98 to about 0.86. For a 100mm plate B varies from 0.94 to about 0.85. For a thin plate it was found that near surface effects were evident completely through the thickness. For thicker plates (2t > 70mm) B eventually becomes a constant value at a sufficient depth. The evaluation of the through thickness strain ε_{zz} is described in section 3.3.3.

3.3.2. Influence of number of angles measured

If the assumption made that the 2D plane stress analysis is correct, three components of stress are evaluated, respectively σ_{xx}, σ_{yy} and σ_{xy}. This is shown in Figure 3.30. In theory, if only three stresses are to be evaluated, there are only three angles to be measured. However, this provides only limited information regarding the intensity of the residual stresses and their distribution around the reference hole as a function of angle. Since only the two main stresses are evaluated in the two directions x and y, there is uncertainty regarding the principal stress direction and their projections on the two axes. This will be discussed in more detail later. However, increasing the number of angles around the reference hole increases the accuracy of the fit through the strain data as a function of angle. This eventually provides information about second order stress distributions at other angles than 0° and 90°.

Figure 3.31 shows a fit through the strain data as a function of angle for three and sixteen angles respectively. Experimental data were taken from one of the specimens measured during the project. This measurement was carried out using a 16 angle analysis respectively from 0° to 168.75° each 11.25° and fitted strains were also taken using only 0°, 45° and 90°. Figure 3.31c shows a comparison between the two fits. It is clear that good fits are obtained through the experimental results using three angles since there are only three points, however, there is a complete lack of information about the global deformation of the hole using the other angles. This is very clear for the fit with 16 angles, which also shows that more accurate results are obtained.

Another point concerning the accuracy of measurements is the reliability of the results. If one measurement is incorrect for the three angle analysis, this strongly influences the evaluation of residual stresses. For this reason, there is more scatter in the stress evaluation using only 3 angles. However, if 16 angles are used and one measurement is incorrect, this does not influence the results significantly.

3.3.3. Evaluation of stresses in the third direction

Initial work in this project assumed a 2D plane stress analysis for converting strains to stresses. The stresses were evaluated in the *(x, y)* plane and assumed that $\sigma_z = 0$. However $\varepsilon_z \neq 0$. In this case, only specimens having a small stress intensity in the *z* direction or being thin will be suitable for this analysis.

A new measurement system was developed to measure the relaxed strain in the *z* direction (the axis of the reference hole). This is the capacitance gauge system presented in section 3.2.5. The system measured strain relaxation during EDM process. However, the EDM process generates heat during trepanning and therefore increases the specimen dimensions at the same time. This is in addition to the mechanical strain deformation caused by residual strain relaxation during trepanning. Figure 3.32 shows an example of the capacitance gauge reading during trepanning process of a 65mm thick stainless steel specimen. This was shown to be the influence of heating from the EDM electrode added to the Poisson's effect from the σ_x and σ_y stresses.

Calibration tests were carried out to measure the temperature distributions through the wall thickness during EDM. These tests were undertaken on stress free blocks shown in figure 3.33. Several blocks of thickness between 10mm and 60mm were used. A hole of 3,175mm diameter was drilled through the specimen thickness and the capacitance gauge system fixed on it. Then the trepanning operation is undertaken to record the thermal expansion of the specimen. Due to different thickness, the transient heat effect in each specimen is recorded via thermocouples on each the front and back face of the specimen. An example of the recorded temperature at each surface is shown on figure 3.34. The core elongation during trepanning can then be plotted versus the elevation of temperature on the surface. This provides a

direct temperature/elongation variation, which can be extracted from capacitance readings on welded specimens.

In figure 3.35, the results show a good correlation with the coefficient of thermal expansion of the specimen. However, the heat generated depends very much on the heat input of the EDM electrode. Also, the temperature distribution depends on the transient heat transfer during the trepanning process since the electrode moves through the specimen. This effect could be evaluated through finite element analysis. The heat transferred through the specimen depends on its size and geometry and measured temperatures at the outside faces may correlate between calibration tests and welded specimens.

If it is assumed that at a given trepan depth there is a constant heat distribution through the wall thickness, it is possible to evaluate the global core expansion since temperatures are measured on both faces of the specimen. The thermal strain is obtained by dividing the core extension for a length increment by the trepanning depth. Since a cumulative displacement curve is obtained from the capacitance gauges during trepanning, the strain is obtained by taking the derivative of this displacement curve. Further details of using this method are described in chapter 5.

3.3.4. Fourier analysis

In the evaluation of residual stresses in a butt-welded pipe where the weld is around the pipe circumference, geometric constraint ensures that the principal stress directions are generally in the hoop (or longitudinal) and axial (or transverse) directions relative to the weld main axis. Therefore, if an assumption is made that experimental measurement evaluates stresses at one point and in two directions, namely σ_x and σ_y at 0° and 90° (in the transverse and longitudinal directions), then the analysis will provide the principal stresses directly. However, if an assumption is made that the principal stress direction are not known, for example this could be at 45° from the two axis 0° and 90°, then the analysis will provide only a projection of these stresses on the two axis x and y at 0° and 90°.

It is possible to provide measurements of more complex residual stress distributions. Assuming a Fourier distribution of the strains allows the stresses as a function of angle around the reference hole to be evaluated. For a better understanding of the distribution, the number of measured angles is important and using 16 angles (currently) each at 11.25° provides sufficient information for a Fourier analysis.

The Fourier analysis was developed mainly to provide a fuller description of the residual stresses irrespective of the orientation. However, as will be shown later only the first order coefficients of the Fourier series are developed to make a direct comparison with the current deep-hole analysis. The higher order coefficients will need to be developed so that more complex stress distributions as a function of angle around the reference hole can be evaluated. The main features of the Fourier analysis are presented here and more extensive details are given in appendix 3a.

If the assumption is made of an existing random stress distribution as a function of angle around the reference hole, this distribution can be approximated by using a Fourier series of the general form :

$$\sigma = \sum_{i=0}^{n} \sigma_i \cdot \cos(i\theta) + \sum_{j=0}^{n} \sigma_j \cdot \sin(j\theta) \qquad (3.7)$$

with :

$i = 0,\ j = 0 \quad \rightarrow \quad 0 + \sigma_0$

$i = 1,\ j = 1 \quad \rightarrow \quad \sigma^{c1}\cos(\theta) + \sigma^{s1}\sin(\theta)$

$i = 2,\ j = 2 \quad \rightarrow \quad \sigma^{c2}\cos(2\theta) + \sigma^{s2}\sin(2\theta)$

$i = 3,\ j = 3 \quad \rightarrow \quad \sigma^{c3}\cos(3\theta) + \sigma^{s3}\sin(3\theta)$

$i = 4,\ j = 4 \quad \rightarrow \quad \sigma^{c4}\cos(4\theta) + \sigma^{s4}\sin(4\theta)$

etc ...

Equation (3.7) then becomes :

$$\sigma = \sigma_0 + \sigma^{c1}\cos(\theta) + \sigma^{s1}\sin(\theta) + \sigma^{c2}\cos(2\theta) + \sigma^{s2}\sin(2\theta) + \sigma^{c3}\cos(3\theta) + \sigma^{s3}\sin(3\theta) + \sigma^{c4}\cos(4\theta) + \sigma^{s4}\sin(4\theta) + \ldots \qquad (3.8)$$

Since the air probe experimental device is only able to measure a diameter and not a radius, the only terms that can be evaluated in equation (3.8) are the following :

$$\begin{aligned}\sigma = \sigma_0 + \sigma^{c2}\cos(2\theta) + \sigma^{s2}\sin(2\theta) + \sigma^{c4}\cos(4\theta) + \sigma^{s4}\sin(4\theta) \\ + \sigma^{c6}\cos(6\theta) + \sigma^{s6}\sin(6\theta) + \sigma^{c8}\cos(8\theta) + \sigma^{s8}\sin(8\theta) + ...\end{aligned} \tag{3.9}$$

This Fourier development can be written for both the radial and hoop directions relative to the reference hole radius. This becomes :

$$\begin{aligned}\sigma_{rr}(r,\theta) &= \sigma_{rr0} + \sigma_{rr}^{c2}\cos(2\theta) + \sigma_{rr}^{s2}\sin(2\theta) + \sigma_{rr}^{c4}\cos(4\theta) + \sigma_{rr}^{s4}\sin(4\theta) + ... \\ \sigma_{\theta\theta}(r,\theta) &= \sigma_{\theta\theta 0} + \sigma_{\theta\theta}^{c2}\cos(2\theta) + \sigma_{\theta\theta}^{s2}\sin(2\theta) + \sigma_{\theta\theta}^{c4}\cos(4\theta) + \sigma_{\theta\theta}^{s4}\sin(4\theta) + ...\end{aligned} \tag{3.10}$$

The equations of equilibrium in a body are:

$$\left.\begin{aligned}\frac{\partial\sigma_r}{\partial r} + \frac{1}{r}\frac{\partial\sigma_{r\theta}}{\partial\theta} + \frac{\sigma_r - \sigma_\theta}{r} + R = 0 \\ \frac{1}{r}\frac{\partial\sigma_\theta}{\partial\theta} + \frac{\partial\sigma_{r\theta}}{\partial r} + \frac{2\sigma_{r\theta}}{r} + S = 0\end{aligned}\right\} \tag{3.11}$$

If the body forces (R, S) equal zero, then equation (3.11) becomes:

$$\left.\begin{aligned}\sigma_r = \frac{1}{r}\frac{\partial\Phi}{\partial r} + \frac{1}{r^2}\frac{\partial^2\Phi}{\partial\theta^2} \\ \sigma_\theta = \frac{\partial^2\Phi}{\partial r^2} \\ \sigma_{r\theta} = \frac{1}{r^2}\frac{\partial\Phi}{\partial\theta} - \frac{1}{r}\frac{\partial^2\Phi}{\partial r\partial\theta} = -\frac{\partial}{\partial r}\left(\frac{1}{r}\frac{\partial\Phi}{\partial\theta}\right)\end{aligned}\right\} \tag{3.12}$$

with Φ is the stress function that fits the boundary conditions of the problem. The stress function Φ is a complex form of constant and n^{th} order terms of *sinus* and

cosinus components used to solve each part of the unknown stress distribution. The 2D plane stress analysis is simulated by an infinite plate with a small hole in the middle and applied stress on the outer boundary. This case is exactly solved by Timoshenko et al. (1951). The two cases (constant and cos(2θ)) are obtained by solving the compatibility equation in polar coordinates. The radial and hoop stresses are :

$$\left.\begin{aligned}\sigma_r &= \frac{p_e.b^2}{b^2-a^2}\left(\frac{a^2}{r^2}-1\right)\\ \sigma_\theta &= -\frac{p_e.b^2}{b^2-a^2}\left(\frac{a^2}{r^2}-1\right)\end{aligned}\right\} \qquad (3.13)$$

This is the constant term of the Fourier analysis, which will be added to the next term in cos(2θ). This second term can be written by using the second order term of the stress function and developing a similar analysis as :

$$\left.\begin{aligned}\sigma_r &= \frac{S}{2}\left(1+\frac{3a^4}{r^4}-\frac{4a^2}{r^2}\right)\cos(2\theta)\\ \sigma_\theta &= -\frac{S}{2}\left(1+\frac{3a^4}{r^4}\right)\cos(2\theta)\\ \sigma_{r\theta} &= -\frac{S}{2}\left(1-\frac{3a^4}{r^4}+\frac{2a^2}{r^2}\right)\sin(2\theta)\end{aligned}\right\} \qquad (3.14)$$

Finally, the addition of the two calculated terms provides the evaluation of residual stresses at any angle around the reference hole.

$$\left.\begin{aligned}\sigma_{rr}(r,\theta) &= \sigma_{rr0} + \sigma_{rr}^{c2}\cos(2\theta)\\ \sigma_{\theta\theta}(r,\theta) &= \sigma_{\theta\theta 0} + \sigma_{\theta\theta}^{c2}\cos(2\theta)\\ \sigma_{r\theta}(r,\theta) &= 0 + \sigma_{r\theta}^{c2}\sin(2\theta)\end{aligned}\right\} \qquad (3.15)$$

The boundary conditions used to solve the problem are the measured hoop strain at the hole edge and zero radial stress at the hole edge and border of the plate. The evaluation of the higher order terms of the Fourier analysis is mainly defined by developing the corresponding boundary conditions for cos(nθ) terms.

The application of the Fourier analysis using the first two terms was carried out using experimental results from butt-welded specimens described later in chapter 5.

3.3.5. Influence of anisotropic elastic properties

It is expected that in welding, particularly for stainless steel, large grains be obtained. The earlier analysis assumes isotropic elastic properties. Here an analysis is presented that considers elastic anisotropy.

Analysis of the experimental results from the butt-welded samples assumed that the weld had isotropic elastic properties. However, it is well known that there is anisotropy of weld metal elastic properties. Therefore an evaluation of the elastic constants of the anisotropic weld metal could be estimated assuming that there is transverse isotropy. The 'bulk' elastic constants from single crystal elastic constants for transverse isotropic materials can be developed from anisotropic elastic theory developed by Kröner [1958, 1967]. He presented a model where evaluation of the bulk moduli are obtained from the main single crystal constants c_{11}, c_{12} and c_{44}. This is described in detail in appendix 3b.

The largest difference between the bulk modulus and the single crystal elastic modulus was evaluated to be the ratio between E_{bulk} and the largest bulk elastic constant C_{22} (or C_{33}). This ratio is:

$$\frac{E_{bulk}}{C_{22}} = \frac{250}{198.2} = 1.26 \quad \Rightarrow \quad 26\%$$

Assuming single crystal behaviour of the relaxed strains, there would, therefore, be a corresponding increase in the measured residual stresses of 26%.

3.4. Concluding remarks

The deep-hole method was presented in this chapter and developments in improving the reliability of the technique were given. The main aspects in the developments were:

In the experiments, it was shown that front bushes were necessary since this is the only part without residual stresses and must act as a reference and a location for initiation of gun drilling. However, the pins used to locate the front bush were removed since they introduced a localised stress concentration around the reference hole. Glued bushes are used instead.

The gun drilling process results in surface roughness, which appears to be an important aspect since a difference of 1μm in the measurements represents an error of about ±30MPa in the residual stresses. The variation in diameter from the gun drilling process is of the order of 15μm, and is well within the air probe sensitivity. However, for a smaller air probe, this range has to be decreased since the air probe sensitivity decreases with diameter.

The ECM system was replaced by an EDM system. This allowed changes in core diameter to be made, resulting in a lower quantity of material removal and automation of the process.

A capacitance device was developed to measure displacements along the axis of the reference hole during trepanning. The main difficulty using this device was that heat generated during trepanning could not be evaluated accurately.

The air probe system is currently the most appropriate device to measure the reference hole diameter although some limitations in its use near the reference hole entry and exit points. The system was assessed and developed in several ways during the research project. A more accurate driving system was introduced, and included a micrometric screw thread to increase accuracy in locating the air probe down the reference hole, increased measured number of angles and an automated drive via a stepper motor. Calibration tests were carried out. The average repeatability of the

device was found to be about 1μm, which for residual stress measurements in steel represents an error of about ±30MPa.

For the analysis of the measured strains it was assumed that the axis of the reference hole is a principal stress direction and that the through thickness radial stress is small or negligible (in a butt-welded pipe) and a 2D plane stress analysis can be carried out. The main drawback of the analysis is its difficulty to resolve sharp stress gradients due to a large core diameter or by assuming that each measured point in depth is independent to carry out the analysis. It was shown that the number of angles was important for providing good results.

A conventional 2D analysis is adequate as long as the two main direction of stresses are known (x, y). However, if this is not known, it is not possible to evaluate the stress distribution as a function of angle with the current analysis. A Fourier analysis was developed for this purpose and provides residual stress information at any measured angle around the reference hole.

Finally the influence of anisotropic elastic properties was considered for a stainless steel weld.

CHAPTER 4 : EVALUATION OF DEEP-HOLE METHOD

4.1. Introduction

This chapter presents experimental calibration tests carried out to assess the reliability, accuracy and limitations of the current deep-hole technique to evaluate stresses. The aim of the calibration tests was to present an assessment of the accuracy of the deep-hole technique in evaluating stresses and compare these with known stress distributions. Note that these tests were not carried out using trepanning to release an existing residual stress field but to measure the hole distortions under an applied external load.

Simple calibration tests using hydrostatic pressure, bending and torsion specimens were undertaken. Since the stress distribution is known exactly in these cases, it is possible to make comparisons with theoretical stress distributions. The hydrostatic tests consisted of applying external pressure on a cylindrical tube and measuring the hole distortion with the air probe system. Air pressure was applied in a cylindrical pressure vessel. The bending tests consisted in applying a point load at the end of a cantilever beam and measuring the deformations of reference holes drilled through the beam thickness and depth. In the torsion test, the same cantilever beam was used but a torque was applied at the end of the beam instead of a point load. This generated shear stress in the beam, measured at the reference hole edge in the same way as the bending test. The measured stresses were compared with strain gauge readings and simple theoretical strength of material analysis. Also, measurements were carried out in an autofrettaged tube and the measured stress distributions compared with a numerical simulation undertaken on a 3D finite element model.

Finally, finite element analyses were carried out to explore the influence of the hole distortions associated with localised plasticity due to stress concentration. It is shown that these effects have little influence on the 2D plane stress analysis used to convert measured strains to stresses.

4.2. Effect of hydrostatic pressure

4.2.1. Experiments

This was the first calibration study carried out to assess the reliability and accuracy of the measurement technique. Constant hydrostatic pressure was applied to a cylinder inside a pressure vessel. The layout of experimental setup is shown in Figure 4.1.

A cylinder was used of internal diameter 3.175 mm, external diameter 15 mm and length 140 mm. The material for the test specimen was 316H stainless steel with a yield stress of about 400MPa, Young's modulus of 200GPa and Poisson's ratio of 0.3. The specimen was enclosed in a vessel where internal pressure was applied through a manual high-pressure air pump. The applied pressure was measured using a pressure gauge attached onto the pump. Different amplitudes of hydrostatic load were applied ranging from zero to 270MPa in steps of 30MPa and evaluated stresses were compared to the standard strength of materials analysis.

The stresses through the wall thickness of an externally pressurised thick walled cylinder can be calculated using the equation developed by [Timoshenko, 1951]:

$$\sigma_r = \frac{a^2 b^2 (p_o - p_i)}{b^2 - a^2} \cdot \frac{1}{r^2} + \frac{p_i a^2 - p_o b^2}{b^2 - a^2}$$

$$\sigma_\theta = -\frac{a^2 b^2 (p_o - p_i)}{b^2 - a^2} \cdot \frac{1}{r^2} + \frac{p_i a^2 - p_o b^2}{b^2 - a^2} \qquad (4.1)$$

where a and b are respectively the inner and outer diameter of the tube, p_i and p_o are the inner and outer pressure, r is the diameter at which the stress are evaluated and σ_r and σ_θ the radial and hoop stresses. For the calibration test $p_i = 0$, and at the exterior of the tube, $r = b$, $\sigma_r = -p_0$.

The experimental technique uses the displacements measured at $r = a$ and converts them into stresses applied on the outer face. The deep-hole analysis uses the equation presented earlier :

$$\bar{\varepsilon} = -\frac{1}{E}[M]\bar{\sigma} \qquad (4.2)$$

where for the pressurised tube $\bar{\sigma}$ is the optimised external pressure obtained from the fitted strains.

Figure 4.2 shows an example of the hole diameter variation before and after applying hydrostatic pressure for P = 270MPa at the angle of measurement θ=0°.

Figure 4.3 shows evaluated stresses as a function of applied stresses. Also shown is the theoretical estimate. These theoretical estimates should be equal to the evaluated stresses from experimental measurements. At 120MPa pressure the experimental stress was about 10 to 15MPa higher than predicted by theory. Figure 4.4 shows the measured stresses as a function of distance through the specimen for each applied pressure.

It was thought that the surface roughness of the reference hole could have had an influence on the measured stresses. There is one point through the specimen thickness in this calibration test that shows the influence of surface roughness. At a depth of approximately 36mm on Figure 4.4, there was a variation of measured stress compared with the rest of the specimen thickness. Since the applied pressure was constant through the thickness and reference hole diameter variation identical before and after application of pressure (see Figure 4.3), the evaluated stress should be constant. However, if the depth at which the hole diameter is measured is not identical before and after applying hydrostatic pressure (for example say 0.1mm), then the corresponding peaks and troughs of the reference hole do not match. A variation in the evaluated stress occurs at this point. It is also noticeable that the accuracy of measurement from the air probe device was of the order of 1μm (this is discussed

later), which corresponds in this case to about 30MPa. All measurements were found to be within this band.

4.2.2. FE analysis

A simple finite element model was developed to verify the variation in reference hole diameter under load. Figure 4.5 shows the finite element mesh used for the hydrostatic pressure test. The mesh was developed on a square section since the experimental results are evaluated in two directions x and y only. The measured experimental stresses were then applied in the two directions on the square mesh and results compared on the lines at zero and 90° only.

The element type used was 8 nodes cubic elements (C3D8). More complex elements have been used with more nodes but did not increase significantly the accuracy of the results. The boundary conditions used were completely fixed since the specimen is completely constrained at each end (see the displacements shown in figure 4.2). The FE displacements are therefore zero at each end and increased rapidly to reach the applied load condition. No plasticity was modelled since the loading condition in both experiment and numerical simulations were in the elastic region. Young's modulus was 200GPa and Poisson's ratio 0.3.

Figure 4.6 compares the change in reference hole diameter from the FE analysis with experimental measurements. This comparison is made for an applied pressure of 120MPa on the outside surface. The difference in displacement between measured and FE analysis was only 0.5μm and corresponds to an error in stress of about 10MPa.

4.3. Beams subjected to bending

4.3.1. Introduction

In addition to constant hydrostatic pressure tests, further tests were carried out to evaluate stresses in beams containing a constant and linear stress distribution. Two rectangular bars of length 400mm with a square section of width 50mm and height

50mm for the first bar and 19mm width and 50mm height for the second bar were extracted from a larger block of 316H stainless steel. Measurements were undertaken across the width of the beam in the 50mm and 19mm directions so the technique could be tested taking into account the specimen thickness. The bars were clamped at one end in a stiff loading device shown in figure 4.7 and loaded at the other end.

The aim of these tests was to introduce a known stress field within the beams and compare the measured stresses using the deep-hole method with stresses predicted from standard strength of materials theory. It was necessary to introduce simple stress distributions so a direct comparison could be made. It was important to assess the accuracy of the air probe readings of diameter and then to convert the displacements into stresses present in the bars. Three methods were used to determine the stress distribution in the loaded bars. Beam theory using the applied load provided the stress distribution at given locations in the bars. Surface strain gauge readings also provided the stress distribution for the applied load and finally elastic finite element analysis, using a three dimensional simulation of the beams clamped at one end, provided a comparison between the theory and deep-hole stress evaluation.

4.3.2. Background theory

The following theory details the analysis for the applied stress since in this experiment known loads were applied to the beams. From the reference hole deformations, the 2D plane stress analysis enabled the evaluation of σ_x, σ_y and σ_{xy} in the plane normal to the axis of the reference hole. These stresses are compared with theoretical stresses. From simple bending tests, a constant stress distribution was expected across the width (50mm and 19mm) and linear stress distribution through the height (50mm). The linear stress distribution was only measured in the 50mm deep bar.

In these calibration tests, the maximum allowed stress intensity was determined by the plastic deformation at the hole edge and taken as $2/3^{rd}$ of the yield stress (σ_y = 400MPa), which gives a maximum applied stress intensity of 267MPa. Theoretical analysis were carried out using cantilever beam equations since it was decided to use a bar clamped at one end and apply a load at the other end. The deformations of the

loading device were not taken into account since the rig stiffness was about 45 times greater than the test bars (for the 50mm square beam).

The bending stress is determined using:

$$\sigma = \frac{M'.y_c}{I_x} \quad (4.3)$$

where:

$$I_x = \frac{b.h^3}{12} \quad (4.4)$$

M' is the applied moment, y_c is the distance from the neutral axis, b is the width, h is the height.

The maximum load applied to avoid yielding was calculated using:

$$F_{max} = \frac{\sigma_{max}.I_x}{y.z_l} \quad (4.5)$$

where z_l is the distance along the beam at which the moment acts and σ_{max} was 2/3rd σ_y. For the 50mm square bar, F_{max} = 23kN and F_{max} = 8.8kN for the 19mm thick bar.

These maximum load values ensured that the stresses at various points along the beam could be determined and the associated strains found by applying Hooke's law.

4.3.3. Experiments

The material properties of these specimens were determined from standard tests at room temperature. Young's modulus was 200GPa and Poisson's ratio was 0.3. The yield strength at 0.2% strain was 400GPa. Stresses were measured across the width b and through the height t corresponding to constant and linear variations of stress.

For a cantilever beam subjected to an end load, the stresses are distributed linearly through the height of the beam with tension on one surface and compression

of the other surface. Also the surface stresses vary linearly along the length of the beam.

Tests were carried out using a specially designed rig shown in Figure 4.7. The bars were clamped at one end and the load was applied at the other end using a bolt thread of high strength steel of 24mm diameter with a hemispherical head (yield stress of 600MPa). Four similar bolts were used to clamp the bar at the other end since they transmitted the maximum load at the clamped position. The main rig was manufactured from En 24 steel. It was assumed that the experiments were similar to cantilever beams and analyses were carried out in order to compare with experimental results. Strain gauges were attached onto the first bar at locations shown in Figure 4.8 and similarly on the second bar (b=19mm) to record deformations at 0° and 45° before being subjected to simple bending and simple torsion tests. The torsion tests are described in the next section. The type of strain gauges used was EA-06-250BG-120. The strains were obtained on the main axis of the beam and through the height of the beam to obtain the variation from the top to the bottom surface. Strain gauges were placed also at specific locations where the stresses were evaluated and on the main axis of the bar to record the standard stress distribution along and across the bar. The locations of the gun-drilled reference holes for deep-hole measurements are shown in figure 4.8.

For the b=50mm thick bar: Hole 1 was situated in the top section of the bar and across the width and was used to measure a constant compressive stress. Hole 2 was situated in the bottom section of the bar and across the width and was used to measure a constant tensile stress. Hole 3 was in the centre of the bar and through the height and was used to measure a linear stress distribution from tension to compression. For the 19mm thick bar: Hole 1 was situated in the top section of the bar and across the width measured a constant compressive stress. The applied loading conditions for each case are shown in table 4.1.

For various end load conditions the tensile surface strain (stress) through distribution along the length of the bar is shown in Figure 4.9 and figure 4.10 shows the strain (stress) distribution through the height of the bar changing from tension on

the bottom surface to compression on the top surface. The stresses were evaluated from the strain gauges readings using Hooke's law. Also shown in figure 4.9 and 4.10 is the location corresponding to hole location 1. The measured surface strain (stress) distributions show that with an applied load of 10kN, the expected stress across the width at the location of hole 1 was 68MPa. The measured distortion of the gun-drilled hole at location 1 revealed a uniform stress σ_{zz} across the width b. A typical result is shown in figure 4.11 at the location for hole 2. The predicted stress was 68MPa, and the averaged stress across the width was 74MPa. In this case, it can be observed that the experimental measurement was constant across the width of the bar and very close to the applied stress of 68MPa.

Similar results obtained from the 19mm thick beam are shown in figure 4.12. In this case, front bushes were glued onto the specimen. There was a small variation across the width of the beam possibly due to an off axis loading leading to a small degree of torsion applied to the specimen. Nevertheless, there remains a very good correlation between the experimental results and the theoretical stress of 64MPa.

The linear variation of stress σ_{zz} through the height of the 50x50mm beam was measured in hole 3. The results for an applied load of 3.3kN are shown in Figure 4.15. This test was also carried out using a pinned front bush. Similar to the other results, it was found there was a disturbance in the local stress field, due to the presence of the pins for distances up to about 10mm from the top surface. Nevertheless, further away there was good correlation between experimental measurements and theory. Note that experimental tests were initially carried out with pinned bushes since it was not expected to have a large influence on the stress distributions. This was changed after the first set of results to obtain more accurate results. The bushes were, from this point, also glued onto the welded specimens.

4.3.4. FE analysis

An elastic finite element analysis using the ABAQUS code was carried out using the mesh shown in Figure 4.14. Analysis was undertaken on the 50mm square bar. Cubic elements with 8 nodes were used. The boundary conditions were completely fixed at the bottom surface of the clamp and fixed with allowed friction on the top

surface of the clamp. Side faces were left free since no direct load was applied. A 3D mesh was used to assess differences across the depth of the beam because the three included holes were located at different orientations in the beam. The load was applied on a surface area at the bottom face of the mesh. The idealised loading conditions are shown in figure 4.15.

When bending was applied, hole 1 situated at the top part of the bar was under compression whereas hole 2 situated at the bottom part of the beam was in tension. The comparison between measured reference hole and finite element deformed mesh is shown in Figure 4.16. The original circular hole is shown with the deformed hole. The magnification factor for the displacements is 200. Also shown is the measured deformed hole from the air probe readings. It can be observed that there is a very good agreement between the deformed hole measured from experiment and finite element analysis.

4.4. Beams subjected to torsion

4.4.1. Introduction

In addition to the constant and linear stress distributions in the bending tests, torsion tests were carried out to examine the accuracy of measuring pure shear (σ_{xy}) stress distributions. The same test bars were used as for the bending test but load conditions were changed. The schematic of the torsion test rig is shown in figure 4.7b. This is a modified version of the same test rig as for the bending tests.

4.4.2. Background theory

In these calibration tests, the maximum allowed stress intensity was determined using the same conditions as for the bending test. Theoretical analyses were carried out for the case of rectangular (or square) cross section (as shown in figure 4.17), the maximum shear stress can be expressed as :

$$\tau_{\max} = \frac{M^t}{k_2(2a)^2 2b} \qquad (4.9)$$

Where M^t is the torque applied and k_2 is a constant equal to 0.208 for $a = b =$ 0.025m.

4.4.3. Experiments

The same bars as for the bending tests were used for these experiments. A roller bearing was introduced at the free end of the bars to ensure that the neutral axis remained straight and load was applied using a lever arm to rotate the beams. The overall arrangement is shown in figure 4.7b. For the torsion test, two different torques were applied and measurements were taken at the location for hole 3 for the 50mm wide bar. The thin bar (19mm wide) was subjected to one bending load and two torque conditions. The loading states are given in table 4.1.

Strain gauges were fixed on the surface of the bar at the locations of the neutral axis on each side and at 45° from the main axis of the bar. The type of strain gauge was the same as for the bending tests.

Typical results from the torsion tests on the 50mm wide bar with applied torques of 830 and 1660Nm are shown in figure 4.18. Similar results for the torsion test on the 19mm wide beam are shown on figure 4.19. In both cases higher shear stresses were measured close to the edges than predicted using standard theory, as will be shown later in FE results.

4.4.4. FE analysis

Finite element analysis was carried out using the same mesh as for the bending analysis tests. The analysis was also carried out on the 50mm square bar, and the boundary and load conditions were changed.These boundary conditions are shown in figure 4.15. The clamped side of the bar was modelled using a completely fixed boundary condition at the bottom face and fixed with friction on the three other faces. The other end of the bar was assumed to have a Young's modulus 10 times higher over a short distance of the bar to allow the torque to be applied. A distributed load was applied at 45° from the faces of the bar at each corner and in the section with the

high Young's modulus. This generated a small distortion between the two different Young's moduli regarding the stress distribution. However, since the drilled holes were located far away, this feature did not affect the results.

The distortion of hole 3, situated at the centre part of the bar was examined. The hole was distorted at 45° on each side of each face of the bar when the torque was applied and the results are shown in figure 4.20. There is excellent agreement between measured and predicted hole distortions. The results of the FE analysis are also shown in figures 4.18 and 4.19. A very good correlation between the experimental and numerical results can be seen. Also the theoretical analysis carried out on the round bar geometry shows smaller intensity as measured. Both sets of results from the 50mm thick and 19mm wide bars revealed higher near surface stresses when compared to standard theory and non-linear distribution was observed across the specimen width.

4.5. Autofrettaged tube

4.5.1. Introduction

An autofrettaged tube was supplied by DSM and an evaluation of the residual stresses was undertaken using different experimental techniques and finite element analysis. The tube wall thickness was 17.5mm and outside diameter 67mm. The results obtained using the deep-hole technique are compared with results obtained using Sachs method [Lacarac et al., 2000].

The autofrettage process is used widely in industry to improve the integrity and life of components. The process involves introducing an internal pressure that causes plastic deformation at the inner bore. Release of the internal pressure leads to elastic recovery, which introduces compressive stresses in the plastic deformed region. The autofrettage process generates a compressive residual stress on the inner surface. Thus a lower intensity of working stress can be used and thereby enhancing the component lifetime.

To assess the structural integrity of the component, an accurate knowledge of residual stresses acting in the section of interest is required. Many experimental (Stacey, 1985 and Clark, 1984), numerical (Jahed , 1996) and analytical (Chen, 1986) studies have been undertaken to determine residual stresses in autofrettaged tubes. Experimental measurements of the residual stress distribution have been carried out using non-destructive techniques such as X-ray (Clark, 1984), neutron diffraction (Stacey, 1985), and also destructive methods, for example Sachs' method (Stacey, 1988).

4.5.2. Experiments

The tube material was a high strength steel, AISI 433M4 and identical to that used by Lacarac et al. (2000) and Stacey et al. (1985), with a Young's modulus E of 210GPa and Poisson's ratio assumed to be 0.3. The yield strength at 20°C is 968MPa. The thick wall tube was 800mm long, 67mm outer diameter and 17mm wall thickness. A schematic of the specimen is shown in Figure 4.21.

Two methods were used to measure the residual stresses in the tube. The conventional Sachs boring method and the deep-hole method. The Sachs method was used to measure residual stresses in the tube immediately after autofrettage. A ring of thickness 25mm was extracted from the tube. To use the Sachs method four strain gauges in both hoop and axial directions were bonded at 0°, 90°, 180° and 270°. The tube is bored out incrementally using a boring machine. The measured strains for four different angular positions were very similar and for residual stress calculations average strains were used. Further details of the experimental method are given in Lacarac (2000). To determine the residual stresses from measured strains the Sachs equations were used. These equations are for generalised plane strain conditions and are:

$$\sigma_{rr}(r) = \frac{E}{1-\nu^2}\left[\frac{b^2 - r^2}{2r^2}\right]\eta(r)$$

$$\sigma_{\theta\theta}(r) = \frac{E}{1-\nu^2}\left[\left(\frac{b^2 - r^2}{2r}\right)\frac{d\eta(r)}{dr} - \frac{b^2 + r^2}{2r^2}\eta(r)\right] \qquad (4.10)$$

$$\sigma_{zz}(r) = \frac{E}{1-\nu^2}\left[\left(\frac{b^2 - r^2}{2r}\right)\frac{d\xi(r)}{dr} - \xi(r)\right]$$

where $\eta(r) = \varepsilon_{\theta\theta}(r) + \nu\,\varepsilon_{zz}(r)$ $\qquad$ $\xi(r) = \varepsilon_{zz}(r) + \nu\,\varepsilon_{\theta\theta}(r)$

$\varepsilon_{\theta\theta}(r)$ and $\varepsilon_{zz}(r)$ are hoop and axial strains respectively measured on the outer radius of the disc. E and ν are Young's modulus and Poisson's ratio of the material, respectively. r indicates the radius of a removed cylinder.

Measured axial strains during removal of the disc from the tube were taken into account in the calculation of axial residual stresses. It was assumed that hoop and radial residual stresses were not affected. The measured residual stresses using the Sachs method are shown in figure 4.22.

The deep-hole method was also used on the remaining part of the tube. A front bush was glued on the outside surface of the specimen and a core was placed on the inside with similar diameter as the tube. The reference hole of 3.175mm diameter was gun drilled and the core trepanned with a 10mm diameter. The standard deep-hole technique was used to measure residual stresses using 16 angles of measurement around the hole. Typical strain distributions obtained from the deep-hole measurements are shown in Figure 4.23 for $\theta = 0°$, 45°, 90° and 135°. The measured strains are shown as a function of distance through the pipe wall thickness. These strains together with those obtained from other angles were used to determine the residual stresses. The measured residual stresses are shown in Figure 4.24. It is assumed that with $\theta = 0°$ corresponding to the hoop direction, then σ_{xx} is equal to the

hoop stress and σ_{yy} is the axial stress in the thick wall tube. Also shown in figure 4.24 are experimental results obtained using Sachs method (Lacarac, 2000). In the Sachs measurements, residual stresses were obtained starting from the inner wall of the tube. Generalised plane strain conditions were assumed in the Sachs analysis, and therefore provided measured hoop, axial and radial residual stresses. Also shown are residual stress measurements carried out using the Sachs boring technique (Stacey et al., 1988) for a similar autofrettaged tube. There is reasonable agreement between the distributions of the measured residual stresses obtained from the Sachs and deep-hole measurements. The deep-hole method measured a compressive residual stress similar to that obtained by the Sachs method at the inner wall of the tube. However, the deep-hole method was unable to measure the steep distribution of the residual stress profile measured by the Sachs method. It is notable that the deep-hole method indicated that the axial and hoop residual stresses were in compression on the outer surface of the tube. This compressive outer surface was also observed by Stacey et al. (1988) and related to the prior machining of the material. More details of this analysis will be described together with the finite element results in the next section.

4.5.3. FE analysis

In view of the differences in residual stresses obtained by the two measurement methods, a finite element analysis was carried out to simulate the introduction of residual stresses into the tube. To provide an accurate material model, the stress-strain curve for the steel was introduced into the ABAQUS finite element (FE) code. Since during the tensile part of a loading cycle the material showed only limited work hardening, a linear kinematic hardening model was assumed to represent the observed behaviour. However, during unloading into compression after tensile loading a pronounced Bauschinger (Bauschinger, 1886) effect was observed. The Bauschinger effect factor, BEF was determined from the measured material response for cyclic loading and found to be 0.35. This material is identical to that used by Lacarac et al. (2000).

One quarter of the autofrettaged tube was modelled using 14900, 8 noded brick elements of type C3D8. The model is shown in figure 4.25 and illustrates that the axial end loading associated with internal pressure in the hemispherical end cap was

included. Also included into the model was a detailed mesh (Figure 4.25b) that was used to simulate the deep-hole measurement process.

Autofrettage of the tube was carried out using an internal pressure of 690MPa. The internal pressure was chosen to introduce a yield front up to about one half of the wall thickness. The internal pressure was then removed by step unloading and consequently residual stresses were formed in the model.

The residual stress predictions from the FE simulation of the autofrettage process are compared to the deep-hole measurement in figure 4.26. The predicted residual stresses from the FE simulations were very similar to the Sachs results. However, the finite element analysis did not take into account possible residual stresses generated by machining of the outer surface of the pipe. There are similarities between the FE predictions and the deep-hole measurements, but again the detailed stress gradient obtained by the FE simulation is not observed in the deep-hole measurements.

The finite element analysis was then used to simulate the deep-hole technique. The different steps of the deep-hole technique were simulated in the FE analysis as follows:

- Elements were removed from the FE model after the autofrettage simulation to simulate creation of a reference hole by gun drilling.

- The diameter of the reference hole was then taken as the initial state.

- To simulate the trepanning process, elements were removed from a region around the reference hole.

- The change in diameter of the reference hole after the trepanning simulation was introduced into the analysis to calculate the residual stresses.

Two trepanning or core diameters 10mm and 5mm were simulated in the FE analysis. The core of 10mm diameter (figure 4.25c) was modelled to compare directly with experimental measurements. The smaller core of 5mm diameter was modelled

for the reasons described later. The calculated hoop residual stresses from the deep-hole FE simulations using these two core diameters are shown in figure 4.27 together with the original predicted autofrettage residual stresses and the experimental measurements.

The residual stress distribution obtained from the 10mm core simulation exhibited similar characteristics to that obtained from the experiments. The steep stress gradient observed in the original residual stress was not reproduced. An improved match with the original stress distribution was obtained when a core diameter of 5mm was used in the simulation of the deep-hole method.

The area of most interest in autofrettaged tubes is usually the inner bore since it is known that fatigue cracks initiate during service loading. Depending on the material model, the greatest discrepancy between experiments and theoretical (and numerical) predictions has been observed at the inner bore. This is mainly because the process of reverse yielding during unloading has not been accurately modelled. There are then inaccurate predictions of the compressive hoop residual stresses at the bore.

The results from the application of the deep-hole technique have shown there is general agreement with other experimental and numerical results although discrepancies are believed to be due to a number of factors. Each measurement through the depth is assumed to be independent of adjacent measurements. In the case of steep residual stress gradients, assuming those adjacent displacements are independent leads to an under-estimation of the residual stresses at each point. Consequently, the experimental method was not able to measure the zone of reverse yielding generated during unloading after the autofrettage process. The finite element analysis simulation of the deep-hole method revealed that, some residual stresses were retained in the core. Therefore not all residual stresses were completely relaxed. Larger values of residual stress were retained in the 10mm core compared to the 5mm core where most of the remaining residual stresses in the core were relaxed. Consequently, there was a better agreement between the predicted autofrettaged stresses and evaluated stresses from the deep-hole simulation.

The deep-hole and Sachs results showed similar trends as the FE simulations. The Sachs measurements however, were able to reveal the steep stress-gradients predicted by the FE predictions of the original residual stresses. Overall, it is apparent that the deep-hole measurement method can determine the residual stress distribution through the wall thickness of an autofrettage tube. Nevertheless, experimental results, combined with finite element simulation have revealed that further refinements are required. This is particularly the case if the deep-hole method is to be applied to component containing steep stress gradients.

Plotting the differences between the different sets of results and comparing these with the residual stresses remaining into the core (FE model) after trepanning provides the assessment of inconsistencies between the different results. These are presented in Figure 4.26. It is observed that the difference between the FE prediction and FE deep-hole results is exactly the same as the amount of remaining residual stress into the core. Therefore, the assumption of complete elastic stress relaxation into the core for the experimental analysis is not valid and can only be solved by decreasing the core diameter and hence reducing the amount of residual stresses left. On the other hand, the difference between the prediction and experiment show that the evaluation of sharp stress gradient by the deep-hole technique can be achieved by decreasing the core diameter since this reduces the influence each measurement next to each other. This was shown in Figure 4.27 where a better agreement was observed with prediction when the displacements from the 5mm core diameter were introduced into the analysis instead of the displacements from the 10mm core diameter.

4.6. Finite element analysis for plates containing holes

4.6.1. Introduction

This section presents a series of FE analyses carried out to explore a number of features related to the deep-hole technique. Finite element simulations in the previous sections have shown that the deep-hole technique can be used to measure through thickness residual stresses. In this section, results from further studies on the influence of core diameter are first presented. Next, a finite element analysis was carried out to examine the influence of local plasticity at the edge of the reference hole.

4.6.2. Influence of core diameter

The FE analysis presented in the previous section for the autofrettaged tube revealed that the core diameter has an influence in the deep-hole method. In this section, the residual stresses from a set of measurements reported later in the thesis were used to create distortions of the reference hole. The set of experimental deep-hole residual stresses, shown in figure 4.29, were applied on the edges of an FE mesh, respectively in the x and y directions. Rather than using a cylinder containing a reference hole, the FE analysis was carried out using a square bar containing a reference hole. This is shown in figure 4.30. The external dimension, width w of the bar was varied from 8mm to 40mm. The reference hole diameter was constant at 3.175mm and the length of the bar was 65mm (equivalent to the specimen thickness). Three-dimensional elements of type C3D8 were used. The stresses shown in figure 4.29 were applied as a uniform distribution across w but varied along the thickness t as shown in figure 4.30. The displacements at the hole edge were recorded and compared with experimental results.

A comparison of the displacements at the hole edge from the FE analysis with experimental measurements with changes in core width for the same external stress field is shown in Figure 4.31. It can be observed that there are larger reference hole displacements for smaller w and there is a 'smoothing' process in the reference hole displacements by increasing the diameter of the core. Decreasing the core diameter improves the trend in displacements through the specimen thickness and also increases the magnitude of the displacements. On the other hand, increasing the core diameter provides closer agreement with experiment.

The current analysis assumes that the residual stresses are evaluated on the edge of an infinite plate with a small hole in the centre and constant stress distribution across the plate. This approximation is limited since the stress distribution across the core is not known. Each measurement at each section is not independent from the adjacent sections. It is recalled that, although the Fourier analysis presented earlier does not take into account the influence of adjacent measurements, it does take into account the reference hole and trepanned core diameters in evaluating the residual stresses.

4.6.3. Influence of local plasticity

Finite element analyses were carried out to determine the influence of plasticity introduced during drilling to create the reference hole and to show its influence on residual stress measurements. Also plasticity around the reference hole can be created from the presence of residual stresses themselves. This analysis was undertaken for different load conditions and two core diameters, 12mm and 24mm. The diameter of the reference hole was 3.175mm and the plate dimensions were 40mm square.

For the first case, one quarter of a square plate was modelled containing a quarter of the reference hole at one angle. The elements used were 4 noded plane stress CPS4 and axisymmetric boundary conditions were assumed. The edge of the hole was subjected to internal pressure to create plasticity at the hole edge. This was intended to simulate plasticity during drilling, then release the pressure. The pressure was applied at the hole edge causing stresses ranging from 450MPa to 650MPa. External elastic loads were applied at the edges of the plate to obtain displacements at the hole edge and then a "core" was trepanned from the rest of the model to remove the outside load. The procedure is presented in figure 4.32. Displacements were recorded at the hole edge and converted into stresses to compare the calculated stresses to applied stresses at the edges of the plate. The comparison between applied and evaluated stresses is presented in figure 4.33a and 4.33b and the corresponding errors are presented in figure 4.34a to 4.34d.

The same plate was used in this analysis but no initial hole existed. External elastic load were applied and the hole was then included on the corner of the plate generating plastic deformation at the edge due to stress concentration. The "core" was then trepanned by releasing the outside nodes and displacements at the hole edge were recorded. As in the previous case measured displacements were converted into stresses. The procedure is presented in figure 4.35. The analysis was carried out for the cases $\lambda=0$, $\lambda=0.5$ and $\lambda=1$, where $\lambda=\sigma_x/\sigma_y$. The comparison between applied and evaluated stresses is shown in figure 4.36 and associated errors are presented in figure 4.37a to 4.37d.

The analysis was carried out for two different diameter of cores and results show that stress analysis is sensitive to the core diameter as shown in the error plots. If the core diameter is outside of the stress concentration, the current analysis results are very close to the Finite Element analysis and calculated stresses.

A study was carried out concerning the local plasticity introduced by the gun drilling operation but showed that this effect was in fact negligible. The local plasticity in fact increases the local plasticity boundary, which in this case is suitable for our study, because the analysis used to carry out residual stress assumes a linear displacement at the hole edge. The radius of influence of this plastic deformation was found to be very small and without influence over such a big diameter core. It is also clear that if the diameter of the reference hole and trepanned core were to be reduced, this plastic effect may have a bigger importance, which may need to be taken into account.

4.7. Concluding remarks

The calibration tests established that the overall reliability of the technique to measure stress will be high provided that the following features are adopted.

- The EDM diameter should be of the order of three times smaller than the specimen thickness to overcome an average residual stress measurement and to include sharp stress variation.

- The EDM diameter can be within the local stress concentration as long as stresses are below 60% of the yield stress.

- Good comparisons between experiment and analysis were obtained for constant and linear stress distributions in components.

- Torsion calibration tests revealed that a non-linear stress variation close to the edges of square section beam was measured using the deep-hole method and agreed with FE analysis.

- The autofrettaged tube specimen contained a sharp stress gradient. The deep-hole method measured an averaged stress gradient. However, a smaller sampling volume (core size) of the technique should resolve this.

FE studies on the influence of local plasticity revealed that if the radius of plastic deformation within the core was small and did not disturb significantly the residual stress state then there was little or no influence of plasticity.

CHAPTER 5 : EXPERIMENTAL MEASUREMENTS

5.1. Introduction

This chapter presents and compares all the different results for experimental measurement of residual stress in welded components carried out throughout this project using the deep-hole technique. The results will be presented so that comparisons can be made for the influence of wall thickness, weld process and includes the effects of post weld heat treatment, ageing and weld repair on residual stress distributions in stainless steel welded components. Also, whenever possible, results obtained using the deep-hole technique will be compared with experimental measurements carried out using other experimental techniques on the same specimens.

The chapter is written in twelve sections. This covers the description of material and specimens, the influence of specimen and weld geometry on the residual stress distributions, the effect of post weld heat treatment on residual stress relief, the effect of ageing and the influence of weld repair on residual stress redistribution. In general, measurements were undertaken at two different locations, the centre line of the weld and in the heat affected zone. Most measurements were obtained with the axis of the reference hole in the deep-hole method in a direction perpendicular to the specimen surface.

A brief summary of the experimental technique is now given. The same technique was used for all experimental measurements during this project. The main characteristics of the equipment and the modifications made to the system were described in chapter 3.

The deep-hole technique was applied in five different steps:

1- Steel bushes were glued on the surface of the specimen to act as reference.

2- A reference hole of 3.175mm diameter was gun-drilled through the specimen wall thickness.

3- The reference hole diameter was measured accurately at intervals of 0.2mm through the depth of the reference hole and *n* angles around the hole.

4- A core containing the reference hole as its axis was trepanned and the change in core height measured while trepanning.

5- The reference hole diameter was remeasured at the same locations as before trepanning. The stress relaxation in the core provided changes in the reference hole diameter. These changes were used to evaluate residual stresses.

5.2. Material and specimens

In this project, experimental measurements using the deep-hole technique were obtained mostly on stainless steel type 316H butt-welded pipes. The material properties of 316H stainless steel are : Young's modulus and Poisson's ratio are 200GPa and 0.3 respectively and the yield stress of the parent material is 400MPa. A list of the components examined in this project is provided in table 5.1. This table does not include the calibration work presented in chapter 4.

5.2.1. Cylindrical specimens

Three sets of cylindrical components were studied. One set consisted of butt-welded pipes with a wall thickness ranging from 19mm up to 65mm. The second set were butt-welded pipes of 65mm wall thickness and containing welds manufactured using different weld procedures. The third set consisted of 65mm thick butt-welded

pipes (VORSAC components A and B). These components were tested as part of a European project.

Butt-welded pipe 19mm wall thickness

This specimen consisted of a butt-welded 316H stainless steel pipe of dimensions 1020mm long, 385mm inside diameter and a wall thickness ranging from 17mm to 20mm. The arrangement of the component is shown in figure 5.1. A fully circumferential weld was situated at 65mm and 50mm respectively from the location of the original nozzles A and B. The weld had a width of 30mm on the outer surface of the pipe.

The weld was introduced using a combination of tungsten inert gas (TIG) and manual metal arc (MMA) welding. The specimen was fixed horizontally and rotated over 360° for welding with downhand process. The electrode diameters were 3/32 inch of type 'S' for the TIG process and type 'S' British Steel code 910 for the MMA process. The TIG process is used at the beginning of welding for the root pass and 'hot' passes (usually few passes).

Three measurements in the heat-affected zone were undertaken in this specimen. Two measurements were with a core diameter of 20mm, one remote from the last weld pass and one on the last weld pass. The third measurement was undertaken on the last weld pass but with a core diameter of 10mm and trepanning was done incrementally.

a) Location 1 (DH1) was undertaken 15mm from the weld centre line on the remote side from the last weld pass. The measurement point was situated at 120° from top dead centre (TDC), which correspond to the central axis of the nozzle in the pipe. A trepanned core diameter of 20mm was used and the diameter of the reference hole was measured at 16 angles.

b) Location 2 (DH2) was undertaken 13mm from the weld centre line on the side of the last weld pass. The measurement point was situated at 150° from TDC. A core

diameter of 20mm was extracted and 16 angles of measurement in the reference hole.

c) Location 3 (DH3) was located 13mm from the weld centre line on the side of the last weld pass at 100° from TDC. The core diameter was 10mm and 16 angles of diametrical measurement were used. This measurement was carried out incrementally (3 increments) and analysis undertaken at each increment.

Measurements at locations 2 and 3 were undertaken since the result at location 1 did not agree with numerical simulations. This is discussed later. Since the first experiment was undertaken on the remote side from the last weld pass, location 2 was carried out on the last weld pass. In addition, location 2 was undertaken 2mm closer to the weld centre line from the edge of the weld cap. This would bring the experimental measurement closer to the heat-affected zone (HAZ) of the weld. It is observed that for this wall thickness, the sampling volume of the experiment (ie : the core diameter) is of the same order as the wall thickness of the specimen. A third measurement (DH3) with a core diameter of 10mm was undertaken and an improved agreement was observed between experiment and FE analysis. The influence of the core diameter on technique sensitivity was described with more detail in the autofrettaged tube specimen FE analysis in chapter 4.

Butt-welded pipe 35mm wall thickness

This specimen was manufactured from a pair of ex-service AISI type 316H stainless steel forgings. The forgings were joined using a standard manual metal arc (MMA) weld procedure, with type 316L electrodes. The dimensions of the specimen were 1100mm long, 360mm inside diameter and a wall thickness ranging from 32mm to 38mm. The weld was situated at 70mm and 50mm respectively from the two nozzles A and B shown in figure 5.2. The weld has a width of 45mm on the outer surface. The arrangement of the component is shown in figure 5.2a.

Six residual stress measurements were undertaken in this specimen. Three measurements were obtained in the heat-affected zone and three at the weld centre line. The location of measurements is shown in figure 5.2b. Also, three short weld

repairs were introduced into the specimen with repair depth 25% and 75% of the original wall thickness (figure 5.2c). To introduce the repair welds, the pipe girth weld was machined using a hand grinder to create three excavations: two to a depth of 25% and one to a depth of 75% of the section thickness. The effective circumferential lengths of the weld excavations corresponded to a subtended angle of approximately 20°. The excavations were filled with type 316L weld metal using a MMA process. It was assumed that the zone of influence of the original nozzles is about ±60° from TDC. All measurements obtained in this specimen were made with a core diameter of 20mm and using 16 angles around the reference hole.

a) Measurement at location 1 (DH1) was undertaken in the heat-affected zone (HAZ) at 135° from TDC and before any weld repair was introduced.

b) Location 2 (DH2) is situated in the HAZ and in the centre of the 75% depth weld repair at 270° from TDC.

c) Location 3 (DH3) is situated in the HAZ and in the centre of the 25% depth weld repair at 90° from TDC.

d) Location 4 (DH4) is situated in the weld centre line and before any weld repair was included into the specimen. The measurement was at 225° from TDC.

e) Location 5 (DH5) is situated in the weld centre line and in the centre of the 25% depth weld repair at 180° from TDC.

f) Finally, location 6 (DH6) is situated in the weld centre line and after weld repair was introduced into the specimen. The measurement was 25mm above the 25% depth weld repair situated at 90° from TDC. This was to explore the zone of influence of the short weld repair in the specimen.

Butt-welded pipe S5-A

This component consisted of two butt-welded 316H stainless steel nozzle sections of length 600mm, 430mm outside diameter and a wall thickness of 65mm. The weld

was situated at the mid-length of each nozzle section. The fully circumferential weld width on the outer section was 40mm. The two nozzles were located at 180° from each other. The arrangement of the component is shown in figure 5.3 with the overall arrangement shown in figure 5.3a and the details of the weld configuration shown in figure 5.3b.

One measurement was undertaken in this specimen on the weld centre line. The location of the measurement was at 90° to the axes of the nozzles. The deep-hole measurement used a core diameter of about 12mm and 8 angles around the reference hole were measured. This measurement was carried out using the ECM system.

Butt-welded pipe S5-B

Similar to component S5-A, this component consisted of two butt-welded 316H stainless steel nozzle sections of length 600mm, 430mm outside diameter and a wall thickness of 65mm. The weld was situated at the mid-length of each nozzle section. The width of the weld was 40mm on the outer surface of the nozzle section. Unlike component A, the two nozzles were located on the same side of the welded section. The arrangement of the component is shown in figure 5.4. This specimen was submitted to a one hour PWHT at 750°C.

The measurements used a core diameter of about 12mm and 8 angles around the reference hole. Trepanning of the core were carried out using Electro-Chemical Machining (ECM). Two measurements were undertaken in this specimen at the weld centre line. Location 1 was situated at 180° from the nozzle side and location 2 was situated at about 100mm from the first measurement location again at the weld centre line. For the second measurement, the trepanning process was carried out only to a depth of 45mm (figure 5.4b). This was to ensure that where trepanning had not taken place experimental analysis would measure no stresses.

Butt-welded pipe S5-C

This component was again similar to specimen S5-A. It consisted of two butt-welded 316H stainless steel nozzle sections of length 600mm, 435mm outside

diameter and a wall thickness of 65mm. The weld was situated at the mid-length of the nozzle section. The width of the weld was 40mm on the outer surface. The two nozzles are located at 180° from each other. The arrangement of the component is shown in figure 5.5a.

Two sets of residual stress measurements were undertaken in this specimen (figure 5.5b). The measurements for this specimen used a core diameter of about 12mm and 8 angles around the reference hole. Again, ECM was used for trepanning. The difference between this specimen and specimen S5-A and S5-B was that a lower heat input was used for the welding process.

a) Location 1 (DH1) was situated in the weld centre line and at 90° from the centre line of the nozzles.

b) Location 2 (DH2) was situated in the HAZ, situated 2 mm off the edge of the weld, in the parent metal, and 90° from location 1 (as shown in figure 5.5a).

Specimen containing a Narrow Gap TIG weld

This component consisted of two butt-welded 316H stainless steel pipe sections, 700mm long, 430mm outside diameter and a wall thickness of 65mm. The weld was situated at about 100mm from one end of the cylinder. The width of the weld was 20mm on the outer surface. The overall arrangement of the component is shown in figure 5.6a and figure 5.6b shows the details of the weld preparation for the TIG weld.

Two sets of residual stress measurements were obtained from this specimen using a core diameter of about 12mm and 8 angles around the reference hole. Measurements were obtained using ECM to extract the core. Location 1 (DH1) was situated at the weld centre line and location 2 (DH2) was situated in the HAZ, situated 6 mm away from the edge of the weld, in the parent metal, and at 90° from location 1 as shown in figure 5.6c.

VORSAC project, specimen A (V-A)

This component consisted of two butt-welded 316H austenitic stainless steel header nozzles of dimensions 550mm high, 432 mm outside diameter and 65 mm wall

thickness. These headers were welded after they had been exposed to service at about 520-530°C for 65000 hours (called hereafter the service-aged condition). Pairs of nozzles were butt-welded using the manual metal arc (MMA process). The total number of MMA passes in each weld was 42. The general layout of the specimen is shown in Figure 5.7. Deep-hole measurements were undertaken using a core of 20mm diameter and reference hole diameters were measured at 16 angles around the reference hole. Also, the EDM process was used for trepanning the cores.

Residual stress measurements were undertaken on VORSAC specimen A before and after post-weld heat treatment (PWHT) at 750°C for two and a half hours. The locations of measurements and measurement type are illustrated in figure 5.7.

Four deep-hole measurements ("DH1 weld", "DH1 HAZ", "DH2 weld" and "DH2 HAZ") were made in VORSAC specimen A. The location of the measurements is shown in Figure 5.7. This figure shows a cross section through the centre line of the butt weld in this specimen A. Also shown in Figure 5.7 are the positions for the application of the other measurement methods. Two measurements, "DH1 weld" and "DH1 HAZ", were carried out to determine the through wall residual stress distribution prior to PWHT (i.e. in the as-welded condition). Two other measurements, "DH2 weld" and "DH2 HAZ", were carried out after PWHT.

a) Location "DH1 weld" was 225° from TDC. The deep-hole measurement at "DH1 weld" was at the weld centre line of the circumferential butt-weld, as shown in Figure 5.7. This measurement was obtained for as-welded condition.

b) Location "DH1 HAZ" was 135° from TDC. The reference hole for the deep-hole measurement was at 20 mm from the weld centre line as shown in Figure 5.7, and perpendicular to the outer face of the specimen. This measurement was also obtained for as-welded condition.

c) Location "DH2 weld" was 180° from TDC and the reference hole situated on the weld centre line. This measurement was obtained after PWHT.

d) Location "DH2 HAZ" was situated at 90° from TDC, with the reference hole 20mm from the weld centre line perpendicular to the outer surface. This last measurement was obtained after PWHT.

VORSAC project, specimen B (V-B)

This component was essentially identical to VORSAC specimen A. Four sets of deep-hole measurements ("DH1", "DH2", "DH3" and "DH4") were obtained from VORSAC specimen B. The locations of the measurements are shown in Figure 5.8. This figure is a cross section through the centre line of the weld. These measurements were carried out to measure the through wall residual stress distribution for four conditions; as welded and after ageing for 182, 2426 and 6989 hours. The deep-hole measurements for all four cases were at a location 20mm from the weld centre line, and perpendicular to the outer surface, as shown in Figure 5.8.

Location "DH1" was 225° from TDC, "DH2" 135° from TDC, "DH3" 90° from TDC and "DH4" 270° from TDC.

5.2.2. Complex shapes

Three components of complex shape were studied. In each residual stress distributions were obtained at various locations through the thickness of the component.

Cylinder-endcap specimen

This specimen consisted of an end-cap welded to a stainless steel cylinder. Both were forged components. The arrangement of the component is shown in figure 5.9. The cylinder was approximately 1100mm long with a 500mm outside diameter and wall thickness of 110mm. Submerged arc welding was used to join the end cap to the

cylinder. One residual stress measurement was carried out in the centre of the weld in the as-welded condition. The diameters of the reference hole were measured at 18 angles and EDM process was utilised with a core diameter of 20mm for trepanning.

Nozzle specimen

This specimen was part of a super-heater header for a steam power generation system. The nozzle was welded onto the side of a cylinder, with most of the weld preparation made on the nozzle, and only a small amount of machining of the header. The header cylinder and outlet nozzles were both about 63.5mm thick. Destructive examination of the weld has shown that there were between 42 and 54 weld beads at any cross section deposited using the manual metal arc process. Prior-to-service (as-welded) and ex-service nozzles were examined. The ex-service nozzle had been exposed to an internal pressure of 16MPag, at 525°C for 55,000 hours. It was manufactured using 316H stainless steel. The arrangement of the component is shown in Figure 5.10a. The cylinder was 500mm long with a 290mm inside diameter and 70mm wall thickness. The nozzle diameter at the intersection with the main pipe was 300mm.

One deep-hole measurement was carried out at the edge of the weld toe at the intersection between the pipe and the nozzle as shown in detail A, Figure 5.10b. The line was orientated 60° to the axis of the nozzle. This measurement was carried out during this project. Two other measurements were carried out prior to the start of this project. Details of these measurements can be found in Smith et al. [2000]. Diameter measurements were obtained at 18 angles around the reference hole and EDM was used for the trepanning process using a core of 20mm.

'Stub-beam' specimen

This specimen consisted of a rectangular section ('stub-beam') welded to the exterior of a cylinder. The arrangement of the welded component is shown in figure 5.11a. The component consisted of a type 316H stainless steel cylinder, 432mm outside diameter, 63.5mm wall thickness and approximately 560mm long, and a type 316L rectangular beam forging, height 210mm, length 152.4mm and width 177.8mm.

The centre of the beam contained a 89mm diameter hole along its length. The weld of interest for the residual stress measurement was, assuming that the cylinder was upright (with its logitudinal axis vertical), along the top face between the cylinder and the 'stub-beam'. The 'stub-beam' had been welded along three faces of the rectangular beam, two vertical sides and along the top horizontal edge. Young's modulus for the two stainless steels was 195GPa, and yield strengths for the two steels were 245MPa and 400MPa for the weld metal.

Three measurements were carried out in the specimen. The measurement locations are shown in detail in figure 5.11b.

a) Location 1 (DH1) corresponds to a line at 30° to the side of the cylinder (or 30° to the normal to the surface of the 'stub-beam'), offset 45mm from the centre line of the cylinder, and penetrating the top surface of the weld and passing into the parent material of the cylinder wall.

b) Location 2 (DH2), also offset by 45mm from the cylinder centre line, but inclined 10° to the cylinder side, and penetrated predominantly through the weld such that the line passed through the bottom of the weld preparation.

c) Location 3 (DH3) corresponds to a position on the 'stub-beam' centre line, inclined at 20° to the side of the cylinder, and located close to the edge of the weld, and in the parent material of the 'stub-beam'. The line for location 3 runs parallel to the edge of the weld preparation and penetrates into the hole in the centre of the 'stub-beam'.

Note that ECM process was used for these measurements and diameter measurements were made at 8 angles around the reference hole.

5.3. Measured residual stresses

5.3.1. Introduction

For each measurement a set of changes in diameter as a function of position through the wall thickness and angles were obtained. To avoid excessive repetition, for each set of measurement a selection of detailed results of reference hole diameter, strain variation, principal stresses and principal direction, are given in appendix 5A. In all cases the method of analysis of results used eq. 3.6, given in chapter 3. When height changes of the trepanned core were not measured the strain ε_{zz} was set to zero.

In the remainder of this section the measured residual stresses for the various components are summarised.

5.3.2. Influence of weld anisotropy

As indicated in chapter 3, there are different aspects that can influence the measured residual stress distributions and particularly the material properties used in the experimental analysis. These are the bulk properties of the overall material. The anisotropy of the weld metal was expected to have a large influence on residual stresses. An attempt was made to show how the crystallographic orientation of the weld metal and the elastic properties of the material can influence the results.

Cores were sectioned along the axis of the hole and in the direction transverse to the weld (axial direction). After polishing and electro-chemical etching, weld beads were examined on the surface of the samples to assess the crystallographic orientation of the weld beads. Sections through the cores from the 35mm thick cylinder weld are shown in figure 5.12a and sections through the core extracted from specimen S5-A are shown in figure 5.12b. However, whilst weld bead orientations could be determined, there appeared to be no correlation between the different beads and the measured displacement variations. Similarly, there was little evidence to show that the orientation of weld beads had an influence on the measured residual stresses.

5.3.3. Analysis method

The main method of analysis of the measured strains was to use the "conventional" analysis developed by Bonner [1996]. The measured strains were converted to stress using equation 3.6. An alternative approach, using Fourier analysis, was developed in section 3.3.5. Here the results of analyse of strains using Fourier analyses are compared with results from the "conventional" 2D analysis.

The application of the Fourier analysis using the first two terms was carried out using experimental results from butt-welded specimens described later in section 5.4. The evaluation of stresses was carried out using the coefficients σ_0, $\sigma^{2c}.\cos(2\theta)$ and $\sigma^{2s}.\sin(2\theta)$. An example of the residual stress distributions obtained using the Fourier analysis is shown in figure 5.13. The other residual stress distributions obtained using the Fourier analysis are shown in Appendix 5B and compared with stresses carried out using the 2D plane stress analysis. A good comparison between the two different analyses was observed. However, for the 35mm specimen, the peak tensile evaluated stress was 50MPa closer to the original analysis by using only σ_0, $\sigma^{2c}.\cos(2\theta)$ coefficients. Also for the VORSAC specimen B, hole 3, the evaluated stresses on the outer surface converged towards the original analysis using only σ_0, $\sigma^{2c}.\cos(2\theta)$ coefficients. It is not clear whether the introduction of an extra coefficient in the Fourier analysis has introduced additional information for the solution but since experimental measurements are not exact and higher order coefficients were not evaluated, it is difficult to assess the reason for this variation.

5.3.4. Changes in core diameter

The effect of changing core diameter was explored using the 19mm thick butt-welded pipe. Only one measurement was originally intended to be carried out on this specimen in the as-welded condition (DH1) but the correlation between experimental results and the finite element simulation was poor. Aspects of the FE analysis are given in chapter 6. A comparison between measured residual stress and FE simulation is shown in figure 5.14. The measured peak tensile residual stress (150MPa) on the

outer surface was not only lower but also did not show the same distribution as shown by the FE results through the wall thickness.

A second measurement was then undertaken on the side of the last weld pass (DH2, see figure 5.1), and 2mm closer to the weld centre line than the edge of the weld cap. Again, a 20mm core diameter was used and the results are compared with DH1 in figure 5.15. This revealed a higher intensity of residual stresses on the side of the last pass. There is for this location better agreement between measurements and FE simulation compared with results with DH1. Again the variation of residual stresses was not measured accurately through the wall thickness. The intensity of the hoop residual stresses was almost twice that of the measurement for DH1 but a more refined technique was needed to measure the sharp variation in the stress distribution.

A core of 10mm diameter was then used to improve sensitivity for DH3. This reduced the sampling volume of the technique, with the core diameter approximately one half of the wall thickness. The measurements from DH3 are shown in figure 5.16. The FE and experimental results have shown a similar trend through the wall thickness. However, the hoop residual stress in the FE analysis was over estimated by almost 200MPa. The axial stress distributions were very similar. The results using 20mm and 10mm cores are compared in figure 5.17. It is evident that using a 10mm core provides more information about changes in the residual stresses through the thickness.

5.3.5. Evaluation of stress in third direction

The measurement of the residual stress on the axis of the reference hole can be undertaken in two different ways. Measurement of the core deformation can be undertaken while trepanning operation is made. This means that heat effect will need to be removed from the capacitance gauge measurements to obtain the mechanical strain. However, this was found to be difficult. The other option is to trepan the specimen incrementally. This means to stop the EDM process and wait for the specimen to cool down until mechanical displacement can be recorded on the capacitance gauge device. By increasing the number of incremental trepanning, a variation of core displacement as a function of depth can be produced.

Nozzle specimen

An incremental trepanning operation was undertaken on this specimen. Nine increments were used to measure the core deformation at different depths through the specimen thickness. Out off these nine points, a polynomial fit was made and the derivative of the polynomial fit provided mechanical strain in that direction. The mechanical displacement of the nine points is shown in figure 5.18a. From the "standard" analysis evaluating σ_{xx} and σ_{yy} the Poisson's effect was then calculated and compared with mechanical strain obtained from the incremental analysis. The comparison is shown in figure 5.18b. A close match was obtained considering the assumptions made. Since no important variation were observed between the Poisson's effect and mechanical strain measured, σ_{zz} was then assumed to be small and not taken into account in the analysis.

End cap to cylinder specimen

The other option to measure σ_{zz} was used for the end cap to cylinder specimen. Since the component is very thick, and constrained on one side of the weld due to the end cap, the radial expansion during welding is different on both sides of the weld. An average radial displacement was clearly identified with the capacitance gauge readings. An example of the capacitance gauge displacement for the end cap to cylinder specimen is shown in figure 5.19. The thermal effect is extracted from the capacitance gauge readings assuming a constant heat transfer flow (as presented in section 3.3.3). The derivative of the polynomial fit through the mechanical displacement provides the mechanical strain, which is included into the "standard" deep-hole analysis for residual stress evaluation.

Results are shown in figure 5.20 and 5.21. There is a good average correlation between experiment and numerical simulation, however the trend is in the opposite direction. This comes from the evaluation of the radial strain in the experiment. The radial displacements are recorded at equal time interval during EDM process, which is different to the air probe measurement increment of 0.2mm in depth. This obliges to fit the capacitance gauges data to obtain values at 0.2mm increment interval to include into the air probe analysis. Fitting the capacitance gauge data do not impose to pass through zero at each extremity (since the radial stress must be zero at the specimen

surface). This prevents accurate evaluation of the radial stress close to the edges of the specimen thickness and provides only average value in the centre.

5.4. Measured residual stresses – Assessment of variability

5.4.1. Measurement location

Differences in residual stress distributions at locations adjacent to the HAZ have already been presented for the 19mm thick butt-welded cylinder. This is emphasised again in figure 5.22 where the results for DH1 and DH2 are combined. Although it has been shown that using a 20mm core reduces the sensitivity of the technique for thin sections, the results in figure 5.22 show that small variations in location near the HAZ can lead to significant variations in the hoop residual stress. The axial residual stresses also appear to change with location.

The effect of measurement location can also be judged from results obtained from the 35mm and 65mm thick butt-welded cylinders. Experimental measurements from the weld centre line and HAZ are shown in figure 5.23 and 5.24. In the case of the 35mm butt-welded cylinder the hoop residual stress was found to be larger near to the HAZ rather than at the weld centre line. Lower axial residual stresses were found at the HAZ. In the case of the 65mm thick specimen, VORSAC A, comparison of the residual stresses measured at the HAZ and weld centre line (figure 5.24) showed that there were very similar distributions at the two locations.

The influence of measurement location can also be judged from the section of the extracted cores shown in figure 5.12.

5.4.2. Specimen to specimen variability

For a given specimen thickness, measurement location and welding process, it is possible to compare results obtained from measurements in three specimens; S5-A, VORSAC specimen V-A and V-B. For example, in the as-welded condition measurements were obtained at the weld centre line for specimen S5-A and V-A, and

at the HAZ for specimens V-A and V-B. The weld centre line measurements are compared in figure 5.25 and HAZ measurements for V-A and V-B in figure 5.26. In both figures 5.25 and 5.26 it can be seen that there are for a given location significant variations in the peak residual stresses from specimen to specimen. There is also uncertainty introduced through measurement location particularly for the HAZ location as explained earlier.

The effect of specimen variability can also be assessed from measurements after PWHT, using results from S5-B and V-A. Here results from the weld centre line are compared in figure 5.27. The magnitude of residual stresses is much lower than for the earlier comparisons, but again there are variations from specimen to specimen. The distributions of the residual stresses as a result of PWHT are also presented later in this chapter.

5.5. Measured residual stresses – Effects of welding processes

5.5.1. MMA processes – High and low heat input.

The difference between specimens S5-A and S5-C was that specimen S5-C was welded using a lower heat input together with a smaller diameter electrode and lower current intensity. This lower heat input was supposed to generate a lower residual stress intensity by assuming that the residual stress intensity is directly proportional to the weld heat input. The measured residual stresses for specimens S5-A and S5-C are shown in figure 5.28. Near to the outer surface both hoop and axial residual stresses in specimen S5-C were higher than in specimen S5-A. Deeper into the wall of the cylinder, the residual stresses were very similar.

5.5.2. MMA and Narrow Gap TIG processes

Two welding processes, MMA and TIG are compared in this section. For the MMA process a standard weld preparation was used. For the Narrow Gap TIG process a much narrower weld preparation was used, and hence a lower volume of molten metal for the weld. For the Narrow Gap TIG specimen measurements were

made at the weld centre line and in the HAZ. It is therefore instructive to compare these results with results for the MMA process.

The specimens used for this comparison are respectively the S5-A, S5-C, VORSAC specimen V-A and the Narrow Gap specimen. The comparisons are made for the as-welded condition.

Results for the weld centre line location are shown in figure 5.29. A similar trend is observed from all specimens. However, in the case of the narrow gap specimen, the residual stress distribution is much more variable and generally the tensile residual stresses were higher. For the narrow gap specimen, the outer tensile hoop residual stress in the first 35mm reached a peak between 500MPa and 600MPa then returned into compression between 35mm and 60mm into the wall thickness with an intensity of about 250MPa and finally returned into tension in the last 5mm to reach 400MPa. A similar trend is observed in the case of the axial residual stress distribution although the intensity was about 150MPa lower than the hoop stress. The intensity of the generated residual stresses is clearly higher in the case of the narrow gap specimen compared with the MMA weld. However it is not known why there are sharp variations of stress at various depths through the wall thickness.

In the case of the measurements at the heat-affected zone location shown in figure 5.30, the results show that the residual stress distributions of the Narrow Gap specimen are located in a band similar to the MMA welds. The main difference between MMA and Narrow Gap TIG welds lie with the axial residual stress, which returned into tension on the inner surface to peak at about 200MPa.

It is notable that, in the case of the Narrow Gap TIG weld, when the distribution of residual stresses was such that the inner and outer faces of the specimen are in tension and the inner section of the wall thickness was in compression, the cross-over from tension to compression was shifted from about 70% of the wall thickness for the MMA weld to about 50% of the wall thickness from the outer face. The second cross-over in the TIG weld occurs beween 85% and 90% of the wall thickness.

5.6. Measured residual stresses – Effect of specimen thickness

Measurements for various wall thickness of butt-welded cylinders have been made for the two different locations : At the weld centre line and in the heat affected zone. The wall thickness of the different components ranged from 19mm to 110mm with the outer radius of the cylinder varying from 420mm to 500mm. The specimens used for this comparison are the 19, 35 and 65mm butt-welded cylinders. Results for the 110mm thick cylinder with end-cap are also included. In all cases welding was carried out using a conventional MMA process. Consequently, for the 65mm thick cylinders the results were confined to specimens S5-A and VORSAC specimen A for residual stress distribution at the weld centre line. For the specimens of wall thicknesses 35, 65 and 110mm measurements were carried out in the weld centre line. The cylinders of wall thicknesses between 19, 35 and 65mm were measured in the heat affected zone.

The residual stress distributions at the weld centre line location are presented in figure 5.31a. The depth through the thickness has been normalised with respect to the wall thickness so that zero corresponds to the outer face of the specimen and 1 is the inner face of the specimen. For all cases, the hoop and axial residual stress distribution through the wall thickness is located within a band of approximately 150MPa. The hoop residual stress was tensile on the outer face between 300MPa and 400MPa, crosses into compression at about 70% of the wall thickness and stayed in compression up to the inner surface between 0MPa and –100MPA. The axial residual stress distribution was different in that it was tensile on the outer surface between 200MPa and 300MPa, crossed into compression at about 45% of the wall thickness with the compressive residual stress at about –100MPa to –200MPa and returning into tension at about 90% of the wall thickness of the specimen and attaining between 0MPa and 150MPa at the inner face. The axial residual stress intensity was also slightly lower than the hoop stress. The most notable difference in the distributions occurred for the axial residual stress distribution in the 35mm thick cylinder. The inner surface of the cylinder was found to be more in tension that the other thicker cylinders.

For residual stress measurements in the heat-affected zone of the various thick walled cylinders, the results are summarised in figure 5.31b. Overall, the results are not very different from those at the weld centre line although the intensity of residual stresses was lower, particularly close to the outer surface. The hoop residual stress reached a maximum tensile intensity around 300MPa compared to about 400MPa at the weld centre line. Also, the axial residual stress was about 100MPa lower close to the outer face compared to the weld centre line. It is notable that the results of the 19mm specimen were different from the average trend. This may partly due to the effect of the sensitivity of the technique discussed earlier even though a 10mm core was used.

5.7. Measured residual stress – Effect of geometry of component

The differences in the residual stress distributions are compared in this section for components of complex geometry and simple butt-welded cylinders. Note that although the specimens geometries were different, the weld geometry was always similar using a V type with the large width on the outer surface of the specimen. The intensity and distribution of residual stresses were found to be very different although some aspects remain unchanged.

The residual stresses were always tensile and near to the yield stress close to the outer surface. The hoop or longitudinal residual stress intensity was usually higher than the transverse residual stress. Although the end cap to cylinder component was classified as a complex geometry, it provides the closest residual stress distribution to the simple butt-welded specimens. Since this geometry generated higher constraint in the radial direction during the welding process, the hoop and axial residual stress distributions were not very much different than other simple butt-welded cylinders. The comparison of residual stresses between the end cap to cylinder specimen with butt welded pipes is shown in figure 5.32a as a function of normalised distance through the specimen thickness.

For the two other complex components, branch weld and stub-beam, although the pattern was similar, there were larger residual stress variations in the nozzle and stubbeam components than in the cylindrical specimens. The residual stress distributions are compared in figure 5.32a for the weld centre line and 5.32b for the heat affected zone.

A comparison of the weld centre line results shows that the nozzle developed lower residual stresses than the cylindrical specimens. The hoop residual stress was about half of the yield stress at 200MPa crossing into compression at the mid-wall thickness. Note that the hoop stress was almost asymmetrically distributed from the mid-wall thickness. The stub-beam longitudinal residual stress was very comparable to the cylindrical specimens close to the outer surface. However, the residual stress intensity remained in tension all throughout the wall thickness and reached about +100MPa on the inner surface. The residual stress distribution was almost linear through the wall thickness.

The transverse or axial residual stress, however was quite different. It also had a tensile maximum intensity close to the outer surface of about 200MPa but remained close to zero from 20% to 100% of the wall thickness. No noticeable compressive residual stress were observed in this case. The transverse residual stress in the case of the stub-beam specimen was also tensile and close to the yield stress but higher than for the cylindrical specimens. The distribution was similar to the cylindrical specimens but shifted about 100MPa towards the tensile stresses. This brought the inner surface of the specimen to be slightly into tension, although part of the mid thickness was in compression at about –100MPa. Although a similar trend was observed in all cylindrical specimens, the differences in the stress distributions between the two complex components revealed differences in intensity up to about 300MPa. This difference is shown through all the wall thickness for the longitudinal residual stresses but only through about 50% of the wall thickness from the outer surface for the transverse residual stress.

In the case of the residual stresses in the heat affected zone, figure 5.32b, the results reveal very different residual stress distributions for the hoop or longitudinal directions between the complex components and the simple cylinders. The maximum stress variation was about 400MPa between the nozzle specimen and the stub-beam. The stub-beam residual stress distribution was completely in tension with the stress changing from about 400MPa close to the outer surface to about zero close to the inner surface. On the other hand, the nozzle residual stresses were also close to 400MPa on the outer surface but decreased rapidly towards compression at about 35% of the wall thickness and remained in compression at about –100MPa up to the inner surface. The simple cylinder stress variations lie in the middle of these two distributions except close to the inner surface where they were slightly more in tension than the complex geometry with a compressive residual stress between –50MPa and –150MPa.

The transverse or axial residual stress distribution was very different from the hoop distribution. The complex geometry distributions in this case were very similar to the simple geometry. The stub-beam specimen had a higher tensile residual stress distribution than the others (about 100MPa higher). All distributions started at the maximum tensile residual stress close to the outer surface at about 300MPa and reduced to zero between 40% and 60% of the wall thickness. From this point, the simple geometry showed a compressive residual stress variation between zero and –150MPa up to the inner surface where the complex geometry residual stresses were between zero and –50MPa.

5.8. Influence of Post Weld Heat Treatment (PWHT)

When the welding procedure is completed, residual stresses are known to be high. This generates problems when assessing the structural integrity of the component or the working margins and lifetime. Therefore, PWHT is introduced to reduce the level of residual stresses. The post weld heat treatment consists of inserting the specimen into a furnace at 750°C for 2.5 hours.

Experimental measurements were obtained from two different sets of specimens for assessing the residual stress redistribution after PWHT. Two measurements were located in the weld centre line for the S5-B and are compared with results for the as-welded conditions of specimen S5-A. In addition, four measurements were obtained from the Vorsac specimen A (V-A); two in the as-welded state and two after PWHT. First, the results from specimen S5-B are presented and discussed, and then results from VORSAC specimen A are presented.

Specimen S5-B was measured to obtain the residual stress redistribution after PWHT. Originally, one measurement DH1, see figure 5.4a, was to be carried out in this specimen. The experimental results did not show a good agreement with the expected effect of PWHT obtained from FE simulations. This is discussed later. Nevertheless results are shown in figure 5.33. A second measurement DH2 was undertaken at 100mm around the circumference of the pipe from DH1 and also at the weld centre line. The second experimental measurement was undertaken only to a depth of 40mm through the wall thickness. The results from the second measurement are shown in figure 5.34.

For depths greater than 40mm, the residual stresses in the hoop and axial directions were close to zero. This is as expected since trepanning of the core through the full depth of the wall had not been completed. For depths less than 40mm, it is clear that the residual stresses were much lower than for the first set of measurements. The reasons for the differences are not known, and it appears that the influence of PWHT can depend on location around the circumference of the butt-welded cylinder. The results shown in figures 5.33 and 5.34 are combined in figure 5.35. Figure 5.35a shows the two residual stress measurements compared with the FE simulation. The released residual stresses from DH2 on the first 35mm of the wall thickness from the outer surface are combined with the remaining 30mm of DH1 since trepanning was not carried out all the way through the specimen thickness. This is shown in figure 5.35b where combined measured residual stresses are compared with FE simulation. In this case a good agreement was obtained.

When compared with the as-welded results from the S5 specimen A, the results from hole 2 clearly demonstrated stress relief, whereas results from hole 1 suggested that heat treatment had induced patchy stress redistribution. The possible reasons for this behaviour are local stress variations (from bead to bead) or the presence of a high triaxial stress field. This significantly inhibits thermal stress relaxation. It should be noted that a high triaxial stress field was predicted in the outer 25% of the weld by the FE analysis (Bouchard, 1998).

For the VORSAC specimen A, the results obtained for the weld centre line locations are presented in figure 5.36. Significant stress relief was obtained between before and after PWHT. This relief was of the order of a third to a fourth of the intensity for the hoop stress, which brought the residual stresses to 100MPa and half to a third of the intensity for the axial stress also reducing to 100MPa. The distribution of residual stresses through the wall thickness was the same as for the as-welded case except that the intensity was lower, and the cross-over from tension to compression was at a similar location. It is also remarkable that the intensity of stresses after PWHT was identical for each case although their initial residual stress distributions were different before PWHT. This shows that although there can be differences in the as-welded state due to weld procedure, since the PWHT is exactly the same for both cases and material characteristics identical, the final result was essentially identical.

For the heat-affected zone shown in figure 5.37, results were similar to the weld centre line. It was observed that the intensity of residual stresses could be simply scaled since the distribution through the wall thickness was identical to the as-welded case. For the heat affected zone, the same approach can be used. Also, the intensity of residual stresses after PWHT was also the same (at 100MPa).

5.9. Influence of ageing

Experimental measurements at different stages of the ageing process attempted to reveal the evolution of residual stresses with lifetime of the specimen under working conditions. Only one specimen VORSAC specimen V-B was studied to assess the residual stress variation through ageing. This leads to uncertainty when making a general assessment about how the ageing process changes the residual stresses. A direct comparison of the experimental residual stresses at different ageing times did not in general enable any direct assessment of the influence of the ageing process to be made. However the FE results presented in the next chapter revealed significant changes, which makes the comparison with experiment easier.

Residual stresses were compared from measurements on VORSAC specimen V-B at the different stages through ageing. Deep-hole measurements were carried out at the beginning of life (as-welded state), after 182 hrs, 2426 hrs and 6989 hours. However, results have not shown a big variation in the intensity of residual stresses.

The ageing process was carried out by inserting the specimen into a furnace at 550°C, and leaving it for various times. Experimental measurements were carried out in the HAZ. Surface centre hole residual stress measurements were also made at different locations across the weld on the outer surface. Figure 5.38 shows the hoop and axial surface residual stresses from centre-hole measurements. The through thickness distribution of axial and hoop residual stresses from deep-hole measurements are shown in figure 5.39.

For the deep-hole results, the hoop stress was respectively located between 200MPa and 300MPa in tension on the outer surface and crossed over into compression at about 60% of the wall thickness to reach a maximum compressive stress between 100MPa and 150MPa on the inner surface. The axial stress started in tension at about 200MPa on the outer face, crossed over to compression at about 50% of the wall thickness and reached a peak of compressive stress at –150MPa back to –50MPa on the inner surface. No direct inference about the influence of ageing could be obtained directly from these results but comparisons with FE results in chapter 6 provide an improved understanding.

5.10. Influence of weld repair

Welded components are sometimes repaired during manufacture to remedy fabrication defects found by inspection, or repaired in-service following discovery of cracking. However, non-stress relieved repair welds tend to increase the magnitude and triaxial nature of the weld residual stress field, and therefore may increase the component's susceptibility to degradation mechanisms. In order to assess the effect of a repair weld on the structural integrity of the component, it is important to quantify the repaired residual stress distribution through the wall thickness.

Experimental measurements were carried out in the 35mm wall thickness butt-welded pipes. Three measurements were carried out before any repair was included and three after weld repair.

Experimental results are shown in figure 5.40 and 5.41. For the weld centre line location, the largest measured stress occurred in the hoop direction at about 8mm to 10mm from the outer surface for the centre of the 25% depth weld repair. The insertion of the 25% depth weld repair had increased the tensile residual stress both in the hoop and axial directions from 300MPa to 500MPa for the hoop and from 250MPa to 400MPa for the axial direction. At the inner wall, residual stresses were compressive in the hoop direction at –100MPa and tensile in the axial direction at 200MPa. The axial stress distribution showed a shift of the repaired weld residual stress towards tension where the hoop stress was higher close to the outer face.

A deep-hole measurement, undertaken 25mm ahead of the weld repair, showed a small zone of influence of the weld repair. Since the repairs were of short length, it was expected that the distribution of residual stresses would change from tension in the weld into compression out of the weld along its main axis on the outer face of the specimen. This will be presented in the next chapter with the comparison with FE analysis. It was not observed in the experimental measurement.

The largest measured stress for the HAZ location occured in the hoop direction at a position 8mm below the outer surface. At the inner wall the hoop stress was compressive. It appeared that introducing the 25% weld repair has reduced the peak

tensile hoop residual stress to about one half of the value of the girth weld, whereas the 75% repair peak hoop stress remained unchanged at 400MPa. However, on the inner surface the hoop residual stress increased from about –100MPa to 100MPa for the 75% case. These results can be understood when it is realised that hoop stresses adjacent to repair welds drop very rapidly in the transverse direction, and therefore the measured magnitude will be very sensitive to the exact position of the deep-hole relative the repair weld fusion boundary. The axial residual stress measurements showed that the introduction of repairs induced a net section tensile component of axial stress at mid-repair length, with the deeper repair having the greater effect. In addition, the peak magnitude of measured axial stress at the deep repair was 350MPa, which was much greater than the peak value of 200MPa in the original girth weld. Thus the deep repair increased the biaxial nature of the residual stress field just beneath the outer surface.

5.11. Complex geometry

5.11.1. End-cap to cylinder specimen

This specimen was provided by Rolls Royce Marine (RRM), which showed interest in measuring the distribution of residual stresses through a thick end-cap to cylinder weld of 110mm. RRM carried out the FE analysis on a 2D axisymmetric model using a similar technique as the one employed by British Energy. The schematic of the specimen is shown in figure 5.10. The FE model is carried out using multi-layer of weld passes and final pass after cooling corresponds to the as-welded case. The evaluated residual stresses are shown in figure 5.42.

As expected from the comparative geometry with the butt-welded cylinder, the stress distributions through the wall thickness show similarity to the simple cylinders. The hoop and axial residual stresses are both tensile close to the outer surface with a hoop stress higher and close to the yield stress at 350MPa. The axial residual stress is about 100MPa lower at 250MPa. The residual stresses go to compression at about the mid-wall thickness but due to the constraint of the specimen thickness, the residual stresses reach only –100MPa and return to zero close to the inner surface.

5.11.2. Nozzle specimen

For the ex-service nozzle, measurements were obtained through the thickness of the component at locations, A to C, shown in Figure 5.43 and 5.44. Only one measurement was carried out during this project at location A shown in Figure 5.10. Location A was a line through the cylinder. The line was orientated at 60° to the axis of the nozzle coinciding with observed service degradation. Location B was a radial line, (relative to the axis of the nozzle), through the centre of the weld. Location C was also a radial line in the parent material of the cylinder. For the prior-to-service nozzle, measurements were confined to location A. The lines at each location define the axis of the reference hole used.

For the nozzle-to-cylinder component, measurements were obtained in both the as-welded and post-service conditions. Results at location A for these two conditions are shown in Figure 5.43. The orientation of the measured residual stresses is also shown in the Figure. The largest measured residual stress occurred in the nozzle hoop-cylinder axial plane, normal to line A, towards the outer surface of the cylinder. This residual stress was tensile for depths up to about 25mm. Thereafter, it was compressive through to the inner surface of the cylinder. A similar pattern occurred for the residual stress, σ_y, along the axis of the cylinder, although the magnitude was lower than for the σ_x stress. For the post service condition, both σ_x and σ_y stresses at the outer surface reduced to about one half their as-welded values, with the peak σ_x residual stress at about 200MPa near to the outer surface.

Measured residual stresses at locations B and C for the post-service condition are shown in Figure 5.44. The directions of the residual stresses σ_x and σ_y are also indicated in the Figure. The orientations of these stresses differ at each location. Compared with location A, the residual stresses at B and C were lower, with the maximum tensile residual stresses again on the outer surface of the component. Residual stresses at all locations on the inner surface of the component were either compressive or close to zero.

5.11.3. Stub-beam specimen

The 'Stub-beam' specimen was a square section welded on the side of a thick cylinder, with most of the weld being on the side of the square section. The cylinder was 63.5mm wall thickness and the square section was 60.5mm thick. The weld preparation has the form of a 'J' shape of 1.75" depth on the 'Stub-beam'. The square section was welded to the pipe using a manual metal arc process with waving electrodes of diameter between 4mm and 10mm. Young's modulus for the two stainless steels was 195GPa, and yield strengths for the two steels were 245MPa and 400MPa for the weld metal. Three measurements were carried out both in the weld and the heat-affected zone (HAZ) of the weld. The global arrangement of the specimen is shown in figure 5.11.

Measurements were obtained through the thickness of the component at locations 1 to 3 shown in Figure 5.11b. Location 1 was a line in the heat-affected zone of the weld, through the cylinder wall thickness at an angle of 30° from the cylinder axis. Line 2 was in the weld centre line at an angle of 10° from the cylinder axis and line 3 was in the HAZ of the square section at an angle of 20° from the cylinder axis, following the weld HAZ.

The measured residual stresses are shown in figure 5.45. All measurements show an identical tensile residual stress close to the outer surface around 400MPa. Line 1, which goes directly into the parent material, however decreases rapidly towards compressive residual stresses at about 30mm depth. The other two measurements stay in tension up to about 40mm to 50mm for line 3, which is in the HAZ and over 50mm for line 2 located in the weld. Locations 2 and 3 show tensile residual stresses almost all the way through the wall thickness. In the three cases, longitudinal residual stresses are higher than the transverse residual stress.

5.12. Concluding remarks

This chapter has presented all the experimental measurements carried out in this project. The description of the results presented attempted to give a global understanding of the residual stress distribution through the wall thickness of the different welded specimens. Since any experimental technique has random errors due

to different factors (some have been presented earlier on for the deep-hole technique), it is clearly difficult to assess and compare the exact value of evaluated residual stresses for each specimen. Also, it was presented that although the measurement location and specimen type should be the same (for example: Same welding process or same specimen but two identical location but not at the same point), they have shown different stress distributions. Therefore, a general trend can be obtained for the different cases and give an understanding of the variations both in the axial, hoop and through thickness directions. The deep-hole technique showed good global reliability concerning accuracy of results especially compared with FE simulations (shown in chapter 6).

Specific residual stress characteristics presented earlier on are summarised below :

- The effect of post weld heat treatment for 2.5 hours at 750°C on the 65mm girth-weld mock-up suggest that stress relief processes in real welds are very in-homogeneous. This effect is more evident below the outer cap passes, where hydrostatic stresses are likely to be significant.

- The evaluated residual stresses for the weld centre line in the 65mm thick narrow gap TIG specimen mock-up were found to be greater in magnitude than the MMA procedure stresses and had distinctly different through-wall profiles. However, the measured stresses in the TIG HAZ were found similar in magnitude to the MMA welds.

- The influence of wall thickness of the different specimen, showed small influence on the residual stress distribution through the thickness in the as-welded conditions. Since the observed trend is similar for variation of thickness between 35mm and 110mm, this factor is not of significant importance for the specific distribution of residual stresses in each specimen.

- The measured residual stress profiles after thermally ageing the 65mm VORSAC specimen at 550°C for different times are very similar to the as-welded profiles. A good correlation is observed at the different stage of ageing but the significant

drop shown by the FE analysis at the first stage has not been observed in the measurements.

- It is shown in the 35mm butt-welded specimen that repairs significantly changed the original as-welded residual stress-state. Both repairs introduced a local tensile membrane component of stress transverse to the weld (pipe axial direction). Also the deep repair increased both the peak value of transverse stress and the biaxial ratio of in-plane stresses. It is noticeable that the stress intensity close to the bore for the shallow repair has decreased and is probably due to a reheat of the specimen on the inner part of the wall.

CHAPTER 6 : COMPARISON BETWEEN RESULTS FROM EXPERIMENTS AND FINITE ELEMENT ANALYSES

6.1. Introduction

In chapter 4 a number of calibration experiments were carried out as a means of ensuring that the deep-hole method is an accurate technique for measuring residual stresses. In the case of welded components it is extremely difficult to verify that accurate information about the residual stresses have been obtained. Alternative measurement methods such as neutron diffraction are unable to obtain measurements in many of the thick walled specimens examined in chapter 5. In this chapter the experimental measurements are compared with results from finite elements (FE) simulations. On the one hand, the experiments can be viewed as validation for the FE analyses; on the other hand the FE results act to provide improved confidence in the measurements.

The finite element analysis was carried out mainly by British Energy [Bouchard et al., 1996-1998]. The structure of this chapter follows as much possible the structure of the previous chapter, where aspects of specimen geometry, post weld heat treatment, ageing and weld repair are examined. Also included are FE results for residual stresses along the surfaces of the specimens.

A full description of the finite element technique used for the simulation of multi-pass welding process can be found elsewhere [Bouchard, 1996-1998]. This simulation process is that employed by British Energy although other simulations follow a similar methodology. Note that in most cases the analyses were carried out using a 2D axisymmetric model since the computing requirements to run 3D models were found to be excessive. The FE analysis is carried out in two steps called an uncoupled analysis using the ABAQUS [1998] FE code. First a thermal analysis is carried out where each bead (or lump bead) is included into the model with a specific heat and

record is made of the thermal distribution through the specimen with time. When the weld groove is completely filled up, there exists a full set of data of temperature and time records through the specimen for each pass. The results are then used to carry out an elastic plastic mechanical analysis to generate residual stresses with each lump bead inserted in the same way as for the thermal analysis. Once the process is completed, the state of the specimen after cooling represents the as-welded case. To simulate processes such as ageing or PWHT, further analyses are carried out.

Finite element simulations were carried out by British Energy plc. for the majority of the specimens presented in chapter 5. The material models used during this project were isotropic strain hardening. This was chosen since it was found to be more conservative than kinematic hardening and showed a better correlation with thin walled specimens. Also to avoid strain hardening beyond yield stress levels, the stress/strain curve were cut off at *1%* proof stress. New models are currently being developed using mixed kinematic/isotropic hardening combined with plastic strain annealing for molten weld and parent metal, which lead to more realistic residual stress levels of the order of 20% to 30% lower. Table 6.1 shows the range of simulations carried out. In the following section comparisons are made for results from simulations of welding of cylindrical butt-welds with thickness of 65, 35 and 19mm. Then results are reported for the influence of ageing, PWHT and weld repair. Finally, comparisons are made with simulations involving more complex shapes.

6.2. Cylinder Butt Welds - As-welded conditions

6.2.1. Surface residual stresses

Although different wall thicknesses (and small variations in the radius of specimens) were studied in the experimental work, it was shown that fairly similar trends were found in the distributions of the residual stresses through the thickness both in the longitudinal and transverse directions (relative to the main welding axis). Also, for as-welded conditions, the maximum measured residual stresses were below and close to the yield stress. Measured surface residual stresses using the deep-hole method, for the as-welded condition, on the outer surface is presented in figure 6.1. The hoop and axial residual stresses for different butt-welded pipes are collated.

Results for the inner surface are shown on figure 6.2. Also shown in figure 6.1 and 6.2 are experimental results from centre hole measurements taken from VORSAC specimen V-A. Finally, results from the FE simulation are shown as a function of distance across the weld (i.e. transverse to the main axis of the weld). The FE results correspond to two simulations ; with the weld cap retained, and with the weld cap removed.

The predicted distribution of hoop residual stress along the outer surface, for distance far away from the weld centre line, is consistent with experimental results from surface centre hole measurements. However the predicted magnitude is significantly greater close to the weld centre line and at the HAZ. This overestimation will be shown later in the through thickness residual stress profiles. The predicted residual stresses tended to be larger than the measured residual stresses on the outer surface of the specimen.

The predicted and measured axial residual stress profiles show reasonable agreement well away from the weld centre line. The predicted stresses are generally greater in magnitude when the weld pass sequencing effects, which affect the local residual stresses, are taken into account (Bouchard, 1996, 1998). It is evident that the presence of the weld cap has a major influence on the local residual stresses. The caps are locally machined to facilitate both the deep-hole and centre hole measurement techniques.

The predicted inner surface residual stresses compared with measured residual stresses are shown in figure 6.2. At the weld centre line the predicted values compare well with experiments. It should be noted that the finite element model has not attempted to simulate the weld root details, and therefore cannot be expected to capture accurately the local surface residual stress field.

6.2.2. 65mm thick cylinders

In this section results from FE analysis and experimental measurements for the as-welded conditions are compared. The experimental data are the same as those shown in section 5.4 to 5.7 but only specimens of 65mm wall thickness are

considered. For the FE analyses, results are taken from simulations with the weld cap removed.

As well as the detailed finite element residual stress analysis been carried out using the simulation procedure for thick section welds with 'lumped' passes as described earlier, residual stress analyses were carried out for the VORSAC specimen using SYSWELD by the Institut de Soudure [1999].

The predicted residual stresses for an analysis for specimen S5-A are compared with the measured data in figure 6.3 for the weld centre line. The distribution of the deep-hole and FE through wall residual stress profiles are almost identical. However, the predicted hoop residual stresses below the outer surface weld cap are up to 180MPa greater than measured. At the inner surface, low values of compressive hoop and tensile axial residual stress (<100MPa in magnitude) are predicted compared to the deep-hole measurements. However, again it should be noted that the finite element model carried out by British Energy had not attempted to simulate the weld root details, and therefore would not capture the local residual stress field. It is also noticeable that both FE analyses (ABAQUS and SYSWELD) provided essentially the same residual stress distributions through the thickness.

Overall, the measured residual stresses confirm that the finite element models have captured the general through wall residual stress distributions and over-predict the maximum stress levels.

Comparisons for the heat-affected zone are shown in figure 6.4. The FE simulations are again from ABAQUS at British Energy and SYSWELD at the Institut de Soudure. Here again, the deep-hole and FE through wall stress profiles are very similar, as found for the weld centre line location. The predicted hoop residual stresses below the outer surface weld cap are greater than measured by up to about 170MPa. The compressive axial residual stresses predicted by the FE analysis near the inner surface are also greater in magnitude than measured by the deep-hole method.

6.2.3. 35mm thick cylinder

In this section, comparison between experiment and FE simulations are presented for the 35mm thick butt-welded cylinder. Experimental results from this specimen have already been presented in section 5.10. An axisymmetric (2-D) representation of the girth weld was used to determine the original as-welded residual stress-state using the method developed by British Energy. Figure 6.5 shows the comparison for the as-welded case in the weld centre line and heat affected zone.

Weld centre line

Results for the weld centre line are shown in figure 6.5a. The maximum tensile hoop and axial residual stress near the outer surface are almost identical at 300MPa. However, towards the inner surface the hoop residual stress remains compressive at -150MPa where the axial residual stress returns into tensile up to 150MPa. There is a reasonably good agreement between experiment and FE simulation, however the predicted residual stresses overestimate the experimental measurements. The FE hoop residual stress is overestimated by about 200MPa at the outer surface although a good comparison is observed at the inner surface. On the other hand, the FE transverse residual stresses show a good comparison at the outer surface but more tensile prediction at the inner edge. Globally, the experimental measurements picked up the through wall stress distributions although a 20mm core was used for a 40mm wall thickness.

Heat-affected zone

Results for the HAZ location are shown in Figure 6.5b. The results obtained for the HAZ locations are different to that from the weld centre line. For the as welded case, the largest measured stress occurred in the hoop direction at a position 7mm below the outer surface. At the inner wall the hoop stress was compressive. The peak axial residual stress was about half the value of the hoop residual stress. Overall, the agreement between the prediction and the experimental measurements is remarkably good bearing in mind the assumptions adopted in both the measurement method and

the FE analysis. The shapes of the profiles match extremely well in each direction. The axial residual stresses differ near the inner surface, but this is not surprising because the weld root area was simplified in the FE analysis, the main interest being on correct modelling of the outer weld region.

6.3. Influence of ageing and PWHT

6.3.1. Ageing

The study of the ageing process was undertaken only on one specimen VORSAC specimen V-B. A series of experimental measurements were made after ageing at various intervals. These results were obtained at the HAZ and will be compared with FE analysis results on a line normal to the surface of the specimen and not following directly the heat affected zone. Results are presented in Figures 6.6 to 6.8. The experimental through thickness results were presented in the previous chapter and in figures 5.36 to 5.39.

Figure 6.6a shows the predicted residual stress distribution through the specimen wall thickness for the hoop and axial directions respectively in the weld centre line. Each residual stress component decreases in magnitude during the course of ageing at 550°C with the regions suffering initially high levels of stress showing the largest reduction. The heat affected zone location shown in Figure 6.6b is similar to the weld centre line location.

Figure 6.7a to 6.7d show the comparisons between the predicted and measured residual stress distributions through the wall thickness at different times of ageing. A very good correlation is observed for the different ageing times between 182 and 7500 hours although the predicted residual stresses for the as-welded condition overestimate the measured residual stresses in the as-welded condition. This confirms what was observed in other butt-welded specimens.

The surface measured and predicted residual stresses are compared in figure 6.9. Results are shown for the hoop and axial residual stress from the FE simulation, and experimental surface hole and deep-hole measurements. Conditions are presented for

different ageing times up to 8000 hours. Although the two VORSAC specimens A and B were assumed to be identical, it is observed that the intensity of residual stresses present in specimen A were different on average than in specimen B. This is believed to be partly due to the sensitivity in location of the deep-hole measurement location. When deep-hole experimental results are compared with results from FE simulation, the following observations are made. The as-welded residual stresses in specimen B appeared to have lower residual stress than after ageing. However, when residual stresses for the as-welded case in component A are included with the measurements for different ageing times in component B, there is a definite decrease in residual stresses. This is similar to the FE analysis results both in the hoop and axial directions. It is less clear however why the surface hole measurements are lower in intensity than deep-hole results but follow the same trend. There is a similar pattern between surface hole and deep-hole measurements. There was an increase of residual stresses between as-welded condition and after 182 hours ageing in component B for the hoop stress distribution but not the axial stresses.

6.3.2. After Post Weld Heat Treatment

Comparisons are made between measured and predicted residual stresses in two components, respectively the S5-B and VORSAC specimen A. Through thickness residual stress distributions from FE simulations and deep-hole measurements are shown. Also included are the surface hole measurements for the VORSAC specimen A. FE simulations were obtained by taking the as-welded FE simulations and allowing creep to occur. The details of the method are given by Goldthorp and Bouchard [VORSAC Work Package 2 report, 1999]. In the case of specimen S5-B the measured residual stresses are results combined from two sets of measurements DH1 and DH2 (see section 5.8).

Figure 6.9 shows the results after PWHT for S5-B. The comparison between predicted and measured residual stresses in this case was remarkably good. Experimental results and results from FE simulations for VORSAC specimen A are shown in figure 6.10 and 6.11. Figure 6.10 shows results obtained at the weld centre line, and results obtained at the HAZ are shown in figure 6.11. Overall there is excellent agreement between the measurements and predictions. It is notable that the

residual stresses obtained using the surface hole technique were generally found to be close to zero in the HAZ. The predictions and DH measurements indicate that tensile residual stresses of about 100MPa occurred through the thickness.

6.4. Weld repair

In the previous chapter, residual stress distributions in weld repairs were presented for a cylindrical specimen of wall thickness 35mm. As-welded experimental results for this specimen were compared with results from FE simulations in section 6.2.3. For the repair weld two finite element analyses were carried out to simulate the repair weld residual stresses. Each employed the ABAQUS finite element code. The first finite element analysis consisted of a 3D model of the pipe constructed using composite shell elements and the as-welded residual stress-state from the axisymmetric analysis mapped around the entire circumference. Then, at defined locations, excavation of material was simulated using a layer activation/deactivation scheme. The introduction of repair weld metal was idealised using four "lumped" beads, rather than representing the many passes (greater than 30) used. A thermal transient analysis followed by a mechanical analysis was performed to simulate the development of residual stress arising from the deep repair. This procedure is described by Zhang et al (1997). A second finite element analysis, using the original axisymmetric model, was performed by British Energy to simulate the detailed deposition of each repair weld bead. The stiffness of the axisymmetric model was modified to represent correctly the restraining effect of the un-repaired section. This was achieved by including a dummy beam tied to the model using multi-point constraints. The beam properties and constraints were derived from a 3-D shell model. The repair weld was simulated by first excavating original weld and parent material, and then adding new weld filler, bead by bead, in a similar way to the original girth weld analysis described above. In the following experimental results are compared with results from the FE simulations at several locations, principally at the weld centre line and in the HAZ.

Weld centre line

Results for the weld centre line location are shown in Figure 6.12. The experimental data are for the weld centre line in the as-welded condition, the centre of the 25% depth weld repair and 25mm ahead of the 25% depth weld repair. The FE analysis show results for the as welded case and the centre of the 75% depth weld repair. The experimental data show that the influence of the 25% depth weld repair outside of the weld repair is small since similar residual stresses to the as-welded case were obtained. However, the introduction of the 25% repair gave rise to higher tensile residual stresses in the weld repair and both in the hoop and axial direction. The comparison with the FE analysis is remarkably good. The distribution follows the experiment in the as welded case, except there is a small over estimate on the outer surface, which was observed in all previous cases. For the weld repair case, it appears that the predicted 75% weld repair stresses follow the measured residual stresses for the 25% weld repair stresses. This is probably due to the assumptions made in the FE analysis. The experimental results provided higher measured residual stresses for the 75% repair case than for the 25% repair. The experiments revealed an increase of residual stresses of about 100MPa to 200MPa for the introduction of the 25% depth repair. However, the FE analysis showed small variation compared with the as-welded case with the introduction of the 75% depth repair.

Heat-affected zone

Results for the HAZ are shown in figure 6.13. It appears that introducing the 25% weld repair had reduced the peak tensile hoop residual stress to about one half of the value of the girth weld, whereas the 75% repair peak hoop stress remained unchanged at 400MPa. However, on the inner surface the hoop residual stress increased from about −100MPa to +100MPa for the 75% repair case. These results can be understood when it is realised that hoop stresses adjacent to repair welds drop very rapidly in the transverse direction, and therefore the measured magnitude will be very sensitive to the exact position of the deep-hole relative to the repair weld fusion boundary. The axial residual stress measurements show that the introduction of repairs induced a net section tensile component of axial stress at mid-repair length,

with the deeper repair having the greater effect. In addition, the peak magnitude of measured axial stress at the 75% repair is 350MPa, which is much greater than the peak value of 200MPa in the original girth weld. Thus the deep repair has increased the bi-axial nature of the residual stress field just beneath the outer surface.

Figure 6.14 compares experimentally measured stresses from the 75% repair, with predicted profiles from the 3D and axisymmetric FE analyses for a deep weld repair with a 20° arc. There is good agreement between the shape of the measured distributions and simulated profiles from the 3D analysis, although the latter predicts higher magnitudes of stress. In contrast, the axisymmetric, bead-by-bead, FE analysis for the deep repair predicts more detailed profiles with higher stress gradients. These are broadly consistent with the 3D and experimental results, but do not closely match in detail. Both analyses predict a tensile net section axial stress at mid-length of the repair, as noted in the measured profile. The full results from the 3D FE analysis showed how such transverse stresses local to the repair are equilibrated by compression beyond the ends of the repair.

6.5. Complex geometry

Residual stress measurement using the deep-hole technique were carried out mostly in the cases where residual stresses were known (as in the calibration work presented in chapter 4) or in specimens where measurement locations were reasonably easy to access since the geometry was simple and principal directions known. However, measurements were also obtained in more complex shapes. Results were presented earlier in chapter 5. Measurements were carried out in three specimens of complex geometry, a cylinder end cap specimen, a nozzle-to-cylinder and a 'Stub-beam'.

6.5.1. Cylinder to end-cap specimen

The experimental results regarding the end cap to cylinder specimen were presented in section 5.11.1. The comparison between experimental and FE results is shown in figure 6.15. Results are shown for the weld centre line location.

The hoop stress shows the same type of difference as with the British Energy results since the FE results largely overestimate the measured stresses. The outer face stresses plateau at about 450MPa and drop to compression at about –50MPa at 85% depth of the wall thickness. The FE results follow almost the same trend with an increase factor of 1.8, which is considerably high. Possible explanation is the FE modelling for the welding process since British Energy results were found closer to the experiments although they also overestimated them.

The axial distribution in comparison is remarkably good for comparison between measured and predicted stresses. An exact match has been obtained and error band is less than 50MPa. It shows a tensile residual stress on the outer surface lower than the hoop stress at 350MPa going into compression at 25% depth and reaching maximal at about –100MPa at 75% depth from outer face. The inner subsurface stresses are more uncertain since there is a big variation between experiment and FE model in the last 5mm of the wall thickness. Also it was shown that the deep-hole technique had difficulty to evaluate accurately the residual stress distribution both close the surface and in presence of a high stress gradient.

The radial stress is much more interesting comparatively to the butt-welded pipes measured for British Energy. Since the specimen presents a high constraint on one end due to the presence of the end-cap (which does not exist on British Energy specimens), the radial displacement during welding is different on each side of the weld. This brings a higher radial stress than when both sides of the weld are free. This is shown on figure 6.15. An average of –150MPa measured radial stress exists and was also predicted. It is possible that a good correlation was observed between FE analysis and experiment since the deep-hole technique can easier evaluate constant through stresses than rapidly changing stresses. Since the component is very thick and specimen constrained on one side of the weld, the radial expansion during welding is different on both sides of the weld. An average radial displacement was clearly identified with the capacitance gauge readings. Results are shown in figure 3.36 and 3.37. There is a good average correlation between experiment and FE analysis, however, the trend is in the opposite direction. This comes from the evaluation of the radial stress in the experiment. In fact, radial displacements are recorded at equal time interval during the EDM process, which is different from the air probe measurements

(every 0.2mm in depth). This obliges to fit the capacitance gauge data to obtain readings every 0.2mm but without forcing the fit to go through zero strain at the specimen surface. The obtained radial residual stress gives therefore only an average value through the specimen thickness.

6.5.2. Nozzle specimen

The details of the comparison between measurements and results from FE simulations are given by Smith et al. [2000]. Here the results are summarised.

Predicted and measured residual stresses along the line at location A are shown in Figure 6.16, for both the pre-service (as-welded) and post-service (thermally aged) conditions. Line A represents the centre-line of the reference hole for deep-hole residual stress measurements. It is seen that the predicted residual stresses for the as-welded case are generally greater than measured values. Towards the outer surface of the component, there is reasonably good agreement between measured and predicted residual stresses for both as-welded and post-service conditions. However, for regions where measured and predicted residual stresses were compressive, the predictions appear to overestimate the compressive stresses.

Predicted and measured residual stresses at locations B and C for the post-service condition are compared in Figure. 6.17. At location B, the measured near surface residual stresses are seen to be larger than predicted, although at other depths the predicted stresses are higher. Note that the peak predicted residual stresses have relaxed to approximately one half of the as-welded level after 55,000 hours of service.

6.5.3. Stub-beam specimen

The FE analysis for this component was conducted by British Energy [Holt et al., 1998 and Smith, 1997]. The FE mesh used for this analysis is shown in figure 6.18. This was an idealised 2D generalised plane-strain analysis because a full 3D model was assumed to be time consuming. The boundary conditions were assumed fixed on the side of the idealised cylinder (left of the Figure) and permitted rotation on the side of the square section (right of the Figure). Further details of these analyses can be

found in Anderson and Little, 1999 and Bouchard et al., 1997. The results obtained from FE simulations of the stainless steel "Stub-beam" component are shown in Figure 6.19 together with experimental results. Since the FE analysis assumed quite different conditions, only broad agreement is observed between predictions and experiments.

Measured residual stresses at location 1 were mostly in the parent material of the cylinder section. There was a measured peak tensile residual stress at about 8mm below the outer surface, in the weld, at 400MPa both in the longitudinal and transverse direction. This was completely overestimated by the predictions with a peak stress at 600MPa in the longitudinal direction. The predicted transverse residual stress was underestimated with a peak value at 350MPa. Thereafter, the residual stress decreased rapidly towards low values, both for the experimental measurements and predictions since the location was further away from the weld.

Measured residual stresses at location 2 were at the weld centre line. The comparison between measurements and predictions is probably the worst because of modelling assumptions. The first 20mm of the wall thickness from the outer surface show the same trend as for location 1. There was a measured peak tensile residual stress at 400MPa largely overestimated by the predictions at 600MPa. However, the correlation of results thereafter is broadly representative of the longitudinal direction with stresses going towards zero. The predicted transverse residual stress was not in accordance with the measured stress between 20mm and 50mm depth. However, after about 50mm and onwards the results compare well. Note that the geometry of the square section attached to the cylinder is of slightly different size between the modelling and real geometry.

Measured residual stresses at location 3 were mostly in tension through the specimen thickness and adjacent to the weld. Peak values of the longitudinal and transverse residual stresses were 400MPa and 300MPa respectively at about 15mm from the outer surface to about zero on the inner surface. It is noticeable that force and moment equilibrium are not associated with the measured residual stress distribution across the section adjacent to the weld. The FE analyses overestimated the longitudinal residual stresses, particularly close to the outer surface of the specimen.

There is, however, excellent agreement between the measured and the predicted transverse residual stress.

6.6. Concluding remarks

This chapter compares experimental results with finite element predictions for the different components studied.

The main characteristic from the FE analysis were :

- The outer surface residual stress predictions for cylindrical butt-welds were mainly greater than the experiments. Nevertheless, a very good correlation was obtained for the as-welded, ageing and PWHT condition through the thickness.

- For the repair weld in the 35mm thick cylinder, the overall trends for the FE results and measurements were similar. However, detailed aspects were not good mainly due to the use of the deep-hole technique for thin sections and the assumptions in the FE analysis for the through thickness stress distribution of the weld repair. The sensitivity of the deep-hole technique is to be improved by using a smaller diameter core in presence of steep stress gradient. However, equibiaxiality of the stress was not observed in the FE analysis from the short repair possibly due to the assumptions in using a 2D axisymmetric model.

- A 2D axisymmetric model was used to model the end cap to cylinder specimen. The procedure employed was identical to the one used by British Energy. As for the British energy simulations, a big overestimation of the predicted hoop residual stress was observed. This is particularly true since the predicted residual stress exceeds the yield stress. On the other hand, the transverse residual stresses are very similar all through the wall thickness. Finally, the measured radial residual stress was found to be of the same intensity as the predictions, however, the distribution was not correct due to difficulty in the interpretation of experimental data.

- Only one measurement was carried out in the nozzle specimen during this research project, which is the location A after service aged condition. However, for each measurement, a good correlation between measurement and prediction was observed considering the assumptions used in the FE model.

Significant differences exist between the welded stub-beam specimen and the employed FE model, both in the geometry and boundary conditions. Nevertheless, comparisons between measured and predicted residual stresses show similar trends. As for the as-welded butt-welded cylinders, The FE analysis overestimates the measured residual stresses. Note that line 1 and 3, located in the parent metal, show a better agreement than line 2, which is situated in the weld centre line. This is probably due to the assumptions of the weld modelling.

CHAPTER 7 : GENERAL DISCUSSION

7.1. Introduction

This thesis has presented various aspects of research carried out using the deep-hole method for measuring residual stresses in welded components. First, a detailed assessment of the different steps in the technique was carried out including development of analysis, calibration tests and numerical simulations. These studies revealed the state of the art concerning the deep-hole method and the accuracy in measuring residual stresses in welded components. Second, an extensive set of experimental measurements was undertaken in welded specimens. An assessment has been made of the influence of specimen geometry, the effect of post weld heat treatment, ageing and weld repairs. Third, comparisons have been made between experimental measurements and numerical (FE) simulations. In this chapter a general discussion is given of the research presented in chapters 3 to 6.

7.2. Residual stress measurement using the deep-hole technique

This section examines the different aspects in the use of the deep-hole method. Some of the assumptions employed during the development of the theoretical analysis and their implications are considered. Features about the calibration and accuracy of measurements are also discussed.

7.2.1. Summary of the technique

The initial step in the deep-hole method was to fit bushes on the surface of the specimen, which act as a reference since they are stress free. It was shown in section 3.2.2 that using pins to locate the bushes was not adequate since it generated a stress concentration around the hole on the specimen surface. This was particularly shown when undertaking the bending calibration tests. The intensity of the stress

concentration is directly related to the residual stress present. This stress concentration was found to extend into the specimen thickness by about 10mm to 15mm. It was therefore decided to glue the reference bushes onto the specimen surface.

Another aspect in using the reference bushes was to attempt to reduce the air gap between the bush and the specimen. This enabled air probe measurements of hole distortion to be made near to the specimen surface accurately. Since the bush acts as an extension of the gun-drilled reference hole, it is possible to evaluate the residual stresses very close to specimen surface. However, when there is an air gap between the specimen surface and the reference bush (i.e. there is a thick layer of glue) the minimum distance over which the measurement was accurate was no less than the air probe diameter.

The second step in the experimental procedure was to gun-drill the reference hole. The gun-drilled surface roughness (i.e. ±15μm) was shown to be within the range of air probe measurement calibrations. However, if the reference hole is to be decreased for a miniaturisation of the process, gun-drilling may have to be discarded since the range of air probe measurements decreases with probe diameter. Also, it is not always possible to obtain a small diameter gun-drill.

The only assessment of the reference hole surface roughness was through a comparison of the air probe reading along the reference hole and measurements undertaken using a tallysurf machine. Since the air probe measures only an average diameter over a small surface area ($3mm^2$), the tallysurf was able to measure more detail. However a good comparison of diameter measurement before and after trepanning revealed that the air probe was able to monitor the major peaks and troughs.

The third step was to measure the reference hole diameter using the air probe system. The air probe system has not been changed in this research project compared to the work carried out by Bonner [1996]. However, a thorough assessment of the device as well as its automation and accuracy were developed. The air probe measures the hole diameter using compressed air via two diametrically opposite holes in the

head of the probe. This measurement is an average value of the air pressure and hence diameter. Calibrations were undertaken to assess reliability and accuracy of the measurements along the hole. It was shown that a typical error band taking account of the whole system was of about ±1μm. Since the air probe was calibrated using calibration rings of known diameter, this error band was fairly constant and not dependant on the hole diameter within the calibration range. This accuracy corresponds to an accuracy of about 30MPa for Young's modulus of 200GPa. However, the accuracy will also depend on the residual stress distribution through the specimen (i.e. stress gradient and intensity). For a constant residual stress, which was used in the calibration tests, this error band was decreased significantly (down to about 5MPa). However, for a steep stress gradient (100MPa/mm for the autofrettaged tube) it is estimated there were larger errors (up to about 80MPa).

The two remaining steps in the deep-hole technique were electro-discharge machining (EDM) and capacitance gauge measurements of changes in core height. The capacitance gauge measurement system was developed in conjunction with the air probe system in an attempt to measure a 3D stress distribution in the specimen. The capacitance system was calibrated using a tensile test and revealed that it was reliable, providing accurate displacements with an error less than 0.1μm. However, it was difficult to use on butt-welded specimens. It was not anticipated that the EDM process would generate strong thermal effect that would disturb the capacitance gauge measurements. However, it was found that the heat generated by the electrode during the EDM operation had a major effect of the core expansion measurement. Furthermore, the residual stress in the direction of the reference hole axis was found from finite element analyses to be relatively small. The numerical simulation on multi-pass weld carried out by British Energy did not show residual stresses greater than 60MPa or 80MPa in this direction. The corresponding displacement from the capacitance gauges for 100MPa evaluated over an increment of 0.2mm with a Young's modulus of 200GPa is about 0.1 μm. Also, due to the transient heat input from the EDM process, it was difficult to measure this displacement. However, it was shown in the case of the end-cap to cylinder specimen that if the radial stress is large and the displacement are of the same order as the thermal displacement then it was possible to obtain the residual stress along the axis of the reference hole.

7.2.2. Developments in analysis

This section discusses the assumptions adopted in the analysis for converting measured strains into stresses. It was assumed that the gun drilled reference hole is a principal stress direction. This approach has not been modified in this research project and any attempt to use the technique on a different configuration would lead incorrect estimates of the residual stresses if the third axis residual stress was significant.

At each point measured through the specimen thickness it was considered that there existed a 2D plane stress state. It was clear that each measurement was not independent and depended on the stress distribution. Using a 2D plane stress analysis provided accurate results if σ_z (along the axis of the reference hole) was small. If σ_z was big, this would lead to big errors and a plane strain analysis would be more adequate. Therefore, the choice of the analysis depends on the specimen wall thickness, where small values of σ_z residual stress would be expected for thin components.

It was assumed that the residual stresses present into the core would relax elastically when trepanning the specimen. However, it was shown for the autofrettaged tube specimen that if the core diameter was too large, then residual stresses were retained in the core after trepanning. The retained residual stresses were found to be close to the error in measured residual stress distribution.

The influence of number of angles measured in the stress evaluation was shown to be important. A maximum error of about 50MPa could be expected between the fitted strains using three or sixteen angles measured. If sixteen angles or eighteen angles were measured the error was then minimised. However, the least squares fit through the experimental data became important when only three or four angles were used. If a more complex analysis were to be used to evaluate residual stresses as a function of angle around the reference hole, then more measurements enable a more detailed stress evaluation.

Finally, an attempt was made to assess the influence of weld material anisotropy. No direct evidence was found to indicate that this would have an influence on the measured residual stresses. There was a possible variation of about ±25% in the residual stresses if it was assumed that the local crystallographic Young's modulus varied by ±25%.

7.2.3. Calibration tests

The calibration tests were developed to assess the reliability of the deep-hole method in measuring residual stresses. Since the measured stress distributions matched the expected and predicted stresses, it was observed that the system was reliable for the calibration tests involving bending, torsion and hydrostatic pressure.

The influence of the EDM core diameter was shown to be important in two ways. Initially, the EDM diameter was chosen to be outside the zone of the stress concentration of the reference hole (three times the reference hole diameter, about 20mm). However, since the stress concentration is only significant close to the edge of the hole, this was not appropriate in the case of a steep stress gradient or a thin wall specimen. On the other hand, the core diameter cannot be too close to the hole edge since it would be necessary to include the stress concentration into the analysis. It was shown in the literature review that as long as the stress intensity does not exceed 2/3 of the yield stress (due to stress concentration) then it is possible to decrease the core diameter without incurring large errors. Ultimately, the optimum core diameter should be as small as possible to release entirely the residual stresses, taking account of the stress variations and wall thickness but not to exceed a residual stress $2/3^{rd}$ of the yield stress for elastic analysis. The Fourier analysis given in section 3.3 does allow a full analysis to be carried out since it is able to measure residual stresses at any radius around the reference hole.

The calibration tests for hydrostatic, bending and torsion stresses revealed that the technique was reliable. However, note that for these tests the EDM operation was not carried out. A reference hole was introduced into the different specimens and different load intensities were applied so that deformations of the reference hole were measured. However, in the case of the autofrettaged tube, since a large stress gradient

was generated in the specimen, errors up to about 80MPa were found. This was observed experimentally and a comparison with numerical simulations revealed a similar error. However, FE simulations of the deep-hole technique using a smaller core diameter showed a improved stress relief and less locked-in stresses in the core. Nevertheless, a non-linear stress distribution was found in the square beam subjected to torsion.

Comparative measurements were made between experimental results obtained for the autofrettaged tube and neutron diffraction measurements undertaken on similar specimen by Stacey et al. [1985, 1988]. Results are shown in figure 7.1. Since identical material properties and specimen geometry were used, very similar results were measured. The maximum intensity of compressive residual stresses obtained from the Sachs, deep-hole and a neutron measurement technique is very similar. The results from the Sachs residual stress measurement technique is very much dependant on the curve fitting to the strains near to the bore, which may have influenced the residual stresses associated with reverse yielding at the bore of the tube.

Sachs and neutron results on the outer face of the pipe were found to be slightly into compression and were associated as a influence of the machining process. The deep-hole technique seems to indicate that residual stresses return to compression or close to zero on the outer surface.

7.2.4. Numerical simulations

One of the main assumptions developed for the deep-hole method is that each measurement through the wall thickness of the specimen is independent of adjacent displacements. However, in practice, there will be an influence and this could lead to errors in the measured residual stresses. The most obvious case is for a sharp stress gradient within a component (i.e. the autofrettaged tube). Between the 0.2mm measurement interval, there was a large change in residual stress. Ideally, to obtain complete stress relaxation at each point, the core wall thickness should be as thin as possible (eg 0.5mm). However, this is not currently practical and consequently by increasing the core diameter, there was an influence of adjacent points, which led to

an averaging of the residual stress and also the potential for locked in residual stresses in the core.

Finite element simulations were undertaken to assess the importance of plasticity created during gun-drilling and the influence of plasticity due to the presence of a stress concentration at the hole edge. In the case of simulation of the gun-drill operation, the amount of plasticity generated at the hole edge relative to the core diameter was found to be only about few percent. Therefore it was assumed not to be significant in distorting the existing residual stress state in the specimen. On the other hand, this plasticity is beneficial for the analysis since it increases locally the yield limit, which benefits the elastic relaxation of the residual stresses. For plastic deformation as a result of the stress concentration, it was shown that for a uniaxial stress, the local stress intensity had to be greater than 2/3 of the yield stress to disturb significantly the stress state. However, since there could be a biaxial stress state, the intensity of stress applied to generate this yield behaviour type was even higher. Nevertheless, in practice most residual stresses measured in this research appeared to be below the yield stress.

7.3. Measured residual stress distributions

The majority of the specimens measured for this research project were made using stainless steel AISI 316H. The results and comparison in chapter 5 and 6 are group together in the following discussion.

7.3.1. As-welded residual stress distributions

The question of accuracy of the technique is always difficult to assess. It was assumed that relaxation of residual stresses was entirely elastic so that a simple analysis could be carried out. The possibility of obtaining a measurement only partway through the specimen thickness was explored. This was assessed through an incremental procedure, which was carried out on the third measurement (DH3) of the 19mm butt-welded specimen. The trepanning process was interrupted at various depths through the wall thickness and the air-probe system used to obtain a set of hole

diameter measurements and the analysis of the displacements. Results are shown in figure 7.2. Between increment 1 (after 7mm trepanning) and increment 3 (after the complete trepanning), there was an elastic residual stress redistribution between tension and compression over the first 10mm of the wall thickness and returning to zero since the trepanning process had not finished. This redistribution was also observed in the finite element simulation carried out for the autofrettage tube.

The simulation of the deep-hole technique on the autofrettaged tube provided a comparison with experimental measurement for the measurement of residual stresses. It has also provided information of the elastic residual stress redistribution during the simulated trepanning by removing elements on the FE mesh. Figure 7.3 shows a comparison of the residual stress redistribution in the autofrettaged pipe. The lowest residual stress distribution represents the final state when the trepanning process is finished and the other stress distribution represents the stress state at 70% of the trepanned wall thickness. It is clear in this situation that any analyses carried out incrementally or part way through the residual stress field will not evaluate the correct stress distribution unless the redistribution is taken into account in the analysis. Beaney and Proctor [1974] suggested that an incremental analysis would provide correct results. This is not the case.

Results obtained for the 19mm thick butt-welded pipe in the HAZ using the 10mm core diameter are compared in figure 7.4 with numerical results obtained by Josephson [1983]. Josephson's results were obtained at the weld centre line of a 22mm ferritic steel butt-welded pipe using an FE analysis. It should be recalled that residual stress distributions obtained during this research revealed similar distributions irrespective of wall thickness. Note that the material properties of the weld metal for the ferritic steel were not known so the direct comparison is not possible. A good correlation is only observed between the two specimens for the axial residual stress.

A very similar comparison can be made in figure 7.5 where the 35mm thick butt-welded specimen is compared with results from Leggatt [1997] on a 32mm thick butt-welded ferritic pipe using the BRSL (Bloc Removal Sectioning and Layering) technique. A similar trend is observed between the two specimens, although the

material used by Josephson and Leggatt was a C-Mn steel with different material properties.

Bonner [1996] carried out deep-hole experimental measurements on an 84mm thick ferritic steel butt-welded pipe. These measured residual stresses are shown in figure 7.6 together with experimental measurements carried out during this project on 65mm thick stainless steel butt-welded pipes. Note that the weld geometry in each case was different and the weld width was 70mm on the outer surface for the 84mm thick pipe compared to 40mm for the stainless steel pipes. Two sets of measurements were carried out, one in the weld centre line and the other 24mm off the weld centre line. The residual stress distributions were almost completely in tension for the ferritic steel pipe. However, the residual stress distribution at 24mm away from the weld centre line shows a better comparison with the 65mm thick specimens than the measurement undertaken at the weld centre line.

Finite element simulations were undertaken by Brust [1981] on 33mm thick C-Mn butt-welded pipe. These are compared in figure 7.7 with the deep-hole measurements and FE simulations undertaken by British Energy at the HAZ of the 35mm thick stainless steel butt-welded specimen. A very good correlation is observed both between the experiment and the various FE analyses. Although the results from the FE analysis carried out by Brust provided a smoother through wall residual stress distribution than the British Energy results, it appears that in the latter case more detailed residual stress state were obtained. However, the results from the two FE analyses in the HAZ are very close. Even for the 35mm thick butt-welded specimen, better agreement may have been provided if the the deep-hole measurement used a 10mm diameter core.

Differences in residual stresses between TIG welds are shown in figure 7.8 and 7.9. In each figure a set of measurements obtained by Faure & Leggatt (1996) using the BRSL and centre hole measurement techniques on a stainless steel TIG specimen identical to the Narrow Gap specimen. Since only one measurement was undertaken with each technique, it is difficult to make a good comparison. Nevertheless, at the weld centre line, it is clear that the BRSL results revealed distinctively lower residual stress intensities, in both the hoop and axial directions. In contrast in figure 7.9 the

comparison in the heat-affected zone is very good. The BRSL results on the weld centre line are less convincing since the BRSL method should have produced an axial stress profile with force equilibrium across the weld centre line.

The differences in the residual stress distributions between specimens S5-A and S5-C were due only to the difference in the weld heat input procedure. This generated a higher residual stress state in the case of a lower heat input, which was at first surprising. In fusion welding processes, thermal contraction strains are always large enough to induce maximum stresses approaching the yield level. For thin section structures, the weld heat input has an important influence on the stress distribution associated with the global (long range restraint) response of the structure. However, for thick structures, the weld heat input probably does have significant effects on 'local' cyclic yield behaviour associated with multi-pass welding, and creep/relaxation effects. The possible difference between the two specimens was that the heat input of specimen A was sufficiently high to induce local creep relaxation of residual stresses which was not the case for specimen C.

7.3.2. Influence of specimen geometry

Comparison of residual stresses obtained from components of complex geometry and butt-welded pipes was presented in section 5.7. Significant differences were observed in the intensity of residual stresses. The main features are : The stub-beam specimen exhibited the highest constraint with high residual stresses on the outer surface, and the nozzle specimen appeared to show the lowest constraint with the lowest residual stresses. The butt-welded pipes and end cap to cylinder specimens lie in between these two extreme cases. A direct interpretation of these results would be that a potential site for failure in the stub beam specimen (i.e. the most critical) is in the weld centre line.

Results from all specimens shown in figure 5.27, revealed residual stresses between –200MPa and 100MPa at the inner surface. In the majority of cases the residual stresses changed into compression through the wall thickness, which is comforting for the structural integrity of the specimens. However, this was not the

case for the stub beam specimen, which revealed completely tensile residual stress distributions at the weld centre line. This was partly confirmed by the FE analysis undertaken by British Energy.

In the nozzle-to-cylinder component, there are a number of reasons for the differences between the predicted and measured residual stresses. Approximations and errors in the measurement method described above will give rise to uncertainty in the magnitude of the measured residual stresses. In addition, the finite element simulation relied upon a number of important assumptions in the thermal and mechanical analyses. A 2-D axisymmetric idealisation of a complex 3-D geometry was assumed. The axisymmetric model's stiffness (and therefore its constraint on the weld) will certainly differ from that of a cylinder. Its resistance to the weld hoop stress distribution would be expected to be greater, leading to an over-prediction of stress component, σ_x in Figure 5.19. Except for a region close to the outer surface of the component, this predicted stress is greater than measured. However, resistance to nozzle-axial loading in the axisymmetric model is likely to be similar to that of a cylinder (and a flat plate), leading to better predictions of σ_y stress.

The measured residual stress in the nozzle specimen at location A were compared with measured residual stresses on a 22mm thick T-joint by Leggatt [1997]. Both measurement locations were at the weld toe. The comparison of residual stress distribution is shown in figure 7.10. Although the component geometry was different, a similar stress distribution was observed. The stress distributions are shown as a function of normalised distance through the wall thickness. The hoop or longitudinal residual stress was found almost identical. Only small differences are observed in the transverse direction.

7.3.3. Influence of post weld heat treatment

For a specimen subjected to a post weld heat treatment, the initial as-welded residual stress distributions are changed and probably relatively close to each other with a maximum level of about 100MPa as shown in figure 7.11. It is clear that variations occur but these are reduced when PWHT was undertaken. However,

potential damage could be generated after original welding if the specimens were subjected to loading before residual stress relief. The comparison of results (figure 7.11) shows a very good correlation between experiment and FE analysis. All residual stresses are found between ±100MPa changing from tension on the outer surface to small compression on the inner surface.

However, experimental results presented in chapter 5 show that the influence of PWHT is not always as homogeneous as expected and that the beneficial effect of PWHT should be taken cautiously in the assessment of the structural integrity of specimens. In chapter 5 it was shown that PWHT undertaken on S5-B specimen was not homogeneous around the circumference of the pipe. Two measurements were made at 100mm apart and tensile residual stresses on the outer surface show variations of about 200MPa between the two measurements. However, this PWHT was undertaken for a short period of time and possible stress relaxation may not have occurred.

Experimental measurements undertaken in specimen V-A showed that adequate residual stress relief had taken place. The significant difference between the two specimens S5-B and V-A is that specimen S5-B was subjected to a thermal heat treatment of one hour where specimen V-A was subject to a thermal heat treatment of two and a half hours. In the case of specimen S5-B, it is possible that the PWHT process was too short for a complete residual stress relief. Two measurements have shown two completely different residual stress states. On the other hand, the heat treatment undertaken for two and a half hours revealed fairly homogeneous residual stress relaxation.

7.3.4. Influence of ageing

The influence of ageing was presented in chapter 5 and 6 through experiment and finite element results. Also, Fidler [1982] shows that the influence of heat treatment is a function of time and temperature. The ageing process, to a certain extent, can be assessed in the same way as a post weld heat treatment in terms of residual stress

relaxation. However, since the temperature is lower, the necessary time to relax the residual stresses is much longer. Also the degree of relaxation is lower.

One aspect shown in the experiment is that the residual stress redistribution between the as-welded condition and the first ageing time (182 hours) showed an increase in the hoop residual stresses. This was confirmed by measurements from both the deep-hole and centre hole techniques. However, the opposite trend was obtained for the axial residual stress. On the other hand, the FE analysis predicted relaxation from the as-welded condition (see figure 6.10) for all ageing times. An increase of the ageing time from this point however did reveal residual stress relaxation for both experimental results and also the FE analysis.

The through thickness residual stress distribution showed a very good comparison through the wall thickness between the experiment and FE analysis for the aged condition. However, FE analysis overestimated the residual stresses for the as-welded conditions near to the surface. This was shown earlier and the results imply that as creep analysis is not taken into account in the welding simulation, the as-welded residual stresses are overestimated. However, the specimens were welded over a period of about 40 hours and some degree of relaxation is expected.

7.3.5. Influence of weld repair

It appears that introducing the 25% weld repair has reduced the peak tensile hoop residual stress to about one half of the value of the girth weld, whereas the 75% repair peak hoop stress remained unchanged. These results can be understood when it is realised that hoop stresses adjacent to repair welds drop very rapidly in the transverse direction. Therefore the measured magnitude will be very sensitive to the exact position of the deep hole relative the repair weld fusion boundary. The axial stress measurements show that the introduction of repairs induced a net section tensile component of axial stress at mid-repair length, with the deeper repair having the greater effect. The deep repair has increased the bi-axial nature of the residual stress field just beneath the outer surface.

The comparison of experimentally measured stresses from the 75% repair, with predicted profiles from the 3-D and axi-symmetric FE analyses for a deep weld repair show a good agreement between the shape of the measured distributions and simulated profiles from the 3-D analysis, although the latter predicts higher magnitudes of stress. In contrast, the axi-symmetric, bead-by-bead, FE analysis for the deep repair predicts more detailed profiles with higher stress gradients. These are broadly consistent with the 3-D and experimental results, but do not closely match in detail. Both analyses predict a tensile net section axial stress at mid-length of the repair, as noted in the measured profile. The full results from the 3-D FE analysis showed how such transverse stresses local to the repair are equilibrated by compression beyond the ends of the repair.

A number of simplifying assumptions cause the differences in results observed for the 75% weld repair. The detailed axi-symmetric FE analysis indicates the presence of steep residual stress gradients through the wall of the pipe. In contrast, the 3-D composite shell analysis predicts a more uniform distribution of residual stress. This latter result is the consequence of using just 4 "lumped" beads. Furthermore a composite shell analysis only simulates the global response of the structure to the presence of the local repair. The good agreement between the experimental results and the 3-D analysis suggests that the measurement method using a 20mm core was also unable to detect steep residual stress gradients through the thickness. The work in this thesis has shown that using smaller cores to measure residual stress profiles with steep stress gradients can be achieved.

The measurements revealed that repairs significantly changed the original as-welded residual stress-state. Both repairs introduced a local tensile membrane component of stress transverse to the weld (pipe axial direction). Also the deep repair increased both the peak value of transverse stress and the bi-axial ratio of in-plane stresses. Finite element simulations of the deep weld repair, using 3-D composite shell and modified stiffness axisymmetric models, provided residual stress results with differing levels of detail. The simplified 3-D analysis results show good overall agreement with the measured stresses. However, the modified stiffness axisymmetric

analysis, which modelled each weld bead, indicates a more complex residual stress distribution than shown by either the 3-D analysis or experiments.

Experimental results from the 35mm thick butt-welded specimen at the location of the 25% weld repair are compared in figure 7.12 with residual stress distributions obtained by Leggatt [1997] in a 75mm thick C-Mn butt-welded pipe with a 40% depth weld repair. The position of the weld repair in both cases was different. The 35mm specimen had the weld repair in the weld centre line where the 75mm thick specimen had the 40% weld repair in the HAZ of the original weld. It is nevertheless interesting to compare the residual stress distribution since the depth of the weld repair was similar. Although the weld material properties are different, a good correlation is observed in the residual stress distribution through the wall thickness. The BRSL method for the C-Mn steel used by Leggatt shows almost an identical stress distribution as the deep-hole method for the 35mm butt-welded cylinder.

7.4. Comparison with standard code distributions

It is instructive to compare the present residual stresses with handbook and empirically based weld residual stress profiles which are recommended for structural assessment. These include recommendations of the ASME XI Task Group for Piping Flaw Evaluation [ASME, 1986] and SAQ evaluations [Brickstadt, 1996]. Two sets of comparison are made, one for the 65mm thick specimens and the other for the 35mm thick specimens.

In the case of the 65mm thick specimens the residual stress profiles are compared in figure 7.13 with the range of experimental results. The key points shown in figure 7.13 are:

- The ASME axial residual stress profile gives a good estimate of the peak tensile stress (about 300MPa) but indicates that this occurs on the inner wall. The measured maximum residual stress was on the outer surface rather than the inner. The ASME hoop stress recommendation underestimates the measured residual stress for the outer 40% of the section thickness. However, it is not surprising that

the ASME profiles are poor for 65mm thick welds. The original recommendations were based on residual stress measurements for pipe welds up to 33mm thick.

- The stress profile recommended by SAQ (Brickstad, 1996) are based on parametric FE simulations for austenitic girth welds up to 40mm thick. The axial distribution does not agree with experimental measurements for 65mm thick girth welds. The recommended hoop stress is based on the 0.2% weld yield, and provides an upper bound to all the measured 65mm specimens.

Similar to the thick section specimens, the estimated profiles for the 35mm thick specimen are shown in figure 7.14:

- The ASME axial residual stress profile gives a good estimate of the peak tensile stress at the inner surface, but greatly underestimates the tensile residual stresses towards the outer surface. Furthermore, the ASME hoop stress recommendation again underestimates the outer half of the section thickness.

- The FE based axial residual stress profile recommended by SAQ should be relevant to the 35mm thick stainless steel girth weld geometry. It provides roughly the correct through wall distribution over the inner half thickness but significantly underestimates the measured maximum tensile and compressive stress levels. Again, the recommended hoop stress is based on the 0.2% weld yield, and provides an upper bound to the measured stresses.

Similar observations can also be made for the residual stress distributions in the heat affected zone, which generally exhibit similar profiles but have lower magnitudes for both 65mm and 35mm thick girth welds.

The axial residual stress profiles recommended for integrity assessments by the SAQ and ASME for thick section austenitic girth welds are inaccurate and non-conservative when compared with experimental measurements. The hoop residual stress profiles recommended by ASME for non-stress relieved austenitic girth welds, are non-conservative compared with experimental measurements on the 35mm and

65mm thick girth welds studied. The profiles recommended by SAQ conservatively bound measured residual stresses for both the 35mm and 65mm thick MMA welds but do not cover peak stresses towards the outer surface.

CHAPTER 8 : CONCLUSIONS AND FUTURE WORK

In this thesis, the use and calibration of the deep-hole technique for measuring residual stresses in thick welded components were investigated. New developments were made to the measurement system and method of analysis. A careful assessment and calibration of the technique was also undertaken. The technique was used to measure residual stress distributions in a variety of components. The influences of section size and weld geometry, as well as the effects of heat treatment and weld repairs, were studied. In this chapter, general conclusions about the assessment of the deep-hole technique and residual stress measurements undertaken during this research are given.

8.1. General conclusions

It has been shown that the deep-hole technique is very reliable for measuring residual stresses. Nevertheless, the method requires further refinement particularly where there are steep stress gradients.

The experimental system was improved by avoiding the use of pins to locate the reference bushes onto the specimen. This was found to introduce a local stress concentration within the residual stress field. The front bushes were then glued onto the specimen surface to avoid this. Furthermore, the absence of an air gap between the bush and specimen improved the resolution of hole diameters near to the specimen surface.

The ECM trepanning system was replaced by an EDM system. This enabled a change of core diameter to be introduced. However, the EDM system introduced large thermal strains during trepanning, which made interpretation of the mechanical displacement in the direction of the reference hole difficult. Nevertheless, a new capacitance device was developed to measure the displacement in the direction of the reference hole. Calibration trials found that this device was reliable but difficult to use

in the presence of thermal strains. However, good accuracy was found if the displacement were of the same order as the thermal effects.

The air probe system continued to be the most appropriate method to measuring the reference hole diameter. The probe was not modified but a thorough assessment of its characteristics and improvements in the air probe rig improved its performance. The standard air probe reading accuracy was about ±1μm. An increase in the number of measured angles was developed. This allowed improved fits to strain data to be achieved and hence reduce errors in residual stress measurements.

A 2D plane stress analysis together with core height changes was used to convert measured strains to residual stresses. A new Fourier analysis was developed using stress coefficients. The first two terms in this analysis correspond to the 2D plane stress analysis. However, for more complex residual stress distributions, the Fourier analysis enables measurements of residual stresses at any angle around the reference hole, and also calculates the residual stress field by taking into account the reference hole diameter and the radius of the trepanned core.

It was found that the influence of anisotropic elastic properties could not be observed in the distortions of the reference hole although the differences in elastic properties were up to 26%.

The calibration tests undertaken to assess the deep-hole technique have shown that :

- The EDM diameter should not be of the same order as the specimen thickness but smaller to overcome averaging of the residual stress through the wall thickness.

- It is possible to use a core diameter within the stress concentration zone as long as residual stresses are below 2/3rd of the yield stress.

- Bending and torsion calibration tests revealed that errors in measured stresses were found to be within 10MPa.

- The measurement of steep stress gradients showed that much larger errors occurred because of the influence of stress distribution through the wall thickness.

- The simulation of gundrill plasticity was found to have a negligible effect on the residual stress measurements.

8.2. Residual stresses in welded components

The conclusions regarding residual stress distributions in welded components are now presented.

The overall influence of wall thickness on the butt-welded cylinders between 35mm and 110mm was shown to be small.

Residual stresses measured in a Narrow Gap TIG specimen was found to be higher than in standard MMA welds. The through-wall profiles of the residual stresses in the TIG weld were also distinctly different than the other MMA weld procedures. This was only at the weld centre line since the residual stresses were found to be identical in the HAZ for both TIG and MMA welds.

The effect of post-weld heat treatment (PWHT) on the 65mm MMA weld specimens was found to be inhomogeneous. Different residual stress redistributions were found for two different locations in the S5-B specimen probably due to a limited PWHT at 750°C for only one hour. However, the measurements undertaken in the V-A specimen were found more homogeneous when a PWHT at 750°C for 2.5 hours was undertaken.

The effect of ageing measured on specimen V-B up to 8000 hours at 550°C was observed. A good correlation was shown between experiment and FE analysis but only after 182 hours. The predicted initial drop in residual stresses was not measured by the experiments.

The introduction of a weld repair revealed a significant variation of the residual stress distribution compared to the as-welded case. The introduction of the deep repair (75%) showed an increase of the peak residual stress and generated biaxial in-plane residual stresses. This may due to the short length of the repair weld (20°). Contrary to this, the introduction of the shallow repair reduced the peak residual stress and also reduced the original residual stress intensity close to the bore due to the reheat of the specimen on the inner part of the wall.

The comparison of measured residual stresses with finite element simulations (carried out by British Energy) have shown the following:

- The predicted residual stresses were found to be greater near the specimen surface than experiment. This was probably due to the creep properties not being taken into account in the as-welded simulation. However, a good correlation between experiment and simulation was observed through the remainder of the wall thickness. Also, good correlation was observed through the complete wall thickness after ageing and PWHT.

- Similar trends were observed between experiments and the two different FE analyses on the 35mm repair weld specimen. A better agreement between experiment and simulation could be expected by using a smaller core diameter to resolve the steep stress gradient. The results from a 3D shell model revealed similarities with experimental results since only four beads were used through the wall thickness. This generated stress averaging through the wall thickness. The FE analysis carried out by British Energy revealed a more detailed residual stress distribution through the wall thickness.

- A similar trend was found between experiment and FE analysis for the radial stress in the end cap to cylinder component but difficulties in the interpretation of experimental results limited the assessment of the results.

- The finite element analysis carried out to simulate welding in the specimens of complex geometry showed that predicted residual stresses were similar to

experimental results. However the differences, particularly in the case of the stub beam specimen, were found to be due to the overconstraint in the finite element model, which generated higher residual stresses.

Finally, the recommendation of the ASME XI Task Group [1986] and SAQ [1996] need reassessment for thick welded components to prevent an underestimation of the residual stress distributions and provide better distributions through the wall thickness. The ASME recommendation was found completely inaccurate for the presented results. The SAQ recommendation is somehow more conservative in that it bounds the maximum residual stress intensity but not at the correct place through the wall thickness.

8.3. Recommendations for future work

This study attempted to provide a complete assessment of the deep-hole technique in measuring residual stresses in welded components. It is clear that a number of improvements can be made to obtain a experimental technique that is more versatile in its potential use. The following points are suggestions for further work to improve the deep-hole measurement technique.

- The deep-hole technique should be able to measure more complex residual stress fields. These are for example steep residual stress gradients or residual stress distributions that are not normal to the reference hole. This aspect could be by taking into account the ratio between the reference hole and core diameter. This would involve assessing the influence of the core diameter versus wall thickness, integration of the Fourier analysis to measure residual stresses as a function of angle around the reference hole and accurate measurement of deformation in the direction of the reference hole.

- A complete development of the measurement of residual stresses along the axis of the reference hole would be very useful since it would avoid using the reference hole axis as a principal stress direction. This would enable a more global stress evaluation.

- The presentation of a standardised procedure would be useful so that a generalisation of the technique could be envisaged. Furthermore, miniaturisation of the process would be very useful since measurements could be taken in situ. This involves redesign of the whole process since miniaturisation assumes a change of the experimental equipment.

REFERENCES

ABAQUS – 1998 – Finite Element Analysis code, Hibbit Karlson and Sorrensen (HKS) UK Ltd., Warrington, Cheshire.

Bainbridge A. T. - 1969 - "*Residual stresses arising from machining and fabrication*", AGARD Conf. Proc. No. 53, Symposium on engineering practice to avoid SCC, Istanbul, Turkey, pp 8-1 to 8-21.

Baldwin W.M. Jr. - 1949 - "*Residual stress in metals*", Proc. ASTM, Technical Papers, vol. 49, pp 539-583.

Bates S.K., Green D. and Buttle D.J. – 1997 - "*A review of residual stress distributions in welded joints for the defect assessment of offshore structures*", OHT 482, HMSO.

Bates S.K., Leggatt R.H., George D., Youtssos A.G. and Bouchard P.J. – 2000 – "*Measurement and Modelling of Residual Stresses in Thick Section Type 316 Stainless Steel Welds*", 6th International Conference on Residual Stresses, Oxford, UK.

Bauschinger, J. – 1886 - "*Ueber die Veränderungen der Elastizitätsgreze und der Festigkeit des Eisens und Stahls durch Strecken, Quetschen, Erwärmen Abkühlen und durch Oftmals Wiederholte Belastung*" Mitt: Mech-Tech Lab., XIII München, Germany.

Beaney E.M. – 1978 – "*Measurement of sub-surface stress*", CEGB Report No. RD/B/N4325, unclassified.

Beaney E.M. and Proctor E. – 1974 – "*A Critical Evaluation of the Centre Hole Technique for the Measurement of Residual Stresses*", Strain, vol. 10, no. 1, pp. 7-14.

Bonner N.W. – 1996 - "*Measurement of residual stresses in thick section steel welds*", PhD Thesis, University of Bristol.

Bonner N.W. and Smith D.J. – 1996 - "*Measurement of Residual Stresses Using the Deep-hole Method*", PVP, vol. 327, pp 53-65.

Bonner N.W., Smith D.J. and Leggatt R.H. – 1994 - "*Measurement of Residual Stresses in Thick Section Steel Welds*", Proceedings of the 10th International Conference on Experimental Mechanics, A.A. Balkema, pp 767-772.

Bouchard J.P. – 1998 - "*Experimental validation for prediction of residual stresses in thick section stainless steel girth welds*", Nuclear Electric Proprietary Report EPD/AGR/REP/0457/98.

Bouchard P.J. and Holt R.H. – 1996 - "*Heysham I / Hartlepool Power Stations – Superheater Outlet Header Weld S6 : A Non-linear Finite Element Analysis of Multi-pass Welding Residual Stresses and Operating Creep Damage*", British Energy Report EPD/AGR/REP/0074/96 Issue 1.

Bouchard P.J. and Morrison D.M. – 1998 - "*Hartlepool/Heysham 1 Power Stations – Superheater Header Weld S5 : Finite Element Analysis of Multi-Pass Weld Residual Stresses and Operating Creep Damage*", British Energy Report No. EPD/GEN/REP/0344/98 Issue 1.

Bouchard P.J., Holt P. and Smith D.J. – 1997 - "*Prediction and Measurement of Residual Stresses in a Thick Section Stainless Steel Weld*", Proc. ASME-PVP Conf., vol. 347, pp. 77-82.

Bouchard P.J., Leggatt R.H., George D., Bates S.K. and Youtssos A.G., "*Thermal Relaxation of Residual Stresses in Thick Section Type 316 Stainless Steel Girth Welds*", 6th International Conference on Residual Stresses, Oxford, UK.

Bradford R.A.W. – 1997 - "*A Summary of Residual Stress Analyses and Crack Initiation Models Completed to Date under the Generic Reheat Cracking Program*", British Energy Report EPD/AGR/REP/0328/97, Issue 1.

Brickstad B. and Josefson L.- 1998 - "*A Parametric Study of Residual Stresses in Multi-pass Butt-Welded Stainless Steel Pipes*", International Journal of Pressure Vessels and Piping, vol. 75, pp.11-25.

Brust F.W and Stonesifer R.B. – 1981 – "*Effect of Weld Parameters on Residual Stresses in BWR Piping Systems*", EPRI NP-1743, Project 1174-1, Final Report.

Chen, P.C.T. – 1986 - "*The Bauschinger and Hardening Effect on Residual Stresses in an Autofrettaged Thick-Walled Cylinder*", J. Pressure Vessel Technology, Vol.108, pp.108-112.

Cheng W. and Finnie I. - 1986 - "*Measurement of residual hoop stresses in cylinders using the compliance method*", Trans. ASME, J. eng. mat. & tech., vol. 108, no 2, pp 87-92.

Chrenko R.M. – 1977 – "*Residual Stress Studies of Austenitic Stainless Steels*", Pressure Vessel Standards : The Impact of Change, Conf. Technical Director J.D. Harrison, vol. 1, Papers, c1972.

Clark, G. – 1984 - "*Fatigue Crack Growth Through Residual Stress Fields Theoretical and Experimental Studies on Thick-Walled Cylinders*", Theoretical and Applied Fracture Mechanics, Vol. 2, pp.11-125.

Darbyshire J.M. - 1985 - "*The origin and nature of residual stresses in welds*", TWI seminar, Newcastle: Residual stresses in welded construction.

De Angelis V. and Sampietri C. – 1990 - "*Report on the state of the art regarding the problem of residual stresses in welds of LMFBR components*", CISE Technologie Innovative, Report No. 5495.

Debiez S. and Granjon H. – 1977 – "*Residual Stresses in Welded Construction and their Effects*", work carried out by the Institut de Soudure (France) on reheat cracking, Proc. Int. Conf., London, Nov. 1997, Publ. The Welding Institute 1977.

Doig P. and Lonsdale D. - 1985 - "*The measurement of stress using the X-Ray diffraction method*", TWI seminar, Newcastle : Residual stresses in welded construction.

Faure F. and Leggatt R.H. – 1996 - "*Residual Stresses in Austenitic Stainless Steel Primary Coolant Pipes and Welds of Pressurised Water Reactors*", Int. J. Press. Ves & Piping, vol. 65, pp. 265-275.

Fidler R. – 1982 – "*Effect of Time and Temperature on Residual Stresses in Austenitic Welds*", Trans. ASME, vol. 104, pp. 210.

Garcia-Granada A.A., George D. and Smith D.J. – 1998 - "*Assessment of distortions in the deep-hole technique for measuring residual stresses*", Proceedings of the 11th International Conference on Experimental Mechanics, pp1301-1306, Oxford.

George D., Bouchard P.J. and Smith D.J. – 2000 – "*Evaluation of Through Wall Residual Stresses in Stainless Steel Weld Repairs*", Materials Science Forum, vol. 347-349, pp. 646-651, 2000.

George D. and Smith D.J. – 2000 – "*The Application of the Deep-Hole Technique for Measuring Residual Stresses in Autofrettahed Tubes*", ", PVP High Pressure Technology, vol. 406, pp. 25-31, 2000.

George D. and Smith D.J. – 2000 – "*Residual Stress Measurement in Thick Section Components*", PVP Assessment Methodologies for Preventing Failure: Deterministic and Probabilistic Aspects and Weld Residual Stress, vol. 410-1, pp. 275-282, 2000.

Hepworth J.K. – 1980 – "*Residual Stresses in Submerged Arc Bead-on-Plate Welds*", CEGB Report RD/M/N1090.

Holt P.J. – 1998 – "*Heysham I / Hartlepool Superheater Weld S4 – Revised Finite Element Residual Stress and Reheat Cracking Analysis*", British Energy Report, EPD/AGR/REP/0326/97, Issue 1.

Holt P.J., Anderson G.P. – 1998 – "*Dungeness B Upper Interbank Stub Beam Welds – Finite Element Residual Stress and Reheat Cracking*", British Energy Report, EPD/DNB/REP/0315/98, Issue 1.

Hutchings M.T. - 1990 - "*Neutron diffraction measurement of residual stress fields - The answer to the engineers' prayer?*", Non-destructive Testing & Evaluation, vol. 5, pp395-413.

Jahed. H., Dubey, N.R. – 1996 - "*Residual Stress Calculation in Autofrettage using Variable Material Properties*", PVP-Vol. 327, Residual Stresses in Design, Fabrication, Assessment and Repair, pp.181-187.

Jesensky M. and Vargova J. - 1981 - "*Calculation and measurement of stresses in thick-walled welded pressure vessels*", Svaracske Spravy, part 4, pp 79-87.

Jones W.K.C. and Alberry P.J. – 1977 – "*A Model for Stress Accumulation in Steels During Welding*", Pressure Vessel Standards : The Impact of Change, Conf. Technical Director J.D. Harrison, vol. 1, Papers, c1972.

Josephson B.L. – 1983 – "*Stress Redistribution During Annealing of a Multipass Butt-Welded Pipe*", J. of Pressure Vessel and Technology, Trans. ASME, vol. 105.

Keil S. - 1993 - "*Experimental determination of residual stresses with the ring-core method and an on-line measuring system*", Experimental Techniques, The Soc. for Exp. Mech. Inc., ISSN 0732-8818, pp 17-24.

Keller H.P., Kerkoff H., Giffeler R. and Meinhardt J. - 1989 - *"Residual stresses and their influence on the integrity of pressure vessel*", T&V Rheinland Institute for Material Testing, report no. SB 203/89.

Kimmins S.T. and Horton C.A.P. – 1986 – "*Anisotropy of Elastic and Plastic Properties of Type 17Cr-8Ni-2Mo and 19Cr-12Ni-3Mo Weld Metals*", CEGB Report TPLD/L/2952/N85.

Kröner E. – 1958 – "*Berechnung der Elastischen Konstanten des Vielkristalls aus den Konstanten des Einkristalls*", Zeitschrift für Physik, Bd. 151, S. 504-518.

Kröner E. – 1967 – "*Elastic Moduli of Perfectly Disordered Materials*", J. of the Mech. & Phy. of Solids, vol. 15, pp. 319-329.

Lacarac, V.D., Pavier, M.J., Smith, D.J., Keltjenz, J. and Lemmens, D. – 2000 - "*Measurement and Prediction of Residual Stresses in Autofrettage High Pressure Tubing Incorporating Temperature and Bauschinger Effect*", PVP conference, Seattle, USA.

Leggatt R.H. – 1986 - "*Residual stresses and distortion in multi-pass butt-welded joints in type 316 stainless steel*", International Conference on Residual Stresses, Germish-Partenkirchen, Germany, Vol. 1, pp 997-1004, DGM.

Leggatt R.H., Smith D.J., Smith S.D. and Faure F. – 1996 - "*Development and Experimental Validation of the Deep-hole Method for Residual Stress Measurements*", J. Strain Analysis, vol. 31, pp 177-186.

Leggatt R.H. – 1997 – "*Welding Residual Stresses*", ICRS 5 Conf., Linköping, Sweden.

Leggatt R.H. and Hurworth S.J. - 1991 - "BRSL - PC : User guide version V 1.0", TWI report.

Lin Y.C. and Chou C.P. - 1995 - "*Error induced by local yielding in hole drilling method for measuring residual stress of materials*", Materials Science and Technology, vol. 11, pp 600-604.

Liu J. – 1997 - "*Handbook of measurement of residual stresses*", Society for Experimental Mechanics Inc., Fairmont Press Inc.

Macherauch E. and Wohlfahrt H. - 1977 - "*Different sources of residual stress as a result of welding*", Residual stresses in welded construction and their effects, vol. 1, ISBN 0-85300119-7, paper 11, pp 267-282.

Macherauch E. and Klaus K.H. - 1986 - "*Origin, measurement and evaluation of residual stresses*", Residual stresses in science and technology, vol. 1, ISBN 3-88355-099-X, pp 3-26.

Macherauch E. - 1987 - "*Introduction to residual stress*", Advances in surface treatment : Technology - Applications - Effects, vol. 4, Residual tresses, ISBN 0-08-034062-8, pp 1-36.

Misra A. and Peterson H.A. - 1982 - "*Examination of the ring method for determination of residual stress*", Experimental Mechanics, Proc. Soc. for Exp. Stress Analysis, vol. 38, pp268-72.

Mitchell D.H. – 1988 - "*R6 validation exercise : Through thickness residual stress measurements on an experimental test vessel rig*", CEGB Report NO. RD/B/6088/R88 (Unrestricted).

Nagai K. and Iwata M. – 1984 - "*Non Destructive Measurement of Residual Stress in a Filled Welded Joint by Photographic X-Ray Diffraction Technique*", IIW/IIS, Doc X – 1065 - 84.

Norrish J. – 1992 – "*Advanced Welding Processes*", New Manufacturing Processes and Materials Series, Institute of Physics Publishing.

Noyan I.C. and Cohen J.B. - 1981 - "*The nature of residual stress and its measurement*", Residual stress and stress relaxation, ISBN 0-306-41102-4, pp 1-17.

Noyan I.C. and Cohen J.B. - 1987 - "*Residual stress - Measurement by diffraction and interpretation*", Springer-Verlag, ISBN 0-387-96378-2.

Parlane A.J.A. - 1977 - "*The determination of residual stress : A review of contemporary measurement techniques*", Residual stresses in welded construction and their effects, vol. 1, ISBN 0-85300119-7, paper 8, pp 63-78.

Parlane A.J.A. - 1981 - "*Origin and nature of residual stresses in welded joints*", TWI report, Residual stresses and their effect, ISBN 0-85300141-3, pp 1-4.

Procter E. - 1985 - "*The basic centre-hole technique*", TWI seminar, Newcastle: Residual stresses in welded construction

Proctor E. and Beaney E.M. – 1987 - "*Advances in Surface Treatments: Technology-Application-Effects*", vol. 14, International Guidebook on Residual Stresses: 165-198, Oxford, Pergamon.

Rosenthal D. and Norton J.T. - 1945 - "*A method of measuring triaxial residual stresses in plates*", Weld. J., Weld. res. sup., pp 295s-307s.

Sachs, G. – 1927 - "*Der Nachweis Innerer Spannungen in Stangen and Rohren*", Zeitschrift fur Metallkunde, 19, pp. 352-357.

Sanderson D.J. and Bate S.K. – 1997 - "*Compendium of Residual Stress Profiles for R6*", AEA Technology Report AEAT-2208.

Schindler H.J., Cheng W. and Finnie I. - 1994 - "*Measurement of the residual stress distribution in a disk or a solid cylinder using the crack compliance method*", Proc. Fourth Int. Conf. on Residual Stresses, SEM, ISBN 0-912053-45-3, pp 1266-74.

Schofield K.G. - 1975 - "*A literature survey of strain and restraint measurements in welded joints*", Int. J. Pres. Ves. & Piping, vol. 4, no 1, pp 1-28.

Smith D.J. – 1997 – "*Residual Stresses in Stub Beam*", University of Bristol Report for British Energy, Contract reference BB/40625.

Smith D.J. and Bonner N.W. – 1994 - "*Measurement of residual stresses in thick section steel welds*", Engineering Integrity Assessment, J.H. Edwards, J. Kerr and P. Stanley Edited, (EMAS Chameleon Press), pp 259-274.

Smith D.J. and Bonner N.W. - 1996 - "*Measurement of residual stresses using the deep hole method*", ASME Pressure Vessels and Piping Conference, Florida, USA.

Smith D.J., George D., Bouchard P.J. and Watson C. – 1999 – "*Prediction and Measurement of Residual Stress in Thick-Section Stainless Steel Welds* I.Mech.E Seminar, London, UK.

Smith D.J., George D. and Bouchard P.J. – 2000 - "*Measurement And Prediction Of Through Thickness Residual Stresses In Thick Section Welds*", Journal of Strain Analysis, Special Issue, vol. 35, no. 4, pp. 287-305.

Smith S.D. – 1991 - "*A review of numerical modelling of fusion welding for the prediction of residual stresses and distortions*", TWI Report 437.

Spooner S., Fernandez Bacca J.A., David S.A. and Hubbard C.R. – 1994 – "*Investigation of Residual Stresses in Multi-pass Weld in 1" Stainless Steel Plate*", ICRS 4, Baltimore, Maryland, USA, pp. 1205.

Stacey, A., MacGillivary, H.J., Webster, G.A., Ziebeck, K.R.A. – 1985 - "*Measurement of Residual Stresses by Neutron Diffraction*", Journal of Strain Analysis, Vol.20, No 2, pp. 93-100.

Stacey, A., Webster, G.A. – 1988 - "*Influence of Residual Stress on Fatigue Crack Growth in Thick-Walled Cylinders*", Analytical and Experimental Methods for Residual Stress Effects in Fatigue, ASTM STP 1004, pp. 107-121.

SYSWELD – 1999 – finite element analysis code, Institut de Soudure, France.

"*The Gundrilling Guidebook*", c/o Eldorado UK Gundrilling, Reed Rolled Thread Die Co. Ltd., Halesowen Road, West Midlands, B62 9BD.

Timoshenko S. and Goodier J.N. – 1951 - "*Theory of elasticity*", McGraw-Hill, 2nd Edition, pp 258-280.

Ueda Y. and Fukuda K. – 1989 - "*New Measuring Method of Three Dimensional Residual Stress in Long Welded Joints Using Inherent Strains as Parameters – L_z Method*", Journal of Engineering Materials and Technology, vol. 111.

Ueda Y., Fukuda K. and Endo S. – 1975 - "*A Study on the Accuracy of Estimated Residual Stresses by the Existing Measurement Methods*", Trans. Jap. Weld. Res. Inst., vol. 4, no. 2, pp 13-27.

Ueda Y. and Kim Y.C. - 1986 - "*New measuring method of three-dimensional residual stresses using effective inherent strains as parameters*", Residual stresses in Science and Technology, vol. 1, ISBN 3-88355-099-X, pp 199-206.

Ueda Y. and Fukuda K. - 1989 - "*New measuring method of three-dimensional residual stresses in log welded joints using inherent strains as parameters - L_z method*", Trans. ASME, J. Eng. Mat. & Tech., vol. 111, pp 1-8.

VORSAC – 1999 – "*Variation of Residual Stresses in Aged Components*", EC Contract No. FI4S-CT96-0040.

VORSAC – 1999 – "*VORSAC Work Package 2, Task 2.5.2: Finite Element Analysis of Multi-Pass Welding Residual Stresses and Stress Relaxation in Thick Girth Weld*", British Energy Report, no. EPD/GEN/REP/0407/99, Issue 2.

Webster G.A. and Webster P.J. - 1985 - "*Measurement of residual stress using high resolution neutron diffraction*", TWI Seminar, Newcastle : Residual stresses in welded construction.

Yen H.J., Lin M.C.C. and Chen L.J. – 1994 - "*Measurement and Simulation of Residual Stress in Type 304 Weld Overlay Stainless Steel Pipe*", Int. J. PVP, no 60, pp 271-283.

Zhang J., Dong P. and Hong J.K. – 1997 - "*A 3D Composite Shell Element Model for Residual Stress Analysis in Multi-Pass Welds*", Trans. 14th Int. Conf. on Structural Mechanics in Reactor Technology (SmiRT-97), Lyon, France, vol. 1, pp. 335-344.

Zhdanov I.M. and Gonchar A.K. – 1978 - "*Determining the Residual Welding Stresses at a Depth in Metals*", Automatic Welding, Vol. 31, No. 9, pp 22-24.

TABLES

Material	α $°C^{-1}$	T_s °C	σ_Y MPa	E MPa	$\alpha(T_s - T_0)$ %	$\varepsilon_Y = \sigma_Y/E$ %
Type 316	18×10^{-6}	1050	300	193000	1.85	0.16
C-Mn	12×10^{-6}	650	350	207000	0.76	0.17
Ti-6Al-4V	7.3×10^{-6}	875	950	106000	0.62	0.89
PEI	56×10^{-6}	219	90	3000	1.11	3.00

Table 2.1 : Contraction strain and yield strain in various materials ($T_0 = 20°C$).

Parameter		Set 1	Set 2	Set 3	Set 4	Set 5	Set 6	Set 7	Set 8	Set 9
Scale	µinch									
Scale	µmeter (40.4)									
Scale	µmeter (40.6)									
Position	Centering									
Position	/ surface									
Position	/ point									

notations :
- Repeatability : difference between two identical measures
- Linearity : difference between reading and linear interpolation
- Precision : difference between reading and theoretical value
- Amplification : difference between theoretical range of reading and experimental

	Efficiency	Repeatability	Linearity	Precision	Amplification	Total inaccuracy
Set 1 (µm)	95 %	± 0.1493	± 0.9016	± 0.2587	± 0.1640	± 1.1361
Set 2 (µm)	95 %	± 0.1233	± 0.7899	± 0.3332	± 0.0369	± 1.0816
Set 3 (µm)	95 %	± 0.2118	± 1.0959	± 0.3359	± 0.1639	± 1.4503
Set 4 (µm)	95 %	± 0.2729	± 0.9448	± 0.4511	± 0.1141	± 1.4562
Set 5 (µin)	95 %	± 0.2352	± 0.8531	± 0.4173	± 0.2538	± 1.3186
Set 6 (µm)	95 %	± 0.1619	± 0.9089	± 0.5564	± 0.2106	± 1.4566
Set 7 (µm)	95 %	± 0.1571	± 0.8477	± 0.1939	± 0.2171	± 1.0281
Set 8 (µin)	95 %	± 0.3345	± 0.9708	± 0.4589	± 0.1576	± 1.5052
Set 9 (µin)	95 %	± 0.2572	± 0.8509	± 0.5647	± 0.1437	± 1.4474

Table 3.1 : Accuracy of air probe measurements.

Bar depth d, mm	Bending stress (stress at hole's location)	Torsion stress (stress at hole's location)
50	Constant : 20, 36, 47, 65 and 68MPa (hole 2) 68MPa = 10kN load Linear : 100MPa (hole 3) 100MPa = 8.6kN load	20MPa (835Nm load) and 40MPa (1670Nm load) (hole 3)
19	Constant : 64MPa (hole 1) (3.8kN load)	40MPa (365Nm load) and 56MPa (508Nm load) (hole 2)

Table 4.1 : Loading conditions for each case of calibration tests.

This list presents a comprehensive survey of the British Energy specimens on which deep-hole experimental measurements were carried out together with the number and location of measurements. Each **x** represents one measurement.

WCL = Weld centre line ; B-W = Butt-welded

Component and material \ Characteristics		As-welded	PWHT (750°C)	Aged (550°C)			In weld repair		In original weld after weld repair
				200 hrs	2000 hrs	6000 hrs	25%	75%	
B-W, 19mm 316H	WCL								
	HAZ	x x x							
B-W, 35mm 316H	WCL	x x					x		x
	HAZ	x					x	x	
B-W, S5 – A t = 65mm 316H	WCL	x							
	HAZ								
B-W, S5 – B t = 65mm 316H	WCL		x x						
	HAZ								
B-W, S5 – C t = 65mm 316H	WCL	x							
	HAZ	x							
B-W Narrow Gap t = 65mm 316H	WCL	x							
	HAZ	x							
B-W, V-A t = 65mm 316H	WCL	x	x						
	HAZ	x	x						
B-W, V-B t = 65mm 316H	WCL								
	HAZ	x		x	x	x			
End cap to cylinder RRM t = 110mm	WCL	x							
	Parent	x							
Nozzle 316H	WCL								
	HAZ	x							
Beam to cylinder Stubbeam 316H	WCL	x							
	HAZ	x x							

Table 5.1 : List of specimens on which experimental measurements were carried out.

Temp. (°C)	Thermal expansion coefficient (/°C)	Young's modulus (GPa)	Poisson's ratio	Parent		Weld	
				0,2% Proof Stress (MPa)	1% Proof Stress (MPa)	0,2% Proof Stress (MPa)	1% Proof Stress (MPa)
20	15.24 E-06	195.1	0.267	358.0	399.0	426.3	476.3

Table 5.2 : Mechanical properties of AISI 316H stainless steel at room temperature used for deep-hole analysis.

Specimen and condition	FE simulation	Experiment
Butt-welded, t = 19mm 316H	X	X
Butt-welded, t = 35mm 316H	X	X
Butt-welded, S5 – A old weld proc., high heat input t = 65mm, 316H	X	X
Butt-welded, S5 – B t = 65mm, 316H	X	X
Butt-welded, S5 – C new weld proc., low heat input t = 65mm, 316H	X	X
Butt-welded, Narrow Gap t = 65mm, 316H		X
Butt-welded, Vorsac A t = 65mm, 316H	X	X
Butt-welded, Vorsac B t = 65mm, 316H	X	X
End cap to cylinder RRM, t = 110mm	X	X
Branch weld, Nozzle 316H	X	X
Beam to cylinder, Stubbeam 316H	X	X

Table 6.1 : Finite element simulation carried out for experimental measurements comparison.

FIGURES

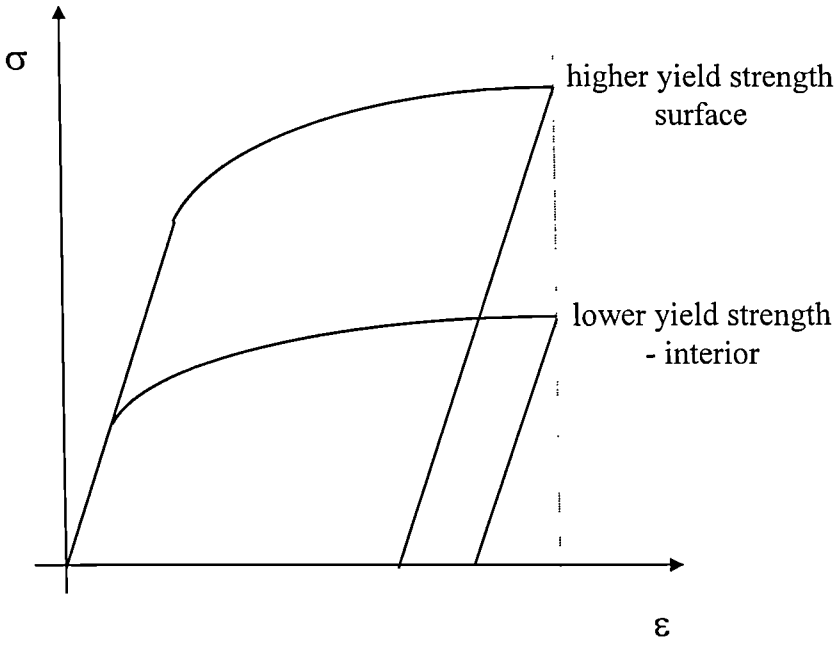

Figure 2.1 : Schematic of possible behaviour of material on loading and unloading [Noyan et al., 1987].

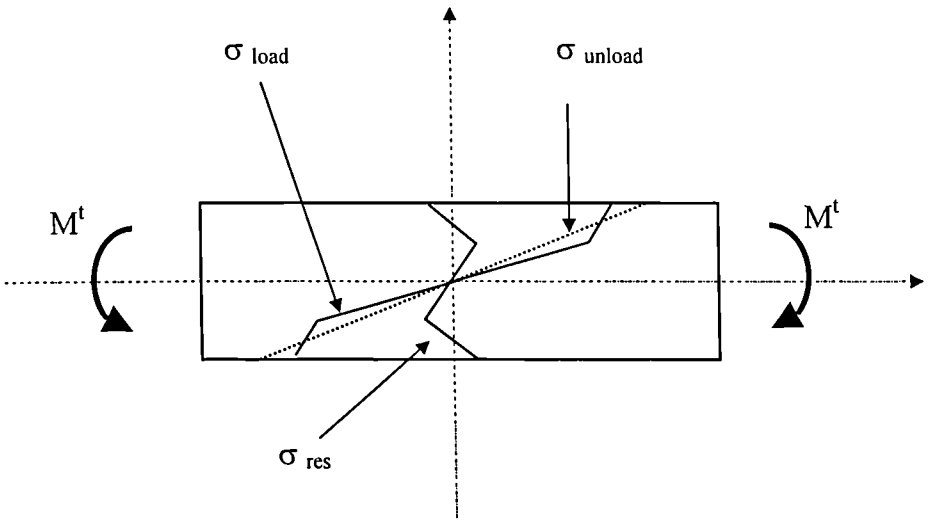

Figure 2.2 : Loading, unloading and residual stresses owing to plastic bending of a bar [Macherauch et al., 1986]

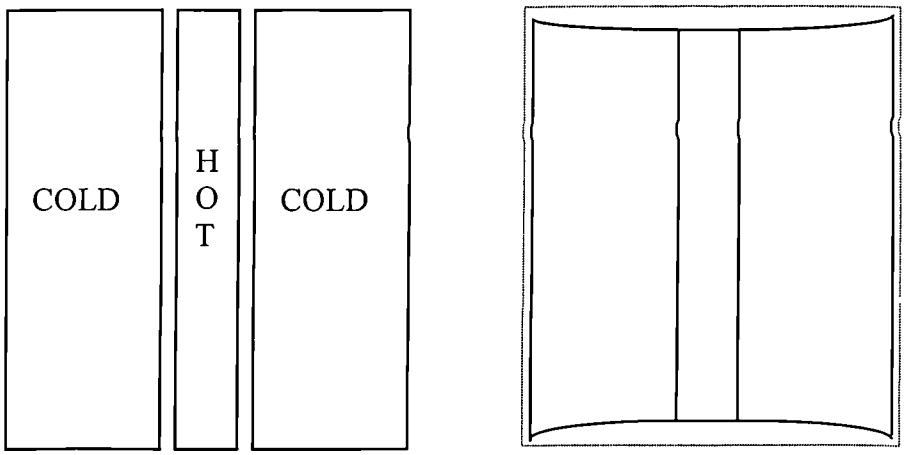

Figure 2.3 : Schematic distortion of a butt-welded plate due to shrinkage of hot weld metal [Parlane, 1981]

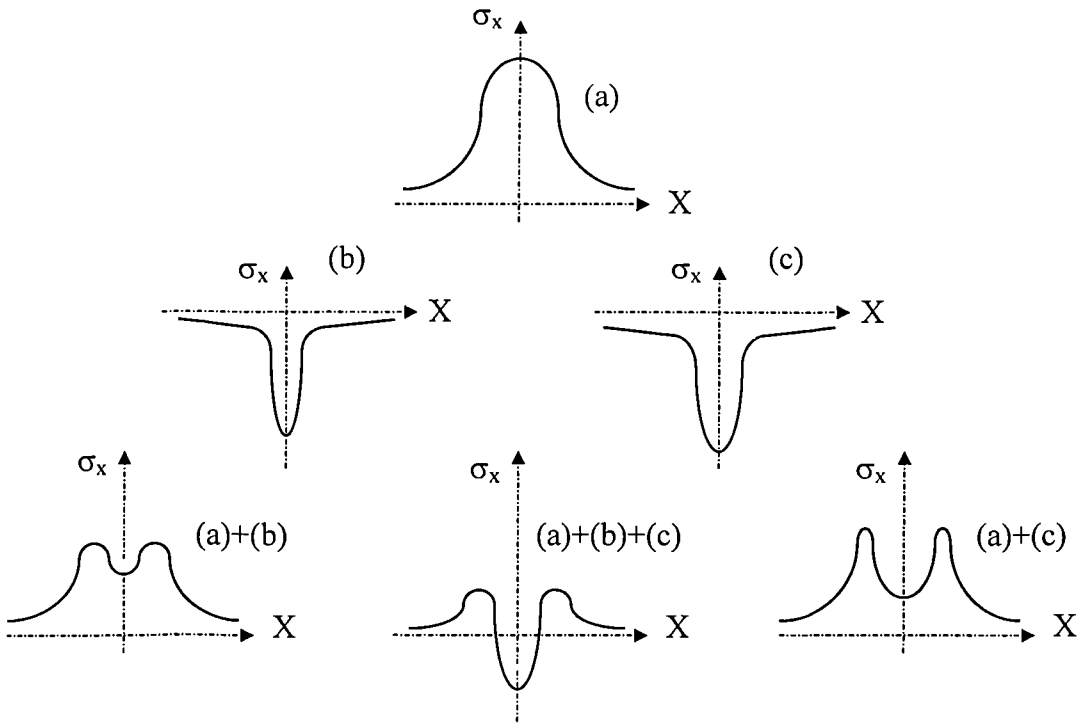

Figure 2.4 : Schematic superimposition of transverses residual stresses due to (a) shrinkage, (b) quenching and (c) phase transformation [Macherauch et al., 1977].

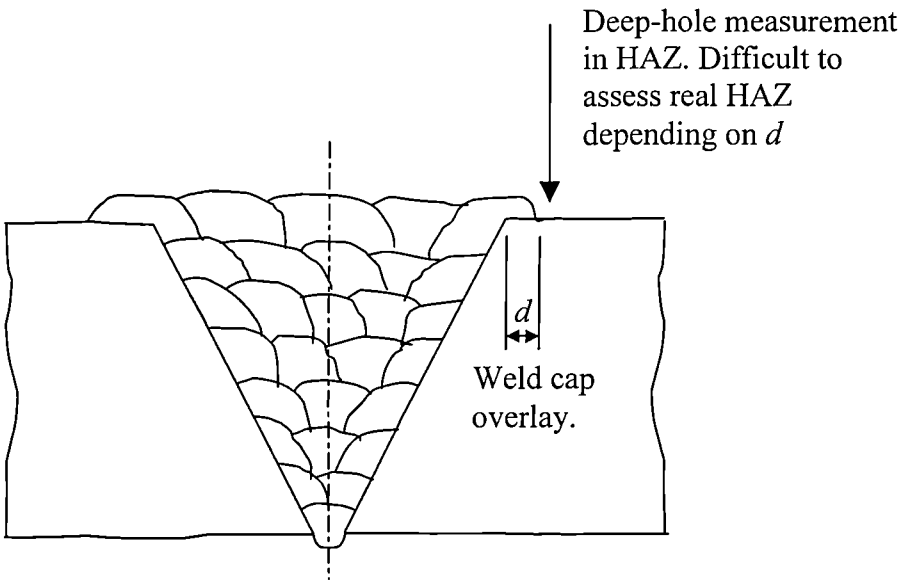

Figure 2.5 : General layout of deposited weld beads (example).

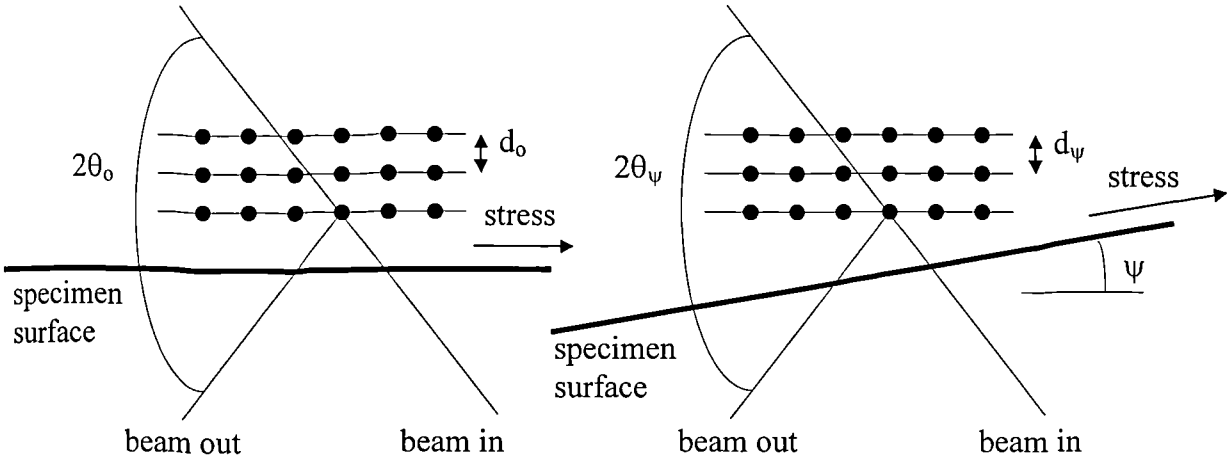

Figure 2.6 : Schematic showing orientations of lattice planes and X-ray beams relative to specimen surface and direction of measured stress [Doig et al., 1985]

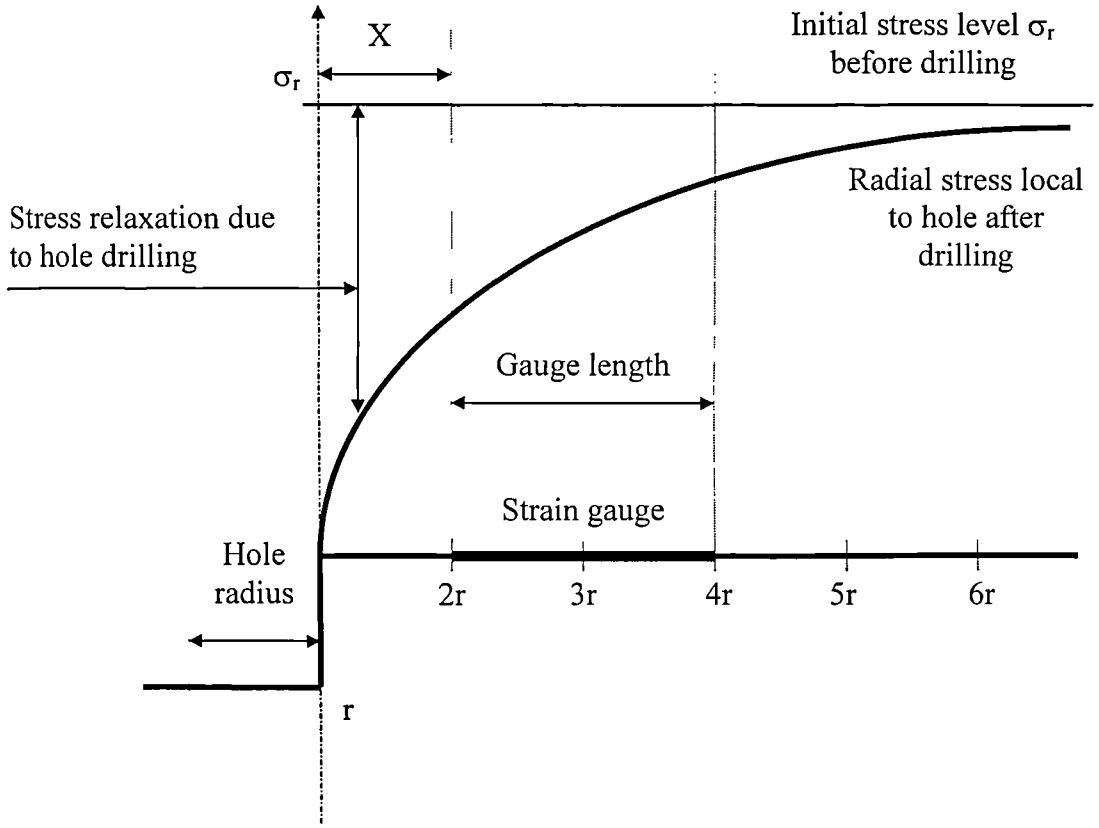

Figure 2.7 : Elastic radial stress relaxation due to drilled hole.

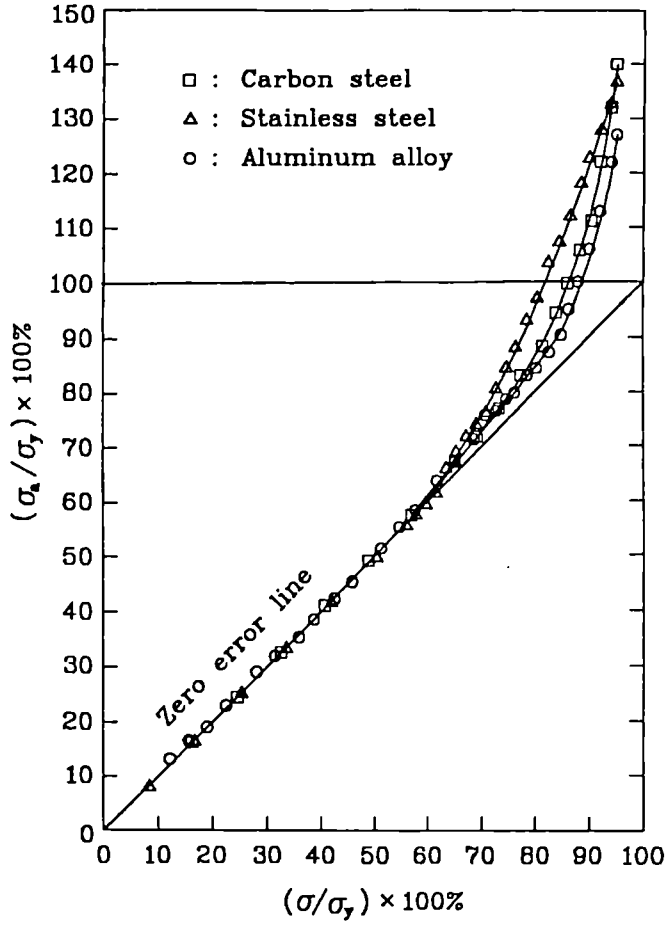

Figure 2.8 : Error induced by local yielding around hole in hole drilling method for measuring residual stress of materials by Lin et al. [1995].

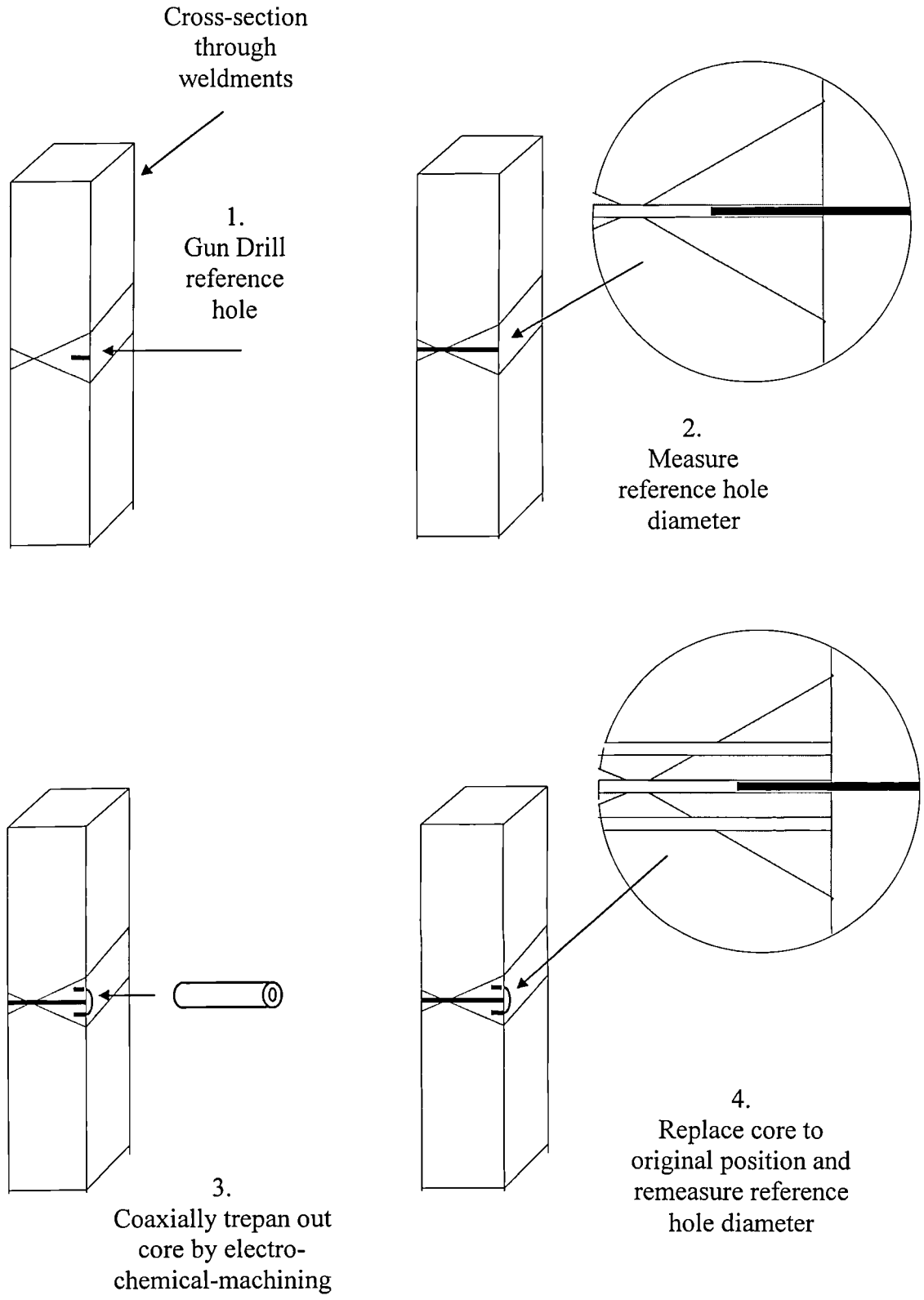

Figure 2.9 : Schematic of basic process of deep hole residual stress measurement.

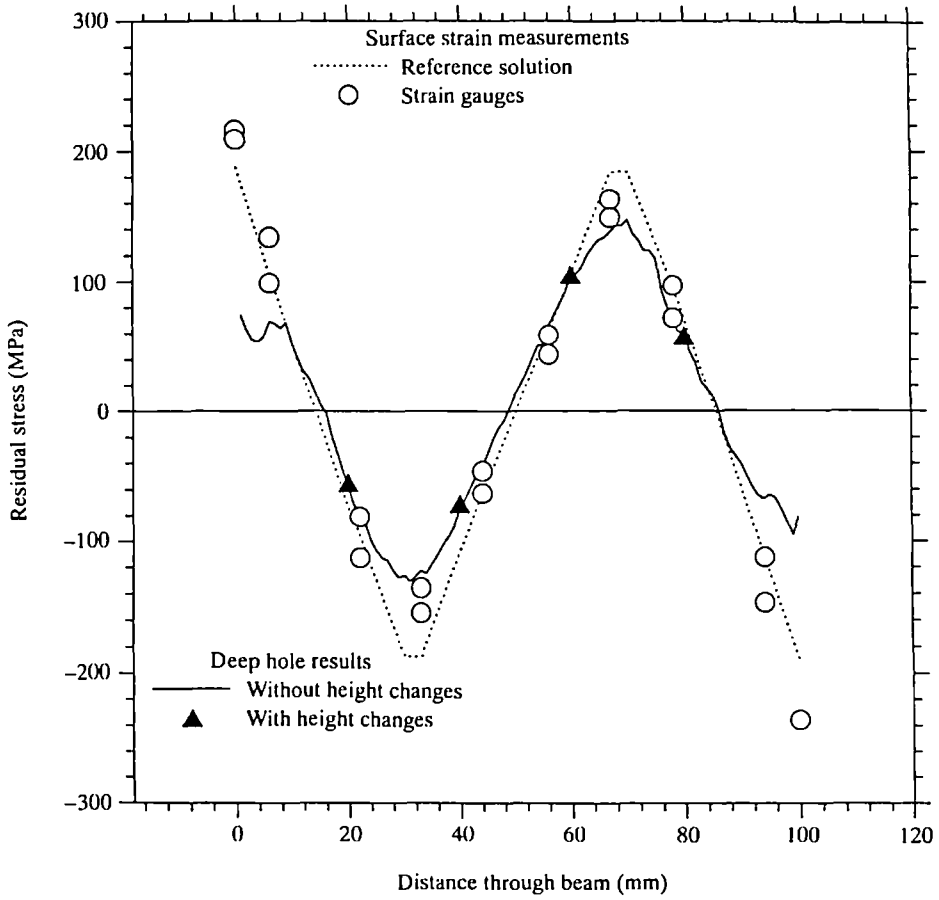

Figure 2.10 : Measured axial residual stress in bar [Leggatt, 1996]

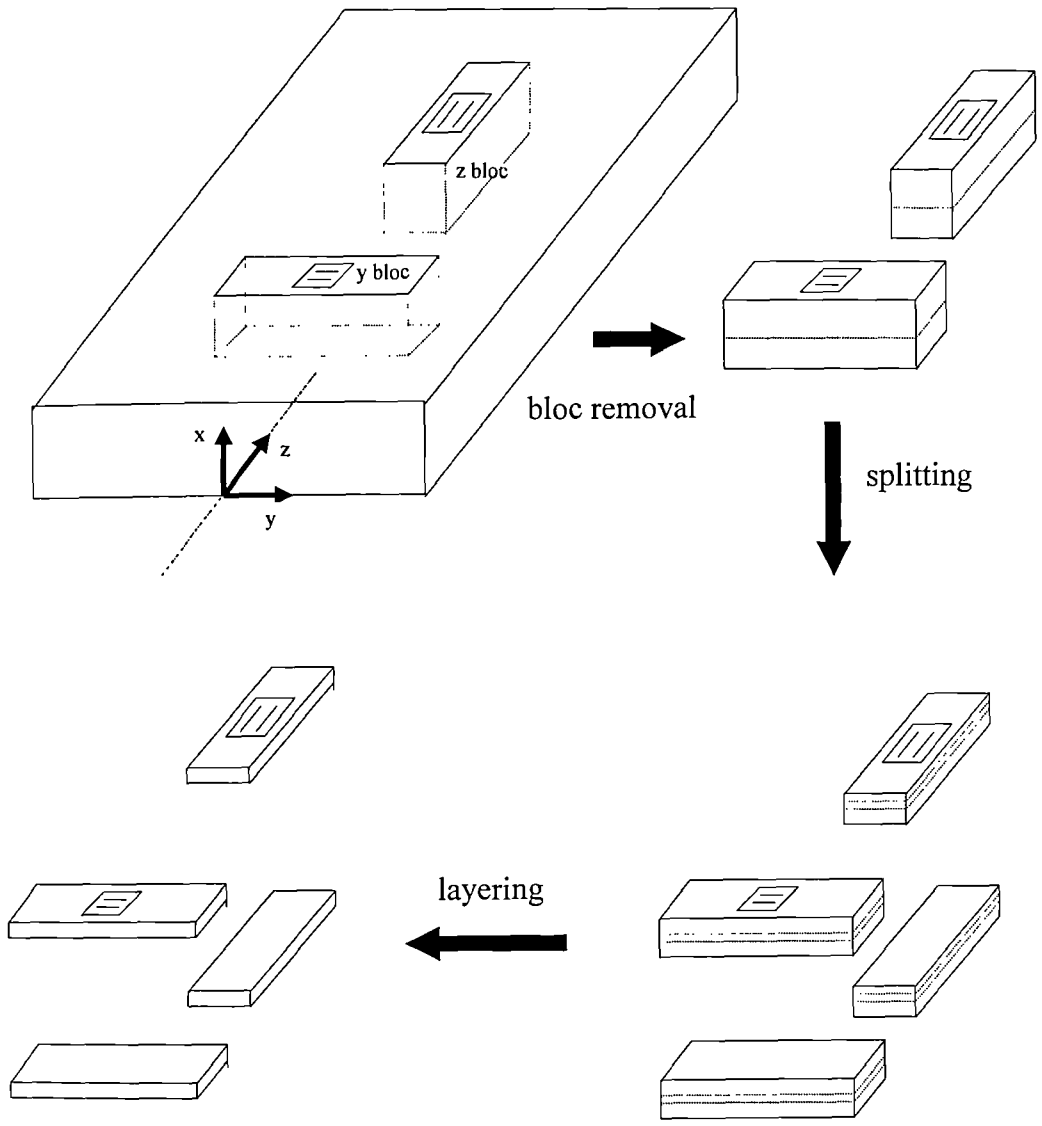

Figure 2.11 : Schematic of basic process of the Rosenthal and Norton (RN) method.

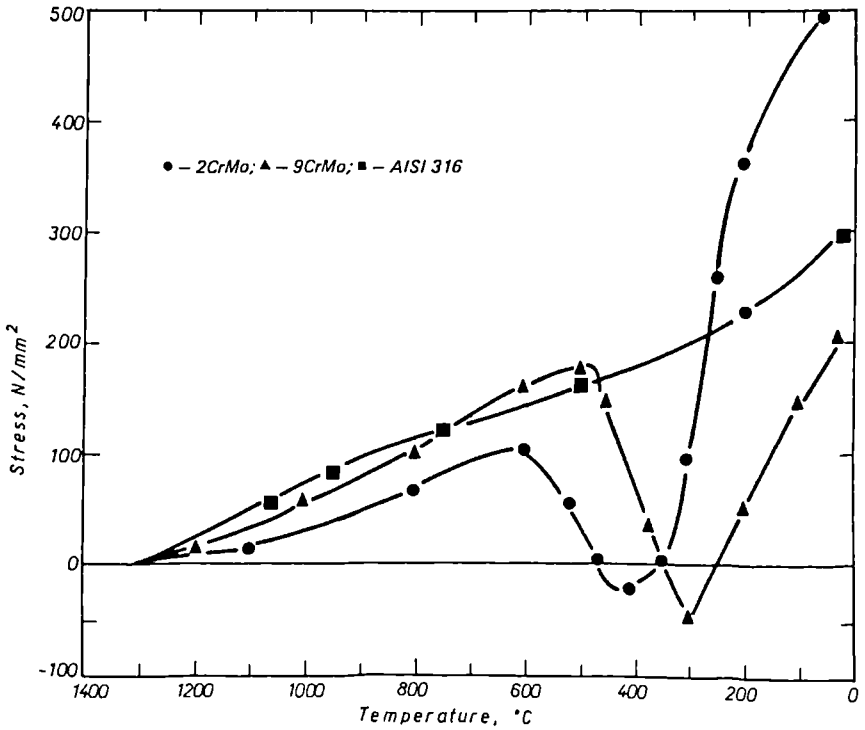

Figure 2.12 : Accumulation of stress during cooling period of a MMA weld from 1320°C by Jones and Alberry, 1977.

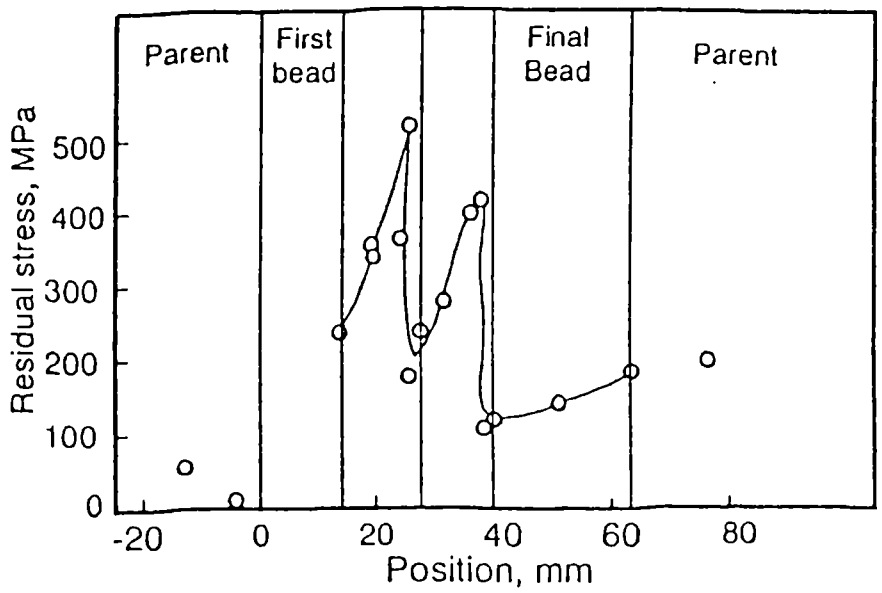

Figure 2.13 : Variation of longitudinal residual stress across surface of a multipass 2CrMo steel bead-on-plate weld with 200°C preheat [Hepworth, 1980].

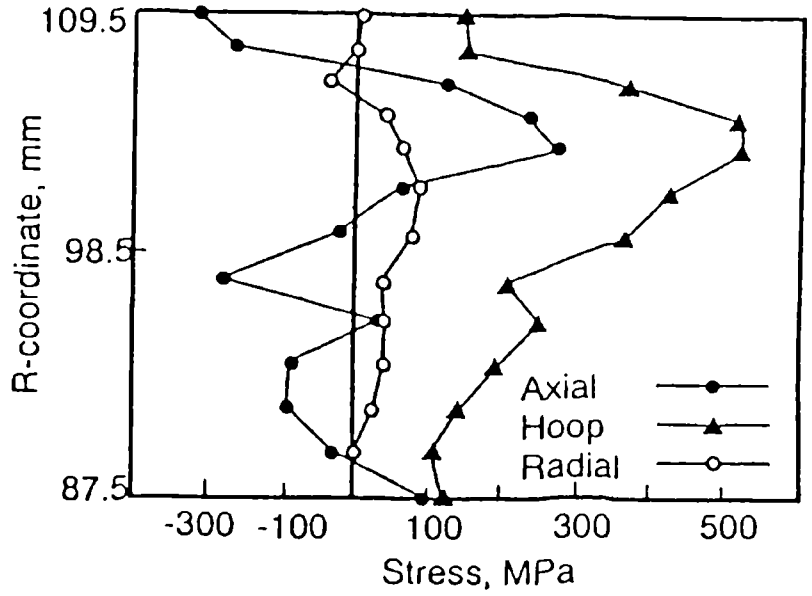

Figure 2.14 : Calculated residual hoop, axial and radial stresses at the weld centre line in a hoop weld of a 22mm thick pipe [Josephson, 1983].

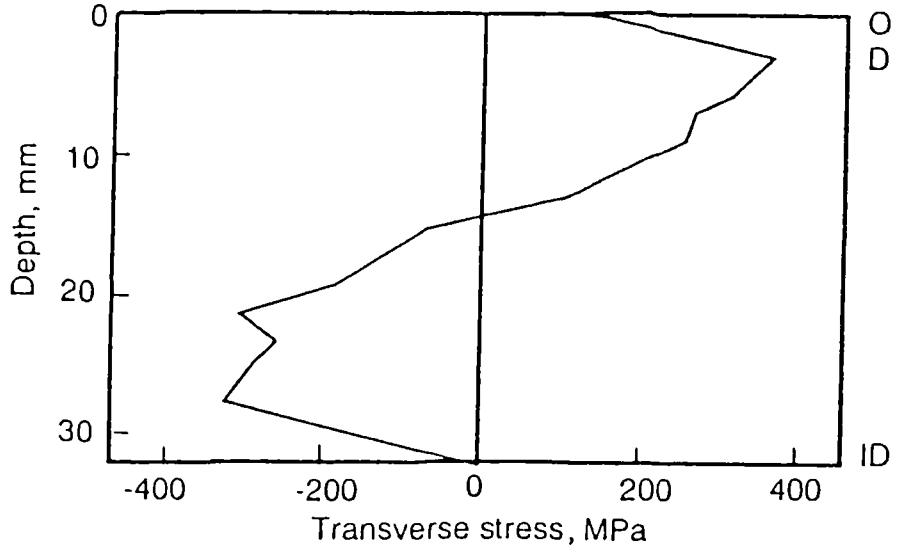

Figure 2.15 : Axial residual stresses at the centre line of a hoop weld in a 32mm thick pipe [Leggatt, 1997]

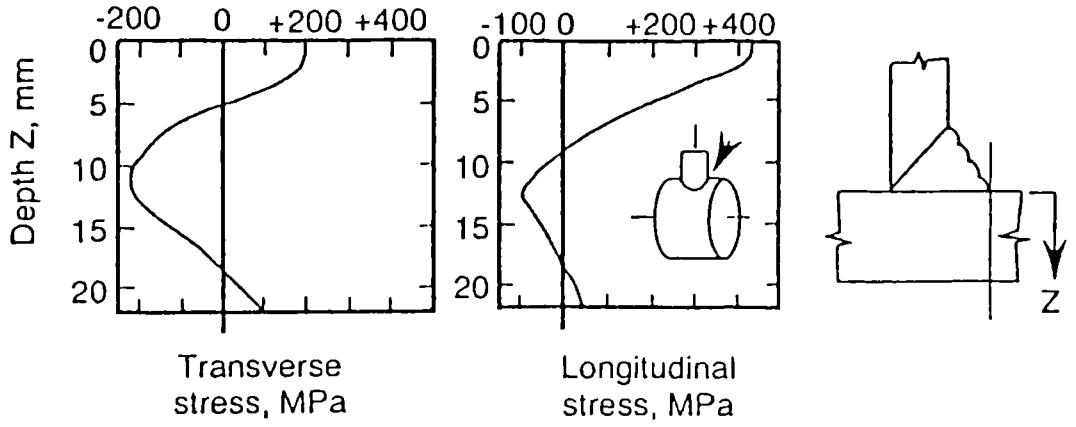

Figure 2.16 : Residual stresses in the chord at the toe of a T-butt weld in a tubular connection [Leggatt, 1997]

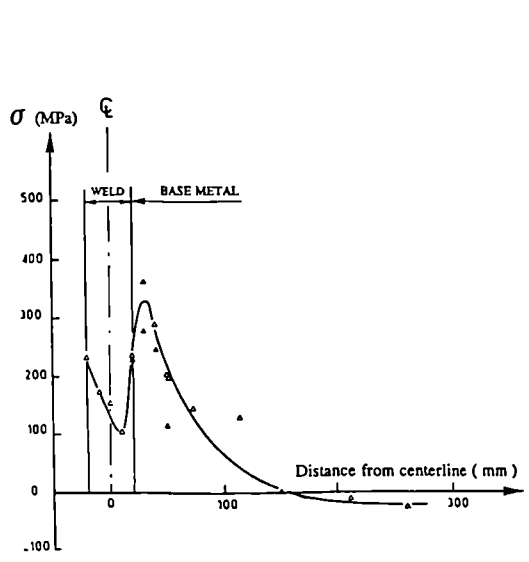

2.10a : axial outer face

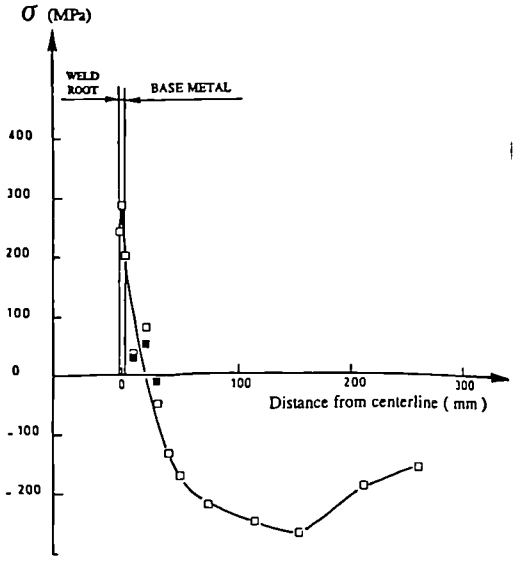

2.10b : axial inner face

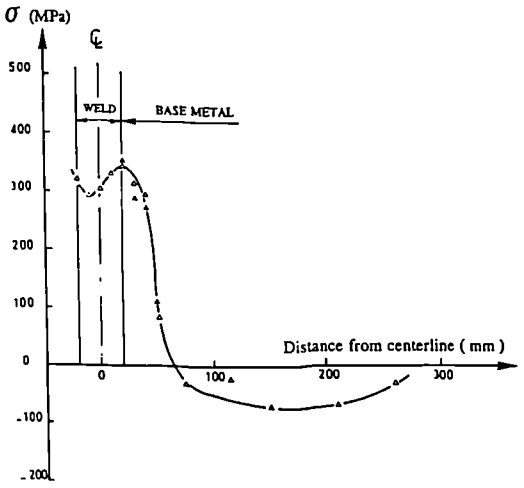

2.10c : hoop outer face

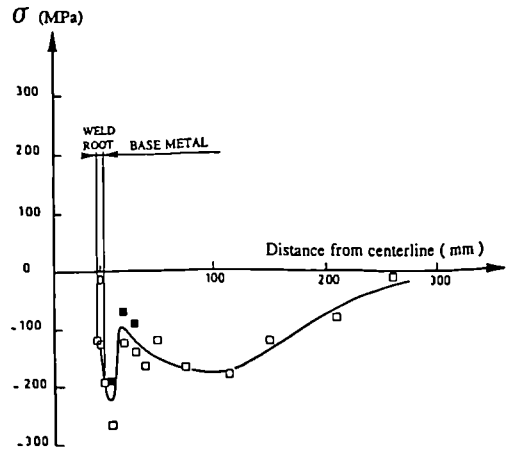

2.10d : hoop inner face

Figure 2.17 : Surface residual stress measurement on orbital TIG weld From Faure et al. [1996].

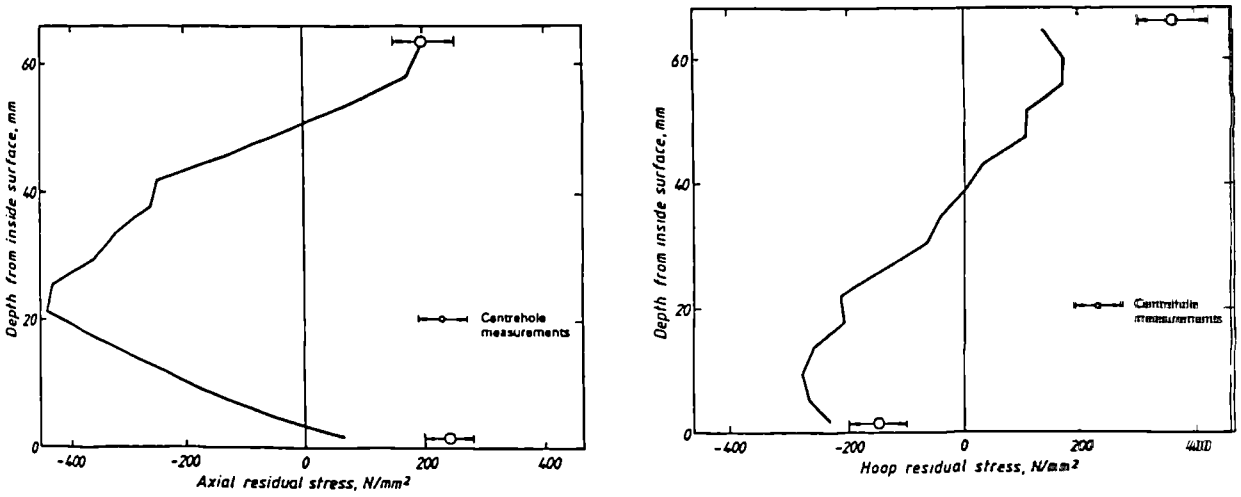

2.11a : axial stress

2.11b : hoop stress

Figure 2.18 : Through thickness measurement at weld centre line in an orbital TIG weld from Faure et al. [1996].

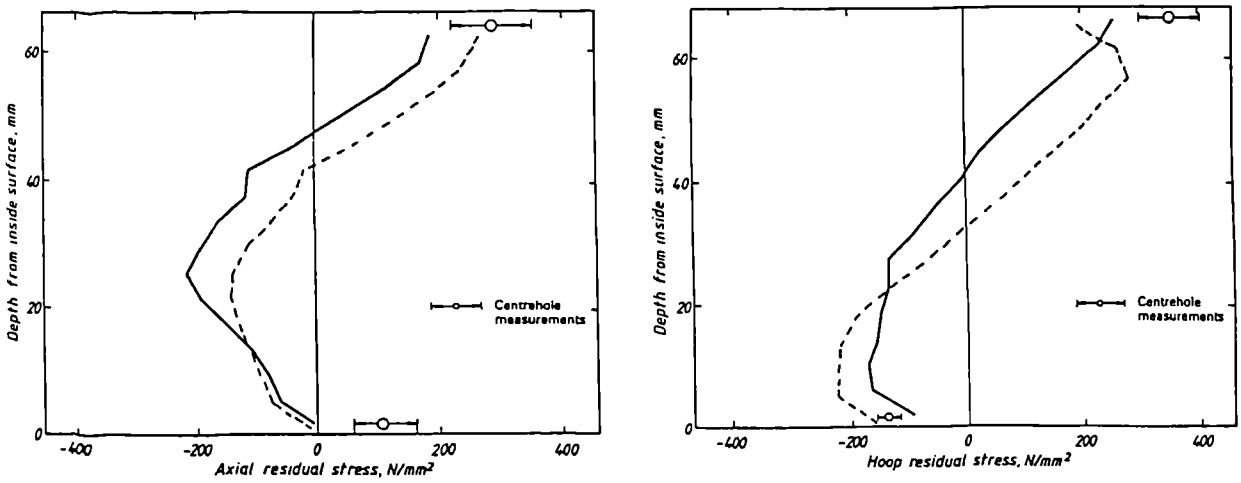

2.12a : axial stress

2.12b : hoop stress

Figure 2.19 : Through thickness measurement at 20mm from weld centre line (HAZ) in an orbital TIG weld from Faure et al. [1996].

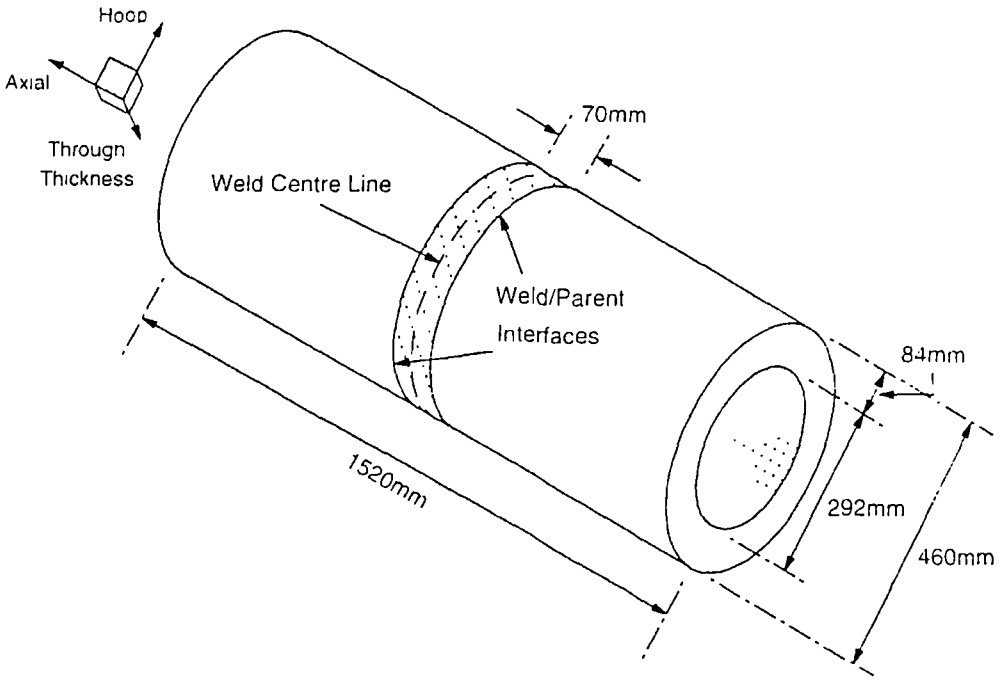

Figure 2.20 : Schematic of thick weld stainless steel butt-welded pipe from Bonner [1996].

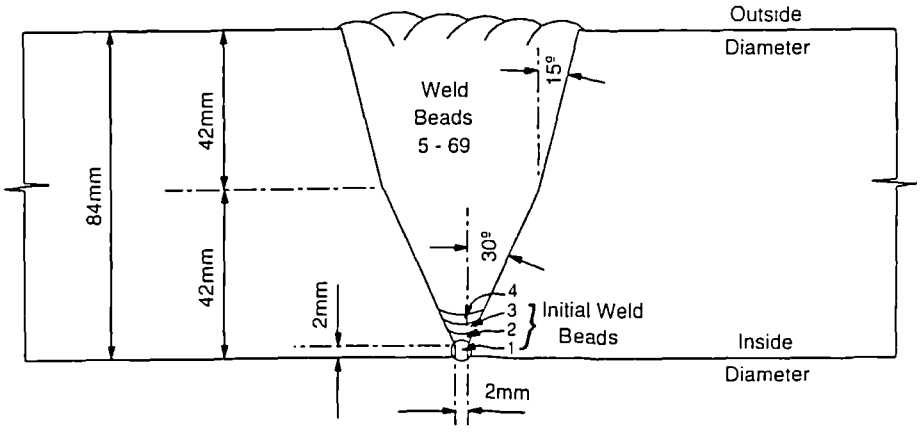

Figure 2.21 : Schematic of the weld geometry of pipe fig. 2.14 from Bonner [1996].

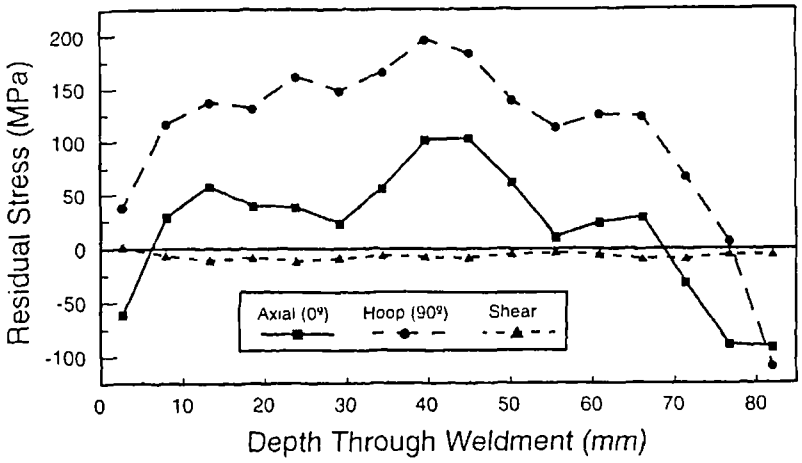

Figure 2.22 : Through wall residual stress distribution at weld centre line, from Bonner [1996].

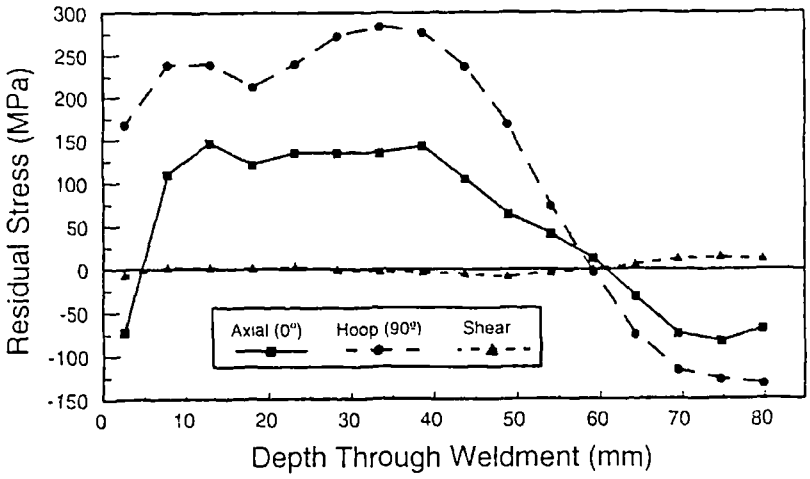

Figure 2.23 : Residual stress at 24mm from weld centre line (not HAZ since weld width is 70mm), from Bonner [1996].

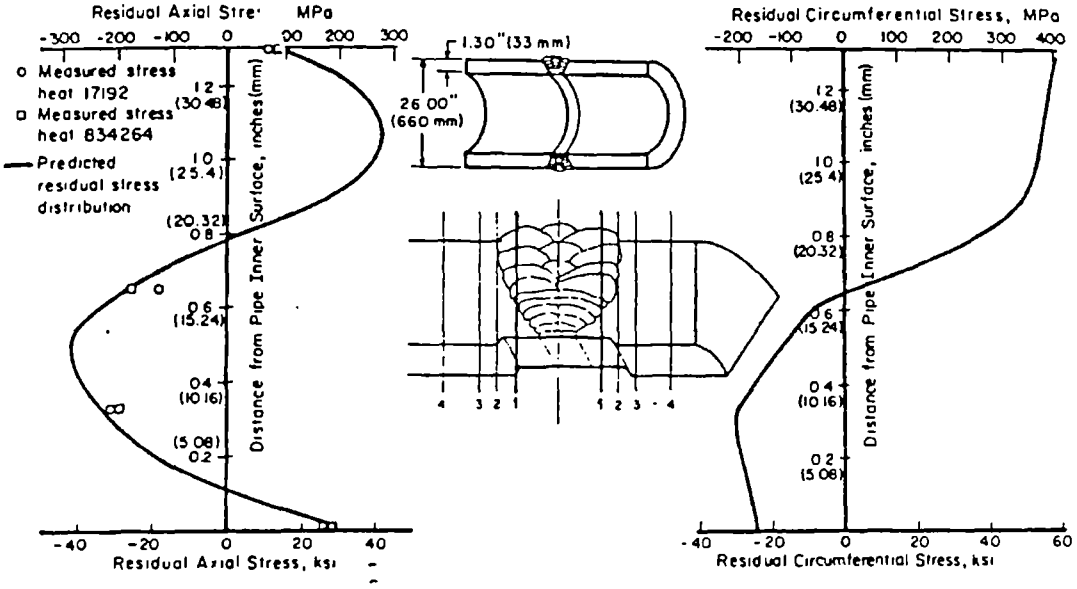

Predicted and measured through-wall residual axial and circumferential stresses at Location 1, 0.33 inch (8 mm) from weld centerline, in a 26-inch (660-mm) pipe welded with high heat input (HI = 1.13 kJ/mm for latter layers)

Figure 2.24 : Simulated residual stresses in 33mm thick butt-welded pipe in weld by Brust [1981].

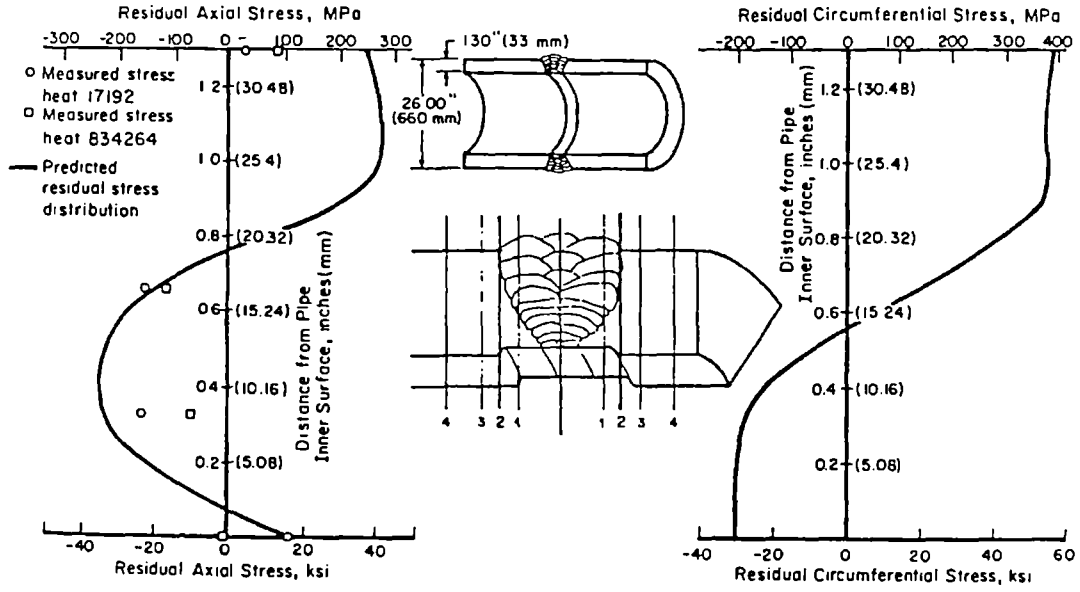

Predicted and measured through-wall residual axial and circumferential stresses at Location 2, 0.50 inch (13 mm) from weld centerline, in a 26-inch (660-mm) pipe welded with high heat input (HI = 1.13 kJ/mm for latter layers)

Figure 2.25 : Simulated residual stresses in 33mm thick butt-welded pipe in HAZ by Brust [1981].

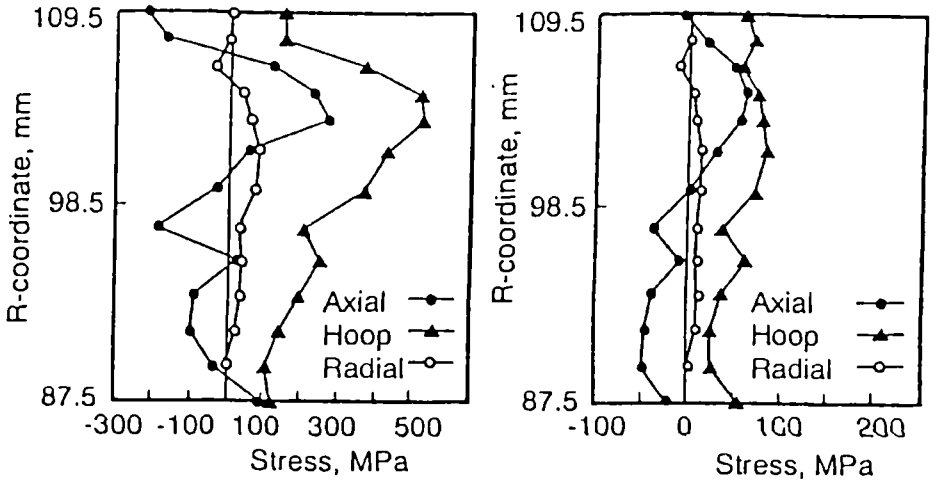

Figure 2.26 : Calculated residual stresses in hoop butt-weld in 22mm thick Pipe as-welded and after PWHT at 575°C by Josephson [1983].

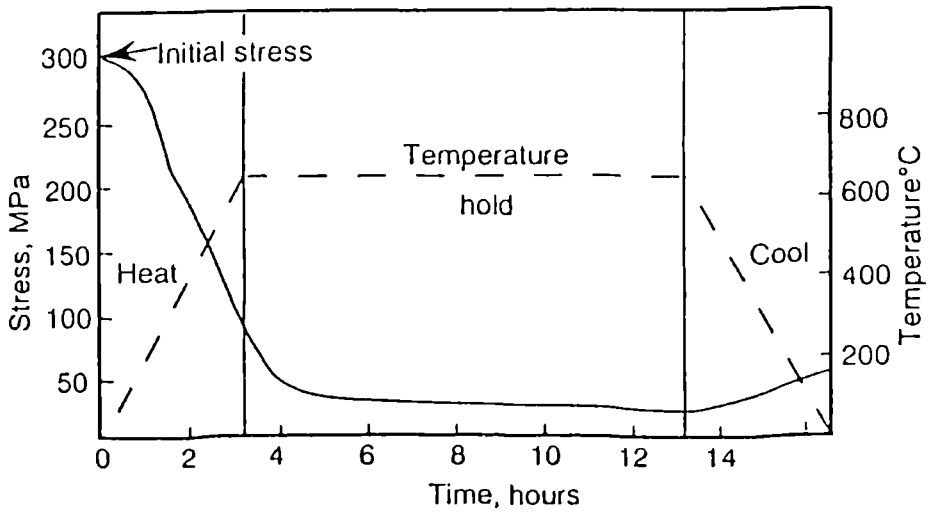

Figure 2.27 : Variation of stress during simulated PWHT thermal cycle by Debiez et al [1977].

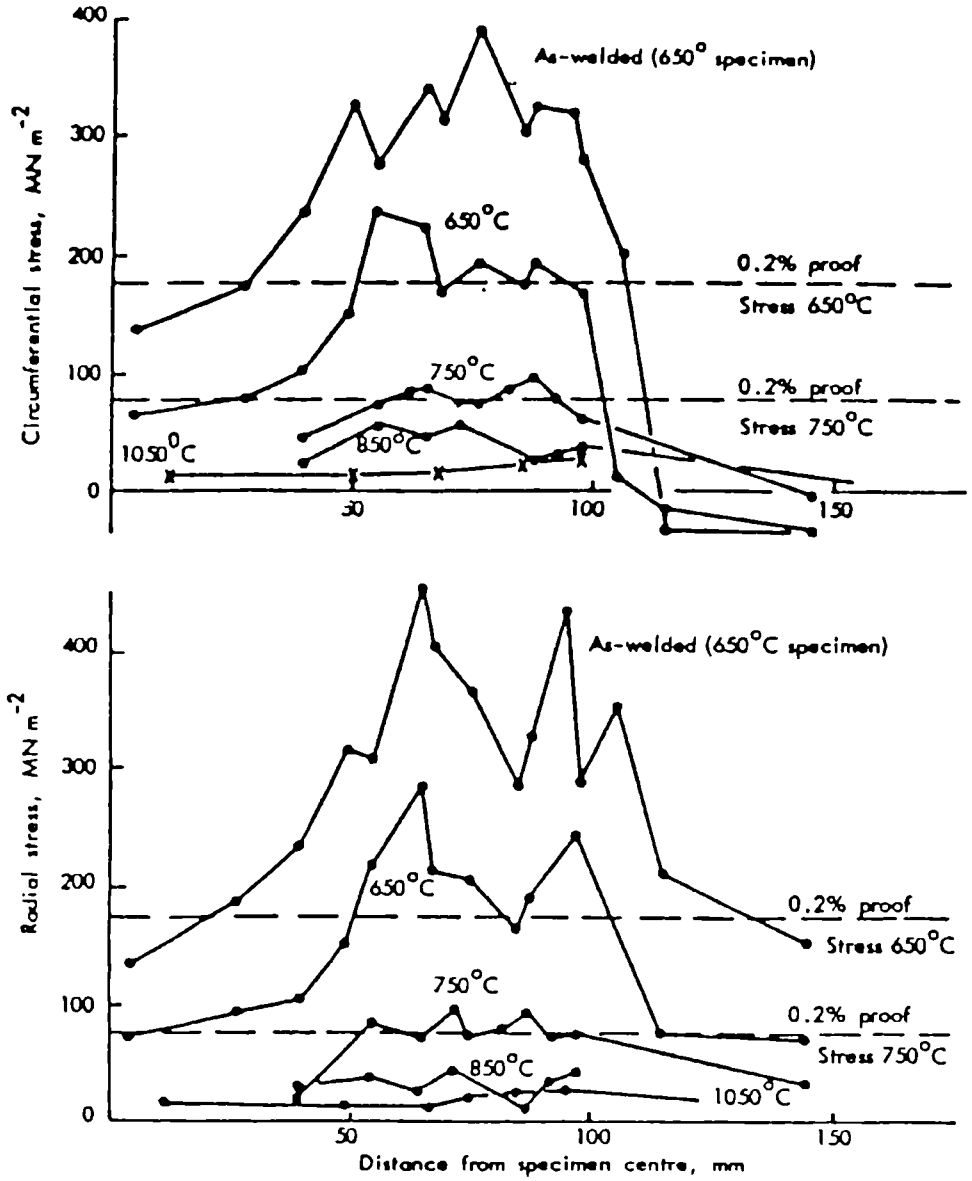

Figure 2.28 : Comparison of residual stresses in the four specimens after heat treatment of 1 hour duration from Fidler [1982].

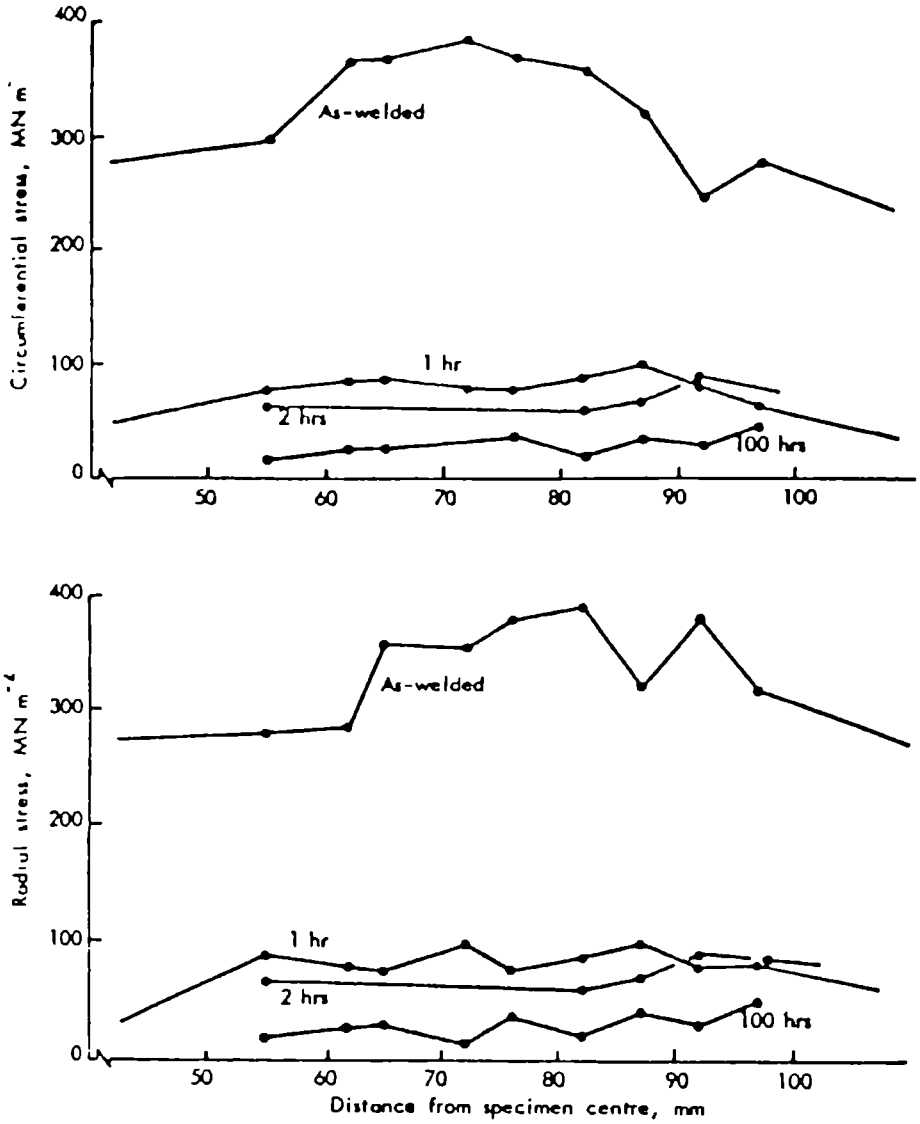

Figure 2.29 : Effect upon residual stresses of various periods of Heat treatment at 750°C from Fidler [1982]

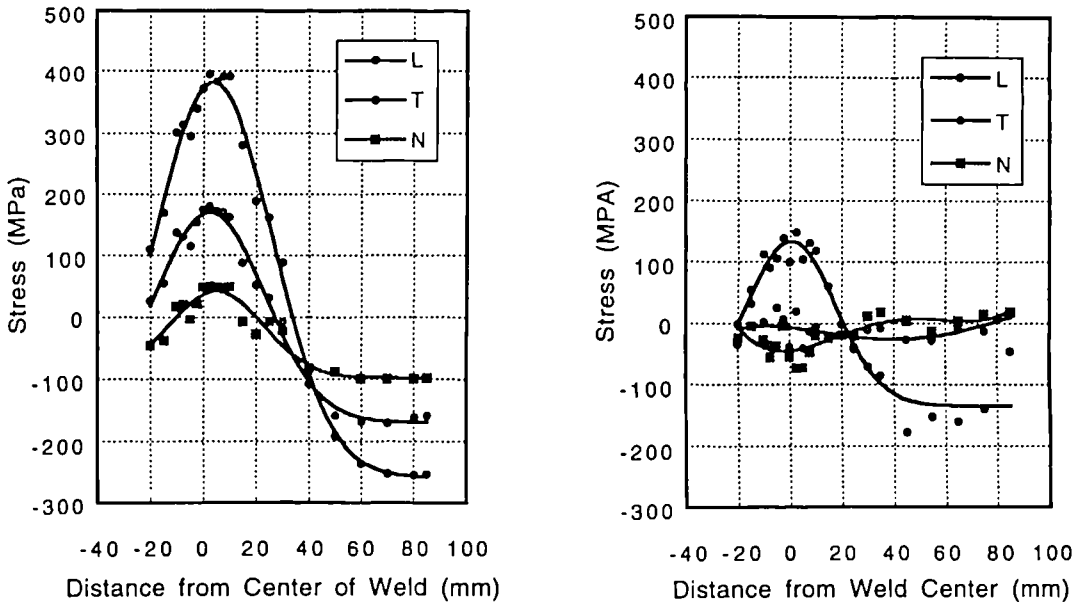

Figure 2.30 : Residual stress distribution before and after thermal stress relief In butt-welded 304 austenitic stainless steel plate from Spooner et al. [1994].

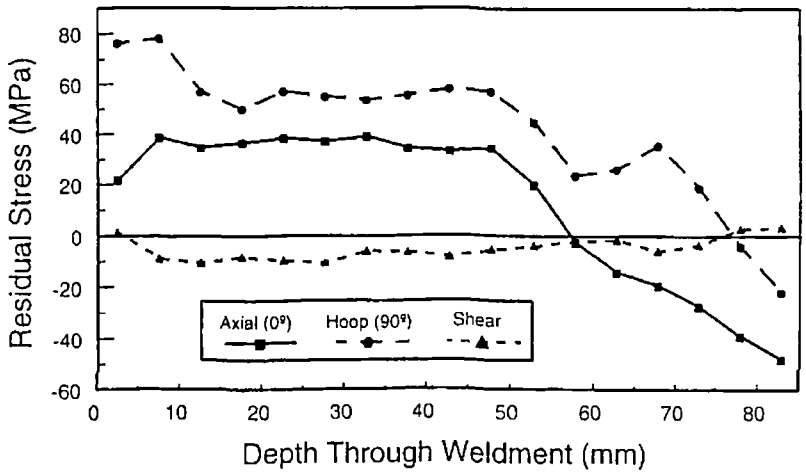

Figure 2.31 : Influence of PWHT on 85mm butt-welded carbon steel pipe from Bonner [1996.]

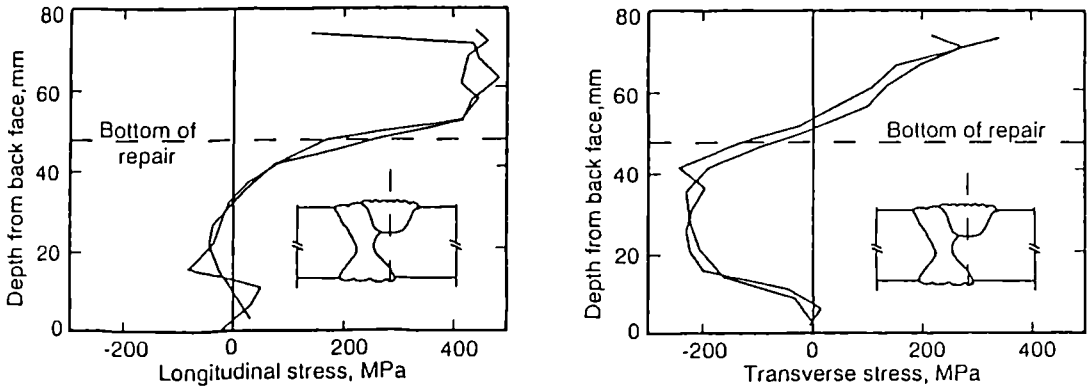

Figure 2.32 : Variation of residual stress through the thickness at centre of 28mm deep repair in 75mm thick C-Mn steel (Leggatt, 1986).

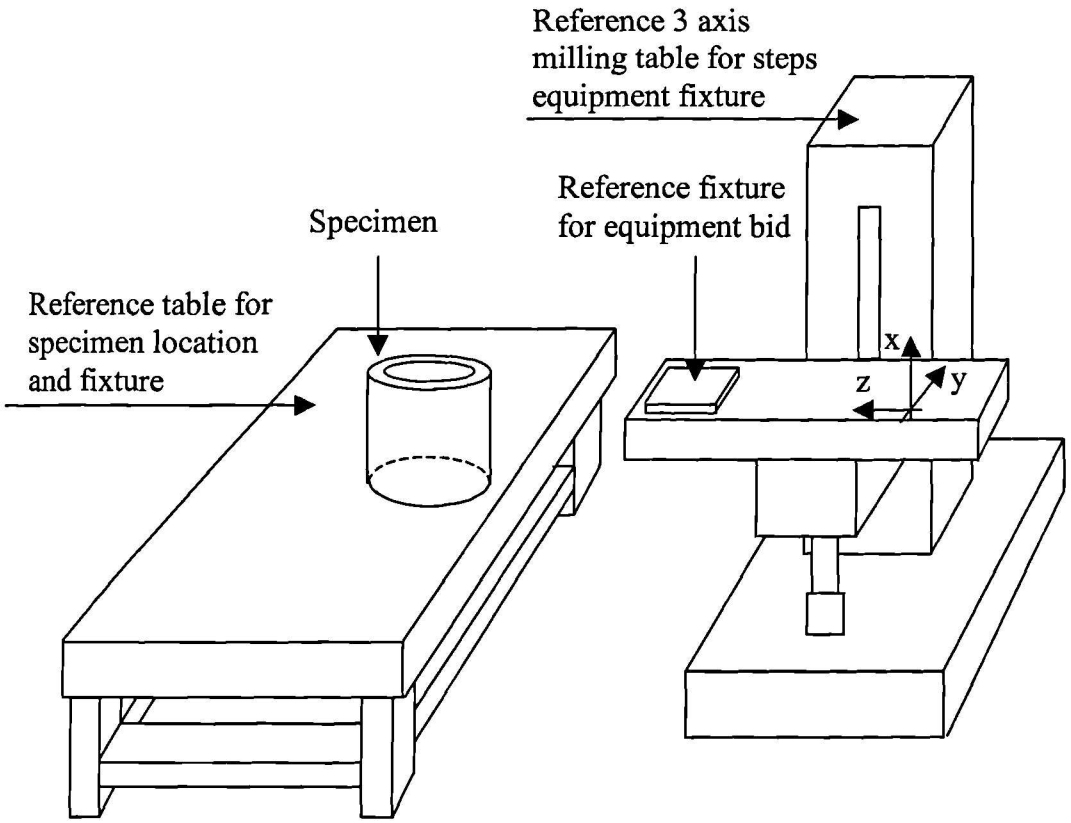

Figure 3.1a : Schematic layout of experimental setup.

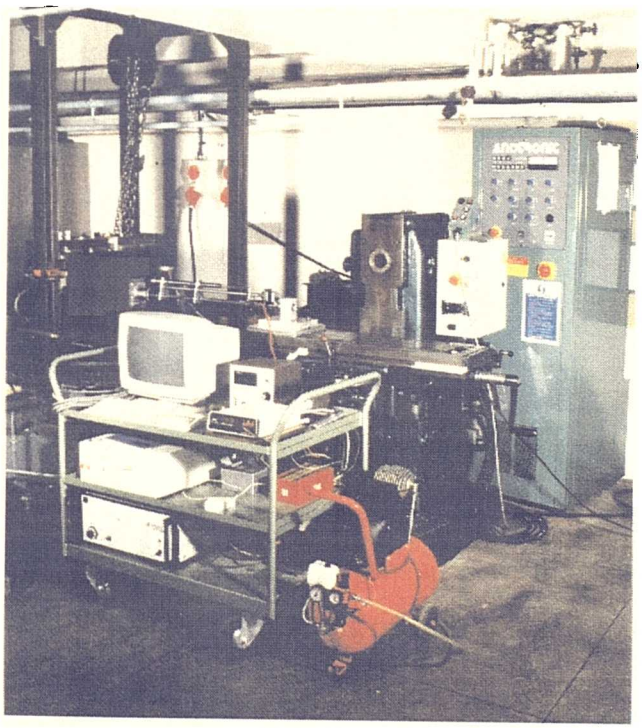

Figure 3.1b : Photograph of experimental setup.

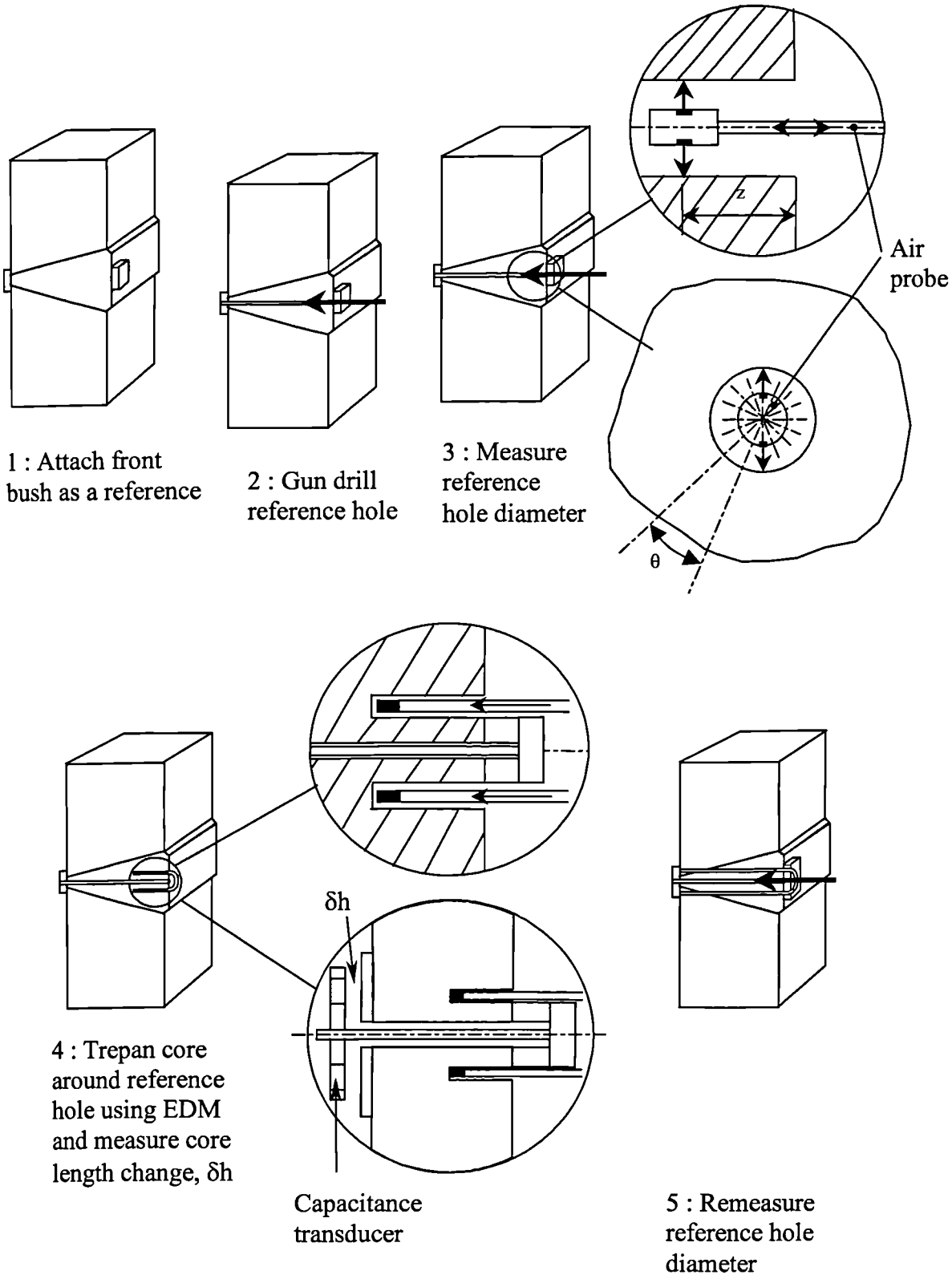

Figure 3.2 : Steps in the experimental technique.

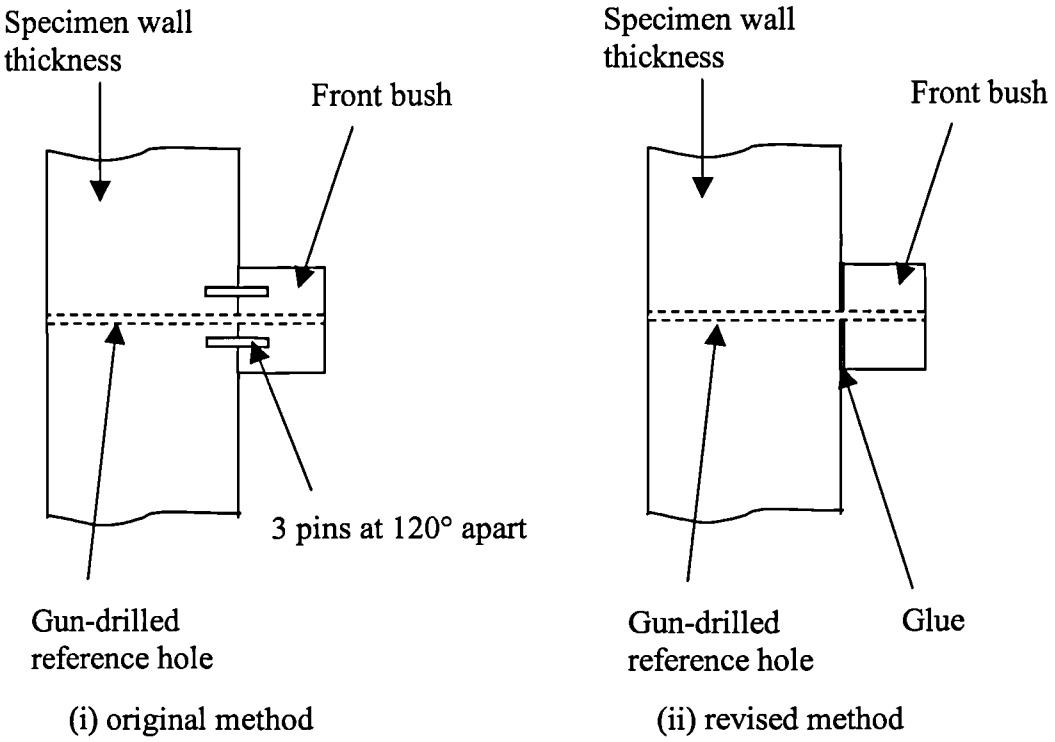

Figure 3.3a : Attachment of bushes onto the specimen surface.

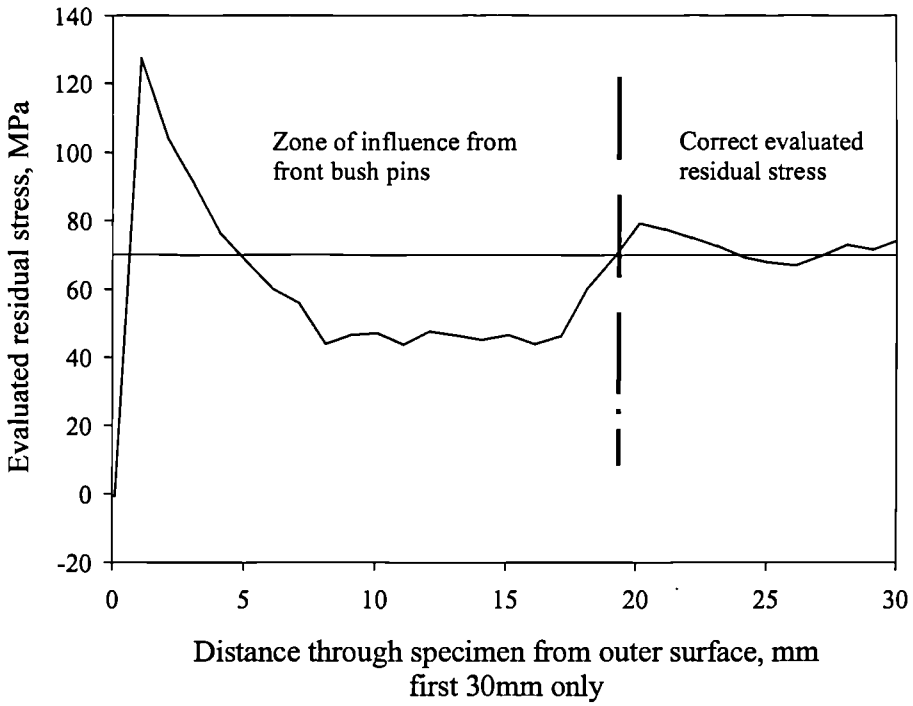

Figure 3.3b : Attachment of bushes onto the specimen surface of a steel bar and influence of attachment pins.

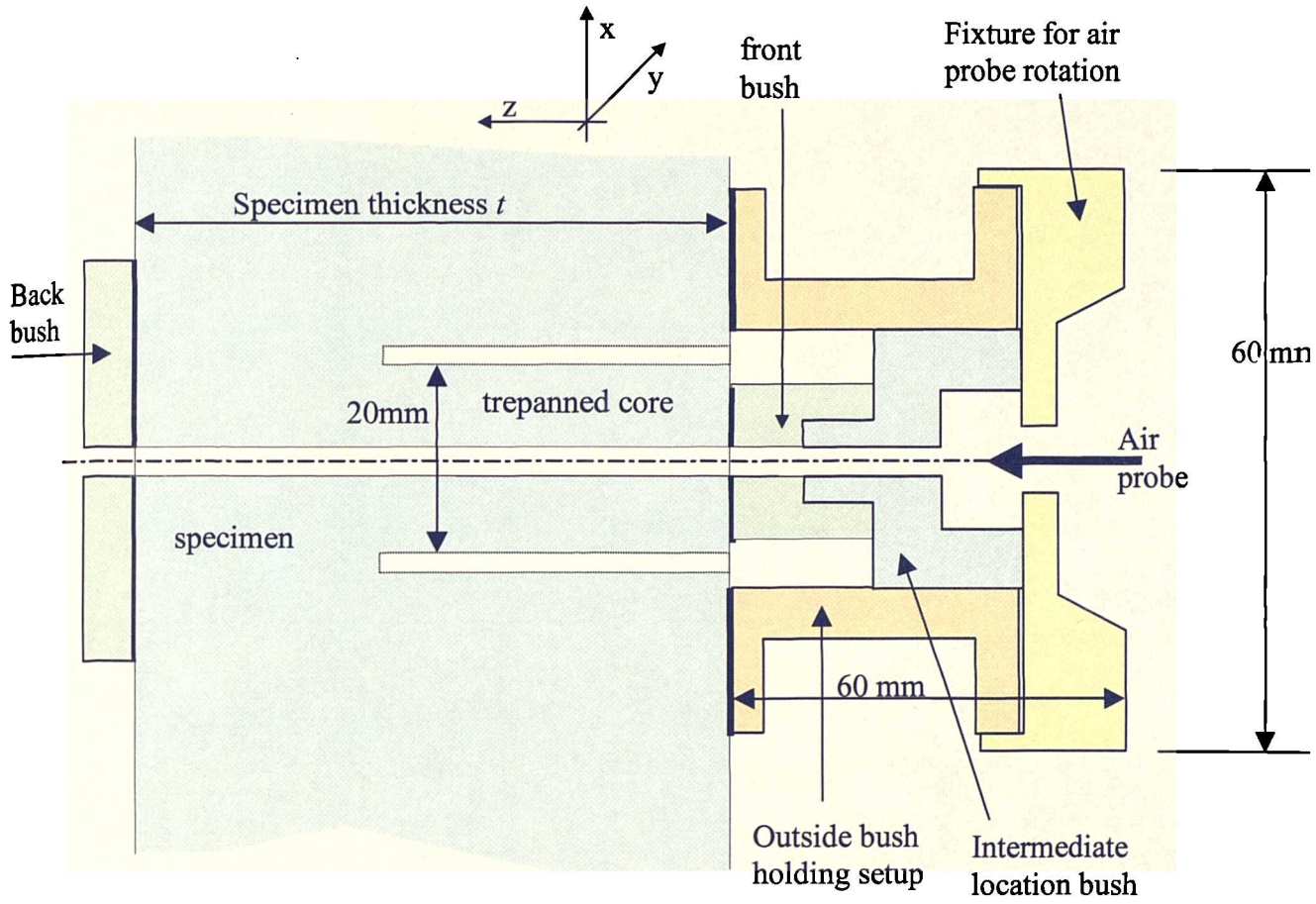

Figure 3.4 : Schematic of attached bushes.

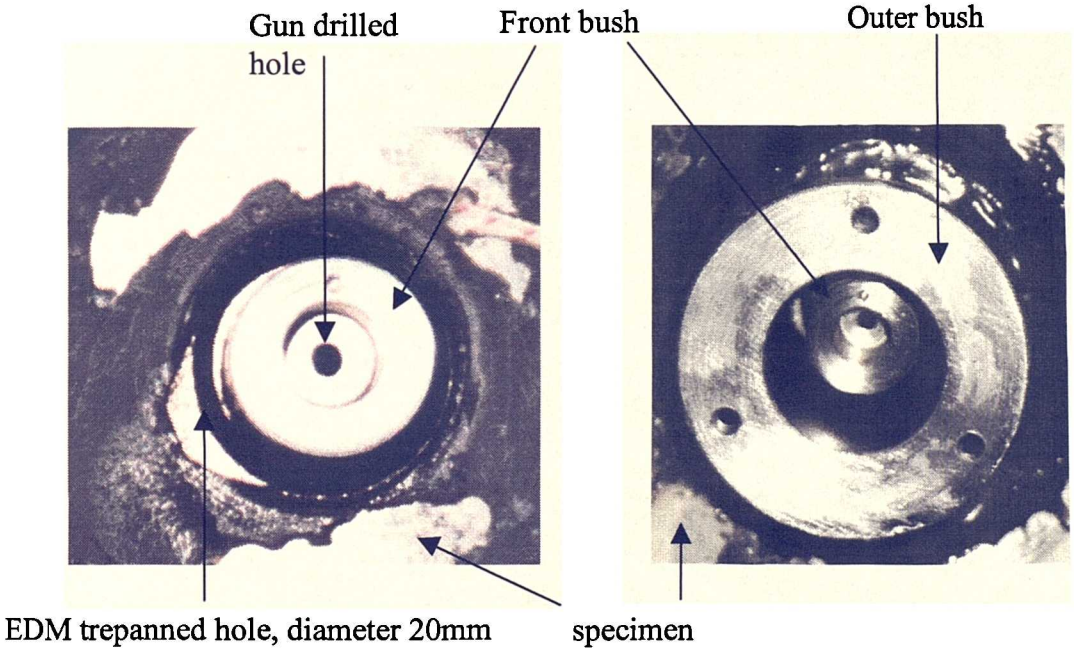

Figure 3.5 : Pictures of the front bush arrangement.

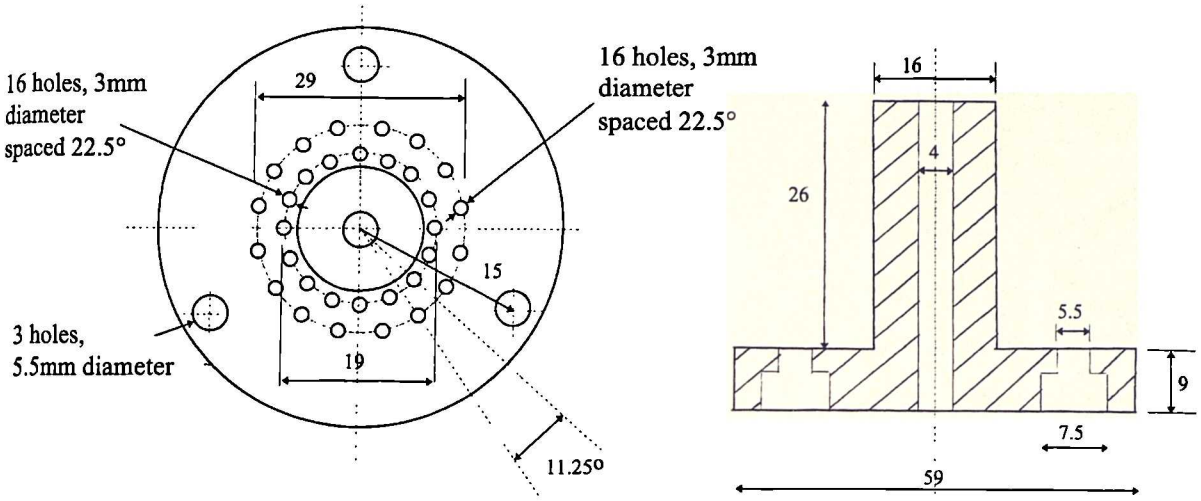

all dimensions in millimetres

Figure 3.6a : Picture of the original location bush.

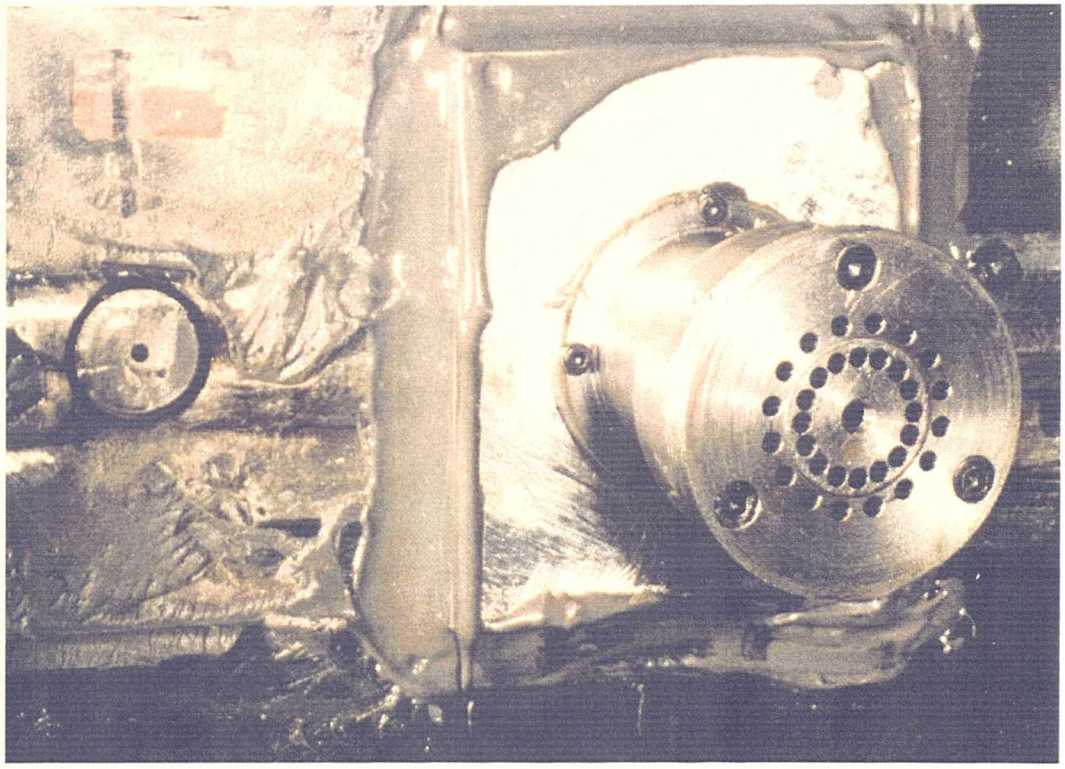

Figure 3.6b : Photograph of the original location bush.

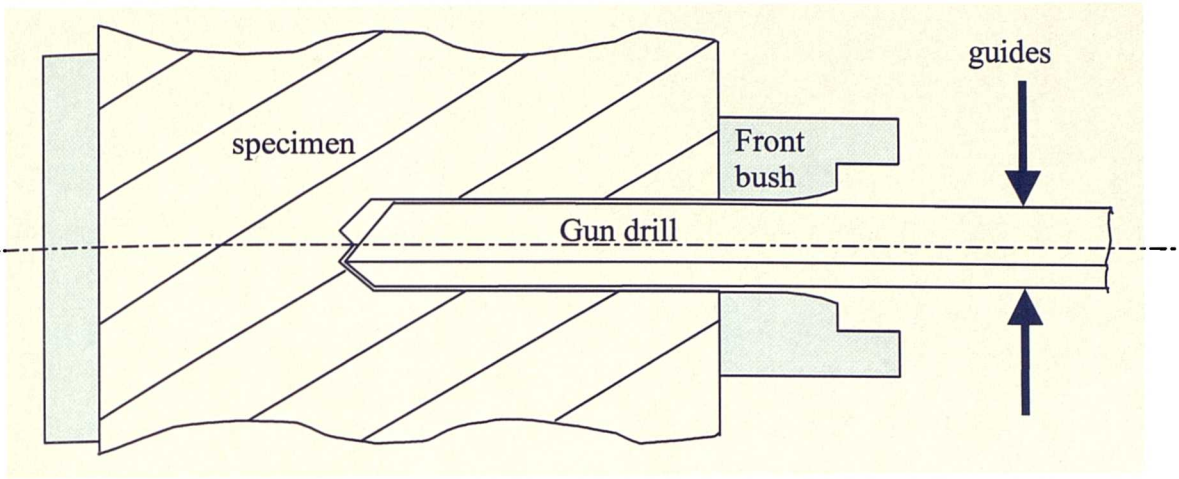

Figure 3.7a : Schematic of gun-drilling.

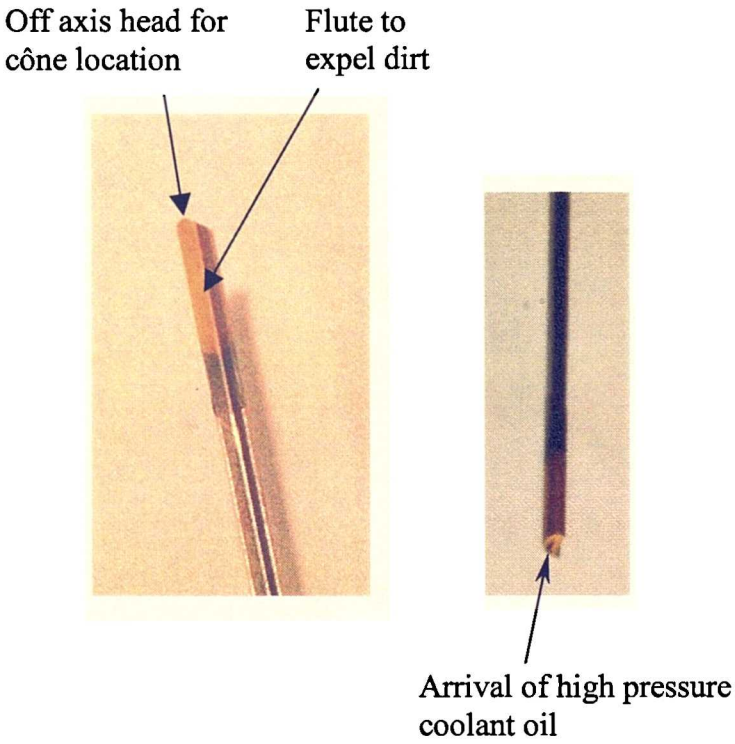

Figure 3.7b : Picture of gun-drill head.

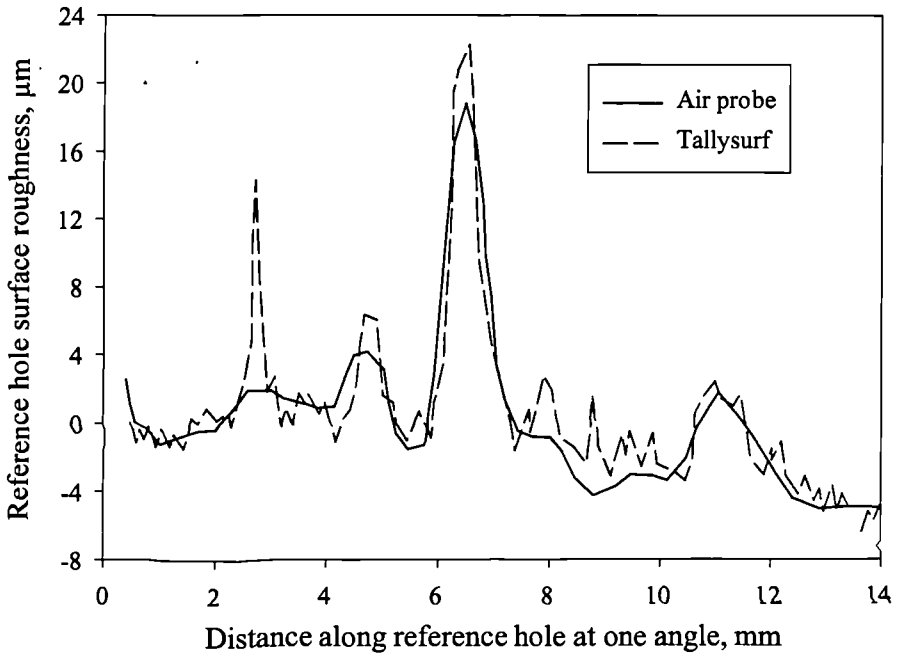

Figure 3.8 : Comparison of tallysurf and air-probe reading.

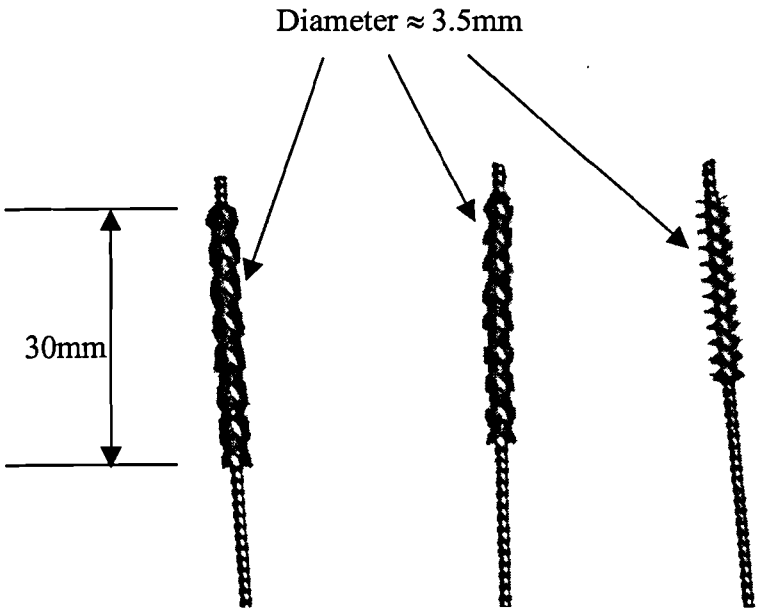

Figure 3.9 : Picture of flex hone used for reference hole surface roughness.

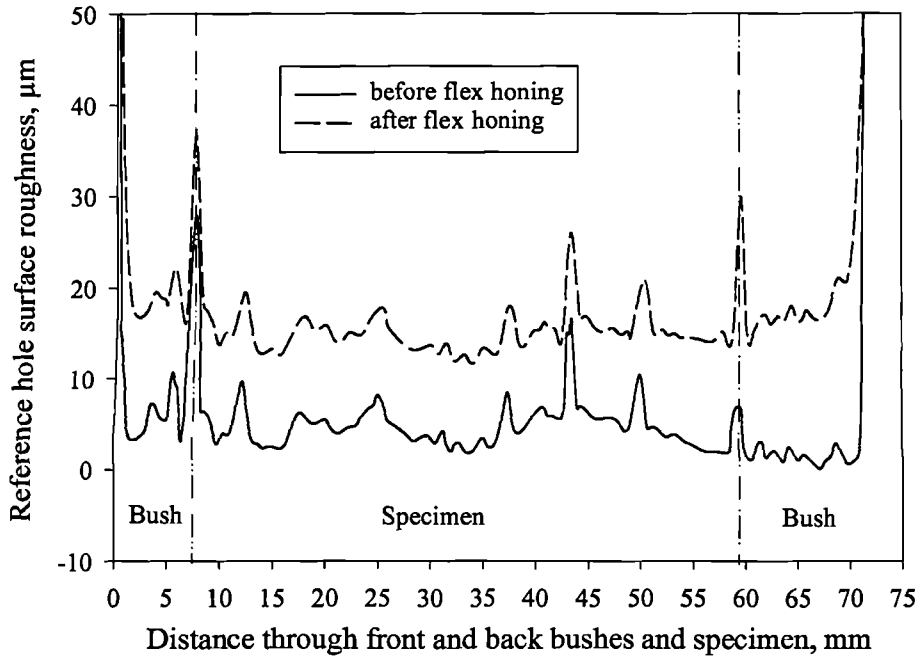

Figure 3.10 : Comparison of air probe reading before and after flex honing.

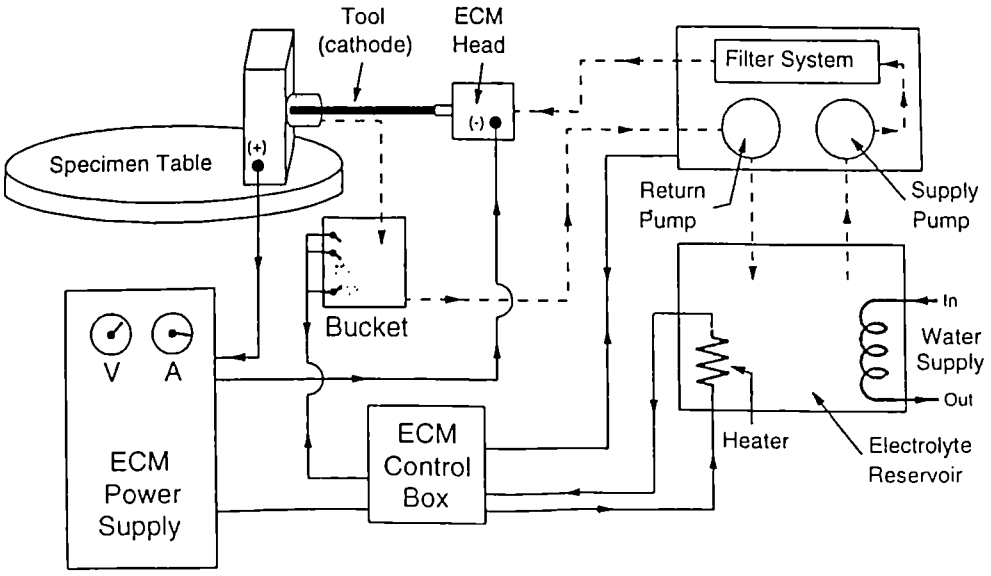

Figure 3.11 : Schematic layout of ECM system.

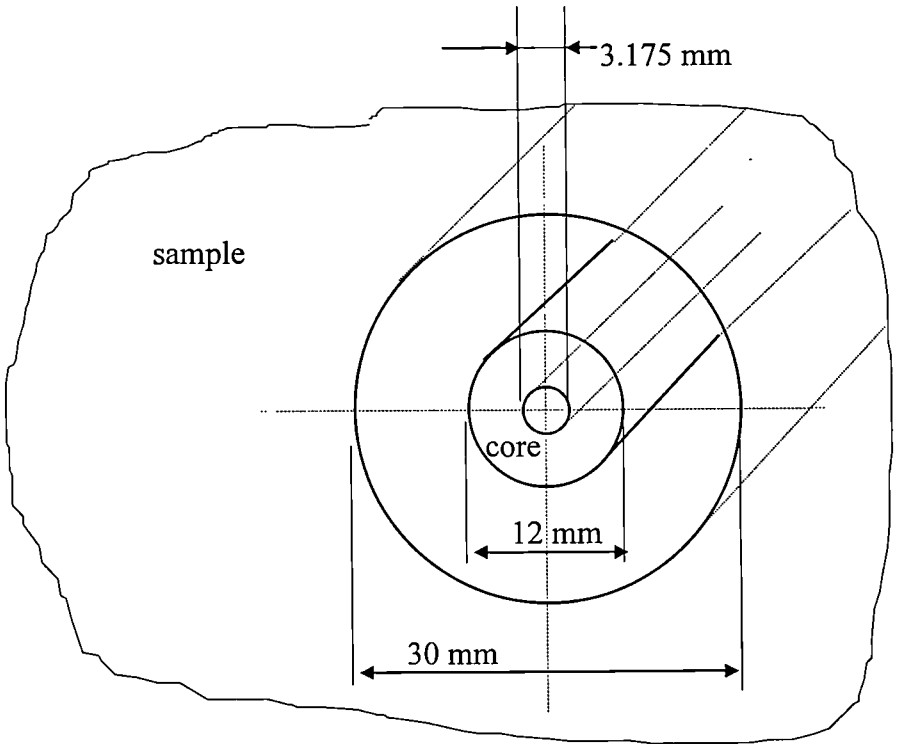

Figure 3.12 : Schematic of the core extracted from specimen using ECM system.

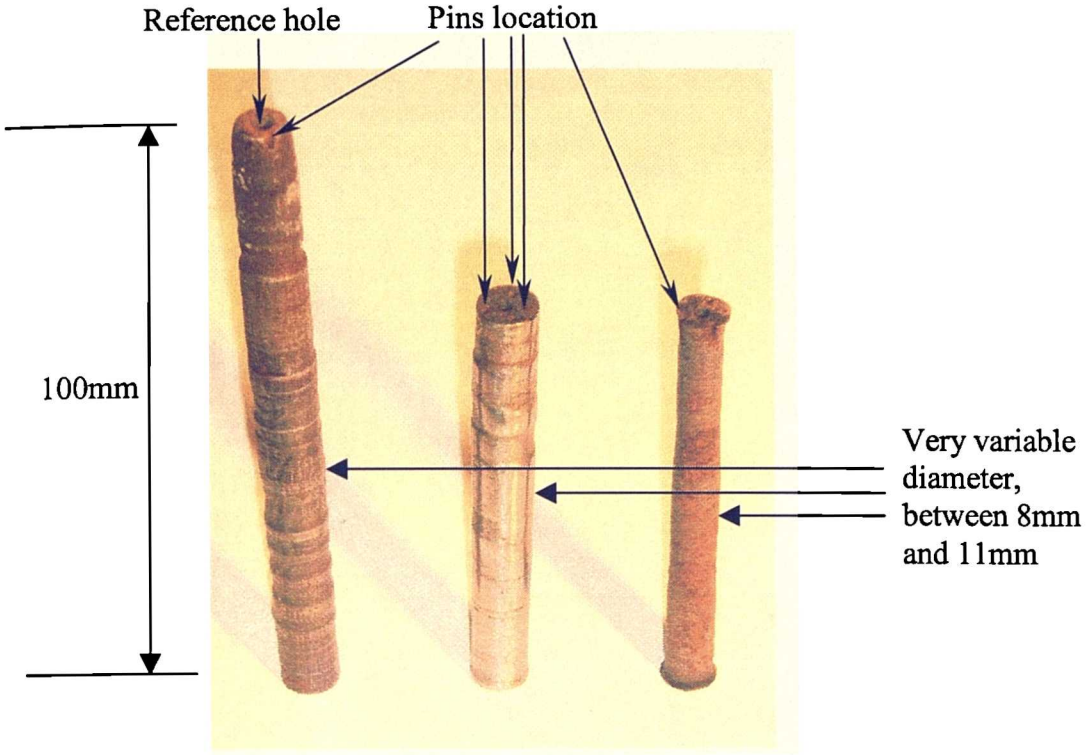

Figure 3.13 : Extracted cores using ECM.

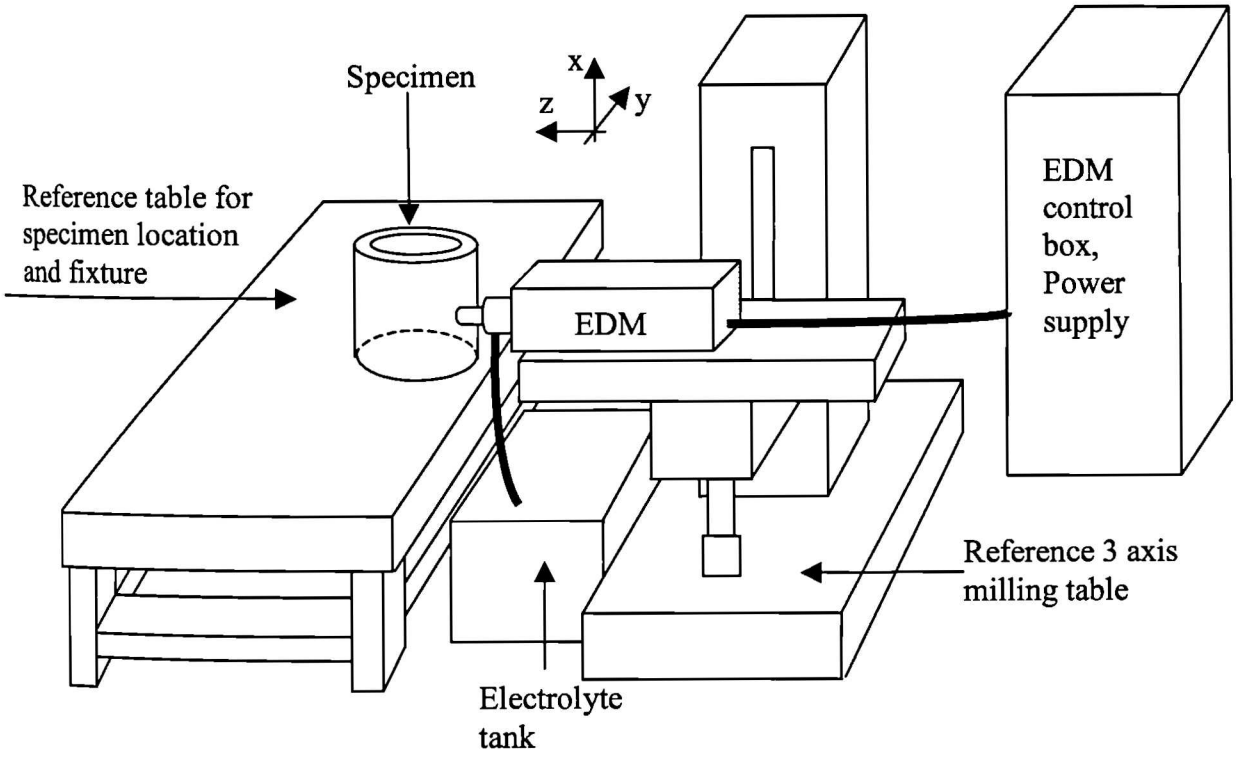

Figure 3.14a : Schematic layout of the EDM system.

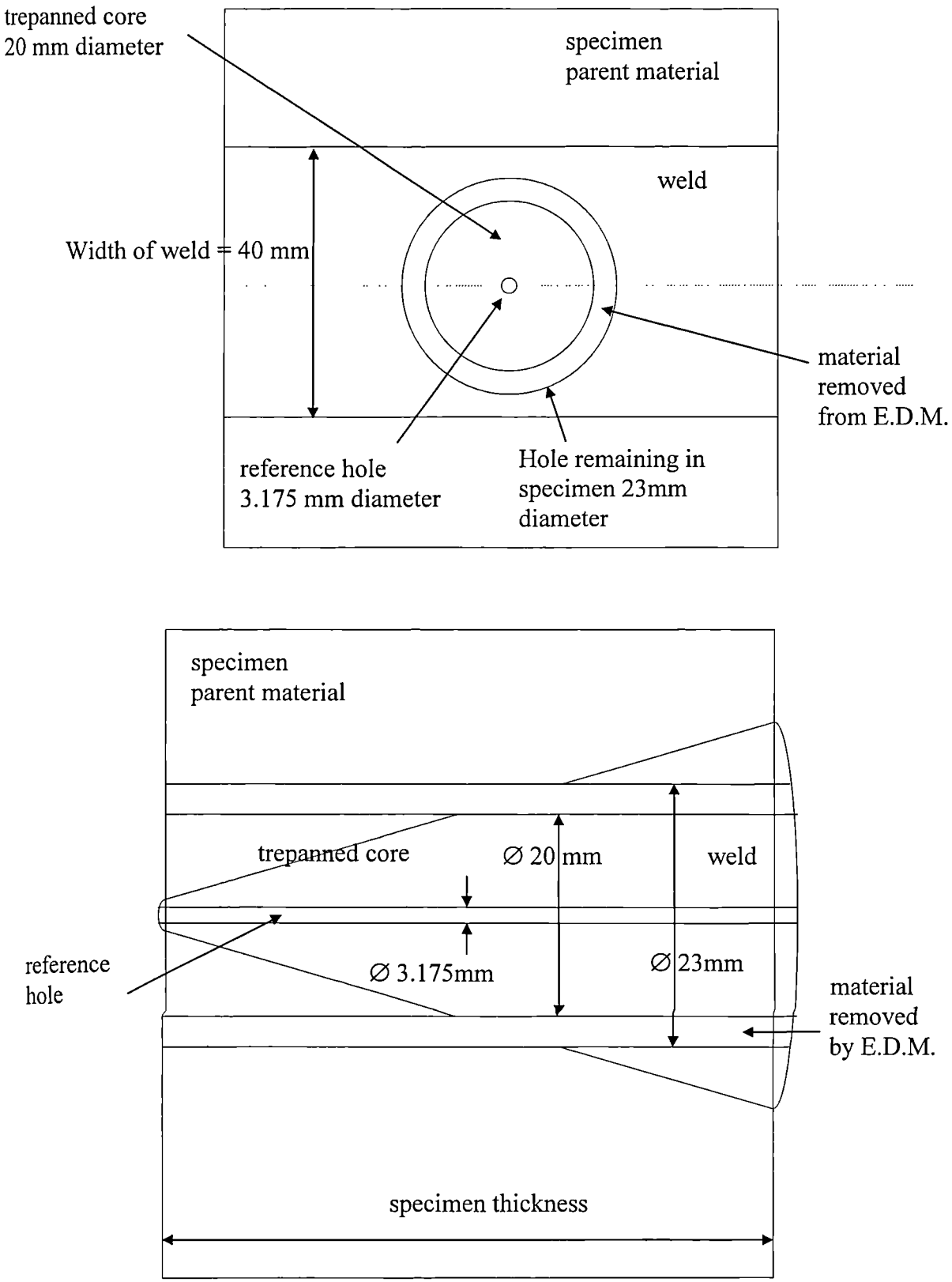

Figure 3.14b : Schematic layout of EDM geometry.

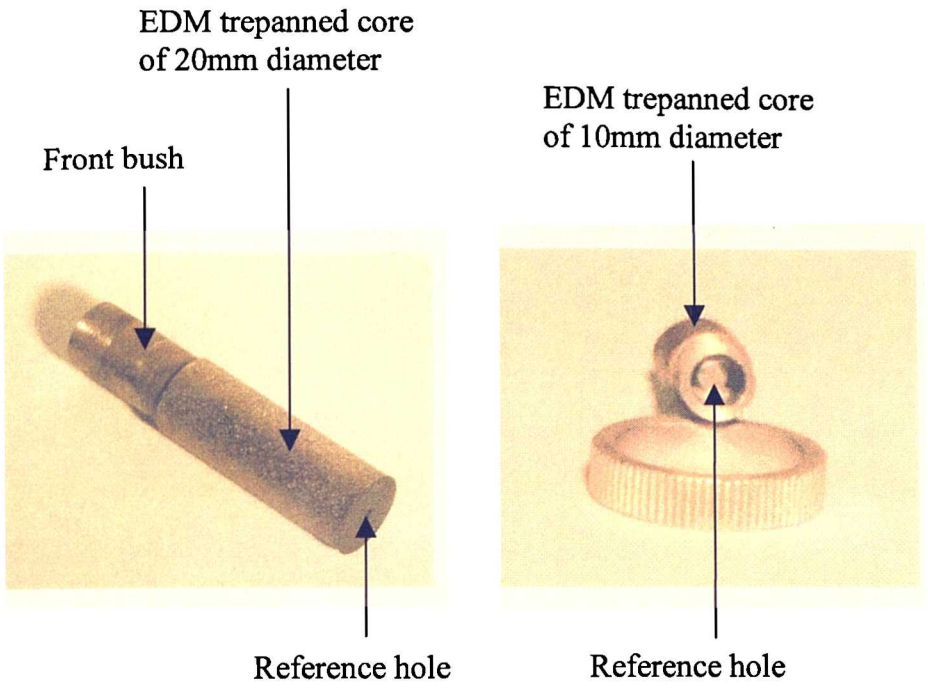

Figure 3.15 : Extracted cores using EDM process.

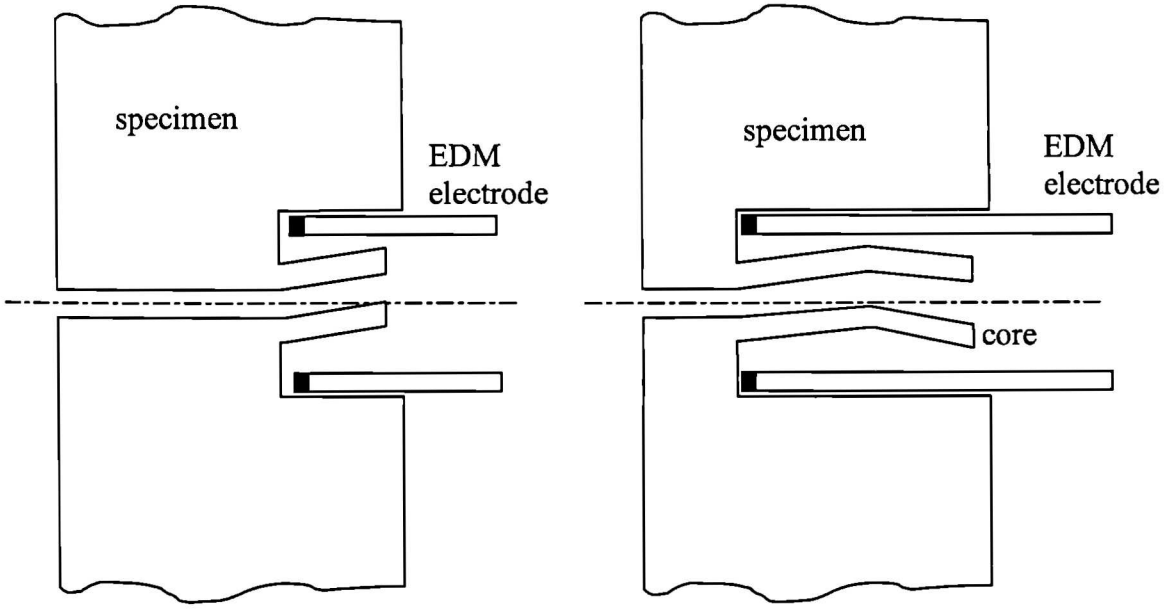

Figure 3.16 : Schematic of core deformation exaggerated during EDM process.

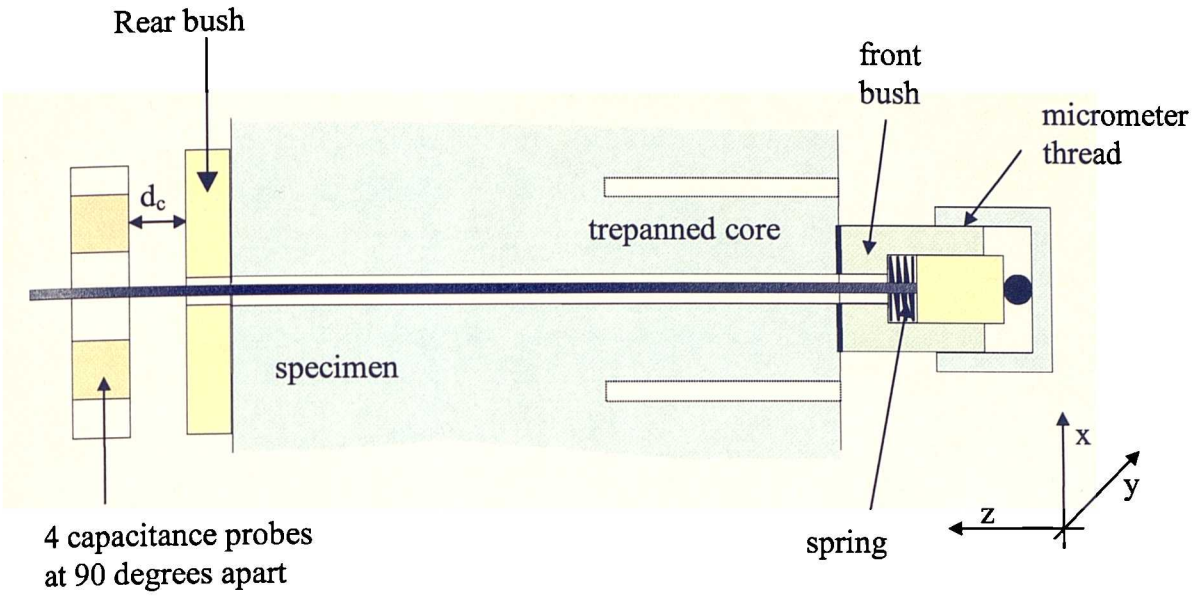

Figure 3.17 : Schematic layout of capacitance probe arrangement.

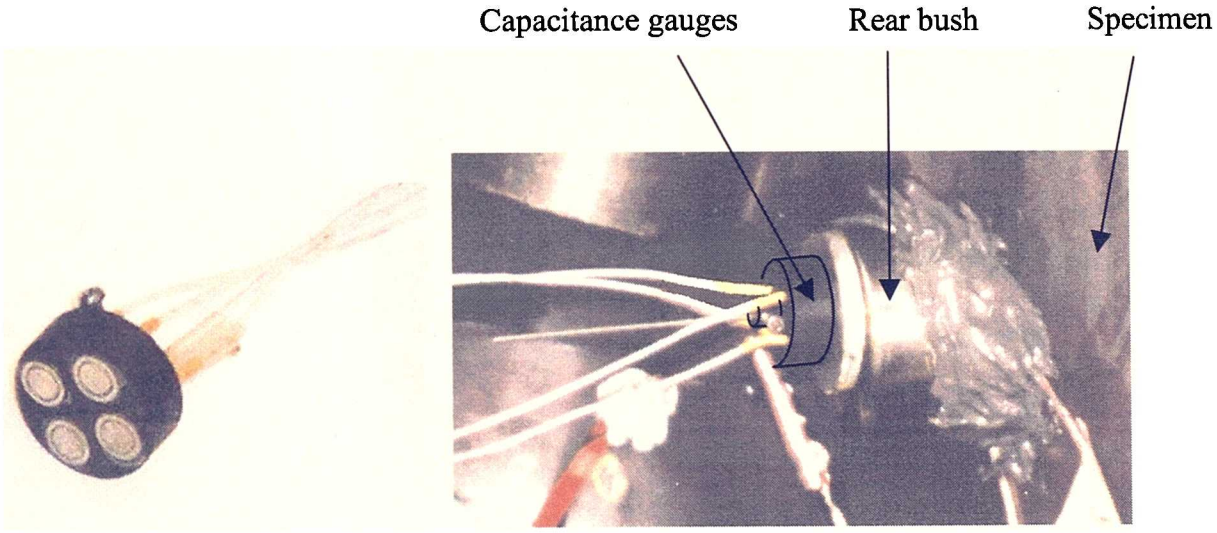

Figure 3.18 : Picture of capacitance probe and arrangement at the back of specimen

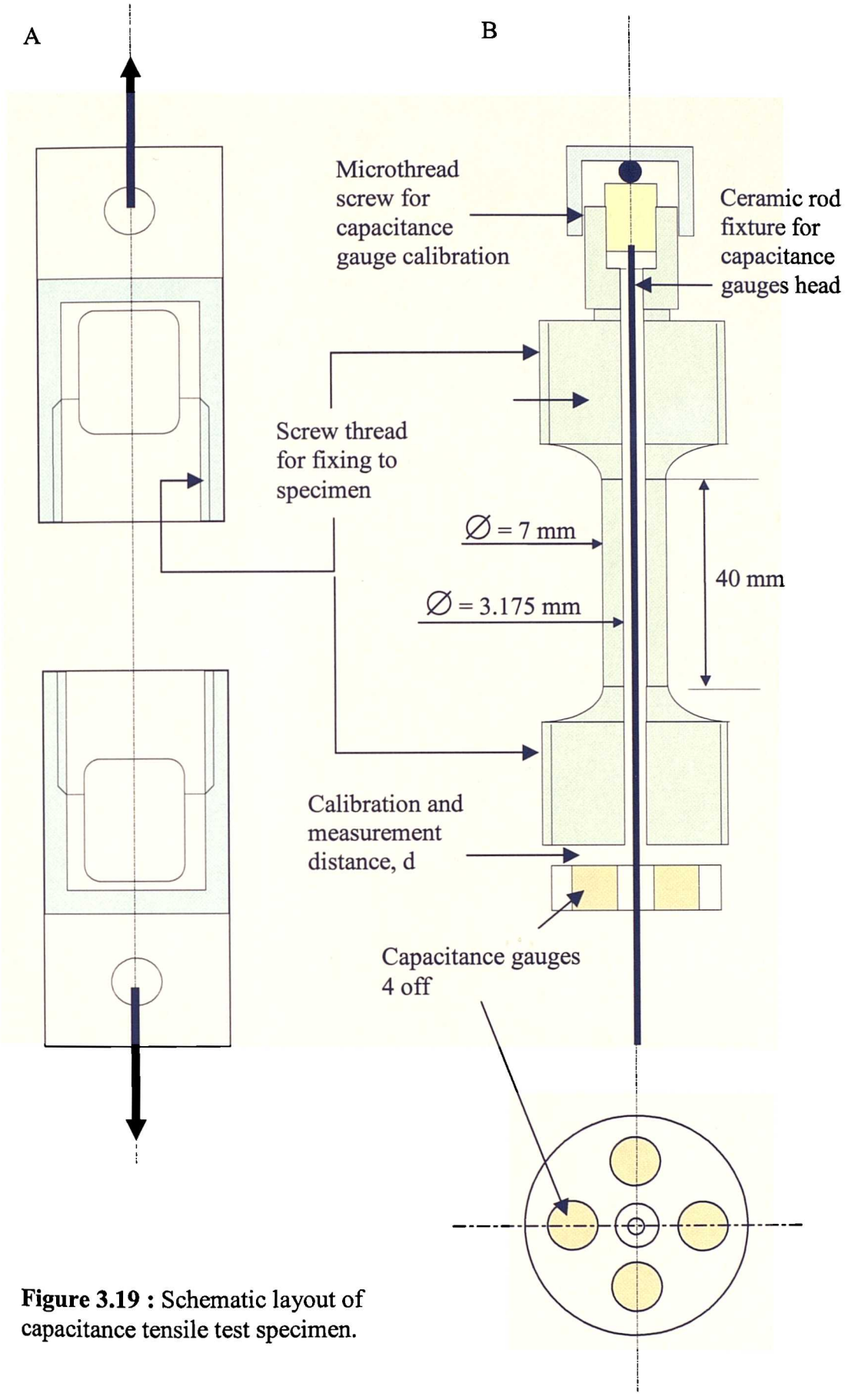

Figure 3.19 : Schematic layout of capacitance tensile test specimen.

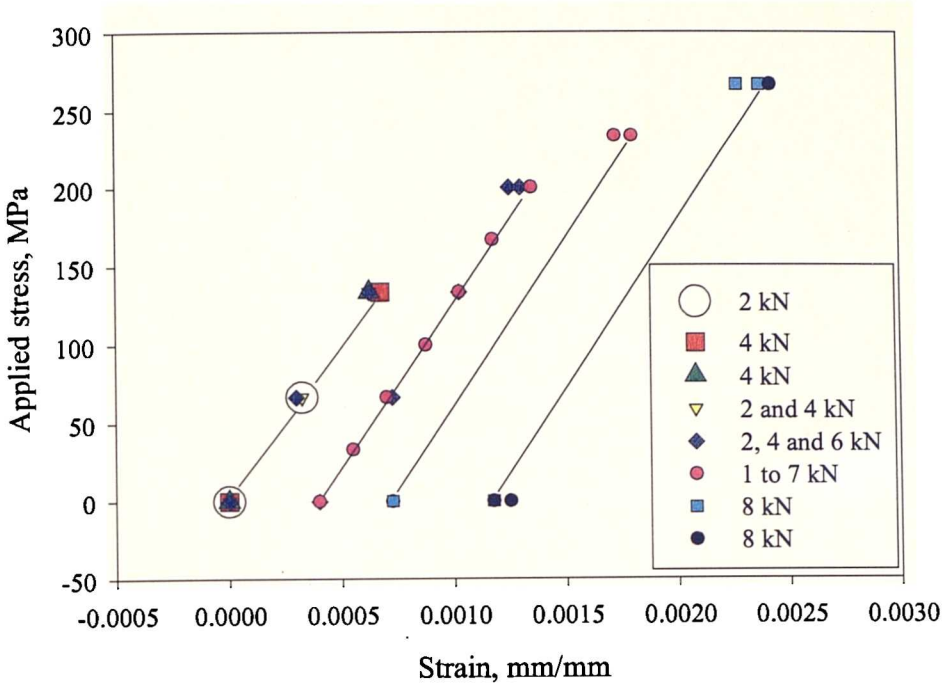

Figure 3.20 : Results of the capacitance calibration test.

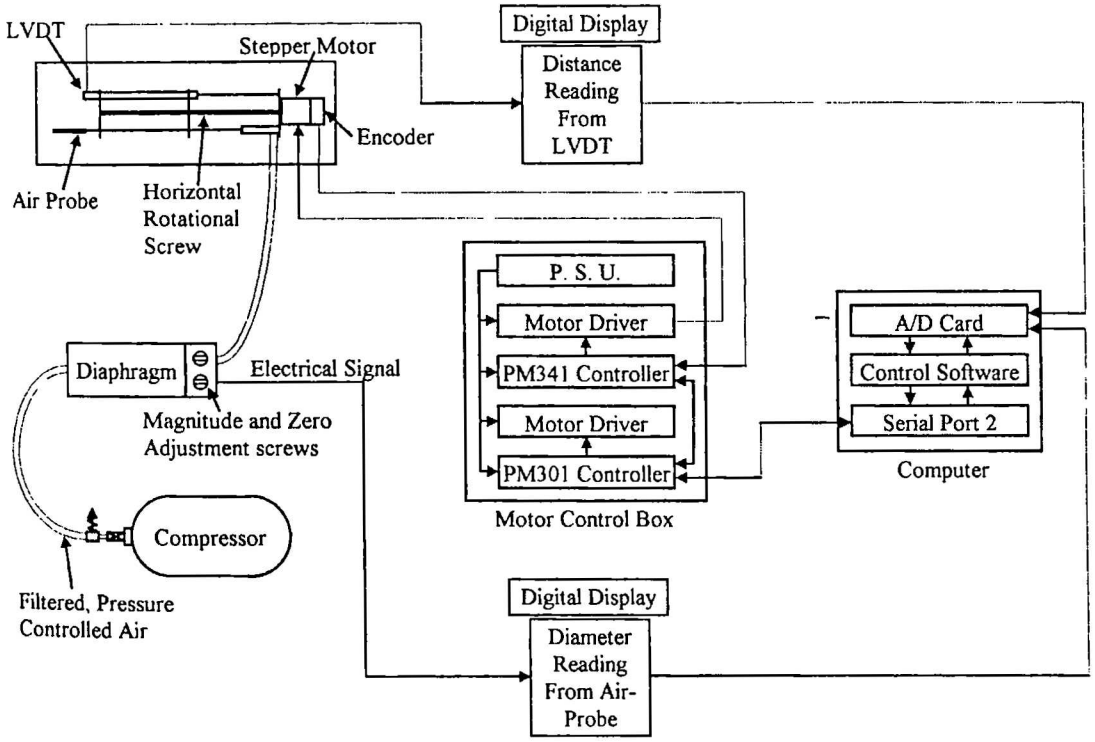

Figure 3.21 : Schematic layout of air probe system.

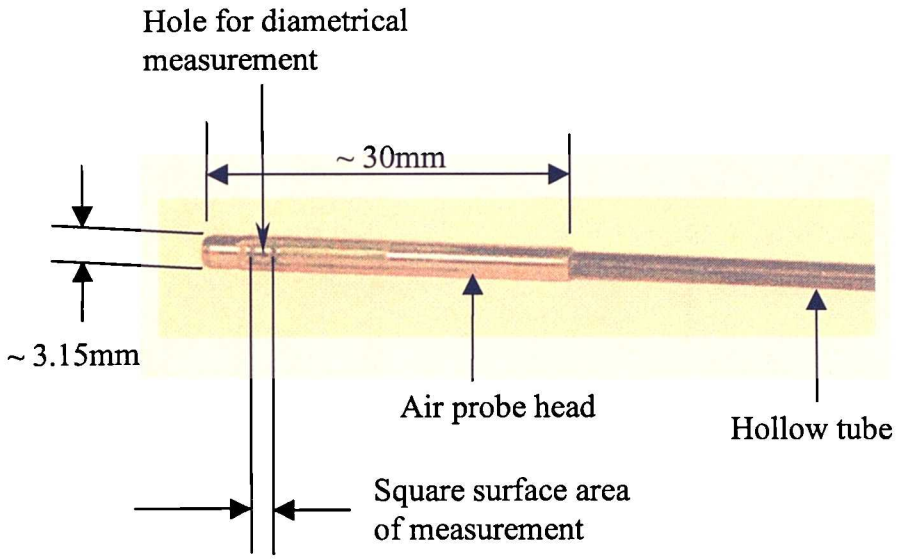

Figure 3.22 : Picture of air probe head.

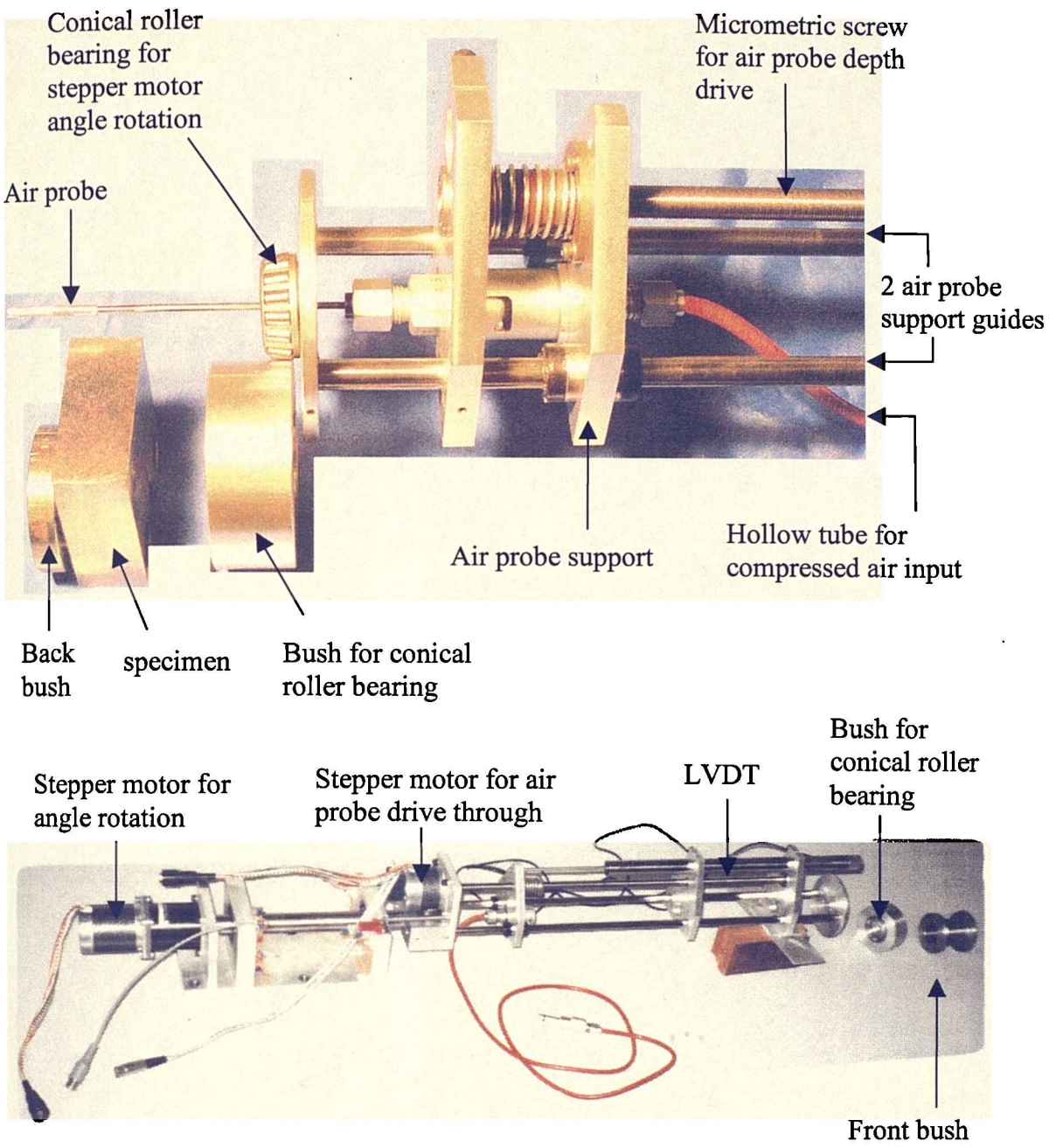

Figure 3.23 : Air probe rig system.

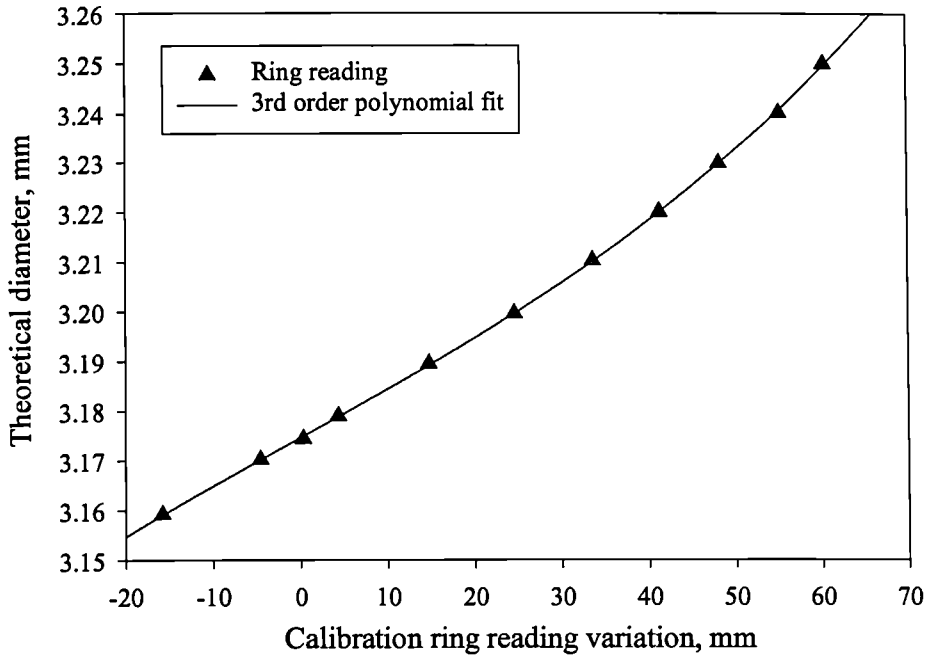

Figure 3.24 : Typical calibration curve for air probe system.

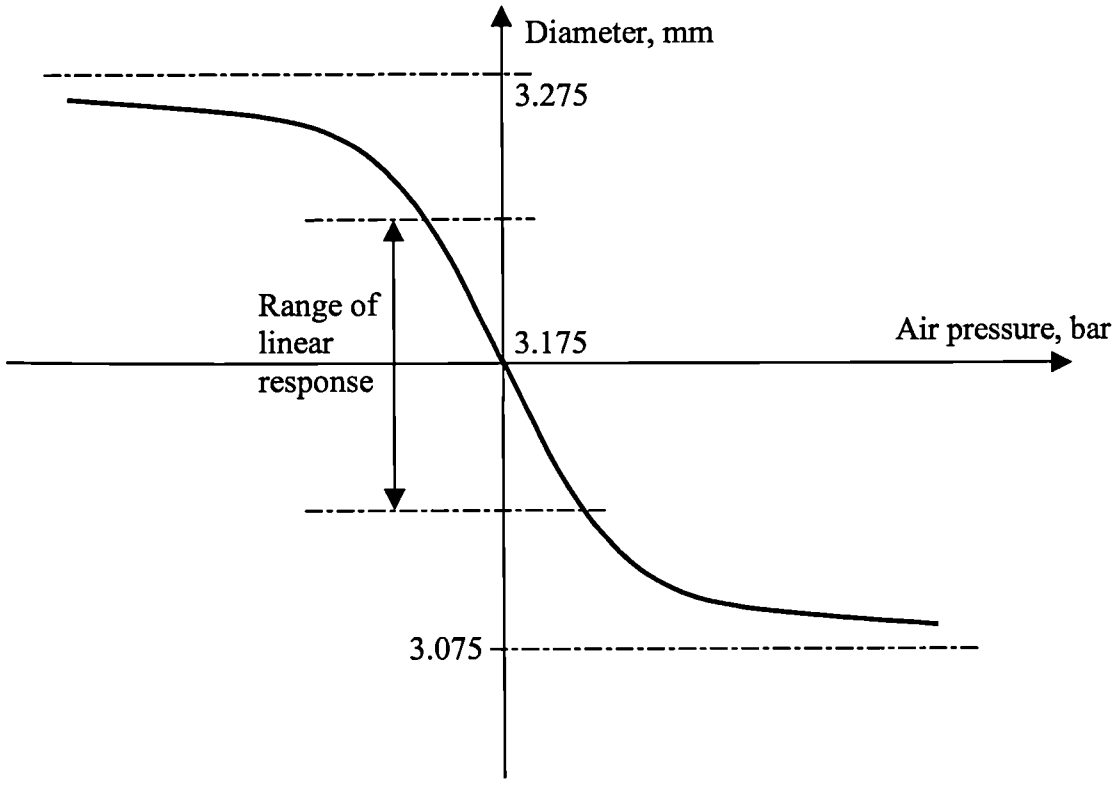

Figure 3.25 : Schematic response of air probe reading.

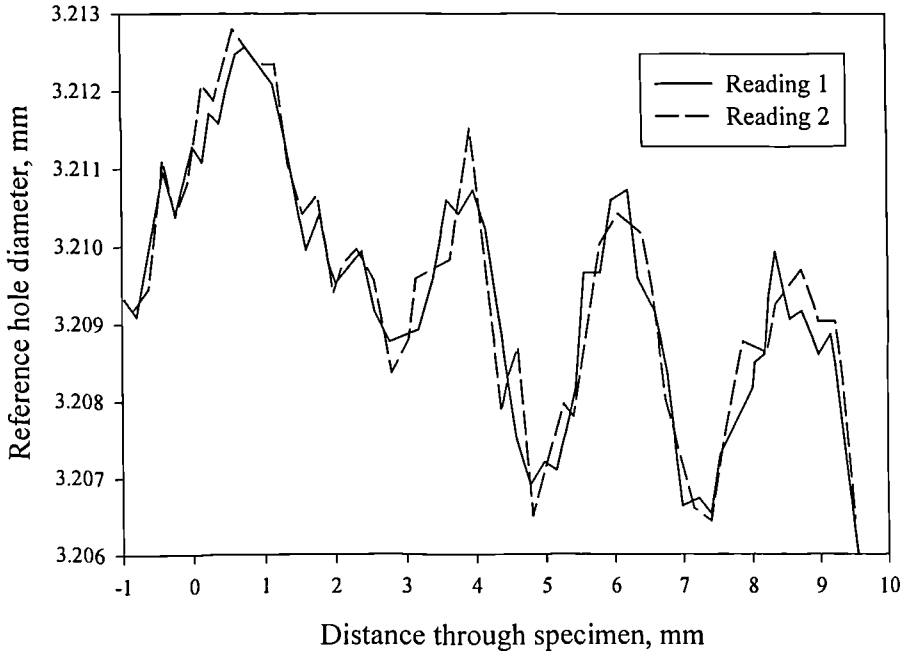

Figure 3.26 : Air probe repeatability of the same measurement position using the same calibration curve.

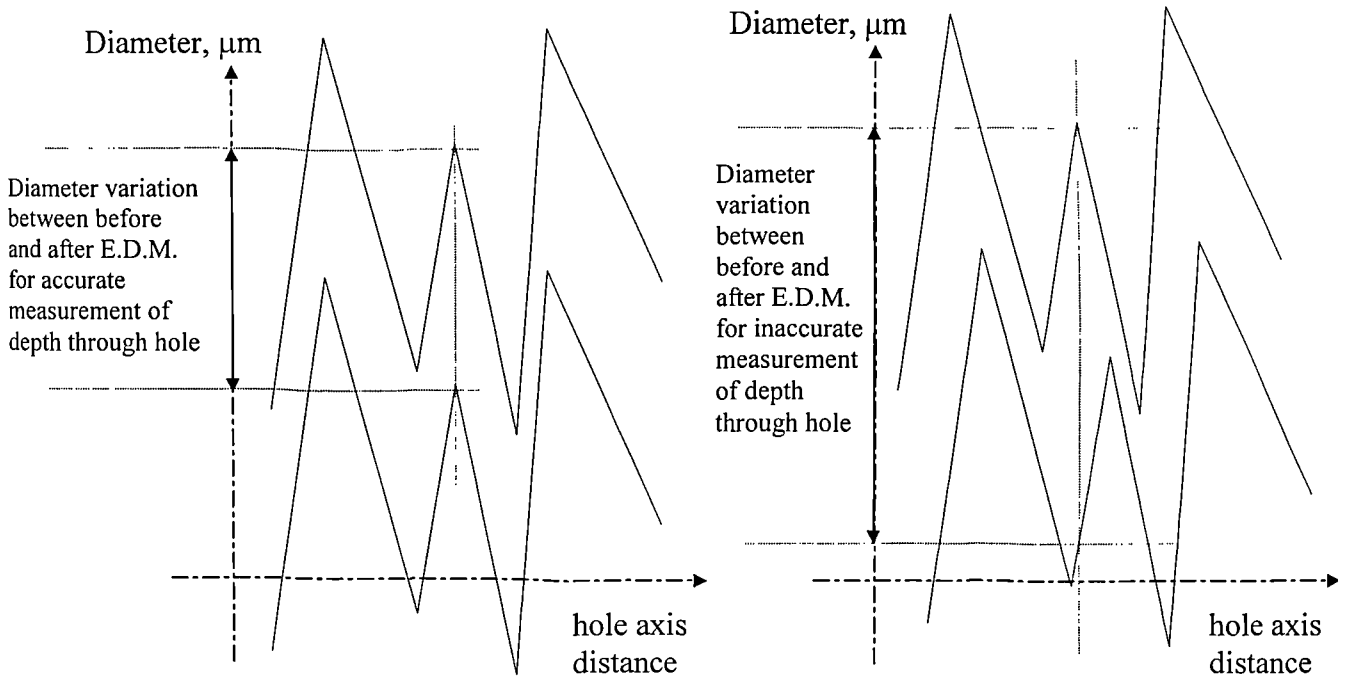

Figure 3.27 : Air probe reading between peaks and troughs.

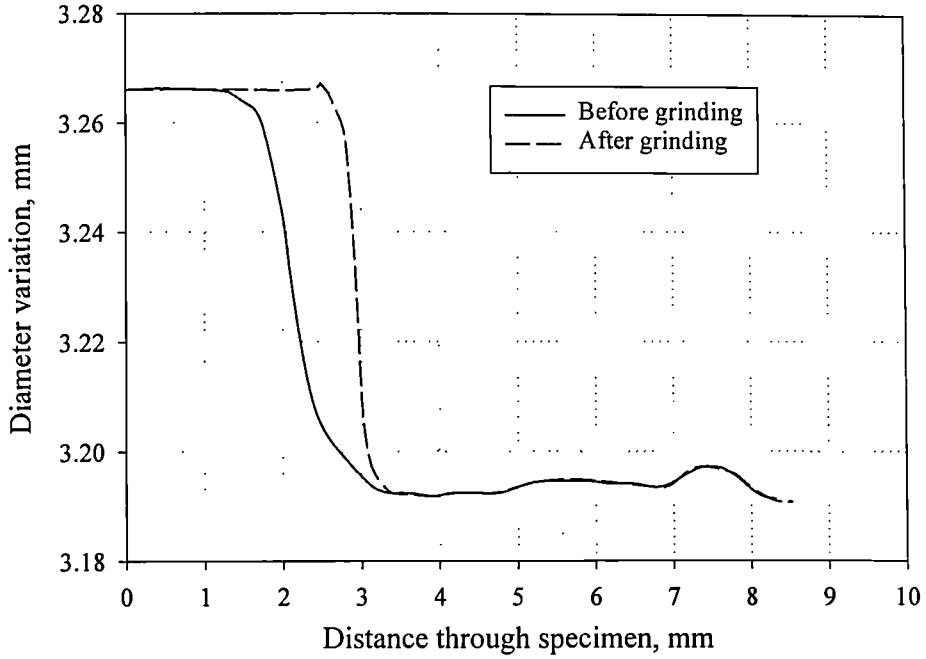

Figure 3.28 : Air probe reading comparison for ground test specimen.

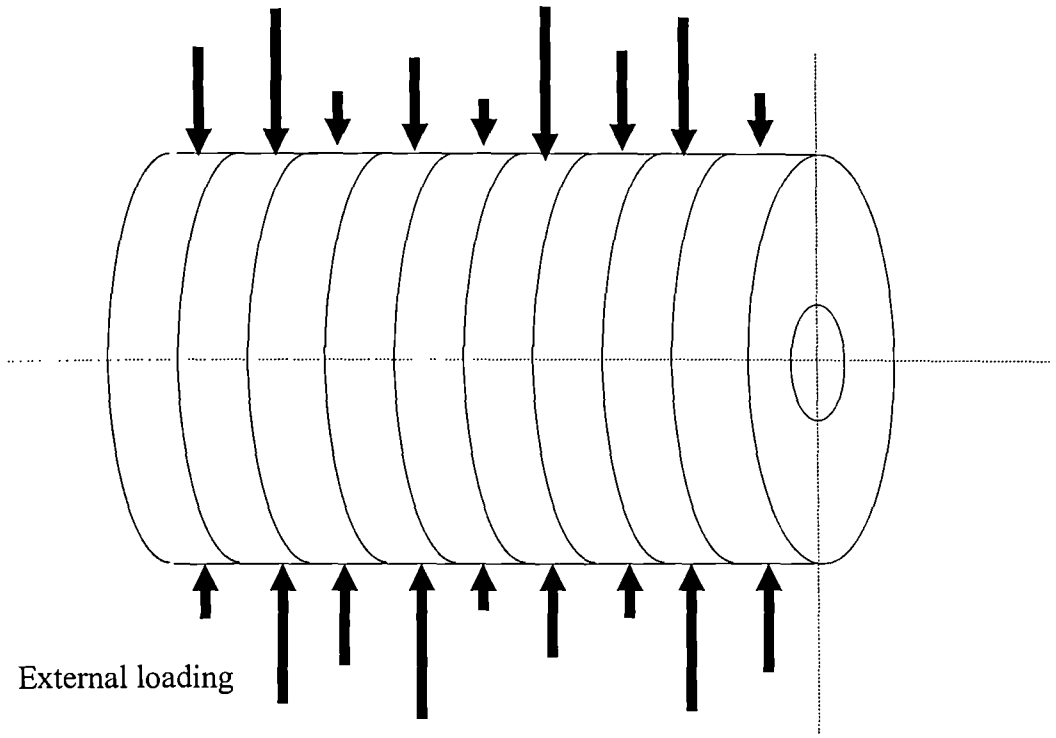

Figure 3.29 : Assumed series of plates.

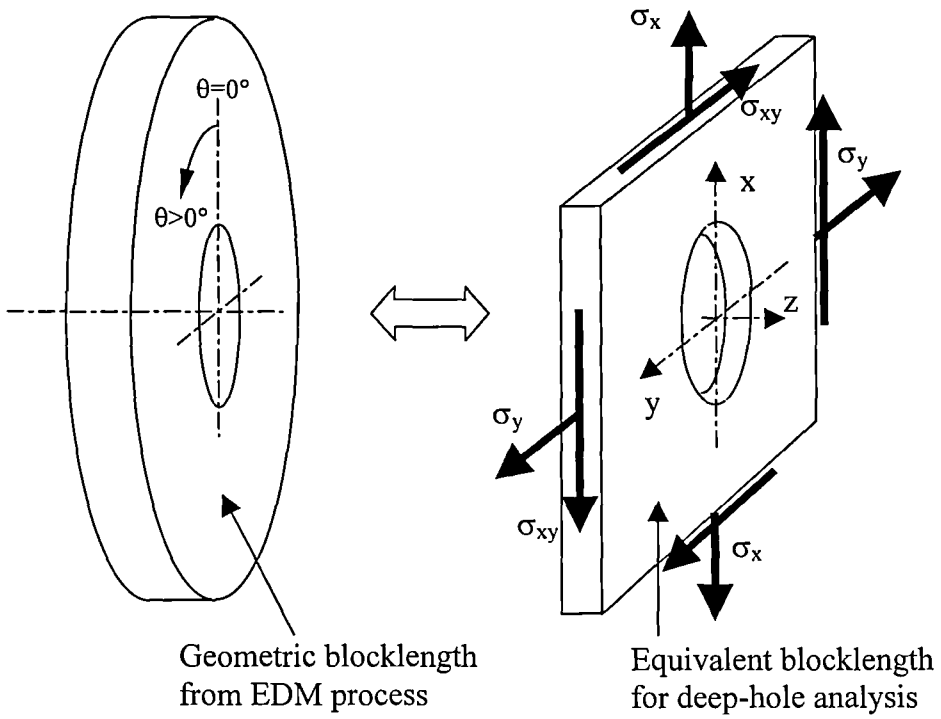

Figure 3.30 : Influence of number of angles.

a) 3 angles

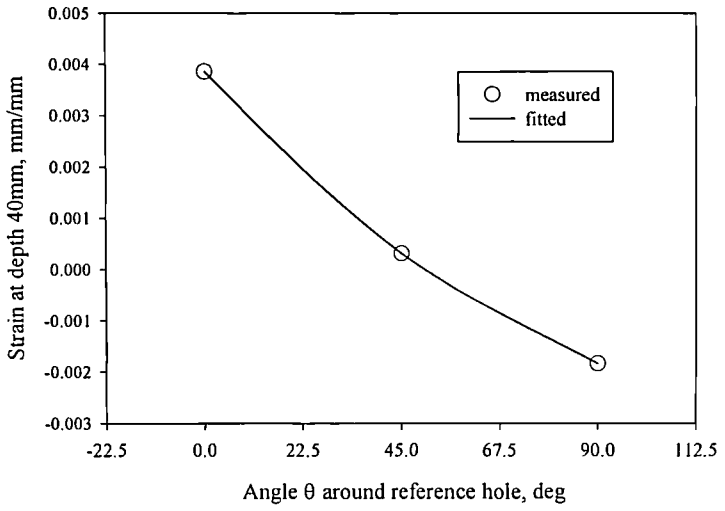

b) 16 angles

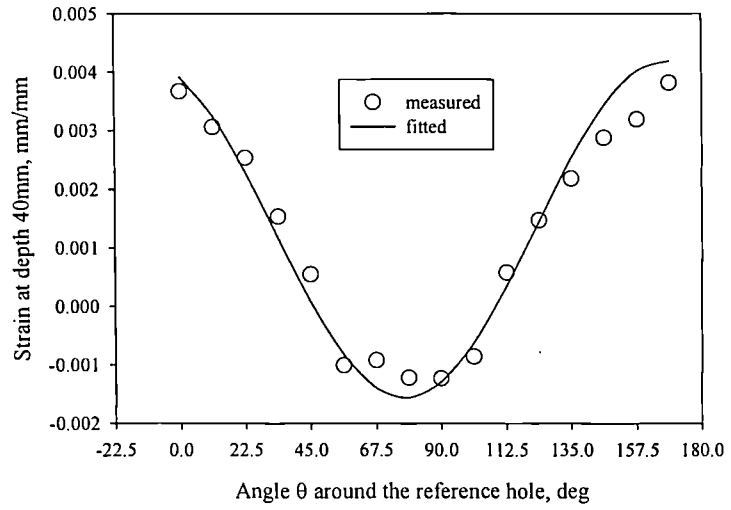

c) comparison

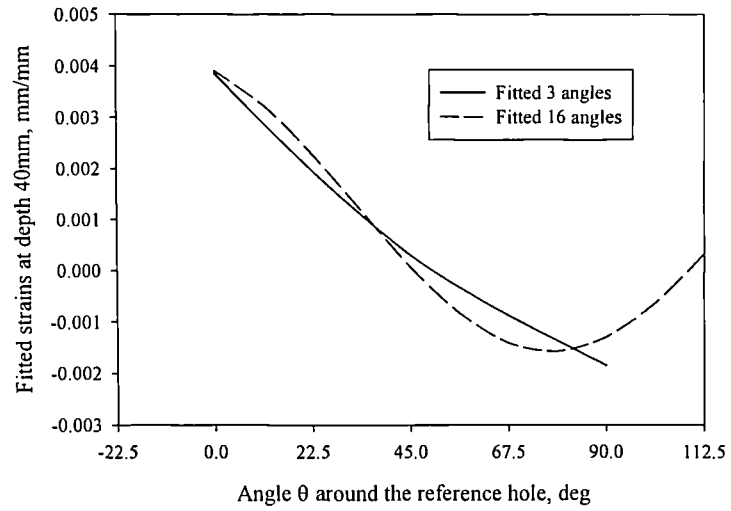

Figure 3.31 : Comparison of strain fit for 3 and 16 angles analysis.

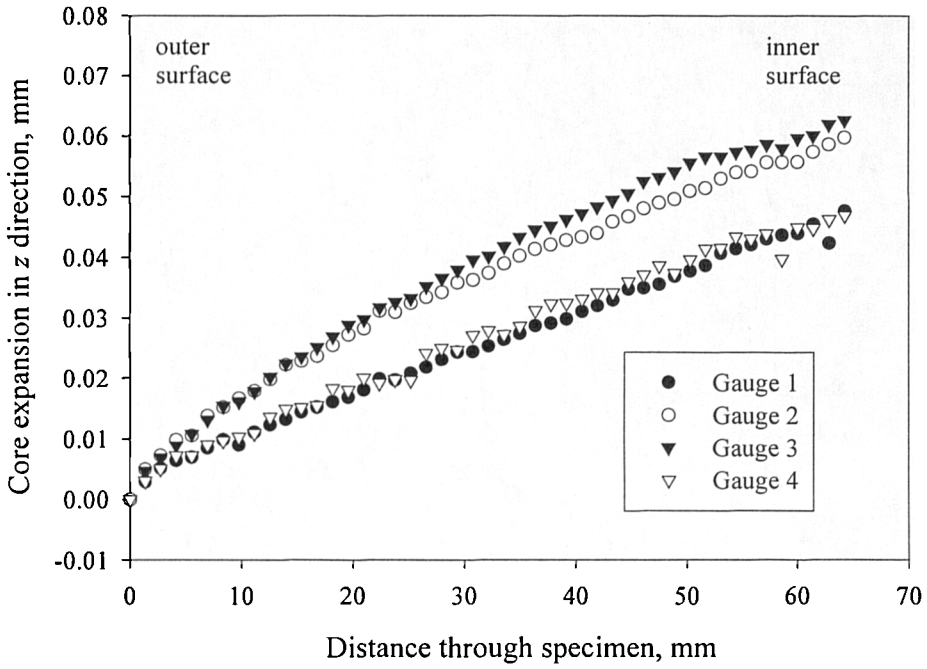

Figure 3.32 : Example of capacitance gauge readings during trepanning.

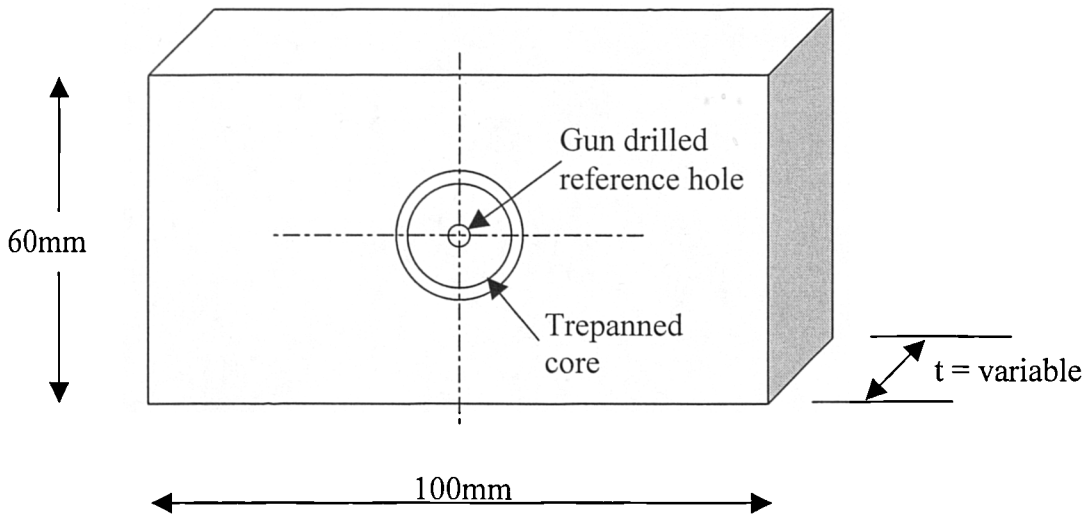

Figure 3.33 : General arrangement of the stress free blocs.

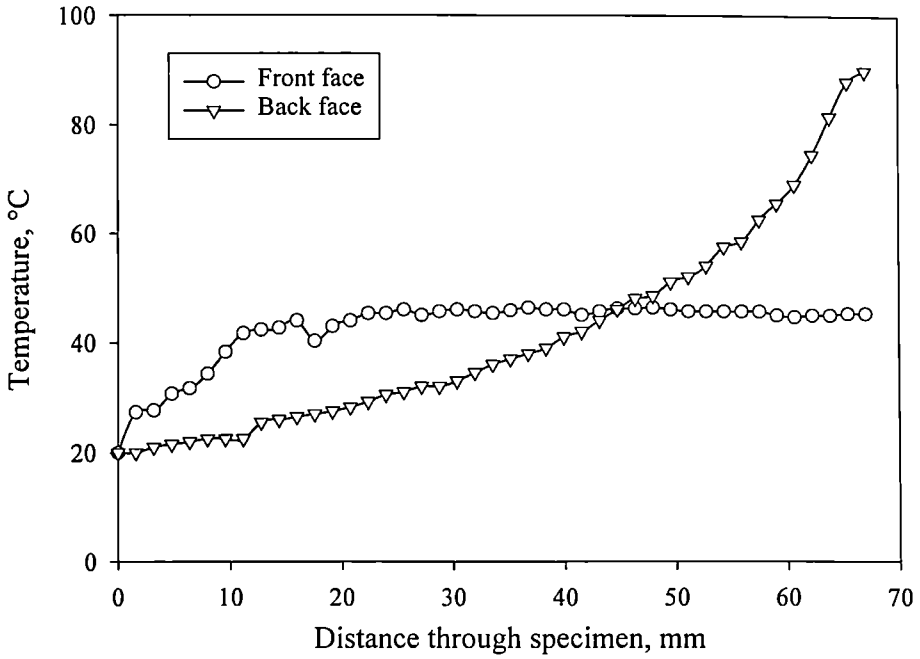

Figure 3.34 : Example of temperature readings during trepanning.

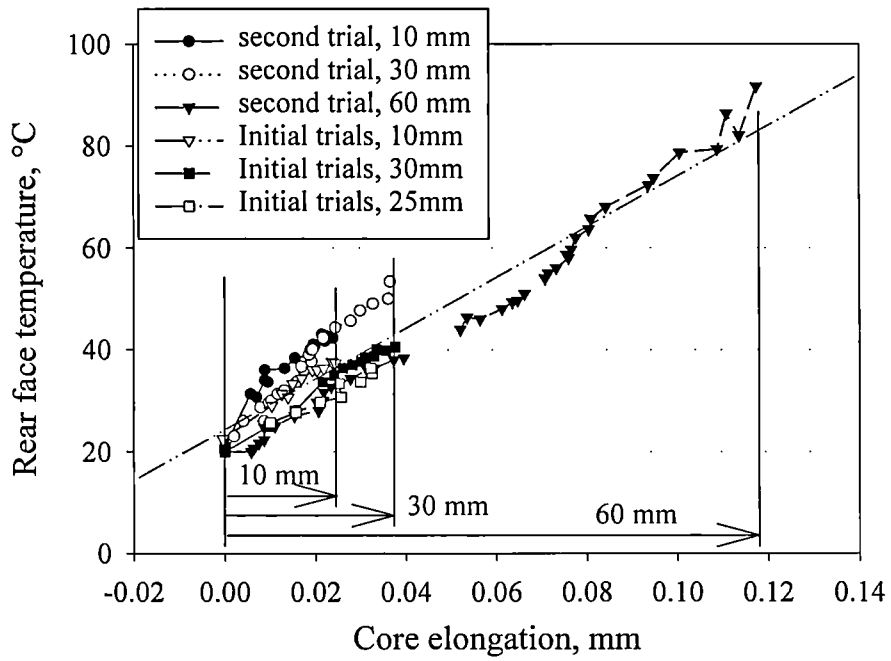

Figure 3.35 : Core elongation as a function of temperature from thermal calibrations.

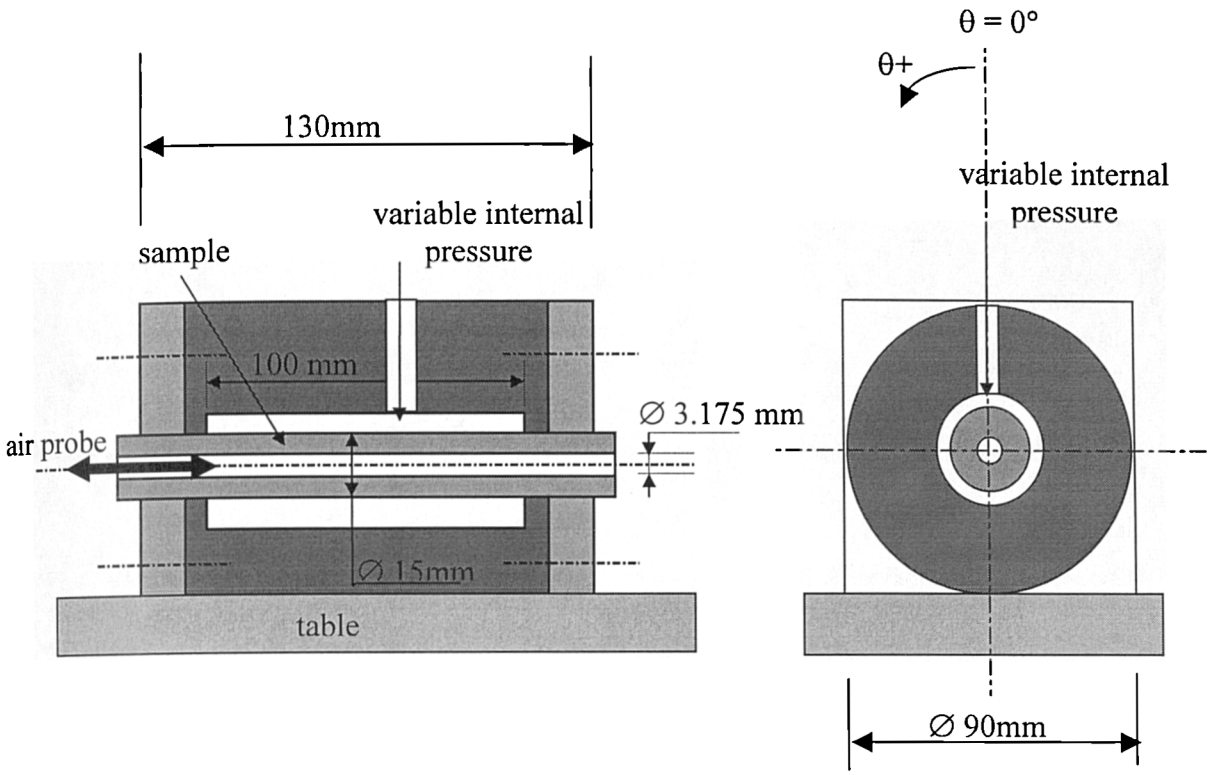

Figure 4.1 : Section through the experimental system for pressurised vessel calibration test.

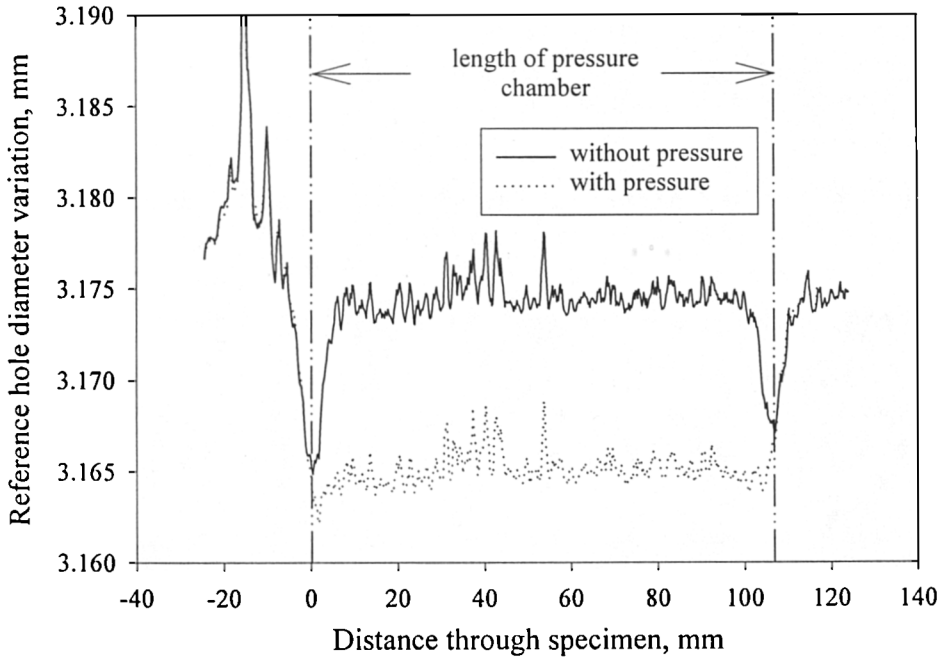

Figure 4.2 : Diameter change corresponding to an applied hydrostatic pressure P = 270MPa.

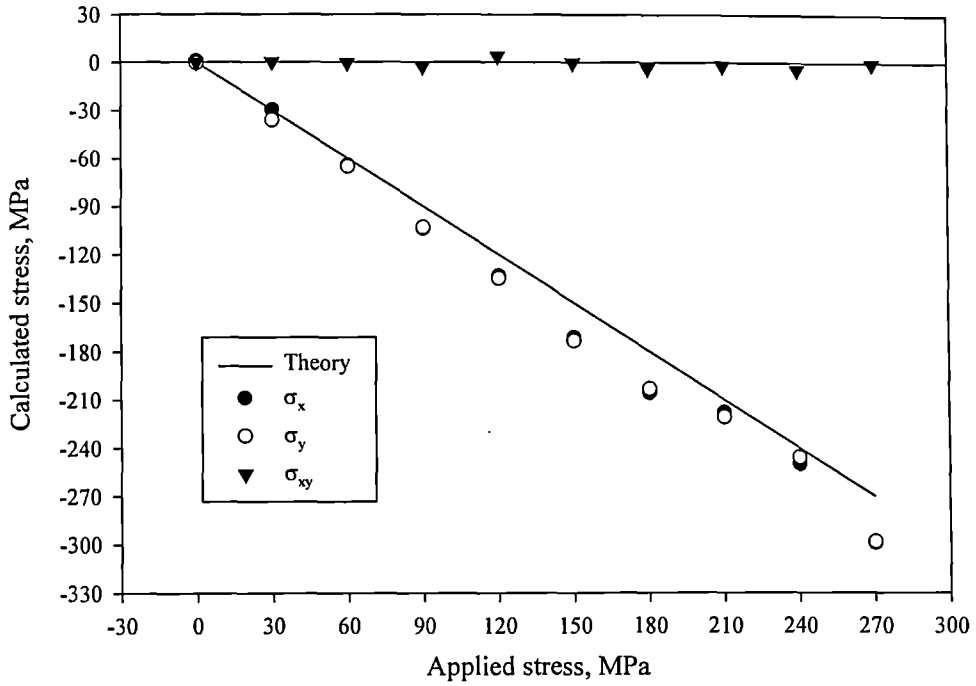

Figure 4.3 : Correspondence between applied and evaluated stresses.

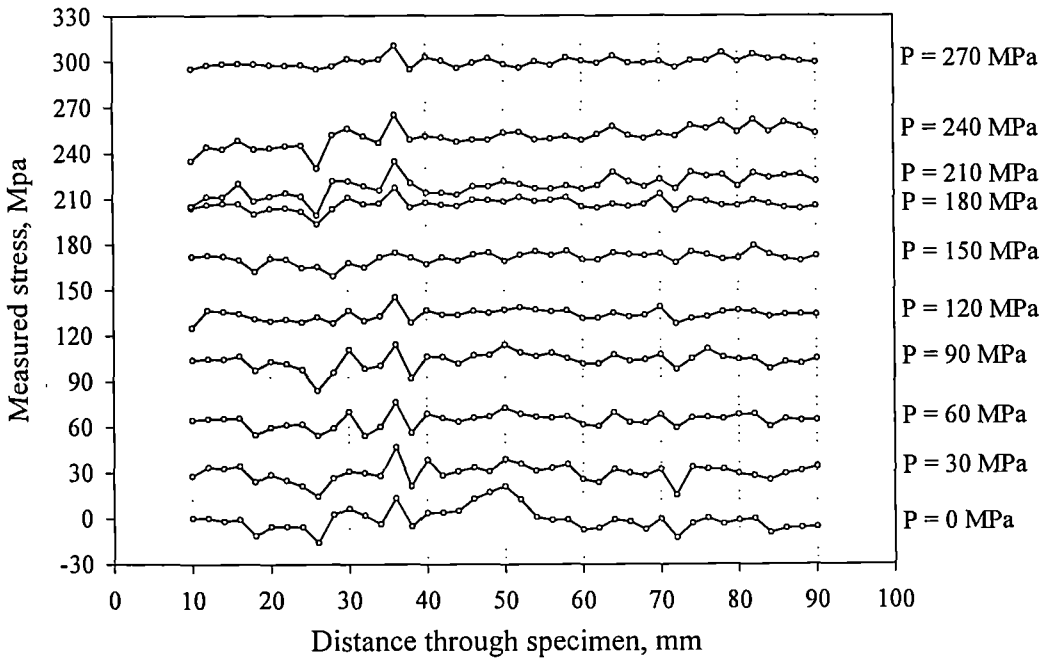

Figure 4.4 : Evaluated stresses for each applied hydrostatic pressure.

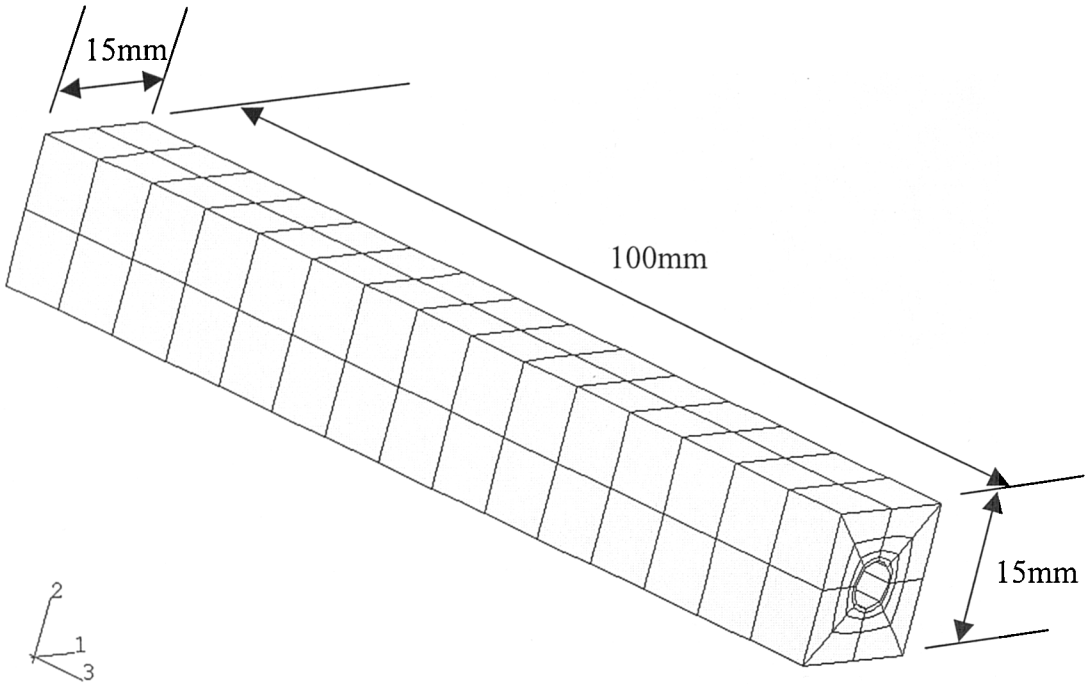

Figure 4.5 : Finite element mesh employed for hydrostatic pressure test.

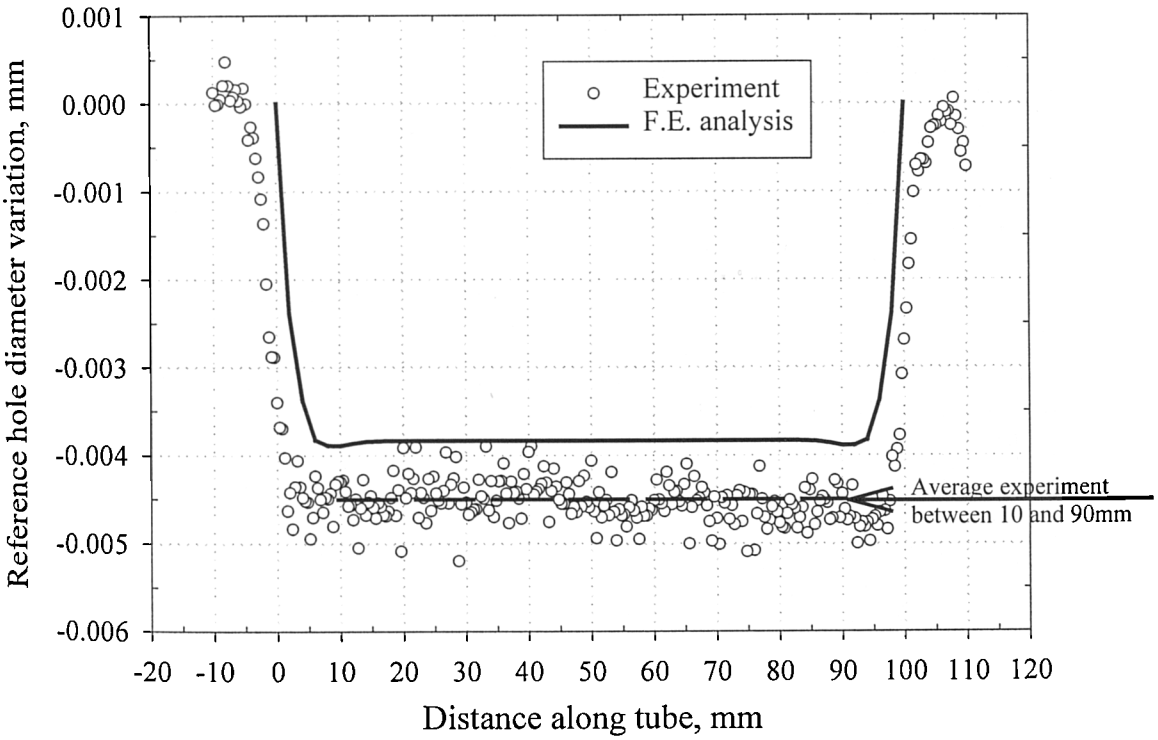

Figure 4.6 : Comparison of experimental and finite element displacement at the hole edge for hydrostatic pressure test – P = 120MPa.

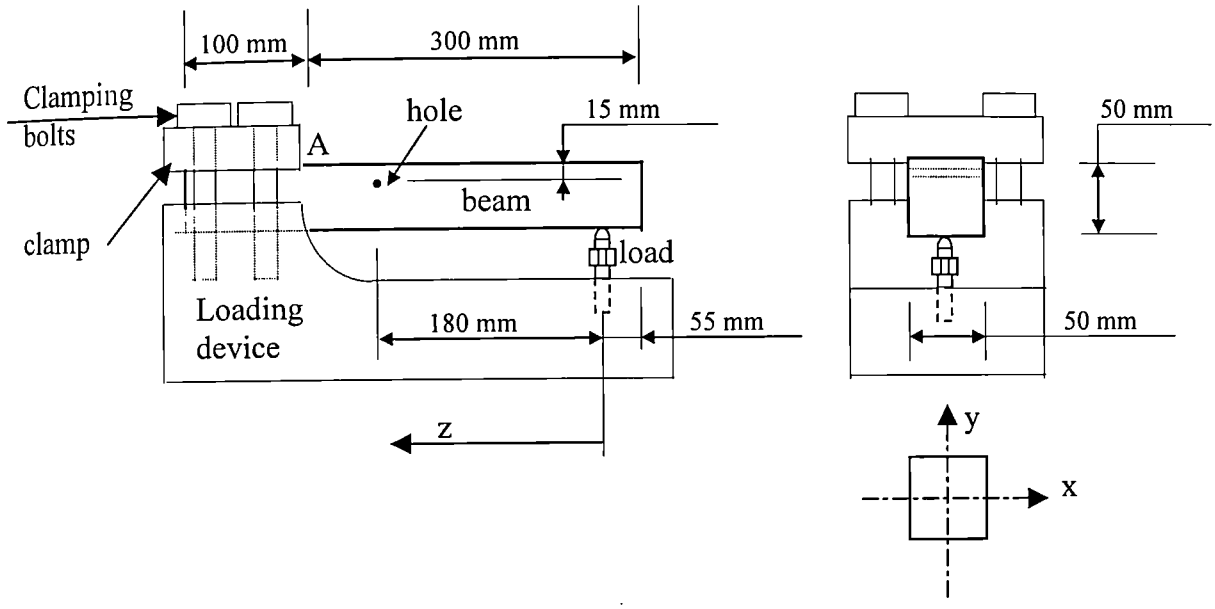

Figure 4.7a : Schematic of the bending test rig.

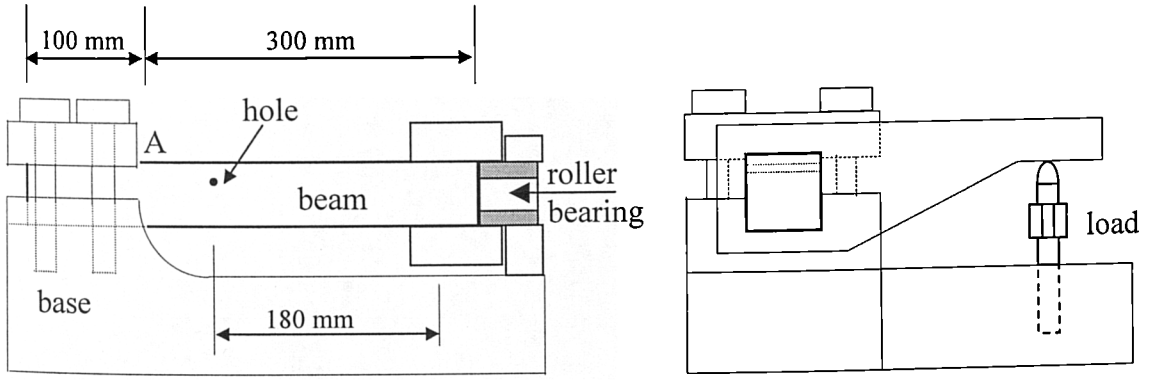

Figure 4.7b : Schematic of the torsion test rig.

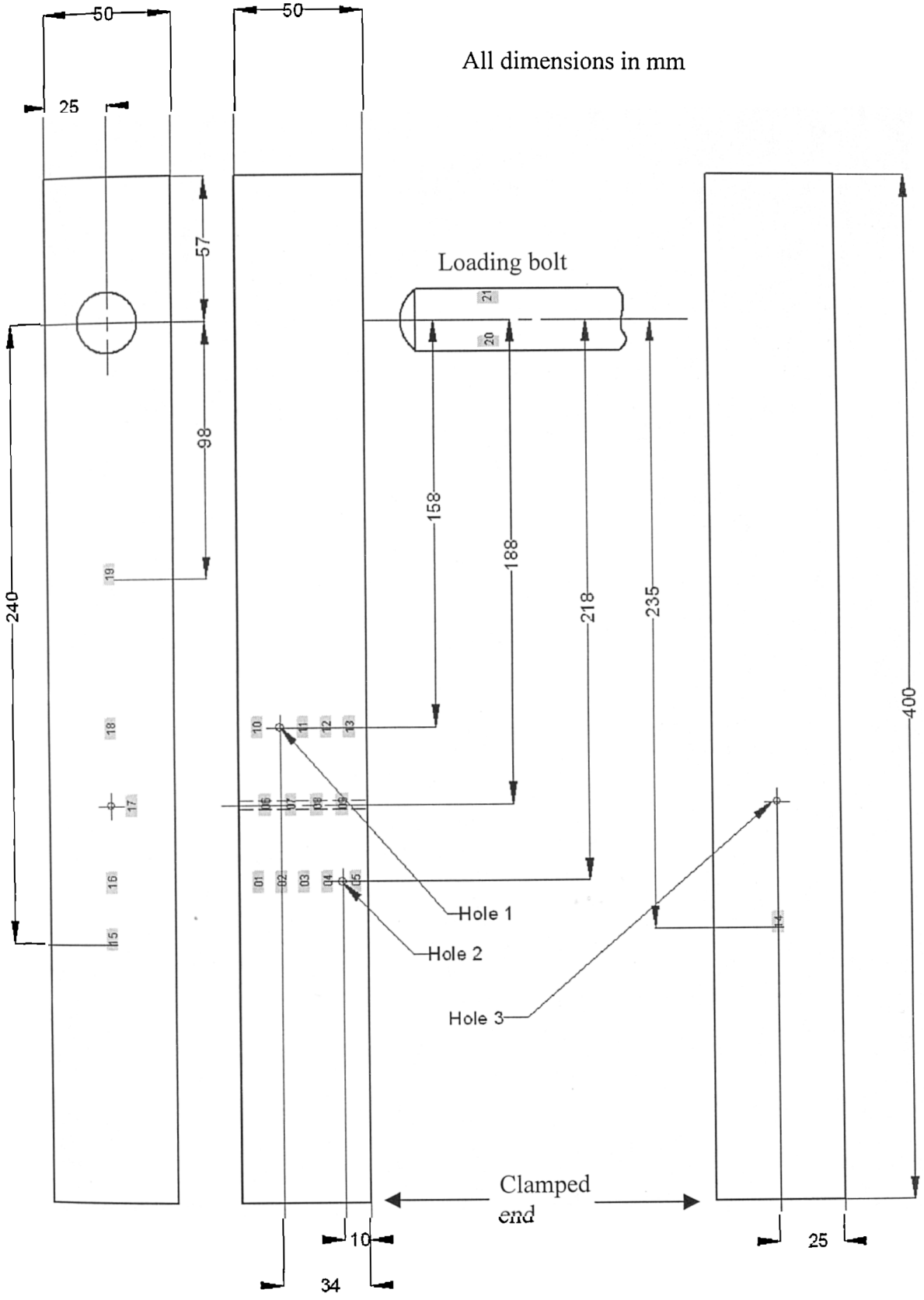

Figure 4.8a : Strain gauge locations for bending tests.

All dimensions in mm

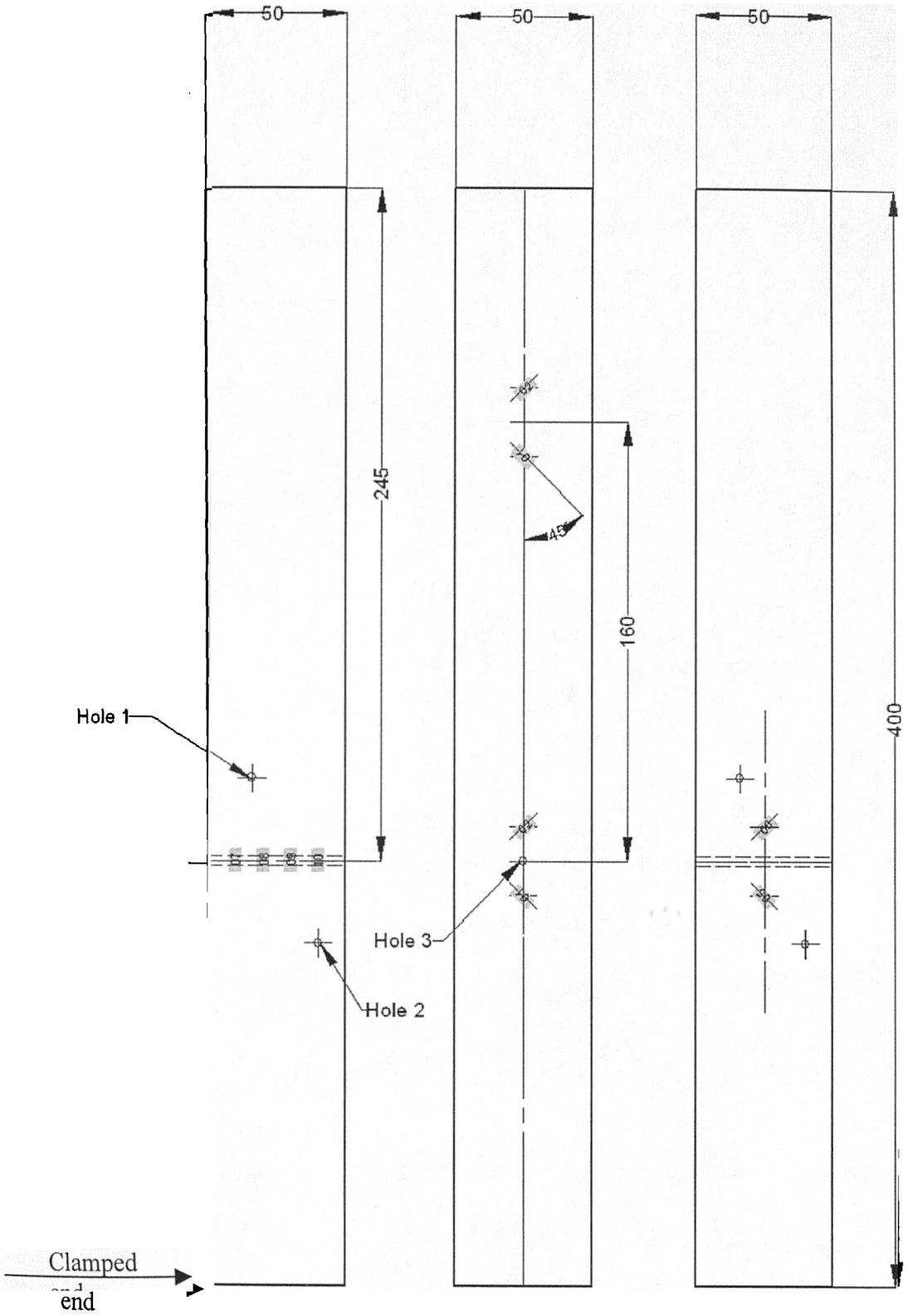

Figure 4.8b : Strain gauge locations for torsion tests.

All dimensions in mm

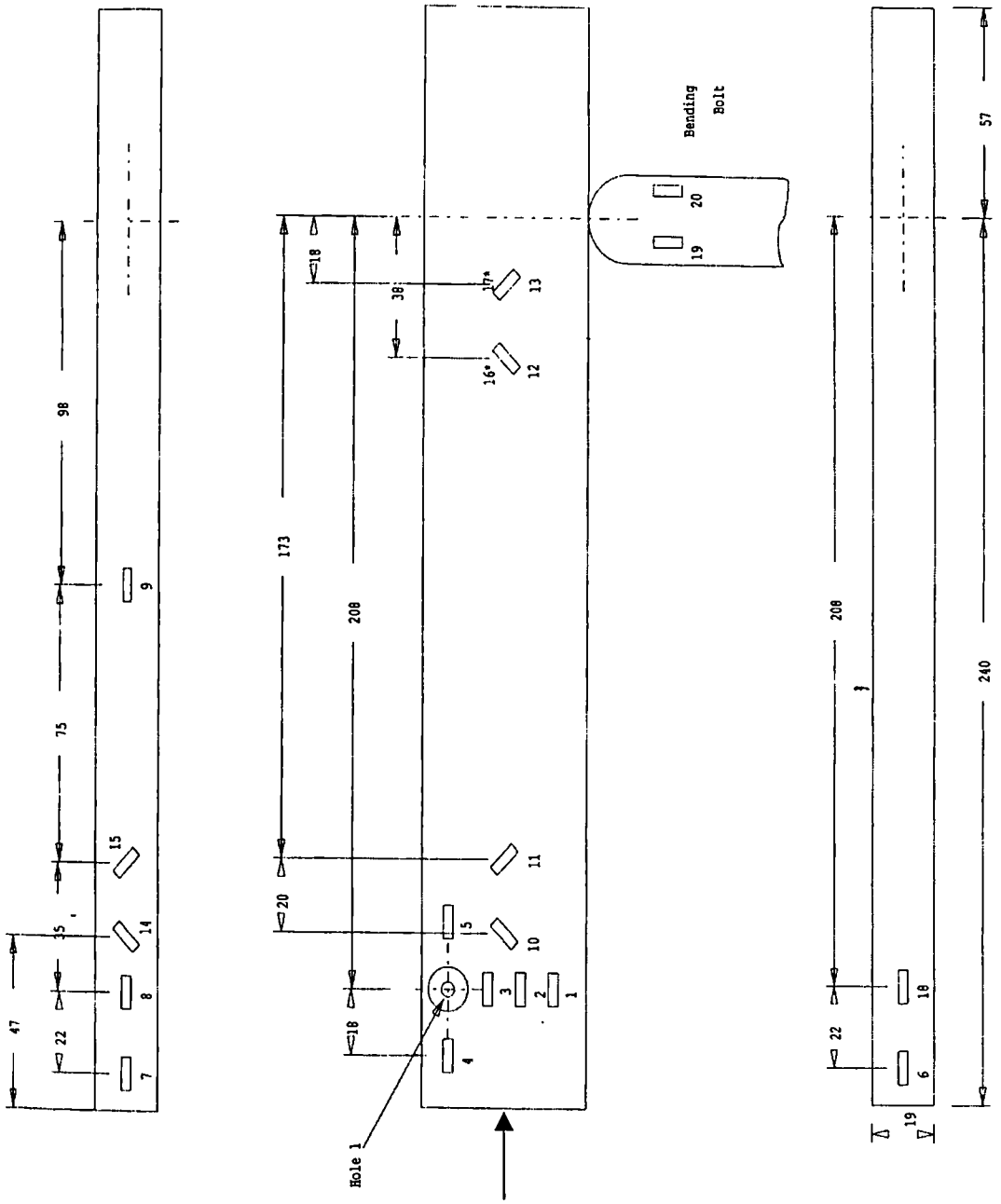

Figure 4.8c : Strain gauge locations for 19mm bar,
Bending and torsion.

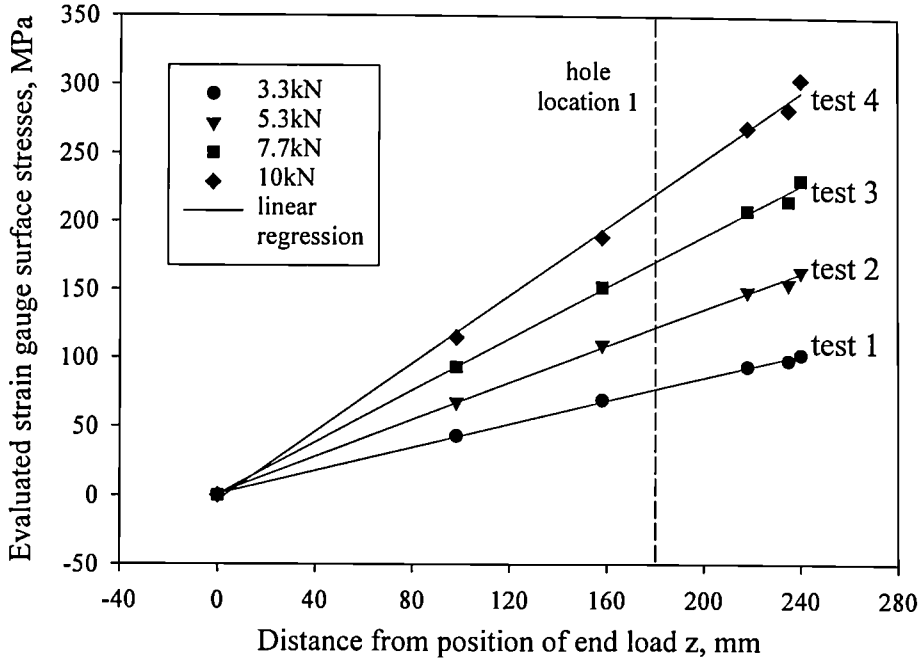

Figure 4.9 : Experimental distribution of stresses obtained from surface strain gauges.

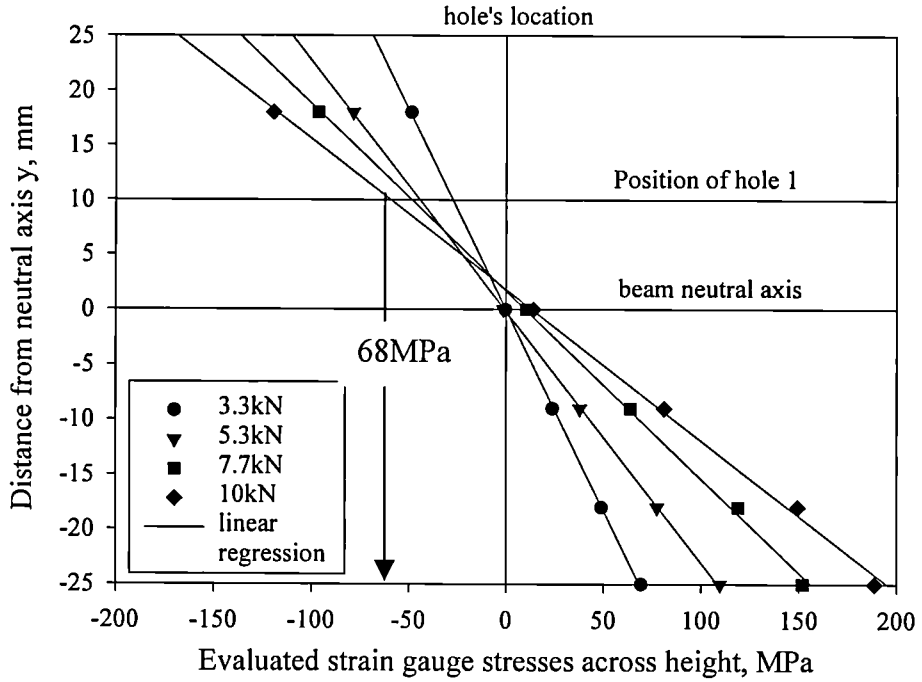

Different applied stresses at hole from strain gauges : -27, -44, -49 and -68MPa.

Figure 4.10 : Experimental distribution of stresses read by strain gauges through beam width.

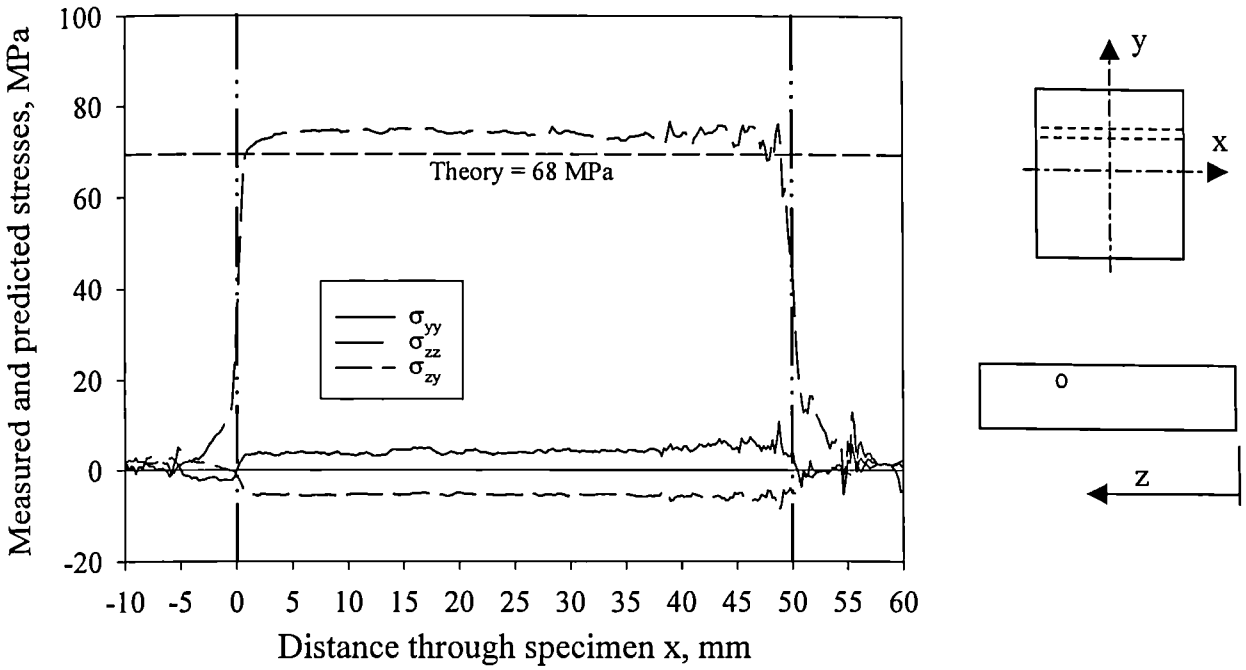

Figure 4.11 : Measured stresses across depth of 50mm specimen, Bending load 10kN.

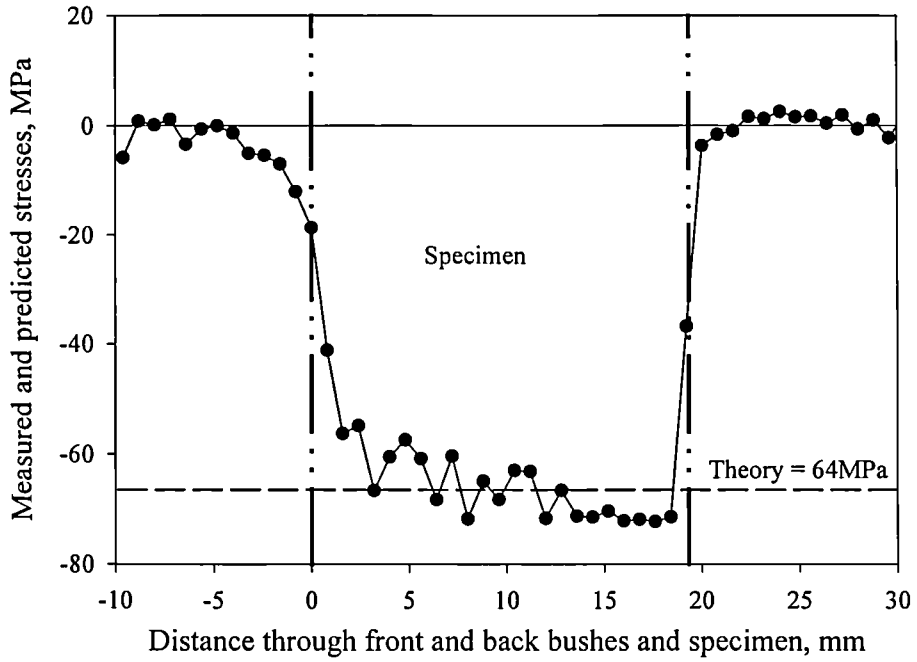

Figure 4.12 : Measured stresses across depth of 19mm specimen, Bending load 3.8kN.

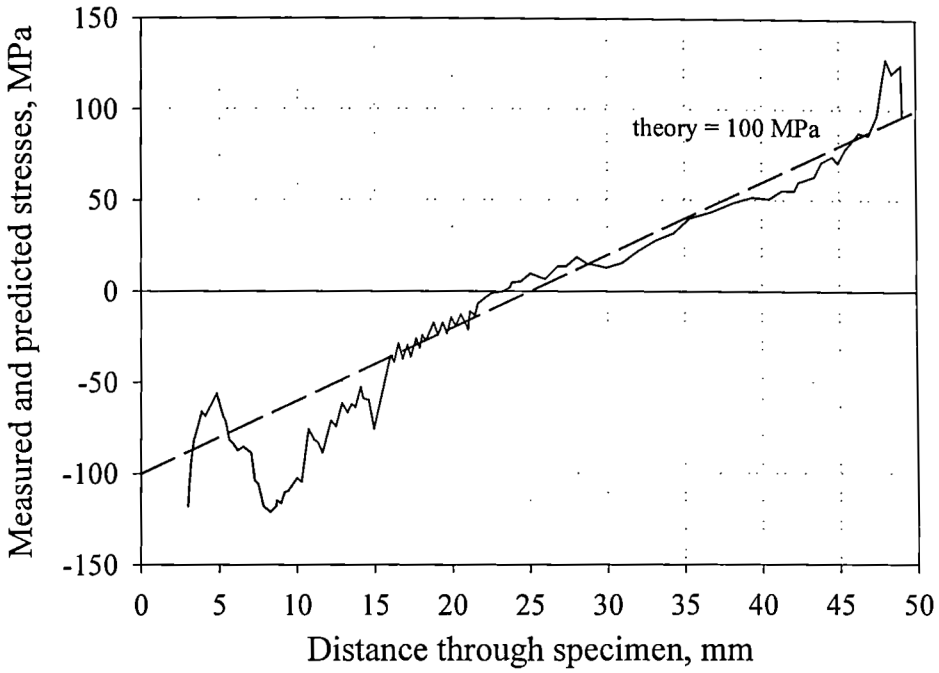

Figure 4.13 : Measured through height stresses in 50mm specimen.

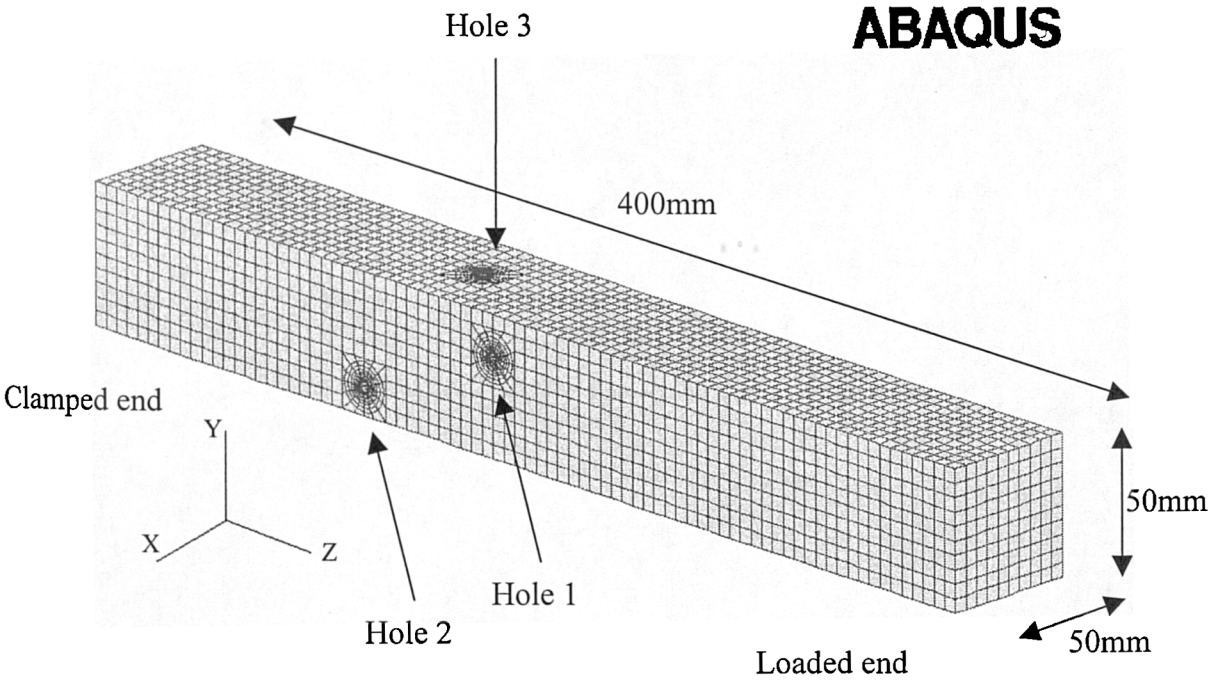

Figure 4.14 : Finite element mesh for 50 mm bar.

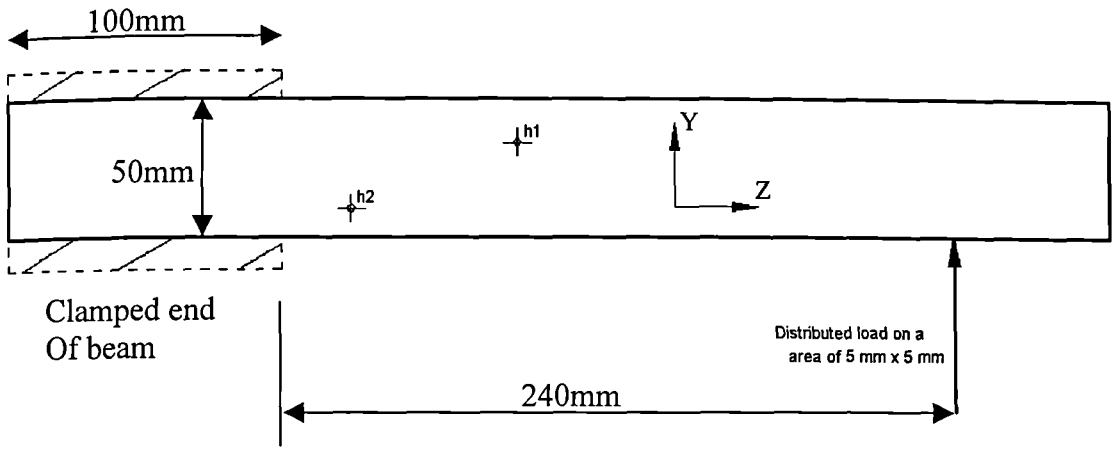

Bending

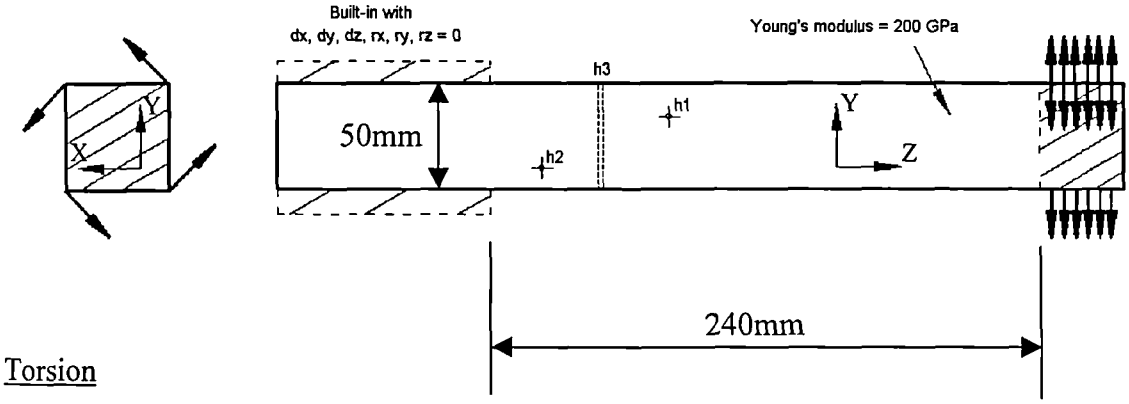

Torsion

Figure 4.15 : Loading conditions for bending and torsion tests.

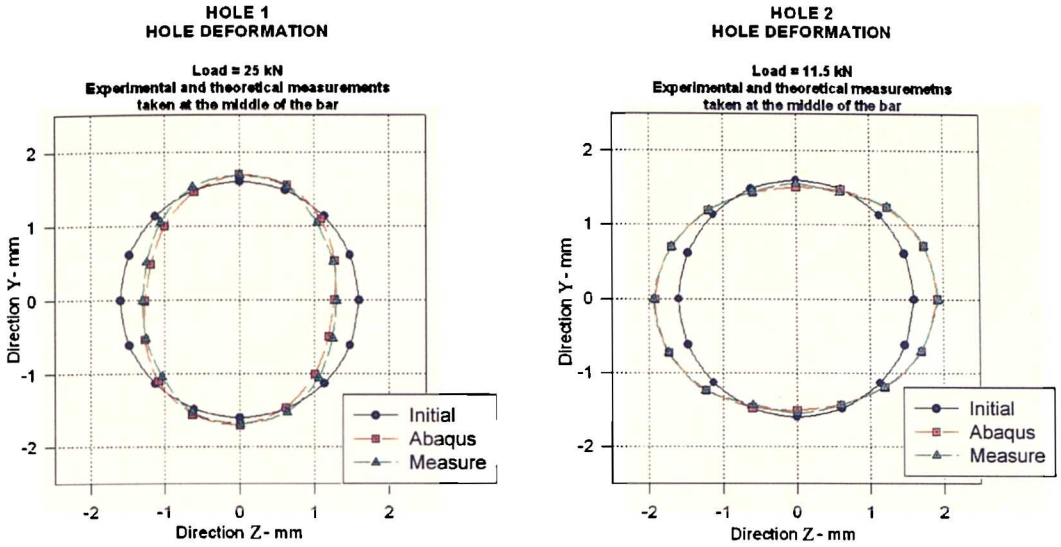

Figure 4.16 : Comparison of measured and predicted hole distortion for bending test.

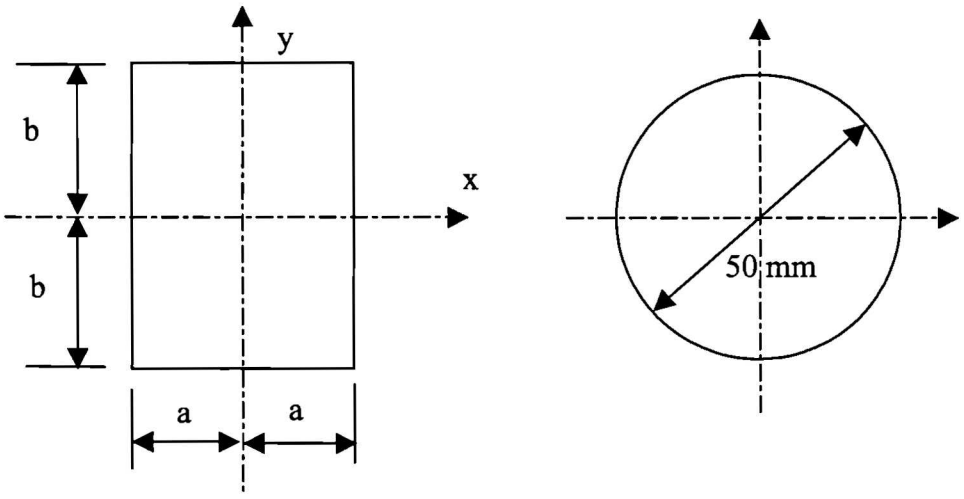

Figure 4.17 : Geometry of specimen for modified torsion analysis

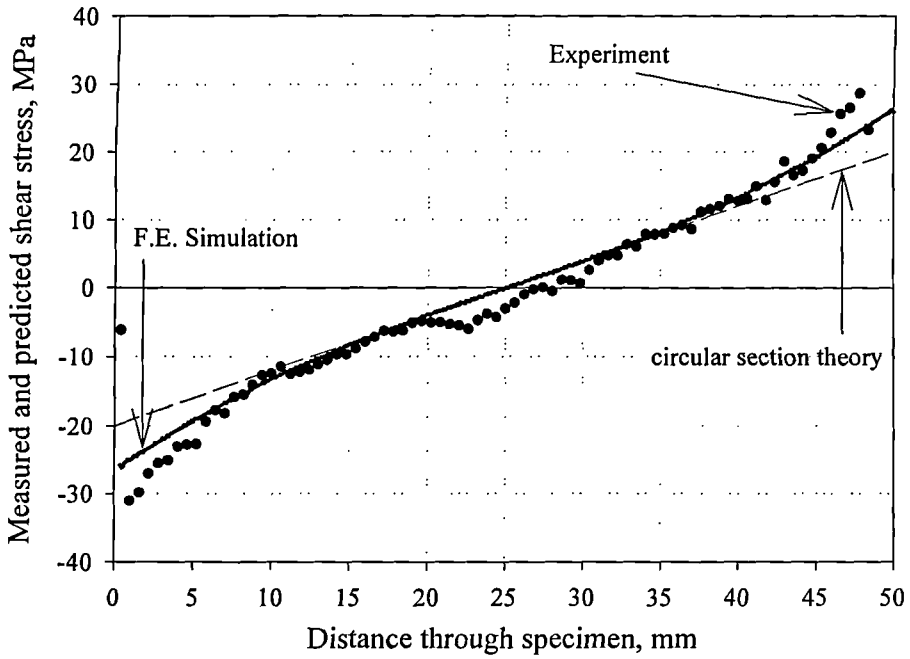

Figure 4.18a : Results for the 50 mm wide bar hole 3 under torsion, $M^t = 830Nm$.

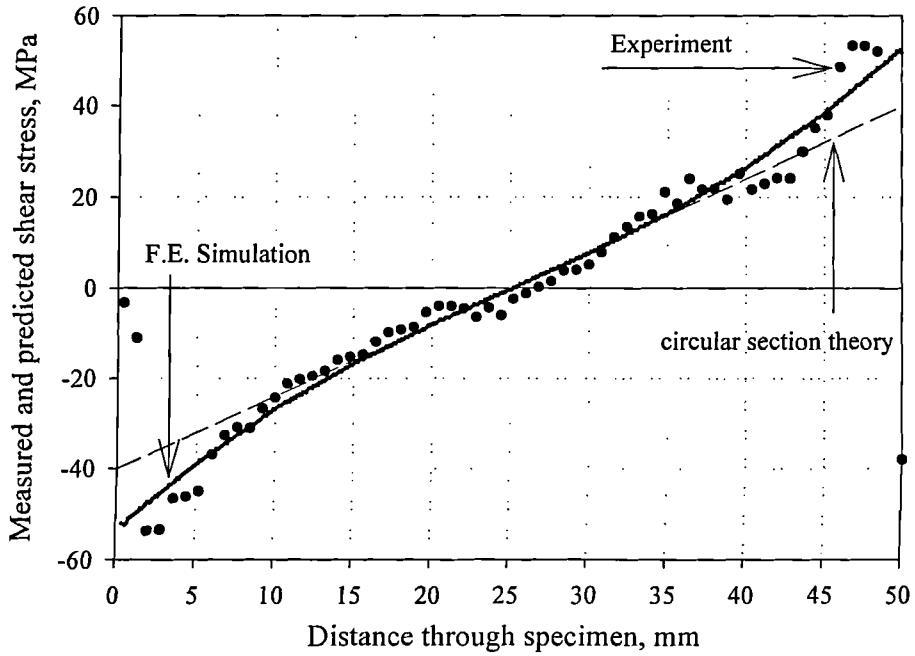

Figure 4.18b : Results for the 50 mm wide bar hole 3 under torsion, $M^t = 1660Nm$.

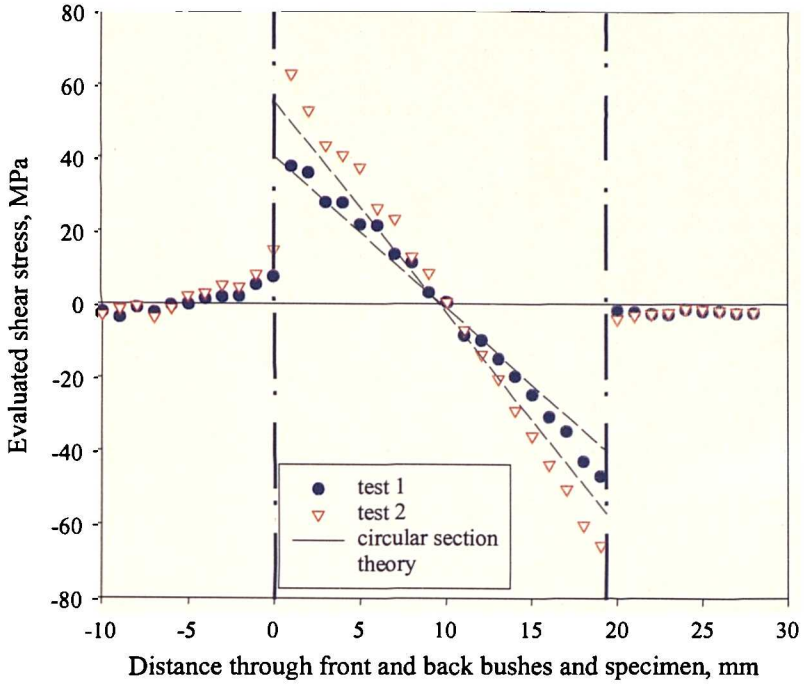

Figure 4.19 : Results for the 19 mm wide bar hole 1 under torsion, $M^t = 365Nm$ and $M^t = 508Nm$.

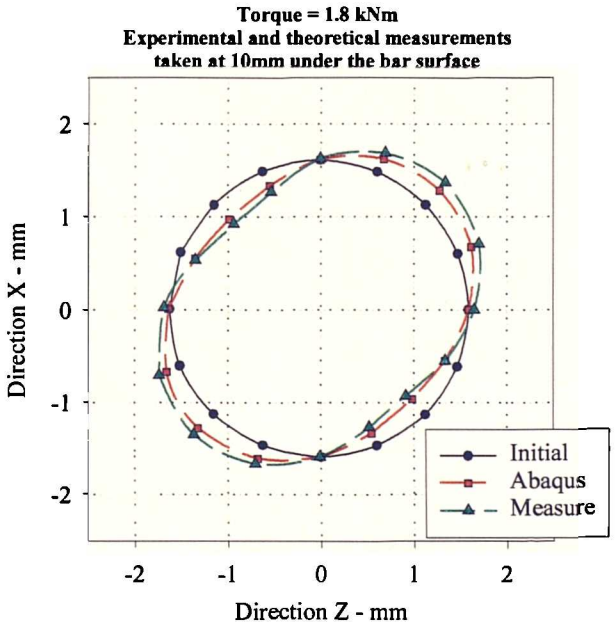

Figure 4.20 : Comparison of measured and predicted hole distortion for torsion test.

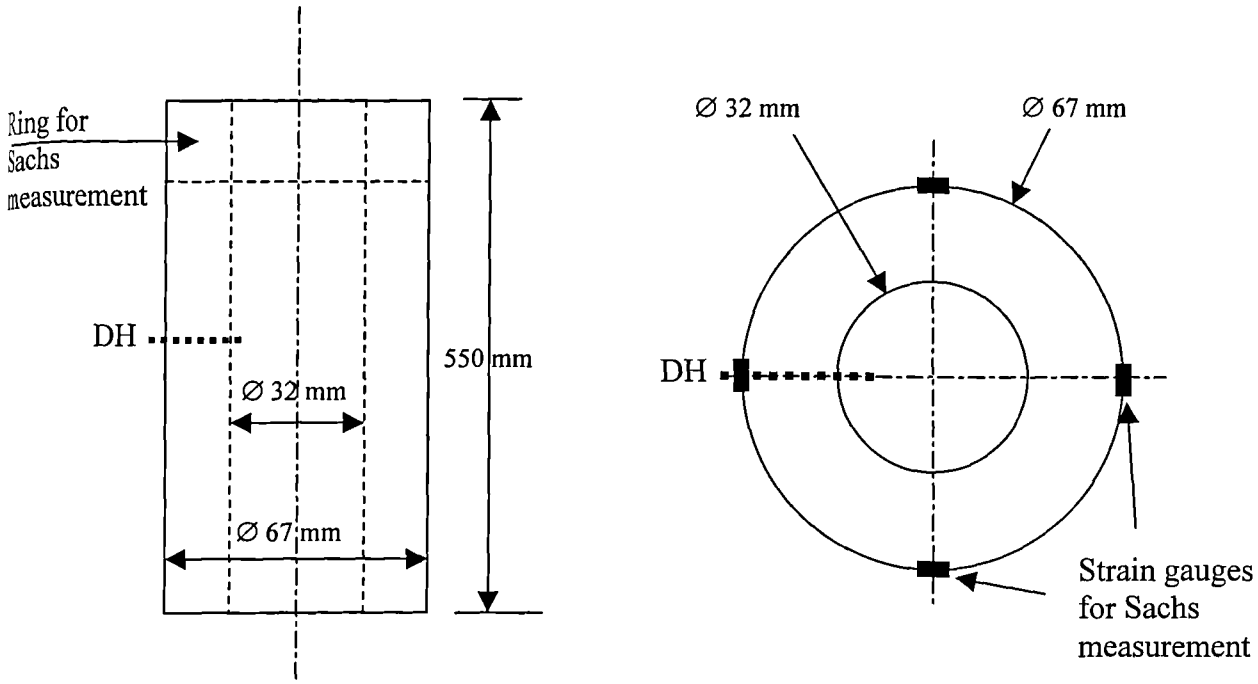

Figure 4.21 : Arrangement of the DSM autofrettaged tube specimen and measurement locations.

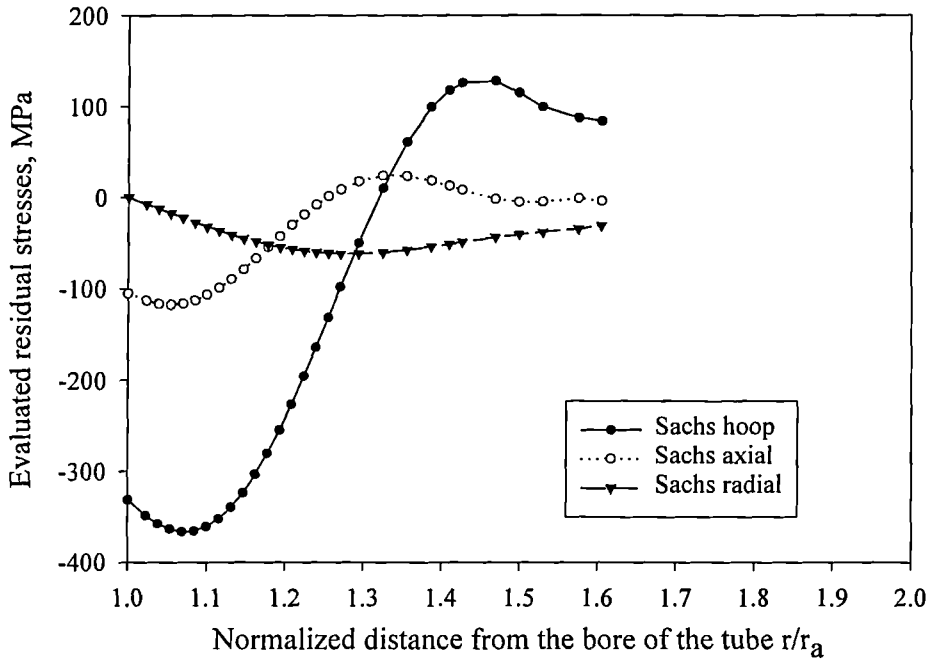

Figure 4.22 : Evaluated residual stresses from Sachs measurements.

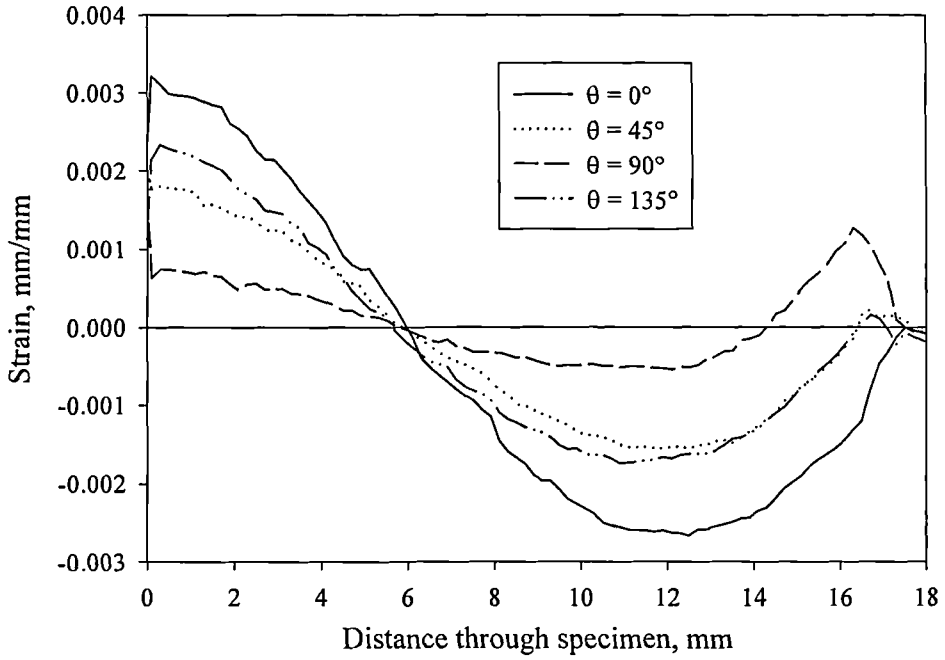

Figure 4.23 : Measured deep-hole strains.

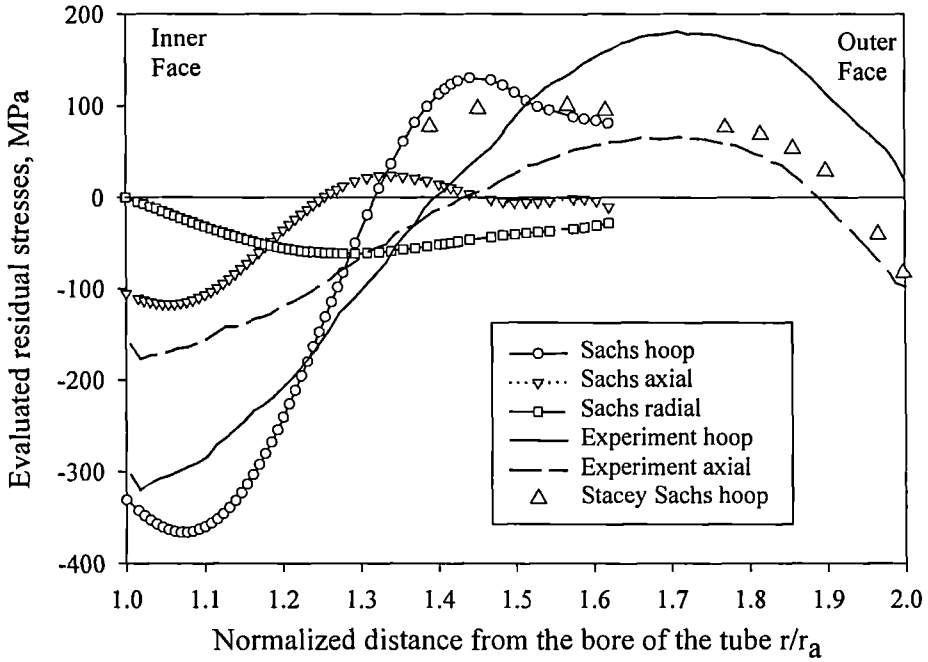

Figure 4.24 : Measured residual stresses in an autofrettaged tube.

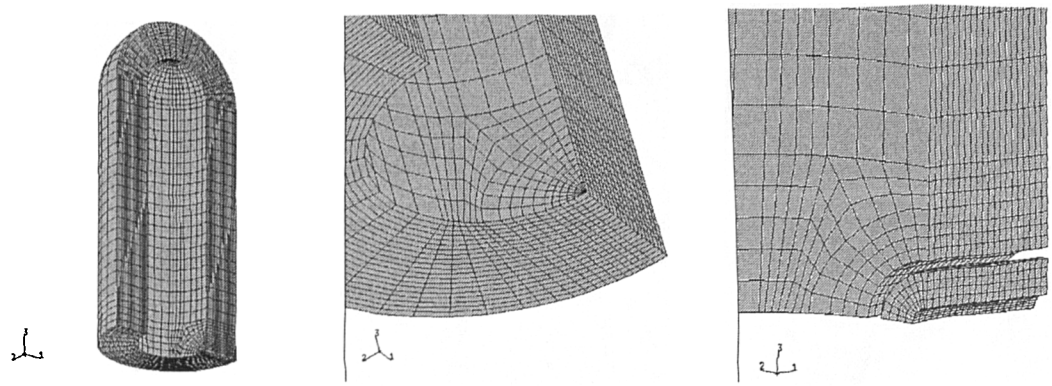

a) ¼ pipe FE model b) detail of tube wall c) deep-hole simulation in tube wall

Figure 4.25 : Finite element mesh for residual stress generation.

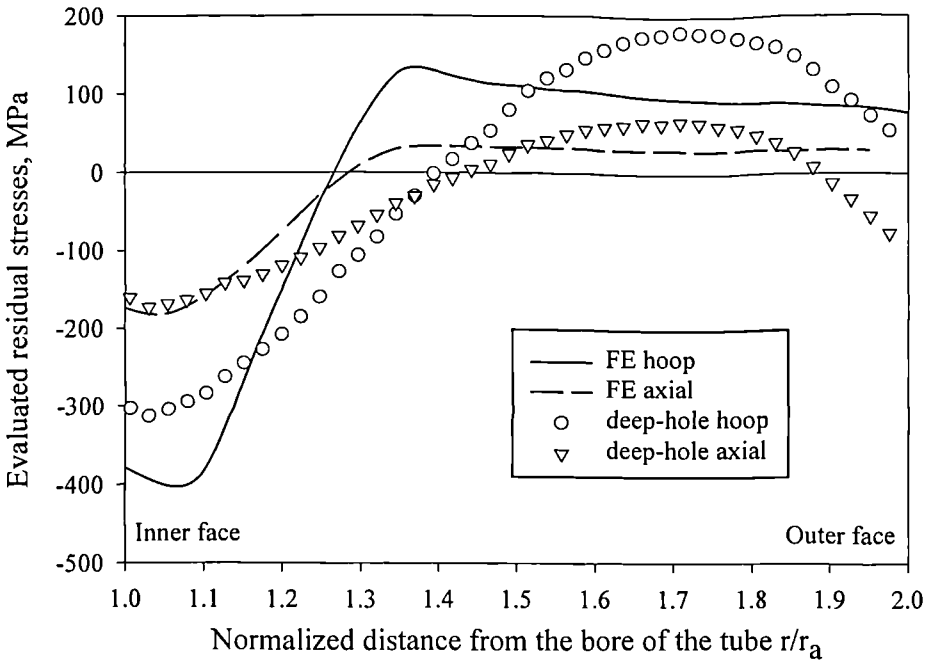

Figure 4.26 : Comparison of residual stresses between experiment and finite element analysis.

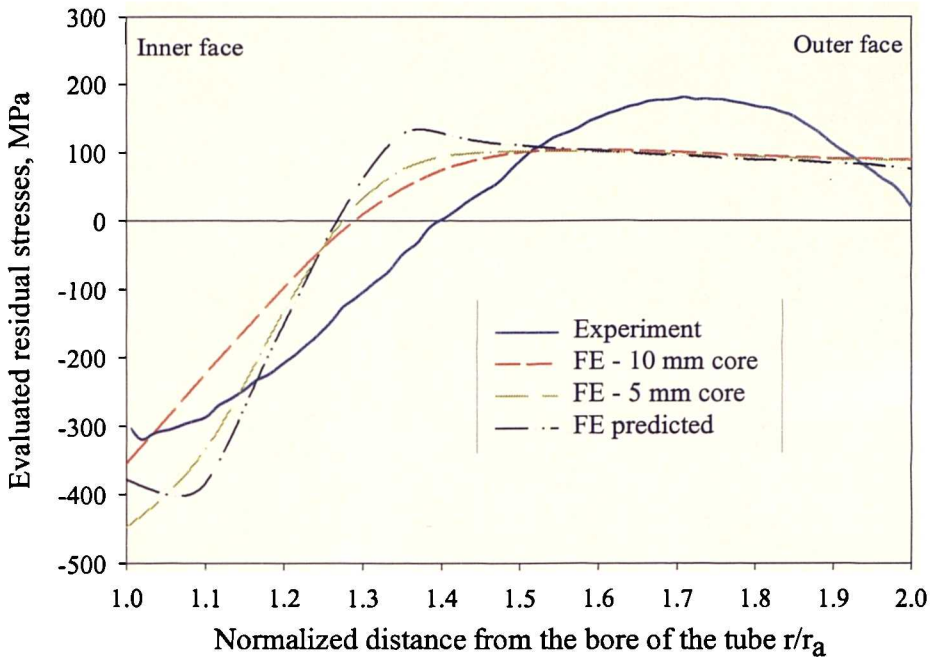

Figure 4.27 : Comparison of hoop residual stresses between original generated residual stresses and evaluated from deep hole technique

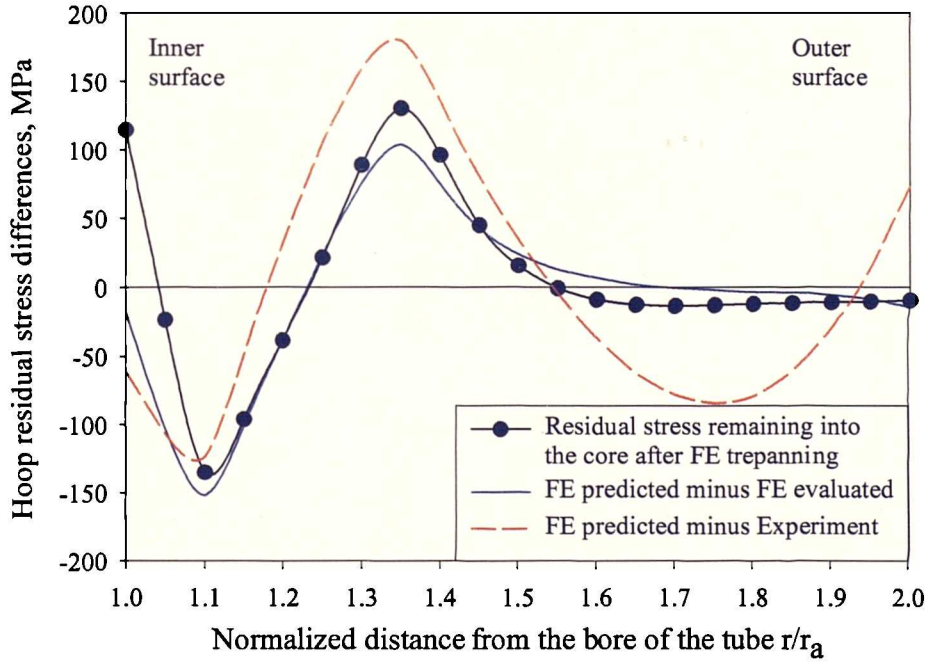

Figure 4.28a : Residual stresses remaining in the core and differences with evaluated stresses, hoop direction.

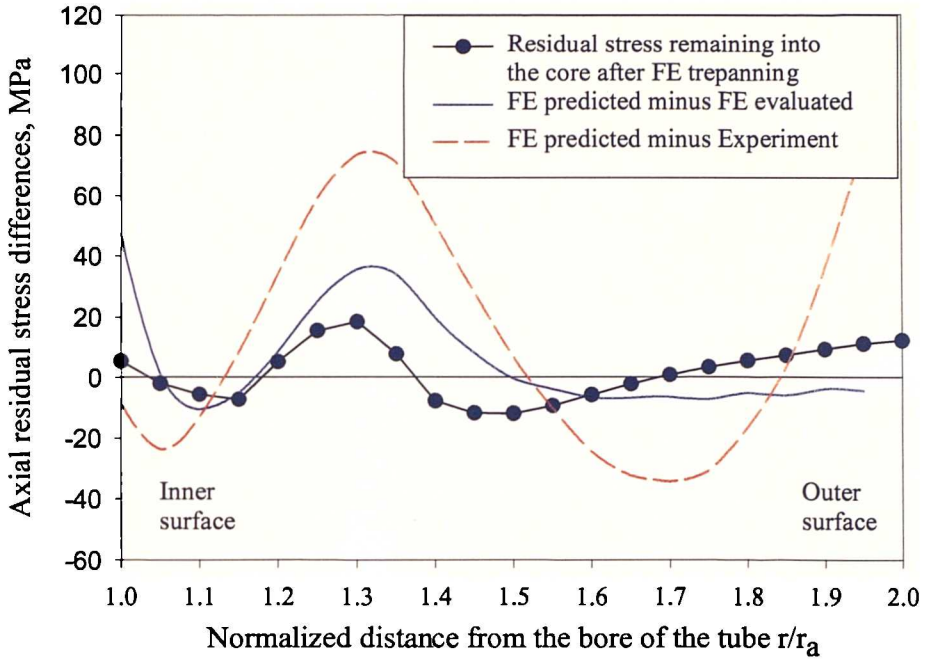

Figure 4.28b : Residual stresses remaining in the core and differences with evaluated stresses, axial direction.

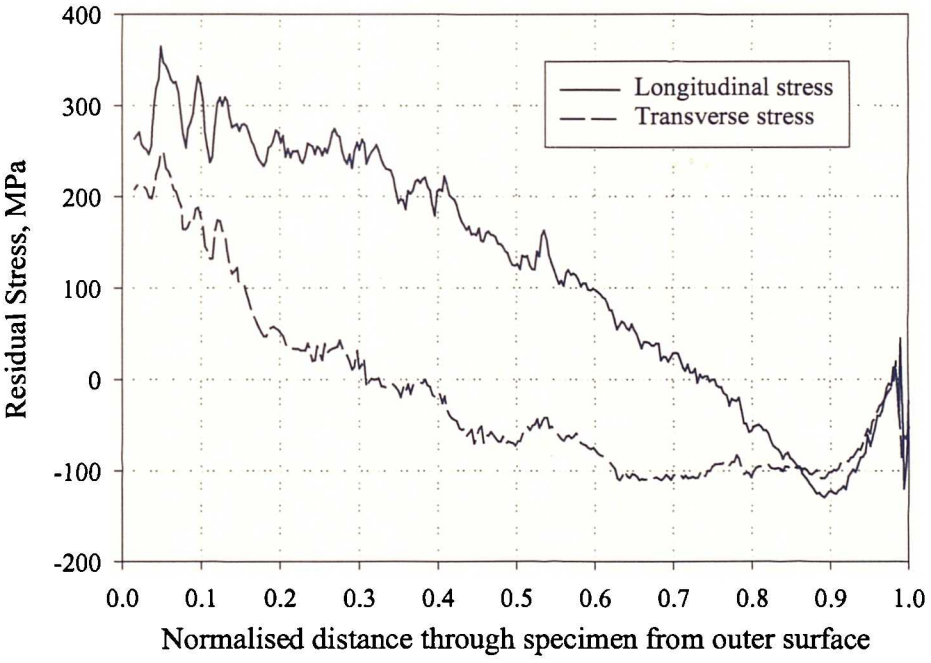

Figure 4.29 : Set of residual stresses applied on FE analysis.

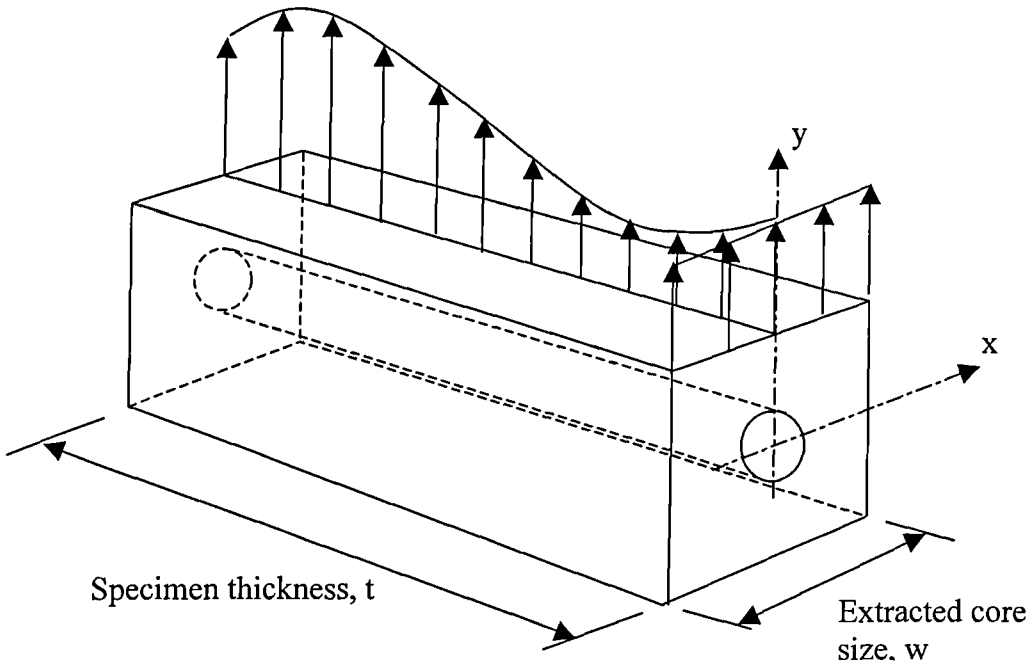

Figure 4.30 : Schematic of the FE mesh for influence of core diameter.

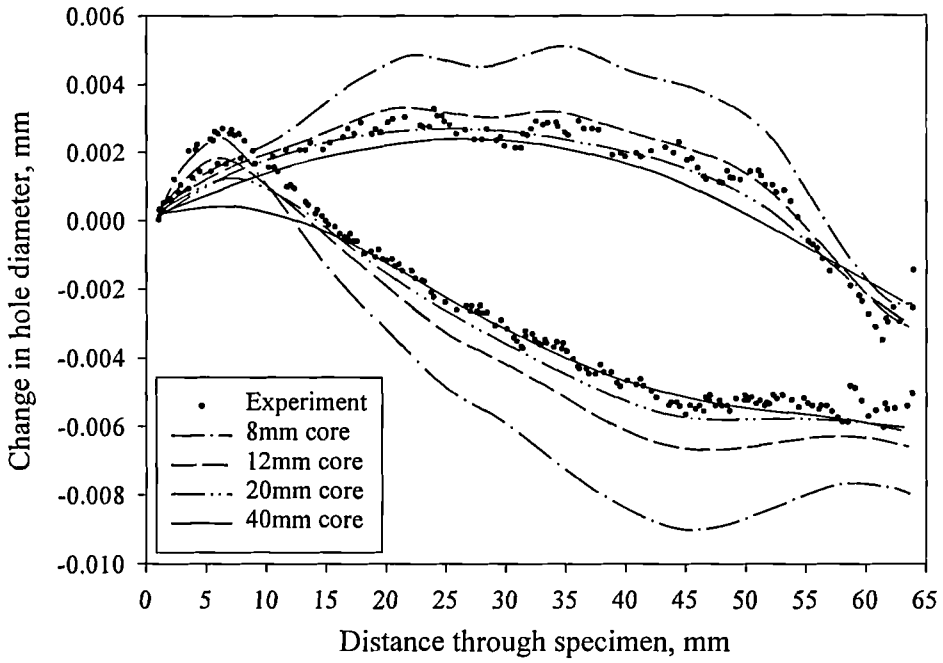

Figure 4.31 : Comparison of displacements between FE and experiments at the hole edge.